الجمهورية الجزائرية الديمقراطية الشعبية

République Algérienne Démocratique et Populaire
Ministère de L'Enseignement Supérieur et de la Recherche Scientifique

UNIVERSITÉ SETIF1-Ferhat ABBAS

FACULTÉ DE TECHNOLOGIE

<u>THÈSE</u>

Présentée au Département de Génie des Procédés

Pour l'obtention du diplôme de

DOCTORAT

Domaine : Sciences et Technologie

Filière : Génie des Procédés   Option : Génie pharmaceutique

Par
MERIR Roufaida

<u>THÈME</u>

Conception de nouveaux systèmes nano/micro encapsulés pour la vectorisation des médicaments.

Soutenue le 20/06/ 2024 devant le Jury :

GUELLAL Messaoud	**Professeur**	**Univ. Sétif1-Ferhat ABBAS**	**Président**
BAITICHE Milad	**Professeure**	**Univ. Sétif1-Ferhat ABBAS**	**Directrice de thèse**
BENYAHIA Azzedine	**Professeur**	**Univ. Mohamed Boudiaf M'sila**	**Examinateur**
BOUGUETTOUCHA Abdallah	**Professeur**	**Univ. Sétif1-Ferhat ABBAS**	**Examinateur**
LAZZARA Giuseppe	**Professeur**	**Univ. Degli Studi di Palermo**	**Invité**
BOUTAHALA Mokhtar	**Professeur**	**Univ. Sétif1-Ferhat ABBAS**	**Invité**

جامعة سطيف 1 - فرحات عباس

Setif 1 University - Ferhat ABBAS

Setif 1 University-Ferhat ABBAS

FACULTY OF TECHNOLOGY

Thesis submitted to the Process Engineering Department for a Doctorate Degree

Domain : Science and Technology

Section : Process Engineering

Option : Pharmaceutical Engineering

BY

MERIR Roufaida

TITLE OF THE THESIS

Design of new nano/micro encapsulated systems for targeted drug delivery.

Defended on 20/06/ 2024 in front of the Jury:

GUELLAL Messaoud	Professor	SETIF1 University-Ferhat ABBAS	Chairman
BAITICHE Milad	Professor	SETIF1 University-Ferhat ABBAS	Supervisor
BENYAHIA Azzedine	Professor	M'SILA University- Mohamed Boudiaf	Examinator
BOUGUETTOUCHA Abdallah	Professor	SETIF1University-Ferhat ABBAS	Examinator
LAZZARA Giuseppe	Professor	Univ. Degli Studi di Palermo	Guest
BOUTAHALA Mokhtar	Professor	SETIF1University-Ferhat ABBAS	Guest

My deepest appreciation also goes to my ***colleagues*** for their unwavering support throughout this challenging but rewarding journey.

I'm thankful to the staff of **LMPMP**, **LGPC**, and **FCL** at Università degli Studi di Palermo, Italy laboratory for their help, support, and consideration.

My acknowledgment to all my Professors whom I had throughout my academic studies.

I'm very grateful to the "*Ministère de l'Enseignement Supérieur et de la Recherche Scientifique de l'Algérie*", "*University of Ferhat Abbas Setif 1*", as well *as "Università degli Studi di Palermo"* for the support of the Ph.D. project.

Dedication

"_To my beloved parents, siblings, and friends, for their unconditional love, patience, prayers and support, which made this journey possible for me_**."**

Roufaida

List of abbreviations

2-CEPA	2-(2-carboxyethyl) phosphonic acid
16-PHA	16-Phenylhexadecanoic acid
5-ASA	5-Aminosalicylic Acid or Mesalazine
5-LOX	5-lipoxygenase
APTES	3-Aminopropyl triethoxysilane
API	Active Pharmaceutical Ingredient
AlO6	Octahedral alumina oxide
BCS	Biopharmaceutics Classification System
CD	Crohn's Disease
COX-1	Cyclooxygenase-1
COX-2	Cyclooxygenase-2
DE	Diatomaceous Earth
DNA	Deoxyribonucleic Acid
DOE	Design of Experiments
DTG	Differential Thermogravimetry
DLS	Dynamic Light Sattering Analysis
EC	Ethyl cellulose
EVA	Ethylene Vinyl Acetate
FDA	Food and Drug Administration
FTIR	Fourier-Transform Infrared Spectroscopy
GI	Gastrointestinal
GPTMS	Glycidoxypropyltrimethoxysilane
HNTs	Halloysite nanotubes
IBD	Inflammatory Bowel Disease
mPEG Silane	Methoxy polyethylene glycol silane
Mg	Magnesium
Na	Sodium
NDDs	Nano/Micro Drug Systems
OTS	Octadecyltrichlorosilane
PEG	Poly ethylene glycol
PDB	Protein Data Bank
PPAR-γ	Peroxisome proliferator-activated receptor-gamma
PLA	Poly lactic acid
PLGA	Poly D, L-lactide-co-glycolide
PMMA	Poly methyl methacrylate
PVA	Polyvinyl Alcohol
PXRD	X-ray Diffraction
RNA	Ribonucleic Acid
SEM	Scanning Electron Microscopy

SGF	Simulated Gastric Fluid
Si	Silicon
SiO2	Silicon dioxide
SiOH	Silanol
TEM	Transmission electron microscopy
TGA	Thermogravimetric Analysis
TNF-α	Tumor necrosis factor alpha
XRF	X-ray fluorescence

List of figures

Chapter IV   Conception of Cellulose/Alginate /Mesalazine microspheres by solvent evaporation technique for drug release: Experimental and theoretical investigations.

Chapter V: Optimizing Colon-Targeted Therapy through Mesalazine Delivery via pH-Sensitive Halloysite/ Polysaccharide Nanocomposites: In vitro, In silico and Computational study.

Chapter VI: Computational Insights and Nanocarrier Technologies with pH-Responsive Polymers for Improving Drug Delivery in Inflammatory Bowel Disease

List of tables

Chapter V: Optimizing Colon-Targeted Therapy through Mesalazine Delivery via pH-Sensitive Halloysite/ Polysaccharide Nanocomposites: In vitro, In silico and Computational study.

Chapter VI: Computational Insights and Nanocarrier Technologies with pH-Responsive Polymers for Improving Drug Delivery in Inflammatory Bowel Disease.

List of contents

Chapter I: Exploring Encapsulation Methods and Materials

Chapter II: Microencapsulation: Solvent evaporation

Chapter III: Exploring clays in Drug Delivery

Chapter IV: Conception of Cellulose/Alginate /Mesalazine microspheres by solvent evaporation technique for drug release: Experimental and theoretical investigations

Chapter V: Optimizing Colon-Targeted Therapy through Mesalazine Delivery via pH-Sensitive Halloysite/ Polysaccharide Nanocomposites: In vitro, In silico and Computational study.

Introduction

Introduction

Targeted drug delivery systems represent a significant technological advancement in the pharmaceutical field, addressing the limitations of conventional drug formulations. Traditional oral or injectable drug administration often results in suboptimal therapeutic efficacy, undesirable side effects, and non-specific biodistribution. This is due to the drugs' inability to selectively reach the intended target site within the body, leading to off-target effects and reduced overall treatment effectiveness.

The design of nano- and micro-encapsulated drug delivery systems has emerged as a promising solution to overcome these challenges. By encapsulating active pharmaceutical ingredients (APIs) within specialized carrier systems, it is possible to improve drug solubility, stability, and targeted delivery to specific tissues or cells. This approach can enhance the pharmacokinetic and pharmacodynamic properties of drugs, ultimately leading to improved therapeutic outcomes for patients.

The primary objective of this thesis is to design and develop innovative nano- and micro-encapsulated systems for the targeted delivery of various drug molecules. The research focuses on the formulation, characterization, and evaluation of these advanced drug delivery platforms, with the aim of enhancing the efficacy and safety of pharmaceutical treatments.

The thesis explores the use of different carrier materials, such as polymers, lipids, and inorganic nanostructures, to encapsulate and deliver a range of therapeutic agents. The encapsulation process is optimized to ensure improved drug solubility, controlled release kinetics, and efficient targeting to the desired site of action. Comprehensive physicochemical, in vitro, in silico, and DFT evaluations are conducted to assess the performance and potential clinical applicability of the developed nano- and micro-encapsulated systems.

The findings of this research contribute to the advancement of targeted drug delivery strategies, providing new insights and innovative solutions to overcome the limitations of conventional drug formulations. The successful implementation of these nano- and micro-encapsulated systems has the potential to revolutionize the way various diseases are managed, leading to enhanced therapeutic efficacy, reduced side effects, and improved patient outcomes.

Chapter I

Exploring Encapsulation Methods and Materials.

1: Introduction

The creation of efficient drug-delivery systems is now a key component of the process of developing novel medications. As a result, researchers continue to look for strategies to distribute medications over time with a well-controlled release profile [1]. Drugs are practically rarely provided as pure chemical compounds; they are usually supplied in the form of prepared formulations or medicines. In addition to the active pharmaceutical ingredient(s), drugs contain several components that help in their creation and enhance drug delivery.

The concept of "drug delivery" has undergone a paradigm shift from erstwhile concept of "right medicine" to that "right target" at the "right time". Covers a broad range of techniques used to get therapeutic agents into the human body to treat disease. The purpose of any drug-delivery system is to deliver a therapeutic amount of medication to the appropriate spot in the body to attain, and then maintain, the target drug concentration and supply the drug at a pace indicated by the body's demands during therapy [2]. The traditional method of treating acute diseases or chronic illnesses depends on prescribing various forms of medication to patients, including tablets, capsules, creams, and injectables. While these options allow for the immediate administration of medication into the body, they can also lead to a swift decrease in drug concentration. Consequently, patients often need to take multiple doses throughout the day to sustain the optimal level of medication in their system for effective treatment. The drawbacks and limits of traditional doses, as well as their negative effects, prompted researchers to the development of novel technical solutions such as micro/nanoencapsulation **[3,4]**.

Micro/nanoencapsulation is an interesting method that has been used to create innovative drug-delivery systems that can: achieve optimum therapeutic drug concentrations in the blood with minimal fluctuation; predict and replicate release rates for extended durations, and improve the pharmacotherapy of drugs with a short half-life. Additionally, they reduce the frequency of dosing and minimize or eliminate dose-related adverse effects, enhancing the overall effectiveness, safety, and compliance of therapy [5]. Micro/nanoencapsulation or micro/nanoparticulate drug delivery is a top option for delivering drugs safely and effectively.

2: Encapsulation

Encapsulation methods allow for the creation of composite particles, which generally consist of a core substance of interest covered by a secondary layer (Capsule) (Fig. 1). Encapsulation can impart qualities such as regulated core material release, protection from non-specific

chemical interactions, ease of handling and transport, and simple separation from matrices to the whole composite particle based on the properties of the coatings [6].

The encapsulation approaches generate microcapsules with varying morphologies depending on the encapsulation approach and the qualities of the core and shell materials. Mononuclear (core/shell), multi-wall, matrix, and polynuclear morphologies for microcapsules with polymeric shells have been observed. These microcapsules find applications across various fields such as pharmaceuticals, personal care, medicine, and food systems **[7,8]**.

The microencapsulation process used is determined by the qualities of the core and shell materials. Encapsulation procedures can be carried out using two approaches: physical and chemical methods. Spray cooling, spray drying, fluidized bed, pan coating, and vibrational nozzle technologies can all be used to physically enclose materials. In another hand, there are various chemical methods used for polymerization, including interfacial polymerization, in-situ polymerization, simple or complex coacervation, layer-by-layer assembly, solvent evaporation, emulsion polymerization, and suspension polymerization **[9-11]**.

The effectiveness of encapsulating microparticles, microspheres, or microcapsules depends on various factors such as the concentration of the polymer, its solubility in the solvent, the rate of solvent removal, and the solubility of the organic solvent in water.

2.1: Encapsulation components

Encapsulated particles are generally made up of two parts: The material inside the microcapsule is known as the core, internal phase, or fill beside the covering material is sometimes called shell, coating, or membrane (Fig. 1). The active components to be coated, known as core materials, can exist in a variety of physical states, including liquid, solid, and gas.
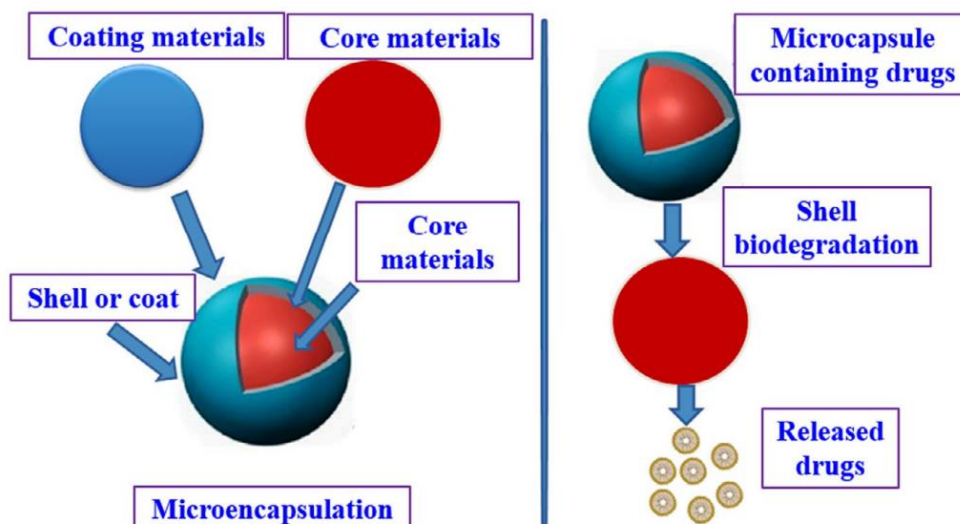
Fig. 1: Scheme showing components, microencapsulation and drug release processes [12].

2.1.1: Core materials

The core material, which is the particular substance that will be coated, might be either liquid or solid. Due to the liquid core's ability to include dispersed and/or dissolved components, the composition of the core material might vary. The active ingredients, stabilizers, diluents, excipients, and release-rate retardants or accelerators make up the solid core. The capacity to change the composition of the core material offers clear flexibility, and making use of these qualities frequently enables successful design and development of the required microcapsule features [13].

2.1.2: Coating materials (Shell)

The choice of coating material significantly impacts microcapsules/microspheres. The selected polymer must meet various product requirements, including stabilization, reduced volatility, and suitable release characteristics while considering environmental conditions. It should form a cohesive, chemically compatible, non-reactive film with the core material, offering essential coating properties like strength, flexibility, impermeability, optical characteristics, and stability.

In microencapsulation, hydrophilic, hydrophobic, or hybrid polymers are commonly used, such as gelatin, polyvinyl alcohol, ethyl cellulose, cellulose acetate phthalate, and styrene-maleic anhydride. The film thickness varies based on material surface area and system characteristics [14].

Microcapsules may exist as single particles or clusters after isolation and drying, appearing as a free-flowing powder suitable for various dosage forms, including compressed tablets, hard gelatin capsules, suspensions, and more. As examples of coating materials:

➢ *Water soluble resins***:** Gelatin, Gum Arabic, Starch, Polyvinylpyrrolidone, Carboxymethylcellulose, Hydroxyethylcellulose, Methylcellulose, Arabinogalactan, Polyvinyl alcohol, Polyacrylic acid.

➢ **Water insoluble resins:** Ethylcellulose, Polyethylene, Polymethacrylate, Polyamide (Nylon), Poly (Ethylene Vinyl acetate), cellulose nitrate, Silicones, Polylactide-coglycolide.

➢ **Waxes and lipids:** Paraffin, Carnauba, Spermaceti, Beeswax, Stearic acid, Stearyl alcohol, Glyceryl stearates.

➢ **Enteric resins:** Shellac, Cellulose acetate phthalate, Zein.

Microcapsules exhibit different morphologies depending on the core material and shell deposition process. They are broadly classified into two groups: matrix and vesicular systems. Matrix systems evenly disperse the core material within the shell, while vesicular systems encase the core within a polymer membrane, forming capsules **[15,16]**. Fig. 2 illustrates how these morphologies can be further defined in terms of composition, coating materials, and manufacturing processes:
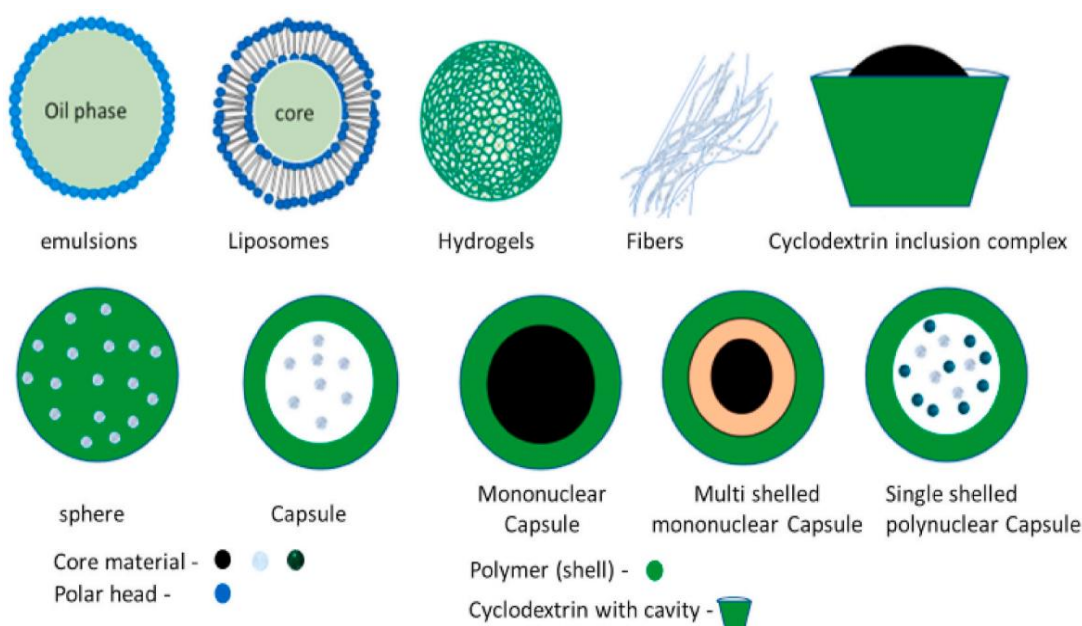
Fig. 2: Illustration of different types of encapsulated particles.

1. Mononuclear (core-shell) microcapsules have a single core surrounded by a shell. The active agents form a core surrounded by an inert barrier in reservoir type. It is sometimes referred to as a single-core mono-core or core-shell type.

2. Polynuclear capsules contain multiple cores within a single shell.

3. Matrix encapsulation achieves homogeneous dispersion of the core material within the shell. The active substance is dispersed or dissolved in a matrix of an inert polymer.

Microcapsules can also exhibit variations such as being mononuclear with multiple shells or forming clusters (Fig. 2) [17].

3: Goals of encapsulation

Microencapsulation guarantees that the encapsulated substance reaches the region of action without being harmed by the environment it passes through. It has also several key purposes, including masking taste and smell, enhancing solubility, protecting from oxidation, reducing irritation, enabling controlled release, delivering targeted release, controlling particle size, enhancing bioavailability, and improving patient compliance. [18]

4: Techniques for the preparation of microcapsules

4.1: Spray drying and spray congealing method

Spray drying stands out as a widely adopted advanced technique for microencapsulation due to its cost-effectiveness, easy availability of equipment, reproducibility, rapidity, and scalability. The procedures of spray drying and spray congealing both involve the drying of polymer and drug droplets in an airborne environment. The procedure is referred to as spray drying or spray congealing depending on whether the solvent is removed or the solution is cooled [19]. In this method (Fig. 3), a polymer is dissolved within a volatile organic solvent, such as acetone or dichloromethane. The solid medication is then homogenized at high speeds within this polymer solution. The resulting dispersion is atomized within a stream of hot air. This atomization leads to the creation of tiny droplets suspended in a fine mist. Rapid evaporation of the solvent from these droplets occurs, yielding microspheres with diameters ranging from 1 to 100 μm. Subsequently, a cyclone separator segregates microparticles from the heated air, and vacuum drying eliminates any residual solvent. Commonly, natural water-soluble polymers like starch, gum arabic, chitosan, Magellan, and sodium alginate are employed as materials for forming the encapsulating walls [20]. A significant advantage of this technique is its suitability for aseptic conditions, as illustrated in Fig. 3 [21].
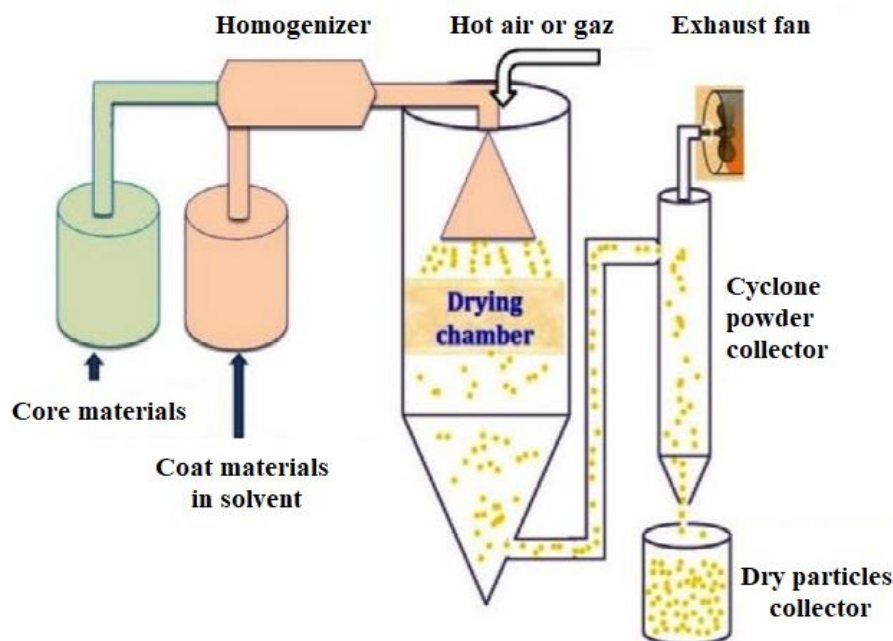
Fig. 3: Scheme showing micro particulate preparation using the spray drying technique [21].

4.2: Air-suspension method

Professor Dale Eric Wurster invented the air-suspension approach [22]. Air-suspension technique entails dispersing core ingredients in a supporting airflow and spraying coating materials onto suspended particles. Particles are suspended on the upwardly flowing air stream in the coating chamber. Because of the chamber's architecture and operating mechanism, the flow of particles recirculated through the coating zone. The core materials get coating materials throughout each cycle through the coating area. According to the goal of microencapsulation, this step is repeated many hundred times during the operation (Fig. 4). The airstream is drying the enclosed goods [19]. For example, the Wurster Process serves to create diclofenac microcapsules [23].
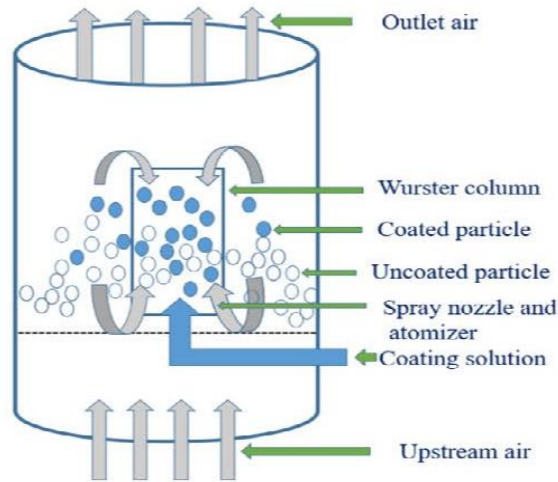
Fig. 4: Air-suspension/Wurster technique for the microcapsule's preparation [19].

a.   **Coacervation method**

Coacervation also known as phase separation, represents an innovative and potentially valuable microencapsulation approach capable of accommodating substantial payloads [24]. In general, this technique is for making microcapsules from various polymers. There are two types: simple and complex. Simple coacervation uses a single polymer, while complex coacervation involves two electrical oppositely charged polymers. Coacervation occurs through the gradual desolvation of polymer molecules. To create microcapsules, a solution is made with a core material and a stabilizer, and then a coacervation agent is added to form partially de-solvated polymer molecules. The mixture is cooled and a cross-linking agent is added to harden the microcapsule wall **[24,25]**. And as whole, the mainly complex coacervation process consists of three steps which are summarized as it follows:

-    Formation of an oil-in-water emulsion;
-    Formation of the coating;
-    Stabilization of the coating. Complex coacervation involves two opposite charges of hydrophilic polymers (Fig. 5). It involves interactions between the two polymers.

Vanessa et al. [26]; created small balls called chitosan microspheres using a method called simple coacervation and then made them stronger using either epichlorohydrin or glutaraldehyde. She did this to control the way diclofenac sodium was released from the microspheres. Vanessa studied how the microspheres reacted over 12 hours by looking at their swelling, hydrolysis, porosity, and cross-linking. She also tested how well the microspheres

held diclofenac sodium and how it was released when the microspheres were in liquids that mimic the gastrointestinal tract. Vanessa did this by testing the microspheres in liquids with a pH of 1.2, 6.8, and 9.0. The results showed that the way the diclofenac sodium was released was slightly different from Fickian transport [26].
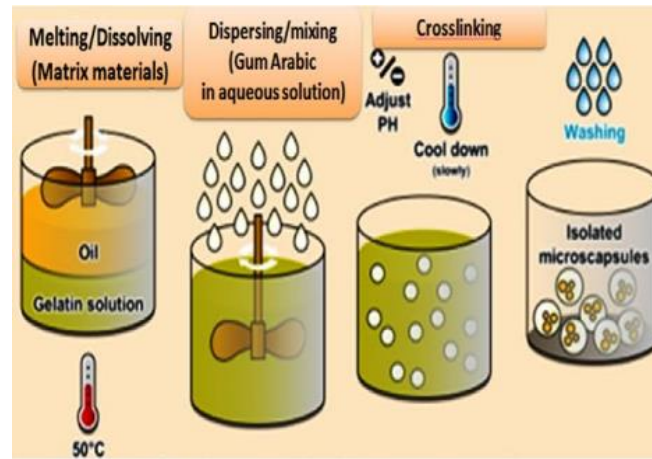
Fig. 5: Scheme showing the steps of the coacervation process [27].

4.3 : Centrifugal extrusion method

Centrifugal extrusion is a type of extrusion technique that consists of concentric feed tubes through which the coat and core materials are fed individually to numerous nozzles. These nozzles are mounted on the equipment's outside surface. The coating material flows through the outer tube as the core material flows through the center tube (Fig. 6). This technique safeguards fragile ingredients, making it suitable for applications like flavor, color, and vitamin protection in beverage mixing, cake preparation, and gelatin dessert and cocktail mixing [28].
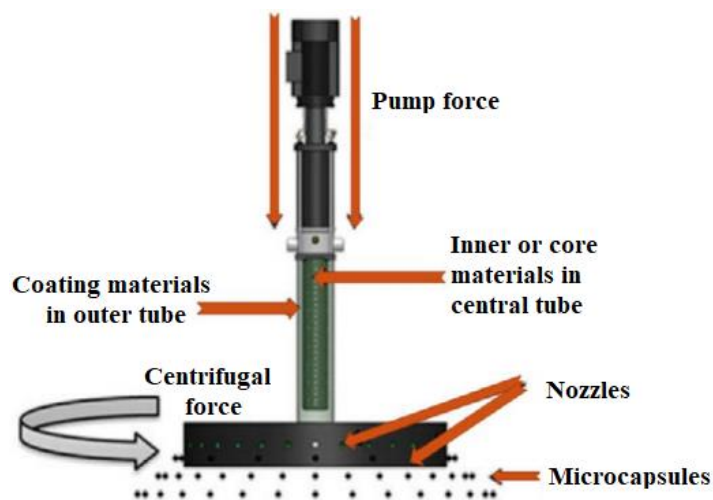
Fig. 6: Microencapsulation by centrifugal extrusion method [28].

Varshosaz et al. [29]; employed the powder-layering technique to create piroxicam enteric-coated pellets, using inert seeds coated with micronized piroxicam and hydroxypropyl methylcellulose. Coating with polymers such as EUDRAGIT L30D-55 and plasticizer triethyl citrate led to effective enteric-coated pellets [29].

4.4 : The pan-coating method

The pan-coating method is an old but widely used production technique in the pharmaceutical industry for manufacturing small particles. The particle is placed in a pan, and the coating substance is gradually added. The outer layer material is applied to the solid component in the coating tray as a solution or atomized spray. Once the coating is applied to the disk, hot air is typically utilized to eliminate the coating solvent as shown in Fig. 7 [30].
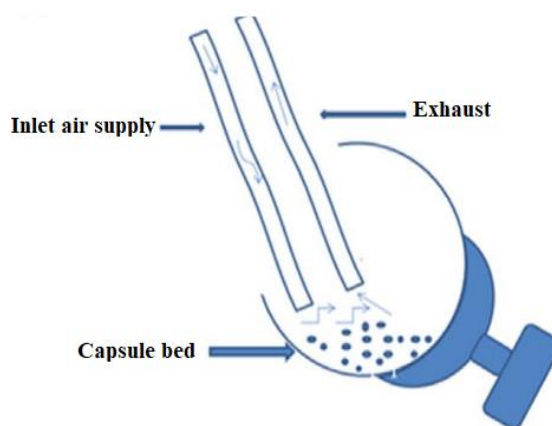
Fig. 7: Illustration of the pan coating method [30].

4.5 : Single emulsion method

According to Giri et al.[31]; the single emulsification approach is a widely used method for producing microparticles. It is effective for encapsulating hydrophobic pharmaceuticals but not hydrophilic medications. This approach involves mimicking oil in water (o/w) to coat hydrophobic medicines. Natural polymer microparticulate carriers are created by dissolving or dispersing natural polymers in an aqueous medium and then a nonaqueous medium such as oil. The dispersed globules are cross-linked using heat or chemical cross-linkers such as glutaraldehyde, formaldehyde, and diacid chloride. The cross-linking process produces distinct particles which are then centrifuged, washed, and separated as presented in (Fig. 8) [31]. The use of dichloromethane (DCM) as a solvent, for example, typically results in microparticles with a greater size distribution. This combination is emulsified in huge amounts of water with

emulsifiers. The solvent of the emulsion is removed from compact microparticles by evaporation at high temperatures or great amounts of water extraction **[32,33]**.
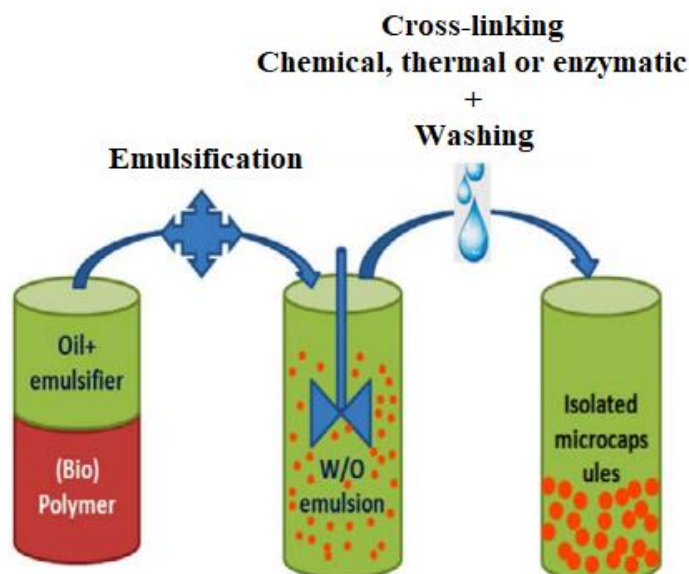
Fig. 8: Design of microencapsulation by single emulsion technique [34].

4.6 : Double emulsion method

The double emulsion approach may be used to encapsulate both hydrophobic and hydrophilic medicines. According to Iqbal et al. [35], this approach may encapsulate a variety of hydrophilic and hydrophobic antibiotic medicines, anticancer treatments, anti-inflammatory pharmaceuticals, proteins, and amino acids. Frequently, the production of double or multiple emulsions of water and oil is required for the production of microspheres. This approach applies to both natural and manmade polymers. The drug, usually present in a dispersed aqueous phase, is encapsulated within the continuous phase of the polymer solution. An essential step involves homogenizing or sonication of the initial emulsion before its introduction to the aqueous solution, yielding a double emulsion. Crucially, the solvent must be effectively removed through either solvent evaporation or solvent extraction to finalize the process [36] as shown in (Fig. 9) [30]**.** In 2014, flurbiprofen microcapsules were prepared using solvent evaporation with co-polymer coatings of Eudragit RS 100 and HPMC, as described by Sohail et al. [37].
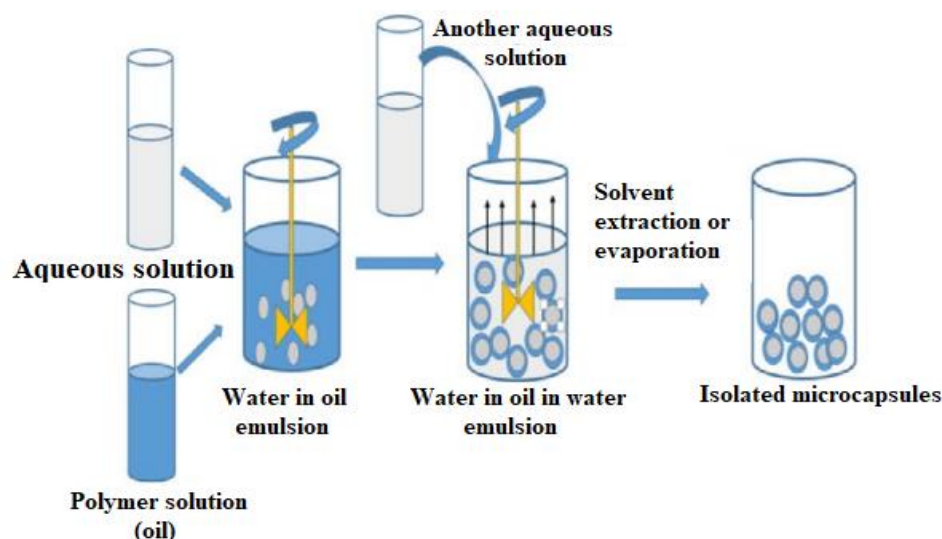
Fig. 9: Strategy of microencapsulation by double emulsion method [30].

4.7: Supercritical fluid micronization techniques

The utilization of supercritical fluid (SCF) micronization technology gained prominence within the pharmaceutical sector industrialization during the early 1970s. Concurrently, SCF-based precipitation and crystallization processes were introduced for advancing pharmaceutical material development. The application of supercritical fluid micronization technology is driven by its multifaceted benefits. Among the frequently employed supercritical fluids, CO_2, alkyl compounds (ranging from C2 to C4), and nitrous oxide (N_2O) stand out. Notably, slight alterations in pressure or temperature exert substantial influence on supercritical fluid density, particularly in proximity to critical points. According to Agnihotri et al.[18]; research; from the various supercritical fluids, CO_2 holds preeminence due to its widespread availability, cost-effectiveness, and exceptional purity. Diverse coating materials, soluble in supercritical CO_2 (such as paraffin, polyethylene glycol, acrylates, etc.), as well as insoluble counterparts (polysaccharides, proteins, etc…), find utility for encapsulation purposes [18]. Noteworthy methodologies within the purview of SCF technology encompass a spectrum of techniques elucidated below.

4.7.1: Rapid expansion of supercritical solution

Supercritical fluids containing active chemicals and coating components stay at high pressure during this procedure and are suspended at atmospheric pressure via a tiny nozzle. The quick reduction in pressure destroys the coating material, which is then deposited on the active ingredient surface and forms a coating layer like in (Fig. 10) [18].
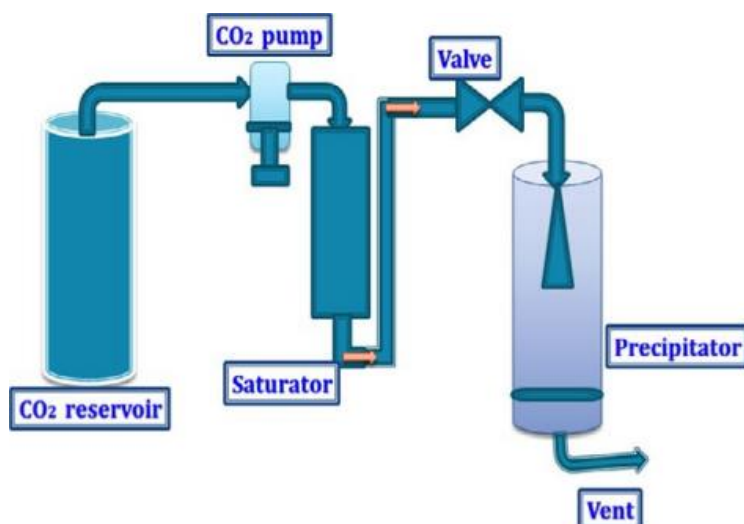
Fig. 10: Design of supercritical fluid micronization techniques [38].

4.7.2: Gas anti-solvent technique

This method is sometimes referred to as supercritical fluid anti-solvent. Supercritical fluids are introduced into a solution of active and shell materials and kept at high pressure. This causes the volume of the solution to expand, resulting in supersaturation and precipitation of the solute. Because water is less soluble in supercritical liquids, this method is ineffective for encapsulating water-soluble compounds [18].

4.7.3: Particles from gas-saturated solution

This process encompasses the blending of core and coating materials within a controlled, high-pressure supercritical fluid milieu. Within this operational schema, the supercritical fluid infiltrates the coating material, inducing pronounced swelling. Upon subjecting the mixture to temperatures surpassing the material's glass transition temperature, the polymer undergoes a transition into a liquefied state. Upon subsequent depressurization, the coating material precipitates onto the core ingredient, thus achieving encapsulation in a defined manner [18].

The distinct characteristics of supercritical fluids micronization technology lie in its exceptional security, ecological compatibility, and economic feasibility. The deliberate adjustment of operational parameters, especially pressure and temperature, amplifies the appeal of supercritical fluid technology in the domain of pharmaceutical research. This methodology has garnered substantial recognition in laboratory settings, enabling the creation of nanoparticles, microparticles, and liposomes for precise drug encapsulation. Additionally, it facilitates the generation of microporous foams, solid dispersants, inclusion complexes, and

macromolecular powders. Consequently, these techniques exhibit considerable potential as pivotal components in the commercialization of various water-insoluble drugs through their solid dispersive formulations **[18,39]**.

4.8 : Solvent evaporation method

This method is commonly utilized for microencapsulation in the pharmaceutical industry. This technology can be utilized to create a controlled-release medication with several therapeutic benefits. Encapsulation is accomplished using insoluble polymers in this process. The biodegradable polymer PLGA is frequently employed as an encapsulating material (Fig. 11). Hydrophobic medications or therapeutic substances such as cisplatin, naltrexone, progesterone, lidocaine, insulin, peptides, proteins, and vaccines have all been successfully encapsulated [39].
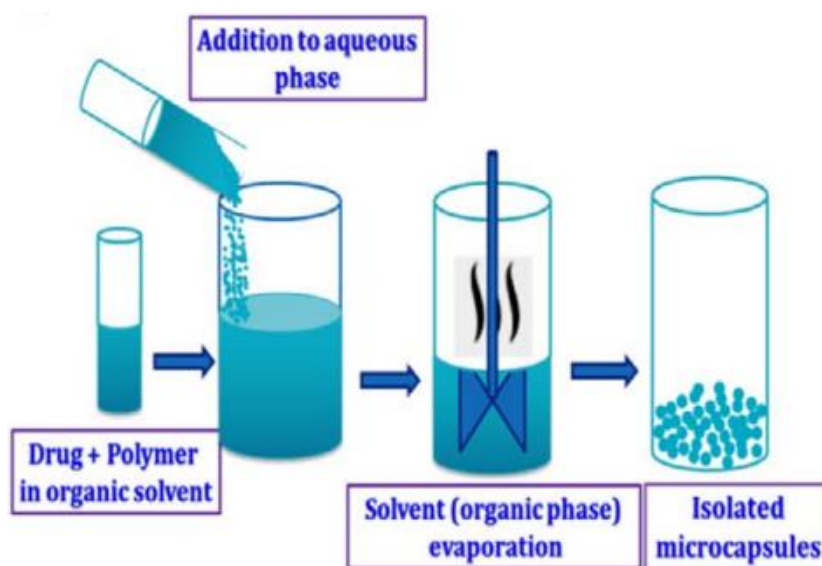
Fig. 11: Scheme showing the steps in the solvent evaporation method.

4.9 : Polymerization

4.9.1: Matrix polymerization

During matrix polymerization, the core components are integrated into the polymer matrix during particle formation. Spray-drying is one example, in which particles are formed by the evaporation of the solvent from the matrix. Chemical alteration, on the other hand, can be employed to stiffen the matrix [33].

4.9.2: Interfacial polymerization

The polycondensation or interfacial of two complimentary monomers at the interface of a two-phase system is used in this technique. An emulsion is formed from the two phases. Each

phase includes a reacting monomer. Thus, one of the reacting monomers is dissolved in the oil phase; the other reacting monomer is dissolved in the aqueous phase. In this process, the oil phase is emulsified in the aqueous phase using constant agitation. During the emulsification process, the polymer is formed at the interface, and this polymer forms a film around the encapsulated active compound. Depending on the solubility of the active compound, it can be placed in either the aqueous phase or the oil phase of the emulsion (Fig. 12) [40]. Usually in the creation of microcapsules a diverse array of polymers was used, including polyamides, polyureas, polyurethanes, and polyesters. The diffusion of reagents between the reaction interface is a critical feature of microencapsulation by interfacial Polymerization. This method may encapsulate a broad variety of core materials, including solid particles, resolutions, and water-insoluble liquids. Because of its average size and membrane thickness, as well as the benefits of permeability, flexibility, stability, and mechanical and chemical properties of the membrane, this method has been used successfully in self-healing and pharmaceutics. Isophorone diisocyanate was encapsulated utilizing polyvinyl alcohol as an emulsifier in an oil-in-water emulsion **[41,42]**.

4.9.3: In situ polymerization

Capsule shell formation, akin to interfacial polymerization, is initiated by introducing polymerization monomers into the encapsulation reactor. Importantly, no reactive agents are applied to the core material during this process. Polymerization transpires when an interface emerges between the dispersed core material and the continuous phase. Initially, a low-molecular-weight prepolymer is generated; however, over time, this prepolymer expands, resulting in material deposition on the dispersed core surface, culminating in a solid capsule shell. The capsule shell formation entails the dispersion of a water-immiscible liquid and polymer in an aqueous medium under acidic pH conditions utilizing urea and formaldehyde.

Broadly speaking, in situ polymerization constitutes a chemical encapsulation methodology reminiscent of interfacial polymerization. However, a crucial distinction arises: in the context of in situ polymerization, the core components remain inert to reactions. Instead, all transformations transpire within a continuous phase, with no differentiation between the two sides of the interface that links the prevailing phase and the internal content. The notable applications of this approach include generating protein nanogels, as demonstrated by Thomas and Maria. Its significance traverses' diverse domains, encompassing cancer therapy, diagnostics, vaccination, regenerative medicine, and genetic disorder treatment, as emphasized by Ye et al. **[41,43]**.
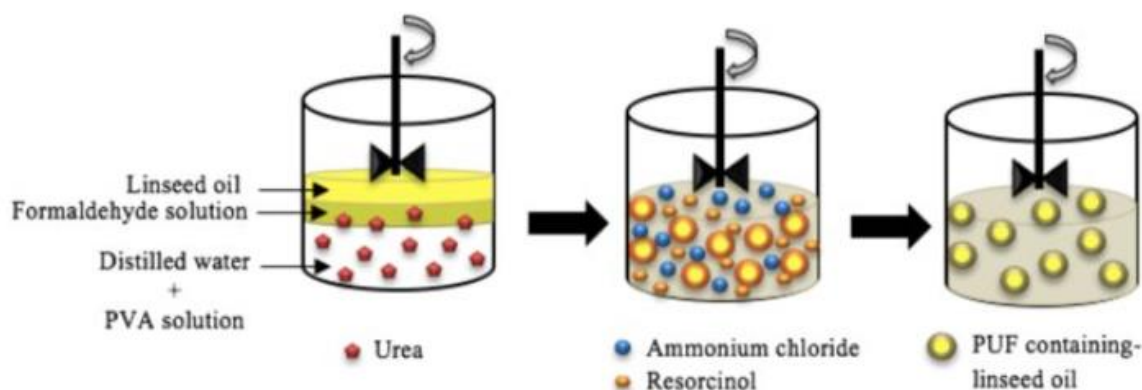
Fig. 12. Schematic illustration of preparation of microcapsules by in-situ polymerization.

5: Applications of microcapsules in biological sciences

On a micrometric scale, micro-encapsulations are tiny containers that successfully combine functional/bioactive compounds like food components, enzymes, cells, and other elements. It is used in veterinary medicine, pharmaceuticals, textiles, chemicals, waste treatment, cosmetics, adhesives, biomedicines, aerospace, food, agriculture, and other fields. Besides microparticles are frequently used to assist with the integration of oily drugs into tablet forms, avoid incompatibility, reduce the odor of active substances, and protect important molecules from oxidation or reactivity. Vitamins, UV filters, moisturizers, and fragrances for example, can be kept in microspheres according to Patravale and Mandawgade [44].

Notably, medications such as insulin, growth hormone, and erythropoietin can benefit tremendously from microencapsulation due to the regulated release it provides, as demonstrated by Orive et al. [45].

Encapsulating vitamins, A and K, for example, protects them against moisture and oxygen. Encapsulated volatile substances can be stored for extended periods without evaporation. In the food industry, some compounds, such as nutrients, are encapsulated to mask their taste and flavor. Fumigants, pesticides, herbicides, and insecticides can all be made less harmful by microencapsulation. The gastrointestinal irritation and hygroscopic properties of several core materials are decreased **[46,47]**.

6: Advantages and challenges of encapsulation techniques

In table 1are gathered some advantages and challenges of encapsulation techniques.

Table 1. Advantages and challenges of encapsulation techniques.

Encapsulation techniques	Advantages	Challenges	Reference
Physical methods			
Coacervation	a) Controllable to produce homogeneously sized particles. b) Compatible method to encapsulateheat-sensitive materials c) High loading capacity d) Specific equipment not required	a) Limited use in certain pH conditions b) Limited to scale up agglomerated particles c) Solvent residue d) High cost of the particle isolation process	[48]
Solvent evaporation	a) Simple technique b) Compatible to encapsulate hydrophilic and lipophilic core materials c) Low-temperature requirement to evaporate the organic solvent	a) Difficulty in removing residual solvent b) High cost	[49]
Sol-gel method	a) Economical method b) Precise microstructural and chemical control c) It can be done at a low temperature	a) Particle agglomeration b) Poor physical, chemical, and mechanical properties	[50]
Liposomal encapsulation	a) Compatible method to encapsulate lipophilic, water soluble, and amphiphilic materials b) Suitable for water activity applications c) Provides highly efficient controlled delivery of bioactive compounds	a) High cost b) Poor physical and chemical stability c) Wide range of particle size distribution d) Complex post-treatment method required to prevent lipid oxidation	[48]
Chemical methods ***Polymerization methods***			
In situ polymerization	a) Suitable for nanoscale production b) Homogenous coating c) Uniform morphological capsule formation d) Good thermal and chemical stability of products	a) Low mechanical stability of products b) High-cost equipment c) High skill requirement for preparation	[49]
Interfacial polymerization	Homogeneous size particle formation Chemically and physically stable products.	Difficulty in control.	[49]
Emulsion polymerization	Low-cost production method, Easy to control.	High technological requirements	[49]
Suspension polymerization	a) High porous material formation b) Controllable particle morphology	a) Both aqueous and organic phases are required for the reaction	**[49]**

	b) Surfactant and stabilizer required. c) The monomer and the initiators are hydrophobic nature.		

Molecular inclusion techniques

Blending	a) Easy application b) High efficiency	a) Low yield	[48]
Kneading	c) Easy application d) High efficiency	a) Low yield	[51]
Coprecipitation and neutralization	a) Simple method b) High efficiency c) Compatible with hydrophobic materials	a) Wastewater production. b) Lab scale production method.	[51]
Solvent evaporation	a) Simple method b) Compatible for thermolabile materials	a) High-cost method b) Issues related to residual solvent	[51]
Milling	a) Economical and time-saving method	a) Industrial application, mechanical equipment required	[51]
Spray drying	a) Large volume production b) Easy and commonly used for industrial application c) Fast drying	a) Restricted use of water-soluble carrier matrix material b) Special equipment required c) Expensive method	[51]
Freeze drying	a) Long shelf-life products b) High structure stability	a) Not compatible for temperature sensitive materials b) High cost	[51]
Supercritical antisolvent system	a) Low reaction temperature b) Easy to separate the final product and supercritical solvent	a) High-cost method b) Highly sophisticated equipment requirement	[51]
Micelle encapsulation	a) Biocompatible b) An easy method of preparation. c) Chemical and physical properties modification is easy	a) Highly unstable b) Low loading capacity c) Must be made fresh and cannot be stored d) Compatible for lipophilic materials e) Dependency of critical micellar concentration	[51]
Air suspension	a) Low cost b) High production volume	a) Practical skills are required. b) Agglomeration of final products	[52]
Spray drying	a) Versatile method b) Sophisticated equipment is required. c) Easy to scale up the process.	a) Agglomeration of particles b) Chances of partially coated particles with final products. c) High-temperature requirement	[52]

7: Release mechanisms of microcapsules

In the case of microspheres, the release of the active ingredient is critical. The release efficiency of microspheres is determined by the type of polymer employed in the formulation as well as the active medication. The structure or micromorphology of the carrier, as well as the characteristics of the polymer itself, impact drug release from both biodegradable and non-biodegradable microspheres [53].Several mechanisms of drug release from microcapsules include: dissolution, diffusion, rupture, osmosis, and erosion (Fig. 13).

7.1 : Dissolution

One significant method of releasing drugs from microcapsules is dissolution. This process involves dissolving the coat when the soluble layer is dissolved in a non-toxic solvent or water at an optimal temperature. As a result, the active ingredient is gradually released from the inside of the capsule to the outside. The rate of dissolution of the polymer shell determines the speed at which the medicine is released from the capsule in solvents, according to Korsmeyer et al. [54]. The thickness of the wall and the dissolution capacity of the coating material in solvents, as stated by Costa & Lobo, also influence the drug release rate [55].

7.2 Diffusion

Throughout this process, the encapsulated materials are gradually released by diffusion through the polymer (reservoir system) or the pores existing in the polymer (matrix systems). into the environment at varying concentrations between the microcapsule and the surrounding environment. As the microcapsule shell dissolves, the core material is liberated, potentially transitioning into a different state depending on its properties, and subsequently traverses through the porous structure of the microcapsule wall [54]. The rate of release is influenced by factors including the core material's penetration rate through the microcapsule wall, its solubility, potential leakage, and surface diffusion [56]. The kinetics of drug or enzyme release can often be described using Higuchi's formulation: $Q = k * \sqrt{t}$, where:

- Q represents the quantity of released substance,
- k is the release rate constant,
- t is time.

7.3 Rupture

When pressure or cracks occur, the core material is released through a process of rupturing. This process is influenced by external forces and extreme conditions. The cover may crack due to various factors, such as pressure, carbon-free copy paper, or scratches [53]. Microcapsule

size is an important factor in releasing the active ingredients through rupture [57]. Several authors have noted that it becomes more challenging to rupture microcapsule coatings as the size of the microcapsule is reduced [58].

7.4 Osmosis

When water is allowed to enter under the correct conditions, osmotic pressure can build up within the particle's interior. As water diffuses into the core through the biodegradable or non-biodegradable coating, sufficient pressure is created to break the membrane, forcing the drug out of the particle. Three elements primarily influence the burst effect:

- ✓ The macromolecule/polymer ratio,
- ✓ The particle size of the dispersed macromolecule,
- ✓ The particle size of the microspheres.
- ✓ The shape of the carrier can help us understand drug release from non-biodegradable polymers.

The overall release profile of a drug or its active ingredients is determined by the geometry of the carrier. This includes whether it is a reservoir type, with the drug present as a core, or a matrix type, with the drug dispersed throughout the carrier [59].

7.5 Erosion

Several coatings can be created to slowly dissolve over time, releasing the medicine contained within the particle. Polymer erosion occurs when the polymer is lost and the monomer accumulates in the release media. The erosion of the polymer begins with changes in the microstructure of the carrier caused by water penetration, which leads to matrix plasticization [60].
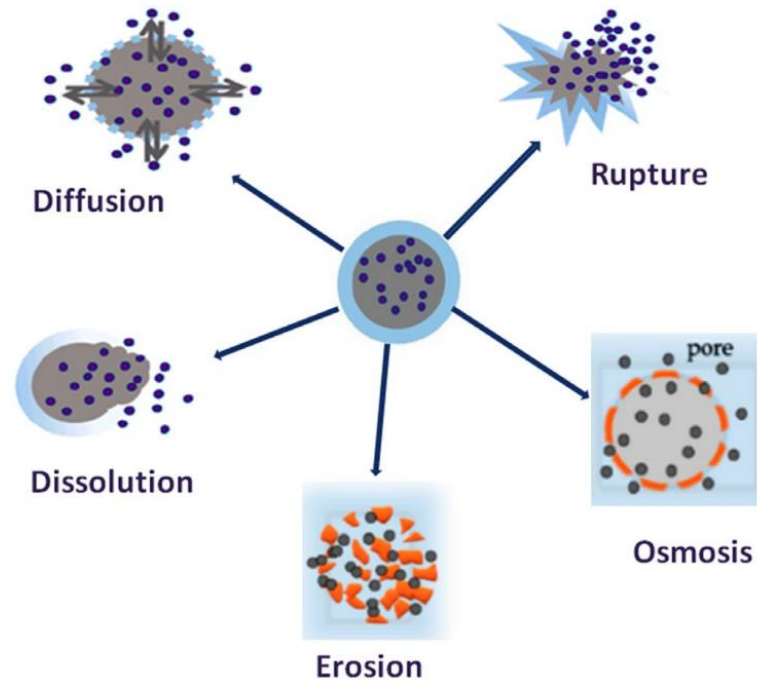
Fig. 13: Scheme describing different drug-release mechanisms from microcapsules [53].

References

[1]   M.K. Thenmozhi, S. Anees Rizwana, M. Vaishnavi, Development of a novel drug delivery system to treat inflammatory bowel disease, IJAPR 5 (2014) 104–114.

[2]   T. Mounika, D.V. Kumar, A REVIEW ON NANOSPHERES, (n.d.).

[3]   N.V.N. Jyothi, P.M. Prasanna, S.N. Sakarkar, K.S. Prabha, P.S. Ramaiah, G.Y. Srawan, Microencapsulation techniques, factors influencing encapsulation efficiency, J. Microencapsul. 27 (2010) 187–197. https://doi.org/10.3109/02652040903131301.

[4]   MICROENCAPSULATIONAREVIEW (1).pdf, (n.d.).

[5]   S. Akhlaghi, M. Ebrahimnia, D.S. Niaki, M. Solhi, S. Rabbani, A. Haeri, Recent advances in the preventative strategies for postoperative adhesions using biomaterial-based membranes and micro/nano-drug delivery systems, J. Drug Deliv. Sci. Technol. 85 (2023) 104539. https://doi.org/10.1016/j.jddst.2023.104539.

[6]   J.C. Matos, L.C.J. Pereira, J.C. Waerenborgh, M.C. Gonçalves, 4 - Encapsulation of active molecules in pharmaceutical sector: the role of ceramic nanocarriers, in: S.H. Sonawane, B.A. Bhanvase, M. Sivakumar (Eds.), Encapsulation Act. Mol. Their Deliv. Syst., Elsevier, 2020: pp. 53–83. https://doi.org/10.1016/B978-0-12-819363-1.00004-1.

[7]   F. Paulo, L. Santos, Design of experiments for microencapsulation applications: A review, Mater. Sci. Eng. C 77 (2017) 1327–1340. https://doi.org/10.1016/j.msec.2017.03.219.

[8]   O. Adeyi, E.O. Oke, A.J. Adeyi, B.I. Okolo, A.O. Olalere, J.A. Otolorin, O.S. Aremu, T. Qwebani-Ogunleye, Microencapsulated anthocyanins powder production from Hibiscus sabdariffa L. calyx: Process synthesis and economic analysis, Results Eng. 13 (2022) 100371. https://doi.org/10.1016/j.rineng.2022.100371.

[9]   J.-F. Su, X.-Y. Wang, S. Han, X.-L. Zhang, Y.-D. Guo, Y.-Y. Wang, Y.-Q. Tan, N.-X. Han, W. Li, Preparation and physicochemical properties of microcapsules containing phase-change material with graphene/organic hybrid structure shells, J. Mater. Chem. A 5 (2017) 23937–23951. https://doi.org/10.1039/C7TA06980D.

[10] Y.-T. Huang, H. Zhang, X.-J. Wan, D.-Z. Chen, X.-F. Chen, X. Ye, X. Ouyang, S.-Y. Qin, H.-X. Wen, J.-N. Tang, Carbon nanotube-enhanced double-walled phase-change microcapsules for thermal energy storage, J. Mater. Chem. A 5 (2017) 7482–7493. https://doi.org/10.1039/C6TA09712J.

[11] F. Ahangaran, M. Hayaty, A.H. Navarchian, F. Picchioni, Micromechanical assessment of PMMA microcapsules containing epoxy and mercaptan as self-healing agents, Polym. Test. 64 (2017) 330–336. https://doi.org/10.1016/j.polymertesting.2017.10.014.

[12] H. Peng, D. Zhang, X. Ling, Y. Li, Y. Wang, Q. Yu, X. She, Y. Li, Y. Ding, N-alkanes phase change materials and their microencapsulation for thermal energy storage:: A critical review, Energy Fuels (2018). https://doi.org/10.1021/acs.energyfuels.8b01347.

[13] Y.W. Chien, M. Nair, Mucosal adhesive device for long-acting delivery of pharmaceutical combinations in oral cavity, US5578315A, 1996.

[14] S. Mantry, A novel approach on microencapsulation in drug delivery system for cancer diagnosis, (2017).

[15] P.N. Ezhilarasi, P. Karthik, N. Chhanwal, C. Anandharamakrishnan, Nanoencapsulation Techniques for Food Bioactive Components: A Review, Food Bioprocess Technol. 6 (2013) 628–647. https://doi.org/10.1007/s11947-012-0944-0.

[16] V. Suganya, V. Anuradha, Microencapsulation and Nanoencapsulation: A Review, Int. J. Pharm. Clin. Res. 9 (2017). https://doi.org/10.25258/ijpcr.v9i3.8324.

[17] R. Singh, R. Bhateria, Core-shell nanostructures: a simplest two-component system with enhanced properties and multiple applications, Environ. Geochem. Health 43 (2021) 2459–2482. https://doi.org/10.1007/s10653-020-00766-1.

[18] N. Agnihotri, R. Mishra, C. Goda, M. Arora, Microencapsulation – A Novel Approach in Drug Delivery: A Review, Indo Glob. J Pharm Sci 2 (2012) 1–20. https://doi.org/10.35652/IGJPS.2012.01

[19] Dr.M. K.M, B. Shivakumar, P. Kumar, Microencapsulation: An Acclaimed Novel Drug-Delivery System for NSAIDs in Arthritis, Crit. Rev. Ther. Drug Carrier Syst. 27 (2010) 509–45. https://doi.org/10.1615/CritRevTherDrugCarrierSyst.v27.i6.20.

[20] Encyclopedia of Controlled Drug Delivery, 2 Volume Set | Wiley, Wiley.Com (n.d.).

[21] F. Casanova, L. Santos, Encapsulation of cosmetic active ingredients for topical application – a review, J. Microencapsul. 33 (2016) 1–17. https://doi.org/10.3109/02652048.2015.1115900.

[22] T.M. Hinkes, ENCAPSULATION OF SMALL PARTICLES, (n.d.).

[23] M.C. Adeyeye, E. Mwangi, B. Katondo, A. Jain, H. Ichikawa, Y. Fukumori, Dissolution stability studies of suspensions of prolonged-release diclofenac microcapsules prepared by the Wurster process: I. Eudragit-based formulation and possible drug-excipient interaction, J. Microencapsul. 22 (2005) 333–342. https://doi.org/10.1080/02652040500100600.

[24] F. Yang, J. Kang, F. Yang, Z. Zhao, T. Kong, Z. Zeng, Preparation and evaluation of enrofloxacin microspheres and tissue distribution in rats, J. Vet. Sci. 16 (2015) 157–164.

[25] D.J. Burgess, J.E. Carless, Manufacture of gelatin/gelatin coacervate microcapsules, Int. J. Pharm. 27 (1985) 61–70.

[26] V.L. Gonçalves, M. Laranjeira, V.T. Fávere, R.C. Pedrosa, Effect of crosslinking agents on chitosan microspheres in controlled release of diclofenac sodium, Polímeros 15 (2005) 6–12.

[27] J. Swarbrick, Encyclopedia of Pharmaceutical Technology, pdf, (n.d.).

[28] A.M. Bakry, S. Abbas, B. Ali, H. Majeed, M.Y. Abouelwafa, A. Mousa, L. Liang, Microencapsulation of Oils: A Comprehensive Review of Benefits, Techniques, and Applications, Compr. Rev. Food Sci. Food Saf. 15 (2016) 143–182. https://doi.org/10.1111/1541-4337.12179.

[29] J. Varshosaz, N. Tavakoli, A. Serri, Preparation and *in vitro* characterization of piroxicam enteric coated pellets using powder layering technique, Pharm. Dev. Technol. 14 (2009) 305–311. https://doi.org/10.1080/10837450802626288.

[30] S.U. Ahmad, B. Li, J. Sun, S. Arbab, Z. Dong, F. Cheng, X. Zhou, S. Mahfuz, J. Zhang, Recent advances in microencapsulation of drugs for veterinary applications, J. Vet. Pharmacol. Ther. 44 (2021) 298–312. https://doi.org/10.1111/jvp.12946.

[31] T.K. Giri, C. Choudhary, A. Alexander, H. Badwaik, D.K. Tripathi, Prospects of pharmaceuticals and biopharmaceuticals loaded microparticles prepared by double emulsion technique for controlled delivery, Saudi Pharm. J. 21 (2013) 125–141.

[32] J. Y, Studies on MEP421 PLGA Microspheres : Preparation and Drug Release, Asian J Pharma Sci 3 (2008) 211–216.

[33] A. Jain, A Review on Various Techniques of Microencapsulation, (2019).

[34] R. Arshady, Microspheres and microcapsules: A survey of manufacturing techniques. Part 1: Suspension cross-linking, Polym. Eng. Sci. 29 (1989) 1746–1758. https://doi.org/10.1002/pen.760292404.

[35] M. Iqbal, N. Zafar, H. Fessi, A. Elaissari, Double emulsion solvent evaporation techniques used for drug encapsulation, Int. J. Pharm. 496 (2015) 173–190. https://doi.org/10.1016/j.ijpharm.2015.10.057.

[36]   F. Pavanetto, P. Perugini, B. Conti, T. Modena, I. Genta, Evaluation of process parameters involved in chitosan microsphere preparation by the o/w/o multiple emulsion method, J. Microencapsul. 13 (1996) 679–688. https://doi.org/10.3109/02652049609026051.

[37]   M.F. Sohail, P.A. Shah, I. Tariq, S. Saeed-ul-Hassan, U. Amin, S.A. Raza, T. Saeed, M. Sultana, N.H. Jawa, Development and In vitro Evaluation of Flurbiprofen Microcapsules Prepared by Modified Solvent Evaporation Technique, Trop. J. Pharm. Res. 13 (2014) 1031–1038. https://doi.org/10.4314/tjpr.v13i7.4.

[38]   A. Martín, M.J. Cocero, Micronization processes with supercritical fluids: Fundamentals and mechanisms, Adv. Drug Deliv. Rev. 60 (2008) 339–350. https://doi.org/10.1016/j.addr.2007.06.019.

[39]   Dr.F. Maulvi, T. Soni, M. Gohel, G. Tejal, Supercritical fluid technology: A promising approach to enhance the drug solubility, J. Pharm. Sci. Res. 1 (2009).

[40]   M. Rosen, Delivery System Handbook for Personal Care and Cosmetic Products: Technology, Applications and Formulations, SERBIULA Sist. Libr. 20 (2005).

[41]   Z. He, S. Jiang, Q. Li, J. Wang, Y. Zhao, M. Kang, Facile and cost-effective synthesis of isocyanate microcapsules via polyvinyl alcohol-mediated interfacial polymerization and their application in self-healing materials, Compos. Sci. Technol. 138 (2016). https://doi.org/10.1016/j.compscitech.2016.11.004.

[42]   L. Lv, E. Schlangen, Z. Yang, F. Xing, Micromechanical Properties of a New Polymeric Microcapsule for Self-Healing Cementitious Materials, Materials 9 (2016) 1025. https://doi.org/10.3390/ma9121025.

[43]   Y. Ye, J. Yu, Z. Gu, Versatile Protein Nanogels Prepared by In Situ Polymerization, Macromol. Chem. Phys. 217 (2016) 333–343. https://doi.org/10.1002/macp.201500296.

[44]   V.B. Patravale, S.D. Mandawgade, Novel cosmetic delivery systems: an application update, Int. J. Cosmet. Sci. 30 (2008) 19–33. https://doi.org/10.1111/j.1468-2494.2008.00416.x.

[45]   F. Cárdenas-Bailón, G. Osorio-Revilla, T. Gallardo-Velázquez, Microencapsulation techniques to develop formulations of insulin for oral delivery: a review, J. Microencapsul. 30 (2013) 409–424. https://doi.org/10.3109/02652048.2012.742159.

[46]   W. Jiang, S.P. Schwendeman, Stabilization of a model formalinized protein antigen encapsulated in poly(lactide-co-glycolide)-based microspheres, J. Pharm. Sci. 90 (2001) 1558–1569. https://doi.org/10.1002/jps.1106.

[47]   K.G. Carrasquillo, A.M. Stanley, J.C. Aponte-Carro, P. De Jésus, H.R. Costantino, C.J. Bosques, K. Griebenow, Non-aqueous encapsulation of excipient-stabilized spray-freeze dried BSA into poly(lactide-co-glycolide) microspheres results in release of native protein, J. Control. Release Off. J. Control. Release Soc. 76 (2001) 199–208. https://doi.org/10.1016/s0168-3659(01)00430-8.

[48]   G. Ozkan, P. Franco, I. De Marco, J. Xiao, E. Capanoglu, A review of microencapsulation methods for food antioxidants: Principles, advantages, drawbacks and applications, Food Chem. 272 (2019) 494–506. https://doi.org/10.1016/j.foodchem.2018.07.205.

[49]   A. Arshad, M. Jabbal, Y. Yan, J. Darkwa, The micro-/nano-PCMs for thermal energy storage systems: A state of art review, Int. J. Energy Res. 43 (2019) 5572–5620. https://doi.org/10.1002/er.4550.

[50]   M. Catauro, S.V. Ciprioti, Characterization of Hybrid Materials Prepared by Sol-Gel Method for Biomedical Implementations. A Critical Review, Mater. Basel Switz. 14 (2021) 1788. https://doi.org/10.3390/ma14071788.

[51]   E. Kahraman, S. Güngör, Y. Özsoy, Potential enhancement and targeting strategies of polymeric and lipid-based nanocarriers in dermal drug delivery, Ther. Deliv. 8 (2017) 967–985. https://doi.org/10.4155/tde-2017-0075.

[52] A. Jamekhorshid, S.M. Sadrameli, M. Farid, A review of microencapsulation methods of phase change materials (PCMs) as a thermal energy storage (TES) medium, Renew. Sustain. Energy Rev. 31 (2014) 531–542. https://doi.org/10.1016/j.rser.2013.12.033.

[53] M. Hu, J. Guo, Y. Yu, L. Cao, Y. Xu, Research Advances of Microencapsulation and Its Prospects in the Petroleum Industry, Materials 10 (2017) 369. https://doi.org/10.3390/ma10040369.

[54] R.W. Korsmeyer, R. Gurny, E. Doelker, P. Buri, N.A. Peppas, Mechanisms of solute release from porous hydrophilic polymers, Int. J. Pharm. 15 (1983) 25–35. https://doi.org/10.1016/0378-5173(83)90064-9.

[55] P. Costa, J.M. Sousa Lobo, Modeling and comparison of dissolution profiles, Eur. J. Pharm. Sci. 13 (2001) 123–133. https://doi.org/10.1016/S0928-0987(01)00095-1.

[56] M.N. Singh, K.S.Y. Hemant, M. Ram, H.G. Shivakumar, Microencapsulation: A promising technique for controlled drug delivery, Res. Pharm. Sci. 5 (2010) 65–77.

[57] C. Perignon, G. Ongmayeb, R. Neufeld, Y. Frere, D. Poncelet, Microencapsulation by interfacial polymerisation: membrane formation and structure, J. Microencapsul. 32 (2015) 1–15. https://doi.org/10.3109/02652048.2014.950711.

[58] J. Yang, M. Keller, J. Moore, N. Sottos, Microencapsulation of Isocyanates for Self-Healing Polymers, Macromolecules 41 (2008) 9650–9655. https://doi.org/10.1021/ma801718v.

[59] R. Dubey, T.C. Shami, K.U.B. Rao, Microencapsulation Technology and Applications, DEF SCI J 59 (2009).

[60] C.R. Rabin, S.J. Siegel, Delivery systems and dosing for antipsychotics, Handb. Exp. Pharmacol. (2012) 267–298. https://doi.org/10.1007/978-3-642-25761-2_11.

Chapter II

Microencapsulation : Solvent evaporation.

1: Introduction

Drug delivery systems are designed to achieve precise drug delivery to specific sites within the body while maintaining the desired drug concentration. Controlled drug delivery systems have shown promise in overcoming challenges associated with conventional therapy, ultimately enhancing the therapeutic efficacy of drugs. Various strategies exist to achieve sustained and controlled release of therapeutic substances as depicted in Figure 1[1].

One effective strategy involves the utilization of microspheres as carriers for drugs. Microspheres are solid, spherical particles with sizes ranging from 1 to 1000 μm. They are typically constructed from biodegradable synthetic polymers or modified natural materials such as gelatin, albumin, polylactic acid, and polyglycolic acid. Researchers have also explored the influence of hydrophilic protective colloids on microsphere properties. Microencapsulation, another critical technique, involves entrapping a drug substance within discrete, free-flowing polymeric particles or microcapsules. Different coating processes can yield various types of coated particles, which may be embedded within a polymeric or protein matrix network or enveloped by a solidified coating [2].One widely utilized encapsulation method is the solvent evaporation technique, extensively employed in the medical industry for encapsulating a diverse range of drugs, both hydrophobic and hydrophilic. This method plays a crucial role in advancing drug delivery technologies [3].
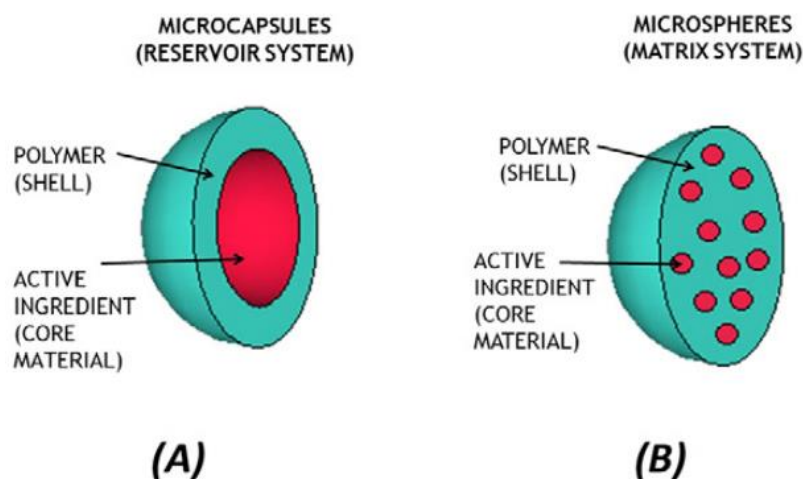
Fig. 1: Inner morphology differences between microcapsules (A) and microspheres (B) [4].

2: Solvent evaporation method

In the realm of formulation processes, the solvent evaporation method holds remarkable appeal due to its user-friendly approach and adaptability in creating micro and nanospherical systems with enhanced characteristics. Its prevalence in practical applications underscores its significance. Originating as a polymer emulsification technique for generating polymeric particles, Vanderhoff et al.[5]; secured its initial patent in 1979. Subsequently, its principles found validation across multiple patents.

The core of this method lies in the distribution of the polymer or micro/nanocapsule coating agent within a volatile solvent, which remains insoluble in the liquid production vehicle phase throughout the procedure. This solvent-bound polymer solution serves the dual purpose of encapsulating the core substance or medicine while allowing its dissolution or dispersion. Controlled stirring facilitates the even spread of the core material within the liquid production vehicle phase, culminating in the formation of microspheres with the desired size range. An emulsion bridge forms between the polymer solution and the continuous phase.

The application of heat or gradual evaporation of the volatile solvent under continuous stirring prompts the polymer to constrict around the core or generate matrix microspheres, facilitated by the core dissolution in the coating solution. Notably, this versatile approach accommodates both water-soluble and insoluble core components within the matrix system [6]. In summary, it can be said that the systems of solvent evaporation method can be based on:

- ✓ The external phase aqueous or nonaqueous nature;
- ✓ The mechanism of the core material's incorporation into the organic either dissolved, dispersed, or emulsified polymer solution;
- ✓ Evaporation or extraction as a method for removing the organic solvent.

3: Materials selection in solvent evaporation method

The selection of appropriate materials has a considerable impact on the successful encapsulation process. The most effective factor in core material microencapsulation is the choice of polymer and solvent in the dispersed phase and emulsifier in the continuous phase.

3.1: *Polymer*

The selection of an effective natural or synthetic polymer as a capsule shell is crucial for the advancement of material encapsulation in medical applications. It was discovered that the physical features of specific polymers had a significant impact on the intended core release rate from microcapsules. Solvent evaporation employs a variety of polymers, including biodegradable, non-biodegradable, and water-soluble polymers. Biodegradable polymers are valued for their biocompatibility and non-toxicity [7]. However, for the microencapsulation of biological components, a variety of biodegradable synthetic polymers have been studied. Natural biodegradable polymers have received a lot of interest because of their availability, abundance in nature, adequate biocompatibility, and ease of modification through simple chemistry [8].

Many studies on drug delivery systems based on natural polymers have been published [9] Encapsulating biological materials is commonly done with biodegradable synthetic polymers such as polyesters, poly(orthoesters), poly-anhydrides, and polyphosphazene. Because of their biodegradability and biocompatibility, lactic and glycolic acid polymers and copolymers are attractive for drug-containing microcapsules in pharmaceutical applications [10]. Poly(D, L-lactide-co-glycolide) (PLGA) and the copolymer of poly(ethylene glycol) and poly(lactic acid) (PEG/PLA) accelerate microcapsule shell deterioration [11]. For medical material encapsulation, biodegradable polymer ethyl cellulose (EC) and biocompatible polymer poly (methyl methacrylate) (PMMA) have been mentioned. As microcapsule shells, biopolymer copolymers such as poly-3-hydroxybutyrate and hydroxyvalerate are used [12].

3.2: *Solvent*

The choice of solvent in the solvent evaporation encapsulation process is crucial, as it significantly affects microcapsule properties. An appropriate solvent must dissolve the polymer, be water-miscible, possess high volatility, have a low boiling point, and be non-toxic [13]. Commonly used solvents for material encapsulation via solvent evaporation include chloroform, dichloromethane, ethyl acetate, and ethyl formate (Table 1) [14]. Dichloromethane, highlighted by Ahangaran et al.[13]**,** stands out due to its low water miscibility of 1.3%. Its rapid vaporization, compared to other organic solvents, expedites microcapsule formation [13]**.** Conversely, ethyl acetate and ethyl formate display water miscibility ranging from 6.4% to 8.8%. These non-halogenated solvents, emphasized by Im et al. [15], are preferred for their low toxicity and minimal environmental impact [15]**.**

Table 1 : Conventional solvents for encapsulation via solvent evaporation technique [16]**.**

Solvent	*Vapor pressure (mbar) at 20°C*	*Boiling point (°C)*	*Solubility in water (g/mL) at 20°C*	*Properties*
Chloroform	212	61	8.1	- Dense than water - Slightly soluble in water - High toxicity
Dichloromethane	453	39.7	20	- Solvent for most polymers - Hightoxicity - Veryvolatile - Miscible with-many organicsol-vents.
Ethylacetate	100	77	90	- Miscible with-many organic sol-vents - Low toxicity - Sweet smell
Ethylformate	259	54	105	- Less dense than water - Low toxicity - Pleasant odor - Less dense than

3.3: Emulsifiers

Over time, a stable emulsion should retain its qualities. The emergence of phenomena such as coalescence, flocculation, creaming and so on can alter the characteristics of the emulsion, making it unstable [17]**.** Emulsifiers provide a protective barrier around particles to avoid droplet buildup and emulsion instability. In the continuous phase, emulsifier type and concentration impact microcapsule properties such as regular size, narrow distribution, spherical shape, and surface morphology [18]. Emulsifiers are classified as ionic or non-ionic depending on their immiscible phase polarity. Amphiphilic structures with hydrophobic tails and hydrophilic heads characterize these compounds. While traditional emulsifiers cover droplets in aqueous solution with hydrophilic heads and hydrophobic parts, polymerizable emulsifiers contribute to stability through emulsion polymerization, forming long-lasting linkages with polymeric particles [19]. Increasing emulsifier concentration decreases interfacial tensions between emulsion phases, allowing microcapsules with smaller mean diameters and narrower dispersion. According to certain research by Ahangaran et al.[20] and Loxley and Vincent, emulsions using polymeric emulsifiers tend to collect microcapsules with broad size ranges, which can be related to their lower colloidal stability when compared to ionic emulsions [20].

4: Solvent evaporation mechanisms

The classification proposed by Aftabrouchad and Doelker [21] is applicable to microspheres prepared using solvent evaporation technique.

4.1: Solvent Evaporation (Emulsification-Evaporation):

The solvent evaporation technique can be executed through two primary methods (Fig. 2.1): oil-in-water (o/w) emulsion and water-in-oil-in-water (w/o/w) double emulsions.
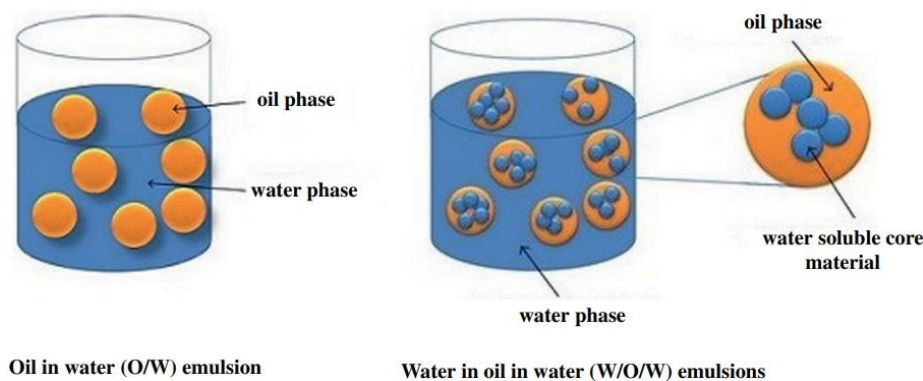
Fig.2.1: Solvent evaporation systems by using O/W and W/O/W emulsions.

The choice of solvent evaporation process is heavily influenced by the core material hydrophilicity or hydrophobicity. An o/w emulsion method can be used to microencapsulate hydrophobic compounds. As water-soluble pharmaceuticals, hydrophilic compounds can be encapsulated in w/o/w double emulsions. The fundamental advantage of the double emulsion technique, on the other hand, is the possibility of encapsulating hydrophilic materials [22].

The oil phase of emulsion systems, the core material, and the polymer as a microcapsule shell are dissolved in a volatile solvent with a low boiling point during the solvent evaporation process. To create an o/w emulsion, the aqueous phase is also prepared by dissolving a suitable emulsifier. The organic component is then introduced drop by drop to the aqueous phase while being mechanically mixed. The polymer chains travel to the oil/water interface through phase separation as the low-boiling volatile solvent progressively evaporates from the oil droplets. The microcapsules are formed as a result of full solvent evaporation from oil droplets. The emulsion system transforms into a suspension system containing microcapsules after the procedure. The interfacial tension interaction between the emulsion's core, polymer, and aqueous phases causes polymer chain phase separation (Fig.2.2) [18].
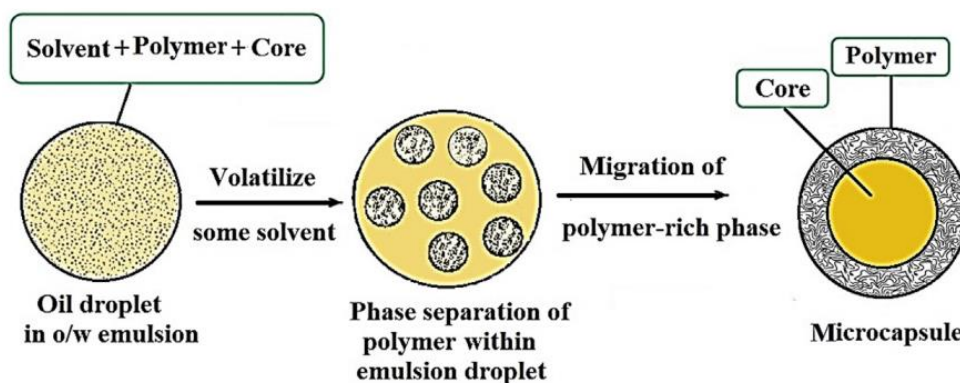
Fig.2.2: Microcapsule formation via solvent evaporation technique [18].

4.1.1: Single emulsion method

This approach is limited to hydrophobic pharmaceuticals due to the possibility of hydrophilic medications diffusing from the dispersed oil phase into the aqueous phase, resulting in decreased encapsulation effectiveness [23]. The oil-in-oil (O/O) emulsification method has gained substantial attention recently as a strategy to encapsulate hydrophilic drugs, including peptides and proteins [24]. This technique involves utilizing water-miscible organic solvents for dissolving both the drug and polymer, while hydrophobic oils serve as the continuous phase within the o/o emulsion. Microparticle formation is achieved by systematically eliminating the organic solvents through processes of evaporation or extraction. The list of nanoparticles prepared by solvent evaporation technique by single emulsion method is given in Table 2.

Table 2: List of some nanoparticles produced by double emulsion method with solvent evaporation.

Drug	Polymer	References
Iron oxide and Rhodamine	PLGA	[25]
Nordihydroguaiaretic Acid [NDGA]	PLGA	[26]
Resveratrol	Different polymers	[27]
Paclitaxel	PLGA	[28]
Bupivacaine	Polyester amide [PEA]	[29]

4.1.2: Double emulsion method

Water-in-oil-in-water (W/O/W) approaches are routinely used to encapsulate water-soluble pharmaceuticals [30]. To make a water-in-oil (W/O) emulsion, an aqueous solution of the water-soluble medication is emulsified with an organic solution containing a dissolved polymer (Fig. 3). For emulsification, high-speed homogenizers or sonicators are used. This initial

emulsion is then vigorously stirred into an excess of water containing an emulsifier, resulting in a w/o/w emulsion. The solvent is then removed by evaporation or extraction in the following steps. A key advantage of this approach lies in its ability to encapsulate hydrophilic drugs efficiently within an aqueous phase. Consequently, the w/o/w emulsion system finds extensive use in the development of protein delivery systems [30]. The characteristics of microspheres produced using the double emulsion method depend on various factors, including polymer properties (composition and molecular weight), polymer-to-drug ratio, emulsifier concentration and nature, temperature, and agitation speed during emulsification. The common research that has been produced by double emulsion (solvent evaporation method) is given in Table 3.
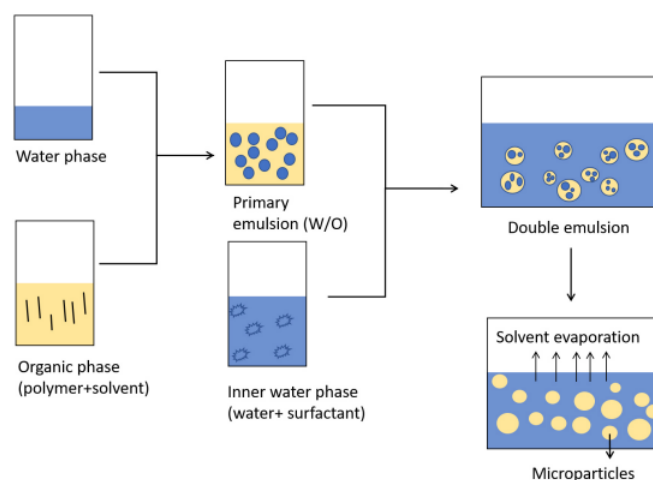
Fig. 3: Scheme of microparticles preparation by the double emulsion
solvent evaporation technique [31].

Table 3: List of nanoparticles produced by double emulsion method with solvent evaporation.

Drug	*Polymer*	*Explanation*	*References*
Cisplatin	PBA	Nanoparticles that enable the release of drug in small concentration in a controlled manner were formulated which thus helped in controlling the nephron toxicity.	[32]
Small interfering RNA	PLGA	Could encapsulate the small interfering RNA.	[33]
5-Flurouracil	PHBHHx	Small co-polymeric microspheres and nanospheres of spherical shape were obtained.	[34]
Paclitaxel, caumarin	Chitosan	Efficacy of chitosan coated PLGA nanoparticles as an efficient delivery system was studied.	[35]

The stability of different emulsions can be affected by the percentage of emulsifiers used in primary W/O emulsions [36]. There are other various phenomena attributed to the instability of double emulsions including coalescence, sedimentation, creaming, flocculation, and so on. Figure 3 depicts a schematic representation of the instability process.

i. Coalescence

During coalescence, droplets mix, resulting in bigger droplet production and evident emulsion phase separation (Fig. 4). Water-water coalescence has little effect on the behavior of the double emulsion. The droplet distribution of the inner emulsion fluctuates, which is mostly determined by the oil droplet size distribution and volume ratio. Larger droplets may display different coalescence behavior, which is controlled by factors such as droplet size and changes in capillary pressure owing to diffusion processes. Unlike water-water coalescence, oil-oil coalescence changes the properties of a double emulsion. Furthermore, increasing the size of the oil droplets reduces emulsion viscosity, intensifying creaming. Double emulsions can break into water and W/O emulsion phases in extreme circumstances [37].

ii. Creaming

The interfacial membrane between droplets has the potential to rupture and cream irreversibly. Creaming in double emulsions can be reduced by reducing droplet size, increasing the viscosity of the continuous phase, and balancing the density. Among these, oil density is a significant element in creaming since it rises when the density gradient grows in both phases [38].

iii. Flocculation

This phenomenon includes the creation of a floc as a result of emulsion droplet aggregation while droplets retain their integrity. When attractive forces (Van der Waals interactions) between scattered phase droplets overcome repulsive forces (electrostatic and short-range interactions), flocculation occurs. It can happen if there is a high concentration of emulsifiers or thickening agents. Flocculation and gravitational separation are connected because flocculation causes an increase in dispersed phase droplet size, which facilitates dispersed phase particle sedimentation. The trapping of continuous phase particles in between the flocs increases the viscosity of the system, resulting in the formation of a gelled product [37].

iv. Ostwald ripening

It is popular in food emulsions containing flavor or essential oils. According to Lamba et al. this phenomenon occurs when the dispersed phase becomes too large and causes an abrupt drop in the emulsion viscosity (Catastrophic phase inversion) or when the inherent environmental parameters, such as temperature and ionic strength, change (Transitional phase inversion) [39].

v. Sedimentation

The density difference between the two phases causes macroscopic separation, as seen in Figure 4. It has been shown that raising the dispersed phase ratio enhances viscosity while decreasing sedimentation. This phenomenon is well-defined by Stokes law, which states that droplet size and the viscosity of the continuous phase have a direct effect on gravitational separation. Droplet size has a direct relationship with the amount of sedimentation index. Small droplet size reduces system density, which is crucial for generating a physically stable emulsion and prevents droplet coalescence [40].
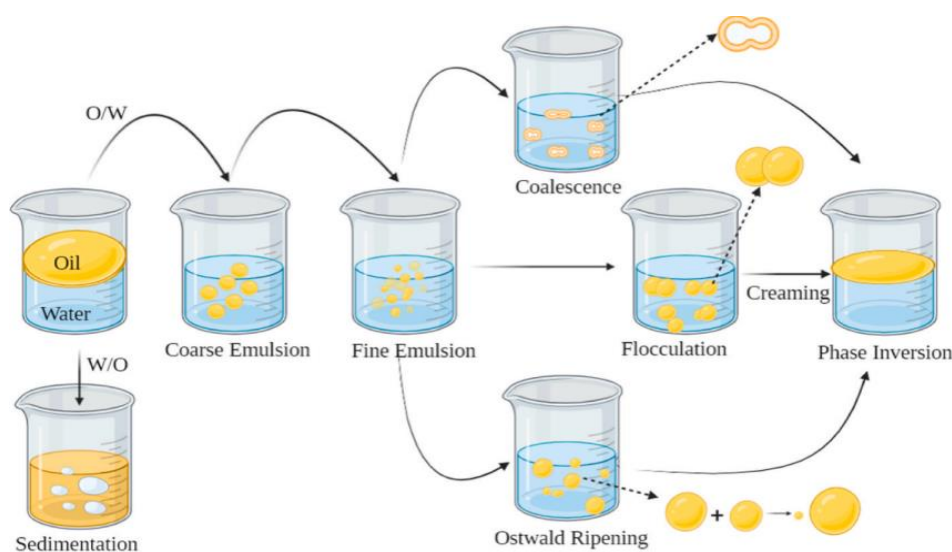
Fig. 4. Schematic illustration of instability mechanism of double emulsion.

4.1.3: Nonaqueous Emulsions method

This technique involves immiscible oily phases for both the continuous and dispersed phases, typically using mineral or vegetable oils or non-volatile organic solvents. It has been primarily used to encapsulate a limited range of drugs, including cytostatics, anti-inflammatories, antimalarials, anxiolytics, and serum albumin. This method forms a protective barrier between the drug and the polymer-solvent phase and prevents highly water-soluble drugs from leaching out of microspheres. For instance, microcapsules of lamivudine and stavudine were prepared using acetone as a solvent and liquid paraffin as a dispersion medium [41]. A variation of this technique involves sublimation through lyophilization after emulsification, resulting in porous microspheres. For instance, a multiunit floating drug delivery system for rosiglitazone maleate was developed using Eudragit RS100 through this method. It offers enhanced entrapment of water-soluble drugs and helps prevent drug or

polymer hydrolysis. However, compared to aqueous emulsions, nonaqueous solvents may be costlier, and removing residual solvents from microspheres can be challenging [42].

4.2: Solvent Extraction (Emulsification-Extraction)

The solvent evaporation process can be modified to bypass the evaporation stage by using an excess of the dispersing phase relative to the dispersed phase or by selecting a dispersed phase containing cosolvents, with at least one having a strong affinity for the dispersing phase, acting as a solvent extractor. This technique has been used to produce microspheres of naproxen and albumin. The solvent extraction process offers advantages over solvent evaporation and spray drying methods, resulting in particles that are more uniform in shape, smaller with a narrow size distribution, and greater porosity [43].

4.3: Phase separation

This approach includes adding an organic nonsolvent to a polymer solution to phase separate it. First, the drugs are disseminated or dissolved in a polymer solution. Under continuous stirring, an organic nonsolvent (e.g., silicon oil) is added to this mixed solution, resulting in the slow extraction of the polymer solvent and the formation of soft coacervate droplets carrying the medication. The rate at which nonsolvent is introduced affects the extraction rate of the solvent, the size of microparticles, and the drug encapsulation efficiency. Non-solvents that are often utilized include silicone oil, vegetable oil, light liquid paraffin, and low-molecular-weight polybutadiene. After that, the coacervate phase is toughened by immersing it in an excess of another nonsolvent, such as hexane, heptane, or diethyl ether. The final microspheres properties are governed by the polymer molecular weight, nonsolvent viscosity, and polymer concentration. The biggest downside of this approach is the increased probability of huge aggregates developing. Before full-phase separation, very sticky coacervate droplets regularly attach to one other **[44,45]**.

References

[1]   J.K. Vasir, K. Tambwekar, S. Garg, Bioadhesive microspheres as a controlled drug delivery system, Int. J. Pharm. 255 (2003) 13–32.

[2]   S. Izumikawa, S. Yoshioka, Y. Aso, Y. Takeda, Preparation of poly (l-lactide) microspheres of different crystalline morphology and effect of crystalline morphology on drug release rate, J. Controlled Release 15 (1991) 133–140.

[3]   D. Tiwari, P. Verma, Microencapsulation technique by solvent evaporation method (Study of effect of process variables), 2 (2011) 998–1005.

[4]   R. Herrero-Vanrell, I. Bravo-Osuna, V. Andrés-Guerrero, M. Vicario-de-la-Torre, I.T. Molina-Martínez, The potential of using biodegradable microspheres in retinal diseases and other intraocular pathologies, Prog. Retin. Eye Res. 42 (2014) 27–43.

[5]   J.W. Vanderhoff, M.S. El-Aasser, J. Ugelstad, Polymer emulsification process, 1979.

[6]   H. Parmar, S. Bakliwal, N. Gujarathi, B. Rane, S. Pawar, Different methods of formulation and evaluation of mucoadhesive microsphere., (2010).

[7]   M. Li, O. Rouaud, D. Poncelet, Microencapsulation by solvent evaporation: State of the art for process engineering approaches, Int. J. Pharm. 363 (2008) 26–39.

[8]   J.H. Park, M. Ye, K. Park, Biodegradable polymers for microencapsulation of drugs, Molecules 10 (2005) 146–161. https://www.mdpi.com/1420-3049/10/1/146

[9]   A.M. Yousaf, D.W. Kim, J.K. Kim, J.O. Kim, C.S. Yong, H.-G. Choi, Novel fenofibrate-loaded gelatin microcapsules with enhanced solubility and excellent flowability: preparation and physicochemical characterization, Powder Technol. 275 (2015) 257–262.

[10] J. Feng, G. Yang, S. Zhang, Q. Liu, S.M. Jafari, D.J. McClements, Fabrication and characterization of β-cypermethrin-loaded PLA microcapsules prepared by emulsion-solvent evaporation: loading and release properties, Environ. Sci. Pollut. Res. 25 (2018) 13525–13535. https://doi.org/10.1007/s11356-018-1557-6.

[11] H. Jeong, H. Lim, D.Y. Lee, Y.-S. Song, B.-Y. Kim, Preparation and drug release behavior of nifedipine-loaded poly (lactic acid)/polyethylene glycol microcapsules, J. Nanosci. Nanotechnol. 21 (2021) 3735–3741.

[12] L. Cao, Y. Liu, C. Xu, Z. Zhou, P. Zhao, S. Niu, Q. Huang, Biodegradable poly (3-hydroxybutyrate-co-4-hydroxybutyrate) microcapsules for controlled release of trifluralin with improved photostability and herbicidal activity, Mater. Sci. Eng. C 102 (2019) 134–141. https://www.sciencedirect.com/science/article/pii/S0928493118324676

[13] A.H. Navarchian, N. Najafipoor, F. Ahangaran, Surface-modified poly (methyl methacrylate) microcapsules containing linseed oil for application in self-healing epoxy-based coatings, Prog. Org. Coat. 132 (2019) 288–297.

[14] Muhaimin, R. Bodmeier, Effect of solvent type on preparation of ethyl cellulose microparticles by solvent evaporation method with double emulsion system using focused beam reflectance measurement: Effect of solvent type on preparation of ethyl cellulose microparticles, Polym. Int. 66 (2017) 1448–1455. https://doi.org/10.1002/pi.5436.

[15] H.-Y. Im, J. Kim, H. Sah, Another Paradigm in Solvent Extraction-Based Microencapsulation Technologies, Biomacromolecules 11 (2010) 776–786. https://doi.org/10.1021/bm9013952.

[16] M. Kutscher, W.S. Cheow, V. Werner, U. Lorenz, K. Ohlsen, L. Meinel, K. Hadinoto, O. Germershaus, Influence of salt type and ionic strength on self-assembly of dextran sulfate-ciprofloxacin nanoplexes, Int. J. Pharm. 486 (2015) 21–29.

[17] R. Al-Shannaq, M. Farid, S. Al-Muhtaseb, J. Kurdi, Emulsion stability and cross-linking of PMMA microcapsules containing phase change materials, Sol. Energy Mater. Sol. Cells 132 (2015) 311–318. https://www.sciencedirect.com/science/article/pii/S0927024814004590

[18] F. Ahangaran, A.H. Navarchian, F. Picchioni, Material encapsulation in poly(methyl methacrylate) shell: A review, J. Appl. Polym. Sci. 136 (2019) 48039. https://doi.org/10.1002/app.48039.

[19] Z.-H. Chen, F. Yu, X.-R. Zeng, Z.-G. Zhang, Preparation, characterization and thermal properties of nanocapsules containing phase change material n-dodecanol by miniemulsion polymerization with polymerizable emulsifier, Appl. Energy 91 (2012) 7–12.

[20] F. Ahangaran, M. Hayaty, A.H. Navarchian, Morphological study of polymethyl methacrylate microcapsules filled with self-healing agents, Appl. Surf. Sci. 399 (2017) 721–731.

[21] C. Bitz, E. Doelker, Influence of the preparation method on residual solvents in biodegradable microspheres, Int. J. Pharm. 131 (1996) 171–181. https://doi.org/10.1016/0378-5173(95)04320-9.

[22] A.M. Bakry, S. Abbas, B. Ali, H. Majeed, M.Y. Abouelwafa, A. Mousa, L. Liang, Microencapsulation of Oils: A Comprehensive Review of Benefits, Techniques, and Applications, Compr. Rev. Food Sci. Food Saf. 15 (2016) 143–182. https://doi.org/10.1111/1541-4337.12179.

[23] M.H. Perez, C. Zinutti, A. Lamprecht, N. Ubrich, A. Astier, M. Hoffman, R. Bodmeier, P. Maincent, The preparation and evaluation of poly (ε-caprolactone) microparticles containing both a lipophilic and a hydrophilic drug, J. Controlled Release 65 (2000) 429–438.

[24] K.G. Carrasquillo, A.M. Stanley, J.C. Aponte-Carro, P. De Jésus, H.R. Costantino, C.J. Bosques, K. Griebenow, Non-aqueous encapsulation of excipient-stabilized spray-freeze dried BSA into poly (lactide-co-glycolide) microspheres results in release of native protein, J. Controlled Release 76 (2001) 199–208.

[25] B.H. Chung, Y.T. Lim, J.H. Han, Polymer particles for NIR/MR bimodal molecular imaging and method for preparing the same, 2011.

[26] R.C.C. Huang, R. Park, C.-C. Chang, Y.-C. Liang, D. Mold, E. Lin, J. Heller, N. Frazer, Methods for delivery of catecholic butanes for treatment of tumors, 2010.

[27] P. Davis, F.B. Davis, S.A. Mousa, H.-Y. Lin, Small molecule ligands of the integrin RGD recognition site and methods of use, 2010.

[28] G. Subedi, A.K. Shrestha, S. Shakya, Study of Effect of Different Factors in Formulation of Micro and Nanospheres with Solvent Evaporation Technique, Open Pharm. Sci. J. 3 (2016). https://doi.org/10.2174/1874844901603010182.

[29] W.G. Turnell, H. Li, Z.D. Gomurashvili, R. Katsarava, Polymer particle delivery compositions and methods of use, 2016.

[30] V.R. Sinha, A. Trehan, Biodegradable microspheres for protein delivery, J. Controlled Release 90 (2003) 261–280.

[31] T.K. Giri, C. Choudhary, Ajazuddin, A. Alexander, H. Badwaik, D.K. Tripathi, Prospects of pharmaceuticals and biopharmaceuticals loaded microparticles prepared by double emulsion technique for controlled delivery, Saudi Pharm. J. 21 (2013) 125–141. https://doi.org/10.1016/j.jsps.2012.05.009.

[32] S. Khoee, A. Sattari, F. Atyabi, Physico-chemical properties investigation of cisplatin loaded polybutyladipate (PBA) nanoparticles prepared by w/o/w, Mater. Sci. Eng. C 32 (2012) 1078–1086.

[33] D. Cun, D.K. Jensen, M.J. Maltesen, M. Bunker, P. Whiteside, D. Scurr, C. Foged, H.M. Nielsen, High loading efficiency and sustained release of siRNA encapsulated in PLGA nanoparticles: quality by design optimization and characterization, Eur. J. Pharm. Biopharm. 77 (2011) 26–35.

[34] X. Lu, Y. Zhang, L. Wang, Preparation and *in vitro* drug-release behavior of 5-fluorouracil-loaded poly(hydroxybutyrate- *co* -hydroxyhexanoate) nanoparticles and microparticles, J. Appl. Polym. Sci. 116 (2010) 2944–2950. https://doi.org/10.1002/app.31806.

[35] B.-S. Kim, C.-S. Kim, K.-M. Lee, The intracellular uptake ability of chitosan-coated Poly (D,L-lactideco-glycolide) nanoparticles, Arch. Pharm. Res. 31 (2008) 1050–1054. https://doi.org/10.1007/s12272-001-1267-5.

[36] N.P. Aditya, S. Aditya, H. Yang, H.W. Kim, S.O. Park, S. Ko, Co-delivery of hydrophobic curcumin and hydrophilic catechin by a water-in-oil-in-water double emulsion, Food Chem. 173 (2015) 7–13.

[37] N. Leister, H.P. Karbstein, Evaluating the stability of double emulsions—A review of the measurement techniques for the systematic investigation of instability mechanisms, Colloids Interfaces 4 (2020) 8.

[38] H.I. Buyukkestelli, S.N. El, Development and characterization of double emulsion to encapsulate iron, J. Food Eng. 263 (2019) 446–453.

[39] H. Lamba, K. Sathish, L. Sabikhi, Double Emulsions: Emerging Delivery System for Plant Bioactives, Food Bioprocess Technol. 8 (2015) 709–728. https://doi.org/10.1007/s11947-014-1468-6.

[40] P. Duque-Estrada, E. School, A.J. Van Der Goot, C.C. Berton-Carabin, Double emulsions for iron encapsulation: is a high concentration of lipophilic emulsifier ideal for physical and chemical stability?, J. Sci. Food Agric. 99 (2019) 4540–4549. https://doi.org/10.1002/jsfa.9691.

[41] R. Narayana, P. Katakam, C. Reddy, B. Krishnaveni, N. Lakshmi, Stavudine loaded microcapsules using various cellulose polymers: preparation and in-vitro evaluation. Int. Jr. pharm, Int. J. Pharm. Sci. Nanotechnol. 2 (2009) 551–556.

[42] M. Mohan Kamila, N. Mondal, L. Kanta Ghosh, B. Kumar Gupta, Multiunit Floating Drug Delivery System of Rosiglitazone Maleate: Development, Characterization, Statistical Optimization of Drug Release and In Vivo Evaluation, AAPS PharmSciTech 10 (2009) 887. https://doi.org/10.1208/s12249-009-9276-4.

[43] F. Pavanetto, B. Conti, I. Genta, P. Giunchedi, Solvent evaporation, solvent extraction and spray drying for polylactide microsphere preparation, Int. J. Pharm. 84 (1992) 151–159. https://doi.org/10.1016/0378-5173(92)90055-7.

[44] D. Mallardé, F. Boutignon, F. Moine, E. Barré, S. David, H. Touchet, P. Ferruti, R. Deghenghi, PLGA-PEG microspheres of teverelix: influence of polymer type on microsphere characteristics and on teverelix in vitro release, Int. J. Pharm. 261 (2003) 69–80. https://doi.org/10.1016/s0378-5173(03)00272-2.

[45] P.W. Heng, L.W. Chan, M.G. Easterbrook, X. Li, Investigation of the influence of mean HPMC particle size and number of polymer particles on the release of aspirin from swellable hydrophilic matrix tablets, J. Control. Release Off. J. Control. Release Soc. 76 (2001) 39–49. https://doi.org/10.1016/s0168-3659(01)00410-2.

Chapter III

Exploring clays in Drug Delivery.

1: **Introduction**

One of the most critical challenges of nanotechnology is the efficient design and production of smart and stimuli-responsive nanosized materials for biomedical applications [1]. Due to both their geometrical and chemical properties, nanotubular particles have received special interest among several nanoscale platforms for drug delivery **[2,3]**. The concept of nano architectonics involves the synergistic integration of multiple types of materials structured into complex super-particles, thereby enhancing and expanding the original functions of the constituent materials **[4,5]**.

In this context, nano-sized tubes emerge as strong contenders to serve as a versatile platform for the development and production of intelligent nanocontainers. In general, nanotubular substances display a shared fundamental structure, wherein a tube-shaped particle contains an inner space (referred to as a lumen) and outer walls, coupled with openings at both ends of the tube. The geometry of nanotubes is highly influenced by their chemical origin; some nanotubes have irregular curly geometry and form bundles of variable sizes and shapes, whilst others have uniform rodlike geometry with little or no spatial flaws. The main advantages of nanotubular structures are strongly linked to the nano-architectonic paradigm, which states that nanotubes of any chemical origin have a similar design (a tube with walls, lumen, and open ends). It enables scientists to conduct the following:

1. Loading products (drugs, therapeutic nucleic acids, etc.) into the lumen, interwall spaces in multi-walled tubes, or onto the walls (or use all of these locations at the same time) [5].
2. Modify the tube extremities with "smart" stoppers (Fig. 1), ideally stimuli-responsive, to adjust product release (i.e., design the stoppers to be permeable only within certain sections of cells or tissues) [6].
3. Adding another degree of difficulty to this strategy is improving the functioning of the tube walls. This functionalization, accomplished by the integration of polymer (multi)layers or nanoscale particles, or a mix of both, enables external triggers or spatial manipulation of the loaded payload. This intentional modification of the drug-loaded nanotubes enables targeted interactions and customized release patterns [7].
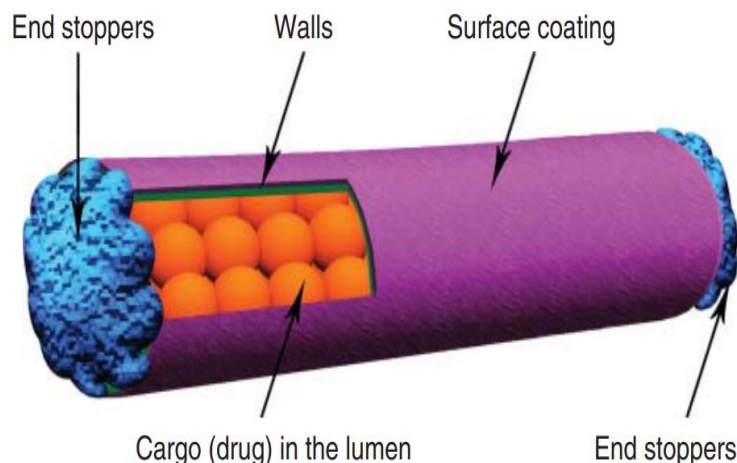
Fig. 1. An illustration depicting a standard drug delivery container based
on nanotubes with the drug cargo carried inside the lumen or
on the outer surface and stimuli-responsive end stoppers [6].

2: Clay Minerals: Structure, Properties and Applications

To fully understand how clays impacts the properties of composites, it is important to highlight the clay definition and its structure. From a chemical standpoint, the word clay mineral denotes a class of the wide category of hydrated phyllosilicates; similarly, from a geological standpoint, this clay constitutes the fine-grained component of rocks, sediments, and soils. Clay minerals are hydrous aluminosilicates with very small particle sizes and a general chemical formula $(Ca, Na, H) (Al, Mg, Fe, Zn)_2(Si, Al)_4O_{10}(OH)_2xH_2O$, where x indicates the variable quantity of water. In general, clay minerals may be divided into two categories: natural and synthetic clays Include Montmorillonite, Hectorite, sepiolite, laponite, saponite, rectorite, bentonite, vermiculite, beidellite, kaolinite, chlorite, natural clay and the synthetic one such as various layered double hydroxides, synthetic Montmorillonite, Hectorite and so on as depicted in Figure 2a outlines the main clay classes. These minerals are used in different fields and their main applications are compiled in figure 2b.

Natural clay type

| 2:1 | | | | | 2:1:1 | 1:1 | Amorphouscrystaline |

| Smectite | Vermiculite | Pyrophyllite Talc | Mica | Brittle Mica | Chloride | Kaolinite | Imgolite |

| Montmorillonite | | Pyrophyllite | Muscovite | | Donbassite | Halloysite | Allophane |

| Saponite | | Talc | Paragonite | | Sudoite | Rectorite | Hisingerite |

| Laponite | | | | | Chamosite | Chrysotile | |

| Sepiolite |

| Hectorite |

| Bentonite |

| Beidellite |

Clay minerals

Natural clays   Synthetic clays

Applications

Adsorbents   Photocatalysis   Pharmaceutical   Feed additives   Packaging

Heavy metals   Wastewater treatment

Excipients   Cosmetics   Biomaterials   Medical devices

Fig. 2: Organizational chart and different applications fields of the main clay classes

.

In general, the different structures of clay minerals are composed of alternating tetrahedral silica sheets "SiO_2" and alumina octahedral layers "AlO_6" in ratios of 1:1 when one octahedral sheet is linked to one tetrahedral sheet as Kaolinite, Halloysite, or in ratios of 2:1 this structure created from two tetrahedral sheets sandwiching an oxygen as seen in Fig. 3, one side of this lamella is still connected to the other by common oxygen atoms. As a result, the clay platelet undergoes structural rearrangement, yielding various configurations (nano-fibers, nano-tubes, and plate-like) as shown in Figure 4.
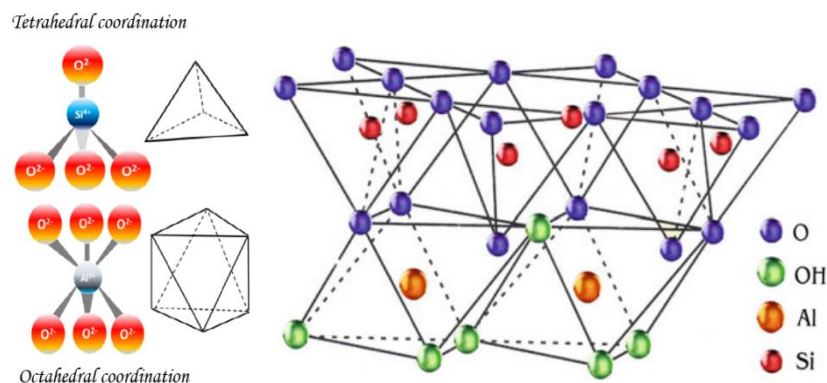
Fig. 3. Basic clay structure
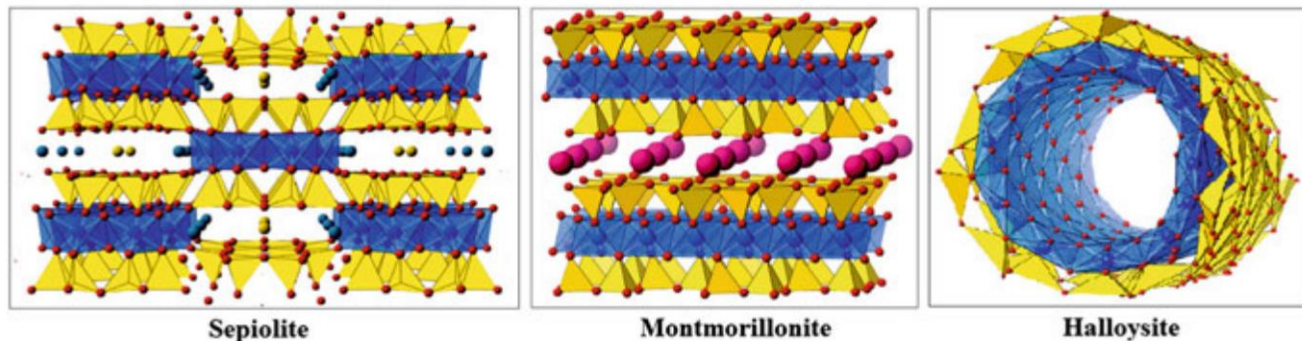
Fig. 4. Crystal structures of nano-fibers, plate-like, and nano-tubes

3: Background history and Terminology of Halloysite

In 1826, Omaliusd Halloy the Belgian geologist provided the first description of halloysite, characterizing it as a kaolin-group clay mineral with high-water content. After two centuries later, we are now beginning to understand the significance of this limited water presence on the nanostructure and the prospective uses of these clays. Halloysite clay mineral structure consists of alternating tetrahedral silica oxide (SiO_2) layers and octahedral alumina oxide (AlO_6). The arrangement and ratio of these layers give rise to different forms of halloysite, including

variations such as halloysite (-10 Å) and halloysite (-7 Å), which denote the presence of interlayer water and its subsequent absence, respectively [8]. Halloysite is defined as a 1:1 phyllosilicate in which a planar layer of tetrahedral silicates alternates with an octahedral geometry layer; these layers are bound together by oxygen bridges [9]. The fundamental unit for the octahedral sheet consists of three octahedrons. In particular, the siloxane groups are bonded via only one oxygen atom to octahedral rings at the outer part and the apical oxygen of tetrahedra becomes the vertices of octahedral[10]. However, under certain geological conditions, halloysite can also take on forms other than classical tubular. It is also possible to distinguish a spheroidal morphology, flat and almost rolled. This unique structure has generated substantial interest for its potential applications, encompassing drug delivery, catalysis, and nanocomposite materials. Pure halloysite is found in various deposits worldwide, including the USA, New Zealand, China, Canada, and Turkey. Pure halloysite exhibits variations in characteristics according to the specific deposit, even within the same deposit site[11]. The unique tubular morphology of halloysite, known as "halloysite nanotubes" (HNTs), arises from specific geological conditions that lead to the wrapping of clay layers into multi-layered tubes.

4: **Structure of halloysite (HNT)**

Halloysite (HNT) occurs naturally as a white mineral that may be easily processed into fine powder. In specific deposits, the mineral hue might range from yellowish to brown or even greenish, attributable to trace amounts of metal ions like Fe^{+3}, Cr^{+3}, and Ti^{+4}, which substitute Al^{+3} or Si^{+4} within the crystal lattice[10]. A very interesting aspect is linked to the different chemical composition between the inner and outer surfaces, in which there are, respectively, the inner surface with aluminolic groups (Al-OH) is composed of gibbsite octahedral sheet and give a positive electrical potential, whereas the external surface consists of siloxanes groups (Si-O-Si) with negative charge **[9,10].** The different charges at the inner and outer faces of the nanotubes are due to the different dielectric and ionization properties of silicon oxides and aluminium which allow for the selective internal loading of negatively charged molecules [12] as it is represented in figure 5 which schematically shows the structure of a halloysite nanotube.
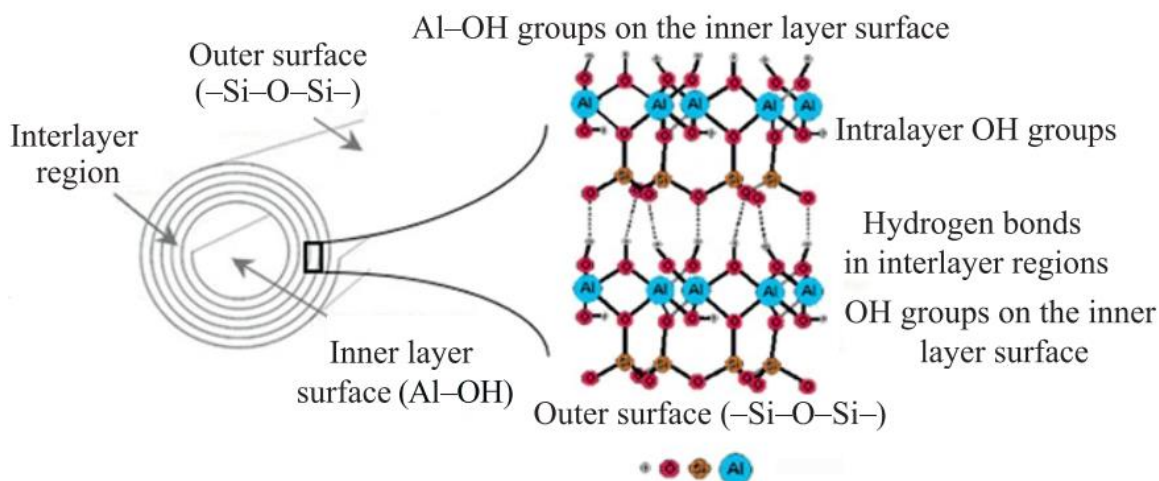
Fig. 5: Scheme showing the structure of the halloysite nanotube.

Within this structure, for pH values of 3–10, the positive charges are distributed in the inner lumen and the negative charges on the external surface; present on the edges is a negative/positive charge. In particular, the tubule lumen is positively charged with pH ≤ 8.5, and the outer surface is negatively charged with pH ≥ 1.5[13].

Generally, because of the O and OH atoms that carry negative charges, the halloysite nanotube is negatively charged. As a result of the tubular shape, on the outer surface only a few hydroxyl groups are present; these are more concentrated in the internal lumen and therefore are more reactive.

In fact, for halloysite tubes, it is possible to classify three types of Al-OH, according to their positioning on the surface, at the ends, and between the octahedral and tetrahedral sheets, as shown in figure 5. All can be reactive and dissociate according to the pH of the solutions, except those placed between the octahedral and tetrahedral sheets, due to steric hindrance [14].

The halloysite nanotubes size may vary depending on the extraction site and the purification process they undergo, but they usually have an internal diameter of 10–30 nm, an external diameter of 40–70 nm, and a length between 200 and 2000 nm **[16,17].** Nanotubes with a length between 3 and 5 µm have been found in some deposits, although those with smaller sizes are more interesting from a biological point of view, as they are more suitable for use as drug carriers [17].

In the first case, the water molecules are placed on the surface of the tetrahedral sheet with different orientations and make hydrogen bonds with the basal oxygens. The "associated" water has a greater degree of mobility at room temperature and is located at a different level in the interlayer space, with an ice-like configuration and forming hydrogen bonds with each other and/or with inner-surface hydroxyls **[19,20].**

Generally, HNT surfaces could be classified into three types:

i.   The inner lumen surface has a positive charge and is covered by Al-OH groups. It can undergo a variety of covalent modifications by which certain functional groups can be added. This method allows immobilizing several organic groups on the surface of the lumen stably.

ii.   The external siloxane surface has a negative charge and can be used to establish covalent bonding with molecules such as organosilanes [20]. Moreover, it can be modified by coating with cationic substances, such as polymers, biopolymers, and surfactants. This type of modification can help to improve the dispersibility and biocompatibility of halloysite.

iii. Interstate surfaces, held together by hydrogen bridges, can be modified by direct or indirect intercalation of small organic molecules and some monovalent cationic salts. This, therefore, can lead to a weakening of the hydrogen bonds interstate and an increase in the surface between the various layers that can be understood as additional space for loading or adsorption [21].

Table 1: General representative analysis data of HNT.

Length	400-1000 nm
Average tube diameter	20-200 nm
Inner diameter	10-70 nm
Aspect ratio (L/D)	9-50
Elastic modulus (Theoretical value)	140 GPa
Mean particle size in aqueous solution	143 nm
Particle size range in aqueous solution	50-400 nm
Typical specific surface area	22.1-81.6 $m^2.g^{-1}$
Pore space	14-47 %
Lumen space	10.7-39 %
Density	2.14-2.59 $g.cm^{-3}$
Average pore size	80-100 Å
Pore volume	1.25 $mL.g^{-1}$
Structural water release temperature	400-600 °C
Cation exchange capability	0.1-0.7 $mol.Kg^{-1}$

5: Halloysite purification

Since the raw halloysite nanotubes were obtained directly from mines, the contaminants, including quartz, kaolinite, illite, feldspar, perlites, and metal ions, were separated before they are used in the experiments. The purification of raw material is based on a dispersion–centrifugation–drying technique. At the laboratory scale, the initial stage of purifying the raw halloysite material involves the elimination of water-soluble components. In this process, 20 g of the material is slowly dispersed in 1 L of distilled water and stirred for 24 hours at room temperature. Afterward, the suspension undergoes centrifugation at 5000 rpm for 5 minutes. Addressing the removal of carbonates requires subjecting the resultant powder to intensive stirring with 2 L of 0.1 M HCl at room temperature for 4hours [22]. Following a second round of centrifugation, the resulting precipitate is meticulously washed using distilled water and subjected to consecutive centrifugation cycles, repeated five times to eliminate chloride ions (tested using AgNO3 solution). Further refinement entails the removal of soil organic matter. This step involves exposing the solid residue to a solution of aqueous hydrogen peroxide (10% v/v, 1 L) and stirring it overnight at room temperature. The residual hydrogen peroxide is then broken down by heating the suspension to 70°C for 30 minutes. The ensuing precipitate is washed using hot water (100°C, 1 L) and dried for 24 hours at 50°C. Subsequently, the material is ground in a mortar, sieved at 45 μm, stored in a container, and safeguarded from moisture. This treated sample is designated as HNT.

6: Structural and morphological changes under chemical activation methods

Several chemical approaches have been investigated to improve the physicochemical properties of HNTs, particularly the loading capacity. By using the different chemical compositions of the inner and outer surfaces, with the possibility to select or remove one layer or the other by working in different pH solutions.

The methods of HNT modification can be divided into two major groups:

    i.   The external modification involves alkaline etching and grafting of nanoparticles, surfactants, polymers, and organosilanes to the outer surface.

    ii.   The internal modification involves acid etching and grafting of surfactants, polymers, bio-compounds, and organosilanes to the inner surface **[24,25]**. Alkaline and acid etching can affect the morphology of HNTs, making them more compatible with various chemicals. Organosilanes, for example, can boost the flexibility of HNTs. Surfactants can improve aqueous solution dispersion by increasing their stability. Biomolecules can induce a variety of qualities, such as the appearance of a zwitterionic

nature at different pH levels and an increase in the thermal and mechanical properties of polymers.

Similarly, the interior space of the nanotubes is modified, resulting in the regulated loading and release of numerous medications. The alteration of the surface of the HNTs is important in halloysite research because it permits the HNTs to be used for a variety of environmental, catalytic, and biological applications [**26**].

6.1: Etching of HNT under chemical manipulation and heat treatment

6.1.1: chemical manipulation

Chemical treatments promise to be a potential technique for increasing the efficacy of clay minerals, particularly halloysite nanotubes (HNTs). For acid and alkaline treatments of halloysite, sulfuric acid, hydroxyl chloride, acetic acid, and sodium hydroxide are commonly used, successfully affecting the lumen diameter of the nanotubes. These treatments successfully impact the nanotubes lumen diameter, offering control over their structural dimensions to match specific needs. Furthermore, the unique chemical compositions of HNTs inner and outer surfaces have been cleverly used to achieve selective layer removal using appropriate pH solutions. This sophisticated approach not only refines the physicochemical features but also emphasizes the precision available in adjusting HNT characteristics for specific tasks, hence increasing their usability and adaptability. Bavykin et al. [26] study; initially demonstrated the long-term stability of Halloysite when immersed in solutions of various acids (H_2SO_4, HCl, acetic acid), a strong base (NaOH), and distilled water, ranging in concentration from 0.001 to 1 $mol \cdot dm^{-3}$ [26]. Notably, the investigation revealed that halloysite exhibited remarkable kinetic stability when submerged in water and mild organic or diluted inorganic acid and alkaline solutions, especially at room temperature. The highest solubility of Al(III) compared to that of Si(IV) in strong acid solutions leads to the formation of small SiO_2 nanoparticles inside the tubes, increasing the sample surface area and pore volume. Conversely, Because Si(IV) is more soluble in concentrated NaOH solutions than Al(III), it engenders the generation of fragmented flaky particles marked by layers of $Al(OH)_3$, as illustrated in Figure 6.
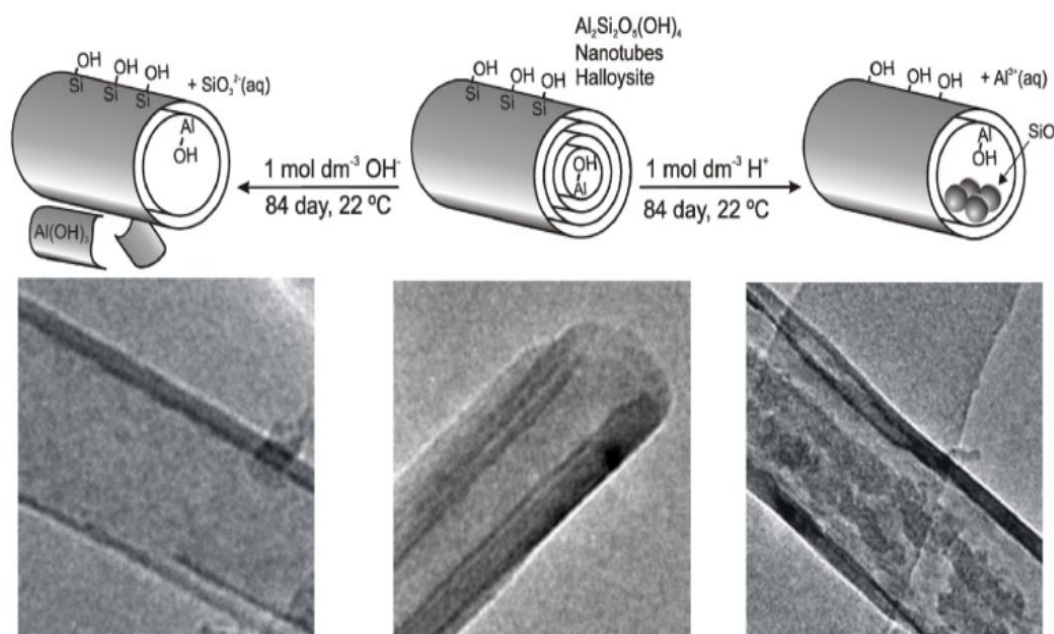
Fig. 6: Scheme presentation of dynamic Evolution of Halloysite Nanotubes in Strong Acid and   Alkaline Solutions: Formation of Amorphous SiO_2 Nanoparticles and $Al(OH)_3$ nanosheets [26].

Likewise, in a study by Chen et al. [27], it was reported that subjecting HNT to sulfuric acid treatment led to the breakdown of its crystal structure, resulting in the transformation into amorphous silica. This treatment dissolved $[AlO_6]$ octahedral layers and caused the fracture of $[SiO_4]$ tetrahedral layers, ultimately yielding porous nanorods. Moreover, Abdullayev et al.[28]; mentioned that the sulfuric acid treatment provides a successful method for controllable enlargement of halloysite lumen diameter. The etching process begins with hydrogen ion diffusion into halloysite pores, followed by a chemical reaction between alumina and hydrogen ions and diffusion of the reaction products out of the lumen (Scheme 7). in summary; The breakdown of alumina sheets begins with the inner halloysite layers and results in clay nanotubes with evenly expanded and uniformly lumen diameters below 70 °C.
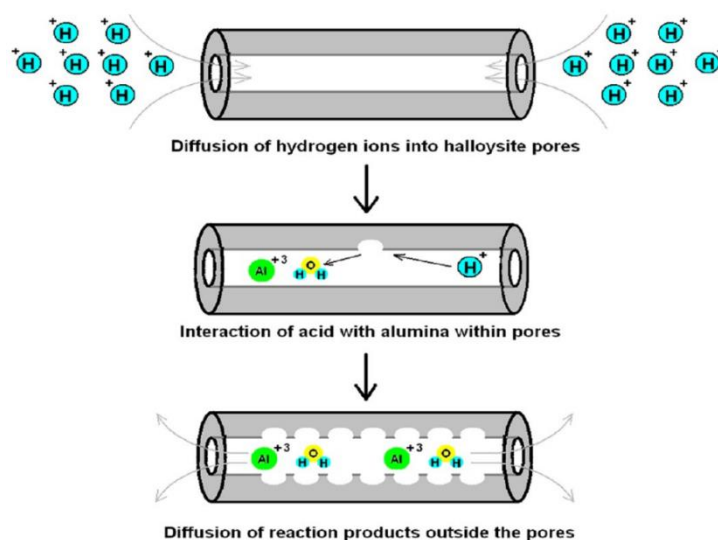
Fig. 7: Selective Acid Etching of Alumina Inner Layers within Halloysite Lumen.

TEM images (Fig. 8) of halloysite tubes acid etched at 50 °C showed the tubes geometry was intact. The outward diameters of the tubes remained constant, showing that etching occurs only in the interior lumen.
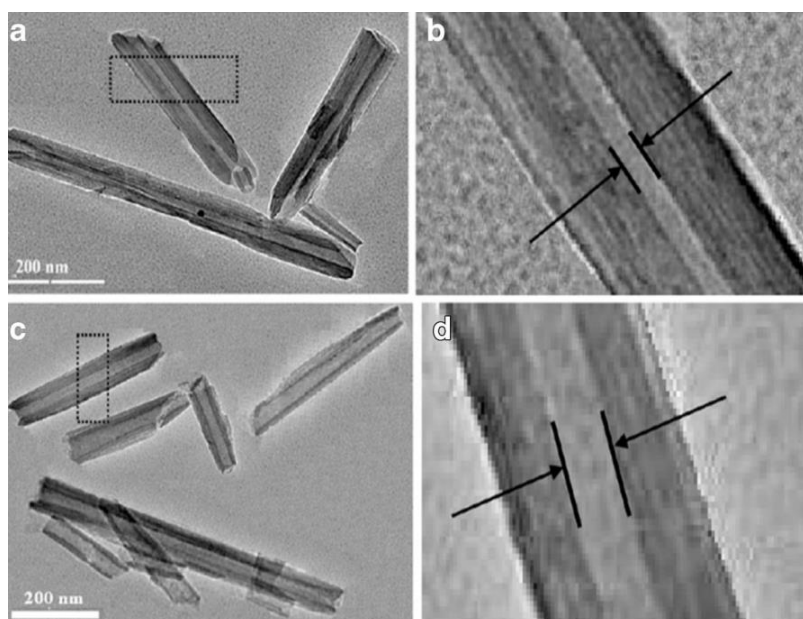
Fig. 8: Morphology of halloysite before acid etching (a, b), after the removal of 20% of alumina at 50 °C (c, d) [28]**.**

Following the complete removal of the alumina, Halloysite undergoes a series of stages leading to the transformation into porous nanorods: First, consistent wall thickness is lost; second, beyond 30-40% dealumination, tubes with varying wall thicknesses develop; and above 50-60% alumina loss, pores in the walls appear and proliferate with additional etching. The

tubular shape is lost and the lumen vanishes when alumina is completely removed. The finished product resembles porous nanorods coated with nanoparticles as presented in Figure 9. Remarkably, the specific surface area of the tubes experiences a more than sixfold increase after 80% dealumination.
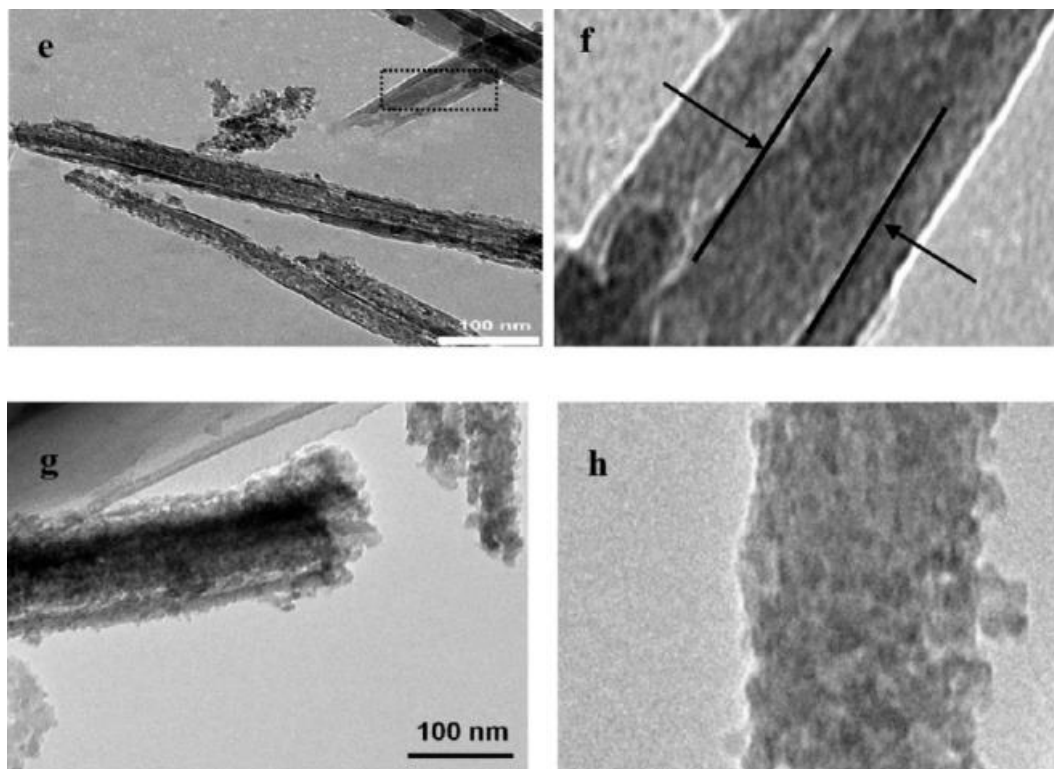
Fig. 9: TEM images of pristine halloysite after the removal 65% (e,f),
and 100% (g,h) of alumina via H_2SO_4 treatment at 50°C [28].

Lvov et al. [28]; validated Abdellah's finding by investigating the kinetics of sulfuric acid treatment of HNTs at various temperatures. The initial step expansion of the lumen proved beneficial in enhancing the loading capacity of the nanotubes. Experiments using corrosion inhibitors, such as benzotriazole, revealed that the loading efficiency of the expanded HNTs was four times that of the pristine one[28].

The research findings of Zhang et al. [27] indicate that acid treatment of HNTs with HCl up to a 12 M concentration had no influence on the halloysite crystal structure and, despite the tubes being shortened throughout the treatment, they preserved a tubular configuration. Because of the leaching of exchangeable cations and the weak electrostatic interaction between the drug-Al^{3+} complexes and the negative halloysite surface, the adsorption capacity of acid-treated halloysite for ofloxacin (selected as the model for biological applications) decreased slightly as

the HCl concentration increased. However, due to the decreased electrostatic interaction, acid-activation was beneficial for the release of all of the adsorbed ofloxacin. In terms of heat treatment, it was discovered that at temperatures below 400 °C, the HNTs showed no modification in crystal structure; however, increasing the temperature to 500 °C caused the HNTs to become amorphous owing to the de-hydroxylation of structural aluminol groups. Similar to the acid treatment, increasing the temperature reduced the adsorption ability of ofloxacin [29].   Liu with his team[30] found that the pretreatment of HNTs with piranha solution enhanced the silanization process [30]. The ability of the piranha solution to activate the surface of HNTs was superior compared to other frequently employed activation agents such as HCl or H_2O_2. The activated HNTs demonstrated increased responsiveness to APTES. Garcia-Garcia team [31]; reported that chemical treatment with strong acids such as sulfuric acid led to an aggressive etching on HNTs characterized by a highly porous structure and partial nanotube decomposition. The specific surface area of HNTs modified with sulfuric acid is of about 132.4 $m^2 \cdot g^{-1}$. On the contrary, the selective etching by using weak acids such as acetic and acrylic acid, led to a noticeable increase in the lumen in HNTs. In detail, the lumen diameter changed from 13.8 nm up to 18.4 and 17.1 nm for acetic and acrylic acid treatments, respectively.

6.2: Heat treatment

Yuan and his colleagues [32] sheds light on the profound structural, porosity, and surface reactivity alterations resulting from a meticulous investigation into the effects of calcination on nanotubular halloysites at varying temperatures. The thermal decomposition of halloysite unfolds through three distinct stages:

❖ **Dehydroxylation (500-900°C):** Within this phase, the original alignment of silica and alumina in the tetrahedral and octahedral sheets undergoes separation, leading to a loss of long-range order. This process primarily occurs as dehydroxylation takes place.

❖ **Formation of γ-Al₂O₃ (1000-1100°C):** In the subsequent stage, spanning from 1000 to 1100°C, the material undergoes a significant transformation, generating nanosized γ-Al2O3 particles in the range of 5 to 40 nm.

❖ **Mullite and Cristobalite Formation (1200-1400°C):** Moving further, the temperature range of 1200 to 1400°C marks the third step. During this interval, a mullite-like phase takes shape, eventually transitioning into the crystalline structure of cristobalite at 1400°C.

Beyond these structural shifts, the heating process penetrates the very core of the material. Remarkably, the most pronounced changes manifest within the material itself rather than externally. For instances where the heating temperature remains below 900°C, the distinctive tubular shape of the halloysite and its mesoporosity remain relatively unchanged. However, the pivotal juncture arrives at approximately 1000°C, initiating the breakdown of the tubular morphology. This results in the distortion of the nanotubes and a significant reduction in porosity. As temperatures surge, the tube ends undergo closure, ultimately leading to the collapse of the tubes. This intricate interplay between heat and the structural resilience within the nanotubes becomes evident**[33,34]**.

7: Halloysite Biocompatibility and toxicity

Mineral clays significance as a drug carrier has been extensively researched due to their rheological features, strong interaction, and high binding capacity with biopolymers. The physical-chemical qualities, such as size, shape, and surface charge density, which vary according to the kind of mineral clay and crystalline structure, are what make them intriguing [34].

7.1: *In Vitro* Evaluation of Halloysite Toxicity

The toxicity of this nanomaterial has been examined on several test species, ranging from bacteria to mammals, according to Vergaro et al. [35], and Massaro et al. [36]; It was discovered that pristine halloysite is practically harmless to living beings and does not damage the environment [37]**.**

7.2: *In Vivo* Biocompatibility of Halloysite Nanotubes

Halloysite toxicity *in vitro* investigations show a good level of biocompatibility; nevertheless, *in vivo*, toxicological assessments can reveal the mechanism of HNTs influence on the entire body. Kirimlioglu et al. [38] created brain-targeted gamma-aminobutyric acid-loaded nanotubes to treat epilepsy. They found evidence for brain delivery and seizure suppression in rat epilepsy models, as well as drug-sustained release and negligible cytotoxicity [39]. In fact, there are just few findings on the *in vivo* toxicity of HNTs to animals. Wang et al. [29]; calculated the liver toxicity of pure HNTs in mice through oral administration [40] they discovered that HNTs increased mouse development at the low dose (5 mg.kg^{-1}) with minimal liver damage, but decreased mouse growth at the intermediate (50 mg.kg^{-1}) and high (300 mg.kg^{-1}) levels. High HNT dosages also resulted in Al buildup in the liver and severe oxidative stress, resulting in hepatic dysfunction and histopathologic alterations [40].

8: Methods for loading drugs in HNTs

The contrasting chemical properties found on the inner and outer surfaces of halloysite nanotubes offer a versatile platform for accommodating a wide array of substances. These substances can engage with the nanotubes through a variety of mechanisms, such as adsorption, intercalation, and tubular entrapment, capitalizing on the nanotubes unique structure and chemistry.

a. Adsorption Mechanism:

This involves the drug, considered as the adsorbate solute, and the halloysite nanotubes, acting as the solid sorbate, being combined through stirring for an extended period, typically around 30 hours. This duration of mixing ensures the establishment of equilibrium between the drug in solution and the drug adsorbate. Following this, the adsorbate referred to as drug-loaded halloysite is separated via filtration and then dried at approximately 50°C in an oven. The equilibrium absorption process is typically visualized through an isotherm as demonstrated by Aguzzi et al. [41]**.** Lee and Kim [42] in 2002 discovered that the adsorption of a cationic surfactant from a solution onto the solid surface of layered clay minerals including halloysite and kaolinite adheres to the Langmuir isotherm. A separate study in 2012 by Krejčová et al**.**[43], used the same approach to demonstrate diclofenac sodium adsorption by halloysite. In this case, the conventional Langmuir sorption theory isn't always fully applicable, especially when employing low concentrations of the drug solution. The binding curve for diclofenac sodium demonstrated an unconventional shape, hinting at the occurrence of multilayer adsorption or two distinct, concentration-dependent adsorption [43].

b. Intercalation Process:

Halloysite nanotubes possess the ability to incorporate a variety of organic and inorganic substances within the gaps between their layers. During this procedure, molecules enter these interlayer spaces, allowing the layers to expand. Consequently, the distance between these layers, denoted as d001 spacing, increases. In particular, substances having functional groups such as -OH or -NH$_2$, such as glycerol, readily intercalate with halloysite nanotubes (HNTs).

In 2019, Cheng and her colleagues [44] found that dehydrated halloysite does not undergo intercalation processes. This is because intercalation requires the presence of interlayer water molecules. Lvov and Abdullayev [45] suggests that interlayer water molecules are crucial in facilitating intercalation between halloysite layers.

c. Tubular entrapment

Tubular entrapment also referred to as the vacuum method. This technique can be executed through two distinct approaches, notably, it holds paramount significance and is the most extensively employed approach for loading halloysite nanotubes (HNTs), as highlighted in works by Massaro et al. [36], Khalida et al. [46] and, Hemmatpour et al. [47]. Method one, an ample quantity of the drug solution is meticulously blended with HNTs that have been previously ground, sieved, and dried. Subsequently, a controlled vacuum is applied to the suspension. The appearance of bubbles on the suspension surface acts as a visual indication, indicating the effective removal of air from the lumens of individual HNTs. The vacuum is gently removed at this indication, allowing the lumens to be supplied with the medicinal solution. This critical procedure is repeated at least two to three times to ensure that the HNTs are properly penetrated with the medication solution, with no gaps remaining unfilled. Upon completing the vacuum cycles, the mixture undergoes centrifugation, prompting the separation of components. Following this, the supernatant liquid is meticulously removed. To conclude this method, the drug-impregnated HNTs undergo a drying process under the controlled environment of a vacuum. This comprehensive procedure ensures the precise and uniform encapsulation of the drug within the HNTs, priming them for further application (Fig. 11) [48].
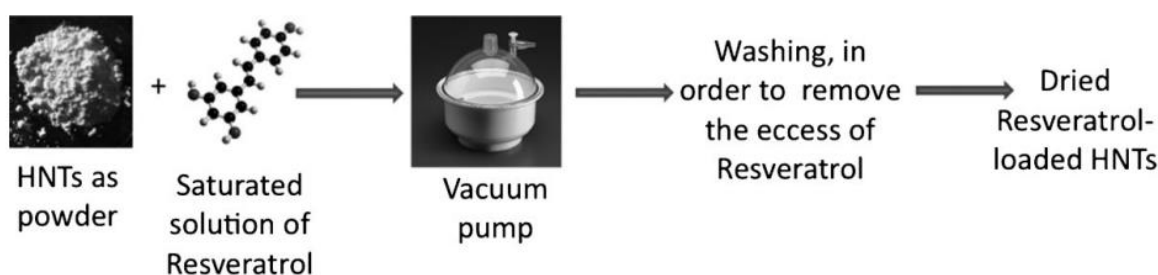
Fig. 11. Scheme of Resveratrol-loading inside HNTs using vacuum method [35].

In the context of the second approach likewise requires the use of a drug solution but in moderation. The drug solution is combined in equal parts with HNTs, resulting in a thick paste rather than a dispersion. The paste is placed in a vacuum, and air pressure is restored two to three times. The mixture is then vacuum-dried within the machine. This approach has several advantages, including the ability to immediately quantify the amount of medication administered to HNTs without evaluating the supernatant and no waste of drug or drug solution [49].

d. Interfacial coating of nanotubes and end-stopper formation:

The creation of artificial caps at the halloysite tube ends has improved control over the release rate of bioactive chemicals. Caps were generated by combining a leaking agent (A) and a complex forming agent it could be a precipitate or insoluble complex, formed by the reaction between the loaded agent and the sealed agent (B) from an external solution to generate thin films or precipitates that partially close the ends of nanotubes. As a result, the complex clogs the tube ends, and loaded agents become imprisoned in the tube lumen, causing the release period to expand from tens to hundreds of hours [50]. This approach was first proposed by Abdullayev and Lvov [51] throw the introduction of benzotriazole to HNT lumen and rinsed it with transition metal salts to form thin films that acted as stoppers (Fig. 12(B)). These stoppers suppressed the release of benzotriazole, but concentrated ammonia solution triggered its release by opening the stoppers [51].
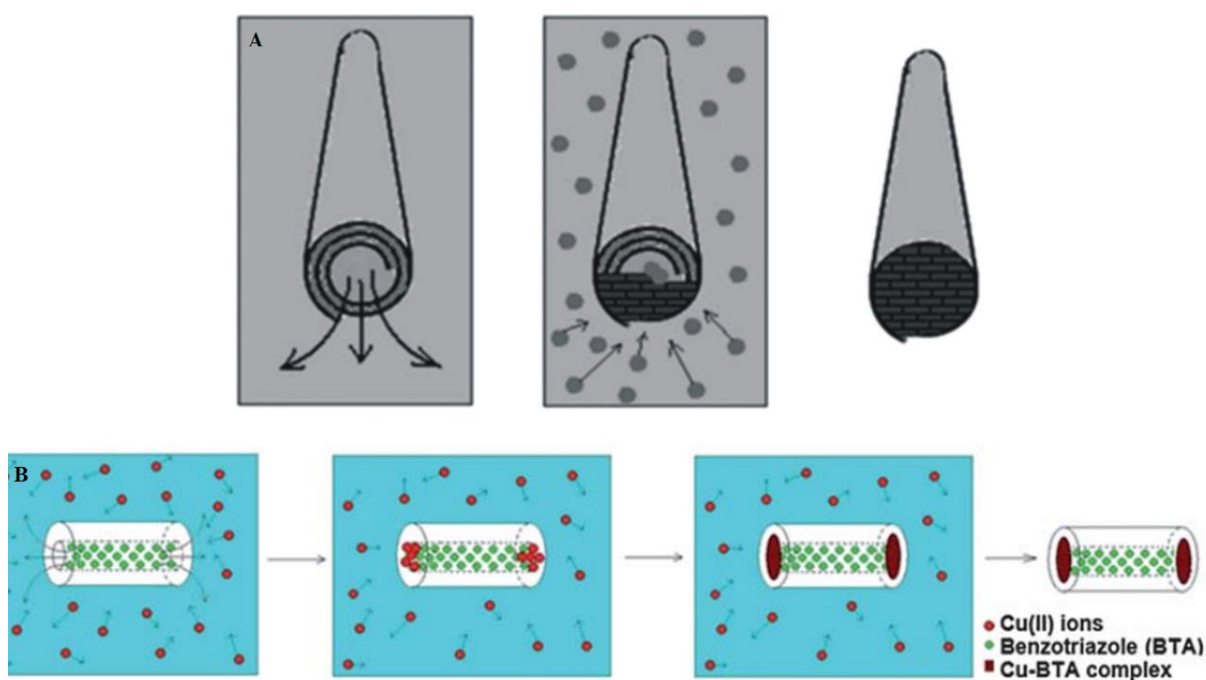
Fig. 12: (A) schematic presentation of the HNT tube stoppers formation [51]**.**
(B) Illustration of stopper formation at halloysite tube endings
by interaction of leaking benzotriazole and Cu(II) ions.

9: Halloysite Clay Nanotubes for Controlled Release

a. Protective Agents

With the variation of internal fluidic properties, the formation of nano-shells over the nanotubes, and by creation of smart caps at the tube ends it is possible to develop various means of controlling the rate of release. Thus, halloysite nanotubes can be used as a protective coating for the loading of agents for metal and plastic anticorrosion and biocide protection [49].

b. Entrapment of active agents (Tetracycline HCl, Khellin, and Nicotinamide Adenine Dinucleotide)

Halloysite nanotubes can entrap active agents within the core lumen and any empty spaces consisted of within the cylinder multilayered walls. Halloysite may hold and release both hydrophilic and hydrophobic substances and may be entrapped following appropriate pre-treatment of the clay to render it lipophilic. A standard release time of 2-5 hours was reported for hydrophilic molecules (such as Kellin, NAD, and tetracycline), whereas a release time of 5-20 hours was observed for molecules with limited solubility in water (such as furosemide, dexamethasone, and nifedipine) [49].

10: Special Delivery System

10.1: Halloysite Nanotube Application in Drug Delivery

When it comes to delivering medication over an extended period, halloysite nanotubes are a more affordable alternative to carbon nanotubes. These tubes have a larger surface area allowing for greater control of drug loading and elution profiles [52].

a. HNTs as a drug-delivery vehicle

Widespread research proved that HNTs are appropriate and efficient nanocarriers for drug delivery systems of chemically and biologically active molecules owing to their unique structural properties and lack of cell toxicity, which is an important requirement for their use in pharmaceutical and biomedical applications. The HNT cavity has been effectively used for protein and DNA encapsulation and controlled release [53], beside a functional molecule with antibacterial, anticorrosion and antioxidant activity **[55, 56]** .

Saturated drug solutions, coupled with cyclic vacuum pumping in/out, may easily load the HNT lumen. According to the HNT geometrical properties, an effective drug loading ranges between 5 and 10% of the nanotube weight, corresponding to full internal cavity filling **[52]**. In

general, there are four major mechanisms for nanoparticle internalization and which are presented in Figure 13: energy-independent membrane piercing by passive diffusion (a), caveolae-mediated endocytosis (b), phagocytosis (c), and clathrin-mediated endocytosis (d).
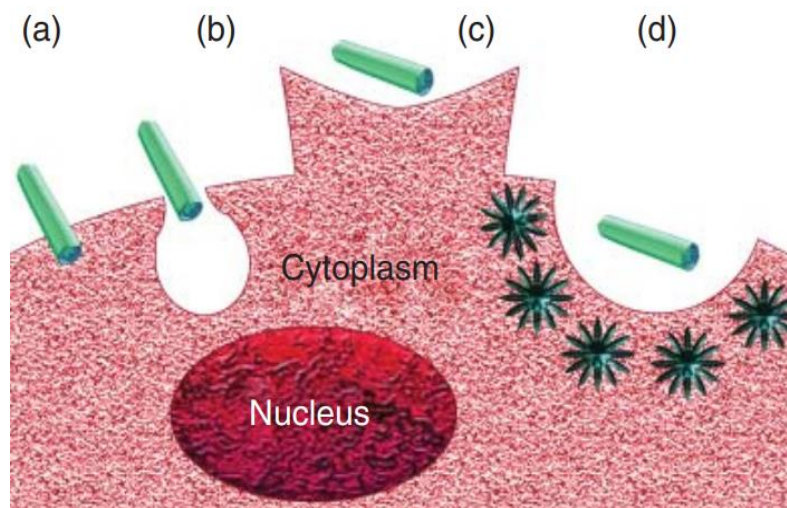
Fig. 13: Biological Pathways of Nanotube Internalization: Exploring (a) Membrane Piercing, (b) Caveolae-Mediated Endocytosis, (c) Phagocytosis,and (d) Clathrin-Mediated Endocytosis Mechanisms.

Several studies are based on the application of energy-dependent endocytosis. For example, Massaro et al. [56] and Liu et al. [57] suggested in their works that the internalization process of halloysite-drug complexes is most likely an endocytosis pathway. They proposed that nanotubular containers might be absorbed into the cytosol via endosomes, as indicated in Figure 14 [57].
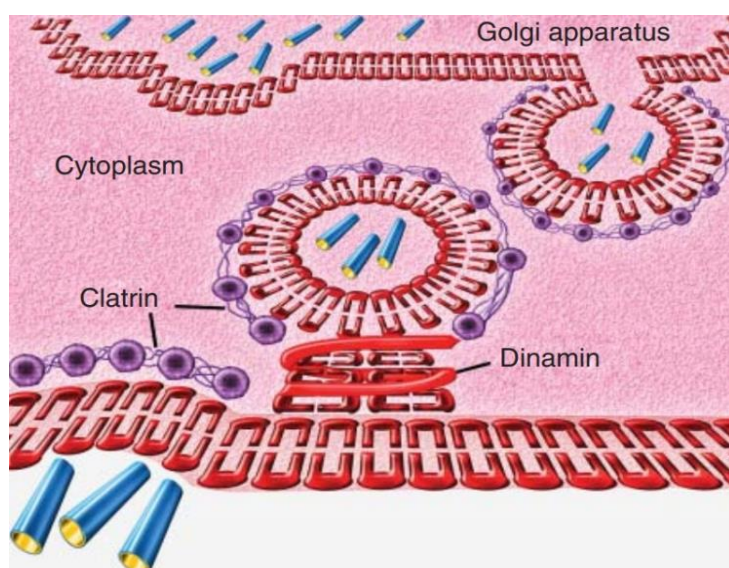
Fig. 14: Illustrating the Endocytosis Process of HNTs [57]

b. Wound care

Wound care solutions improve healing while lowering the risk of infection and damage. In situations of burn treatment, using halloysite as a medicine delivery mechanism can be quite effective. Drugs inserted within halloysite tubes and implanted in the base layer of a bandage can be released slowly over time. This extends the length of medicinal efficacy and minimizes the frequency with which bandages must be replaced [58]**.**

c. Transdermal Patches

When medicines are loaded into halloysite nanotubes, it results in a more regulated elution profile. This has several benefits such as low initial concentrations which eliminates the high initial delivery rate and increases safety, especially with drugs like stimulants or hormones. It also ensures uniform drug delivery, cost efficiency, and less drug loading per patch. Currently, a lot of the drug gets discarded when the patch is removed, but with this method, there will be less wastage [12].

d. HNTs for Cosmetics application

i. Skin cleanser agent

When used alone, the adsorptive nature of the HNT acts as a hypoallergenic skin cleanser capable of eliminating undesirable pollutants and aesthetically unpleasing oils. The clay acts as a mild exfoliant, removing dead skin cells from the surface and leaving the skin looking fresh, youthful, and healthy [59]**.**

ii. Nanotubes in personal care
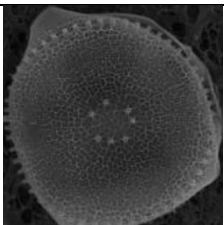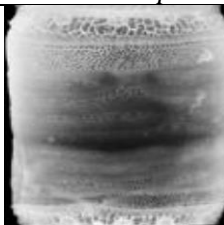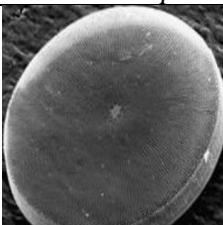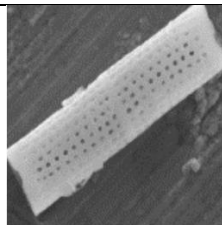
Halloysite nanotubes used in personal care formulae will be subjected to safety and effectiveness studies. Natural nanocontainer for the regulated administration of glycerol as a moisturizing agent for glycerol loading and longer release in cosmetic applications [59]**.**

11. Diatom Diversity: Exploring Structural Features Across Species

Diatomite, a sedimentary fossil material, predominantly comprises diatom frustules siliceous skeletons derived from single-cell photosynthetic algae prevalent in aquatic ecosystems. These frustules, distinguished by their richness in amorphous silica, exhibit a noteworthy specific surface area of up to 200 m²/g[60]. The taxonomic spectrum encompasses approximately 110,000 species, characterized by variations in size (ranging from 2 μm to 2 mm) and morphology [61].

Renowned for cost-effectiveness, abundance, biocompatibility, non-toxicity, and thermal stability, diatomite finds applications from filtration to pharmaceutics [62]. Geologically derived diatomite, comprising 70 to 90% silica alongside other constituents, undergoes meticulous purification processes. Studies, such as those by Fuhrmann et al. [63], Stefano et al. [64], Delalatet al.[65], and Wee et al.[66], explore varied diatom species structural complexities, revealing unique nanostructures and taxonomy categorizations. For instance, Fuhrmann et al. [63] detail the structural features of Coscinodiscus granii, while Stefano et al. [64] unveil unique structures in Mast ogloiaschmidti. Delalat et al. [65]; provide a comprehensive view of Thalassiosirapseudonana sp.'s biosilica, emphasizing pore size range and mechanical strength. Wee et al. [66] shed light on the distinctive traits of Thalassiosiratenera sp., including pore diameter variations. Table 1 summarizes the diameters of various diatom species, relevant to drug delivery applications.

Table 2: Diameter of the diatom species that is relevant in the targeted drug delivery application.

Diatom species	*T. Weissflogiisp*	*Thalassiosirapseudonana sp*	*Coscinodiscus wailesiisp*	*Aulacoseir a sp*
Structural morphology				
Diameter	29 μm	20nm to 2 μm	150 μm	4-6 μm

11.1. Surface Modification of Diatoms:

The inherently adaptable surface of refined diatomaceous earth (DE), primarily composed of silicon dioxide building blocks, offers a captivating prospect for tailoring its properties and creating bespoke bioengineered materials suitable for biomedical applications [67].

The silica surface content exhibits hydroxyl (OH) groups, easily amendable for functionalization through established chemical modification strategies. Over the last decade, significant strides have been made in the surface modification of diatom structures, drawing inspiration from methodologies developed for synthetic silica particles. These diverse approaches encompass the application of organic monolayers, polymers, proteins, and coatings with metal and inorganic oxide layers [67].

The reactive silanol (SiOH) groups present on the diatom surface are highly responsive to functionalization with various reactive species (e.g., NH_2, COOH, SH, and CHO), providing robust coupling points for immobilizing a spectrum of biological or chemical moieties, including drugs, enzymes, proteins, antibodies, aptamers, DNA, and sensing probes [68].

Silanization, a process involving the creation of Si-O-Si covalent bonds, is commonly employed to stabilize the attachment of diverse active moieties on diatom surfaces **[2,7]**. Figure 2 illustrates a prevalent surface functionalization technique utilizing organosilanes to generate a self-assembled layer through Si-O-Si covalent linkages [69].

Modifying the surface with specific chemical terminal groups facilitates the immobilization of a variety of biomolecules, such as antibodies and nucleotides, thereby enhancing drug loading for applications in drug delivery and biosensing. Two widely embraced approaches for immobilizing active biomolecules onto the chemically modified DE surface include non-covalent interactions, encompassing physical adsorption and other weak interactions, and covalent immobilization, characterized by robust covalent binding. Challenges associated with non-covalent binding, particularly its reliance on solution conditions such as pH or changes in ionic strength, contribute to lower stability. Consequently, for real-life applications, the preference often leans towards the covalent binding of biomolecules to the diatom surface due to its enhanced stability and reproducibility [62].
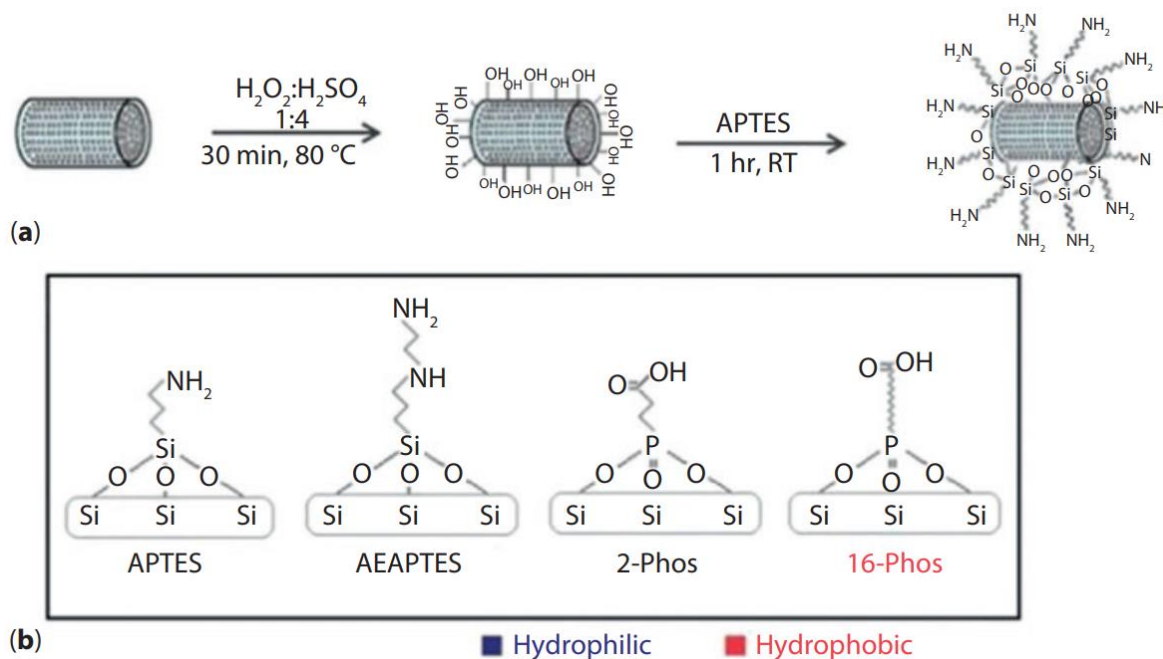
Fig. 15. a) Scheme representing surface functionalization of diatoms using
3-Aminopropyl   triethoxysilane (APTES) [67].
b) Schematic illustration of diatoms functionalization using organosilans
and phosphonic acids with hydrophobic and hydrophilic properties.

11.2.   Diatoms Applications as Drug Carriers

One of the most challenging assignments in drug delivery (DD) is to deliver therapeutic drugs to specified parts of the human body (i.e., sick tissues) with minimal side effects on healthy tissues. Aw et al. [70]; elucidate a compelling paradigm, showcasing the utilization of diatom species (Aulacoseira sp.) sans surface modification for the conveyance of indomethacin nestled within the pores of pristine diatoms (Fig. 2). The narrative unfolds with a burst release of 65-70% in 6 hours, ascribed to a diffusion mechanism liberating the medication from the diatom's surface. This burst phenomenon finds potential roots in the interaction dynamics between silica surfaces and drug molecules. The ensuing gradual release over two weeks is expounded through the lens of zero-order kinetics.
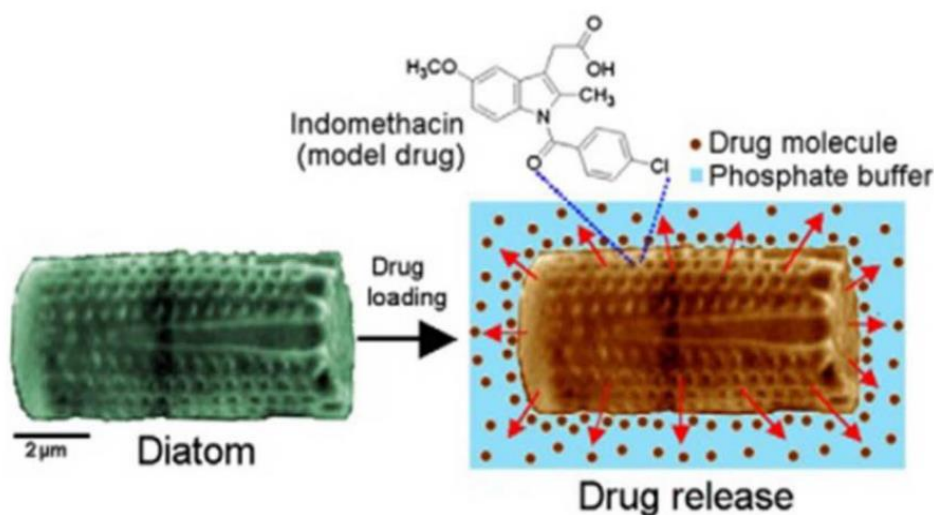
Fig. 16: Schematic elucidating the indomethacin drug release mechanism
from porous diatom micro shells [70]**.**

Bariana et al**.** [71] Clearly demonstrate the augmentation of diatom surfaces functionalities via organosilanes and phosphonic acid. Post successful surface modification, they navigate the encapsulation landscape with two distinct drugs—hydrophobic indomethacin and hydrophilic gentamicin. Hydrophilic surfaces, such as amino-rich APTES, epoxy-rich GPTMS, and carboxyl-rich 2-CEPA, manifest enhanced loading of the hydrophobic drug, coupled with a notably controlled release compared to unaltered diatoms. In contrast, hydrophobic surface-modified diatoms with 16-PHA, mPEG-Silane, and OTS exhibit diminished drug loading capacity and swift release dynamics. Gentamicin, subject to hydrophobic surface modification with 16-PHA, displays improved drug loading and controlled release, while hydrophilic modification with 2CEPA and APTES yields a lesser drug loading with a briefer release profile (Fig. 3).
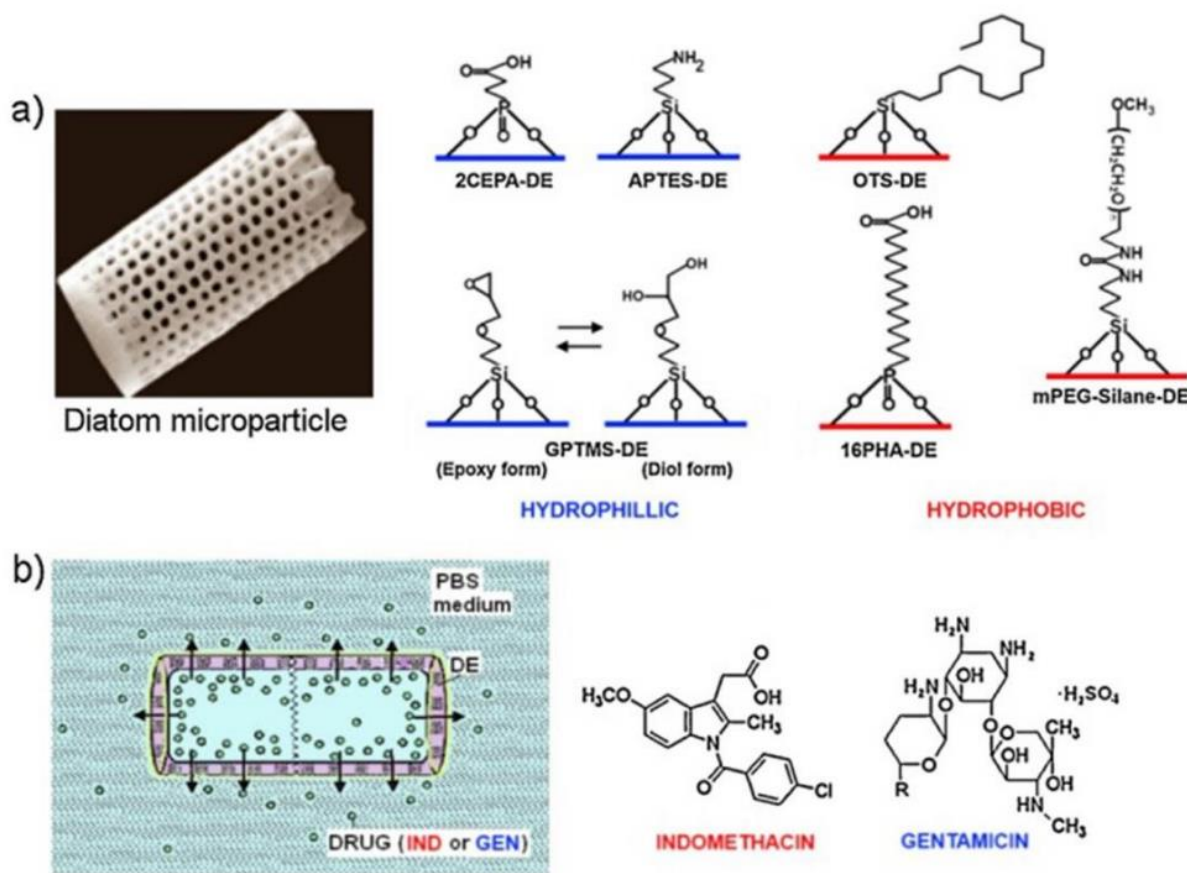
Fig. 17. a: Diatom microparticle structure and surface functionalization to introduce
hydrophobic and hydrophilic features on diatom surfaces modulating
medication release rate.
b: Drug release mechanism for two distinct medications [71].

Zhang et al. [72]; delve into the intricacies of diatom cytotoxicity and their impact on orally
delivered drug permeation. Employing gastrointestinal disease drugs, mesalamine, and
prednisone, diatoms exhibit minimal toxicity for colon cancer cells even at high concentrations
(1000 µg/mL). Extended-release in simulated gastric conditions for both drugs underscores
diatoms potential in enhancing drug permeability across Caco-2/HT-29 co-culture monolayers
(Fig. 4).
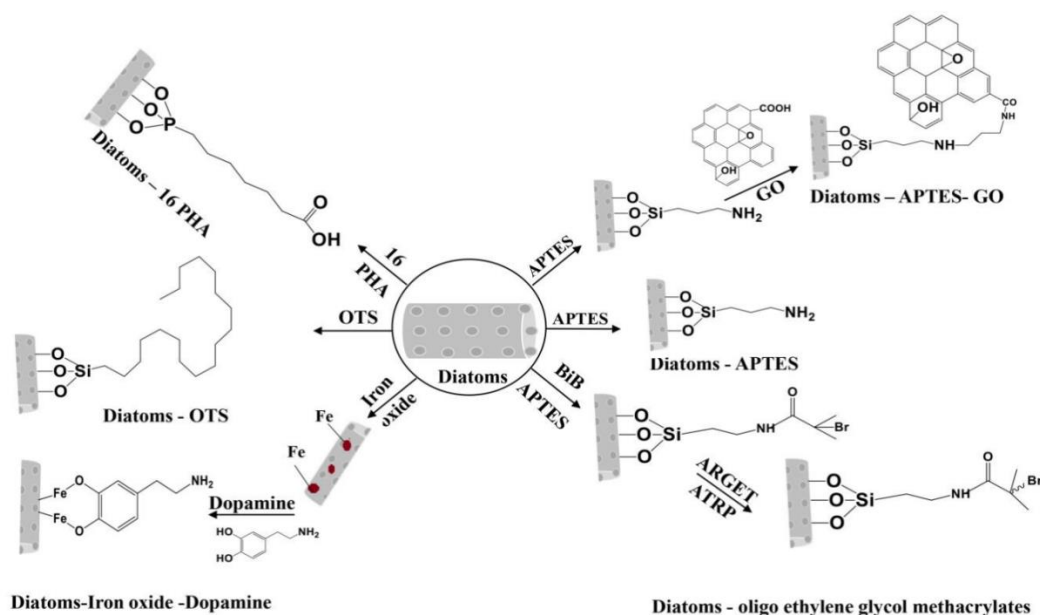
Fig. 18: Various surface modification strategies for diatoms (Aulacoseira sp.) [72]**.**

Vasani et al. [73]; in a sophisticated approach, employ atom transfer radical polymerization (ARGET-ATRP) activators to polymerize a thermos-responsive oligo(ethylene glycol) methacrylate copolymer onto diatom frustules. The resultant matrix facilitates loading and temperature-dependent pharmacological experiments with Levofloxacin. Drug release characteristics explored both above and below the polymer's lower critical solution temperature (LCST), are encapsulated in Figure 5.
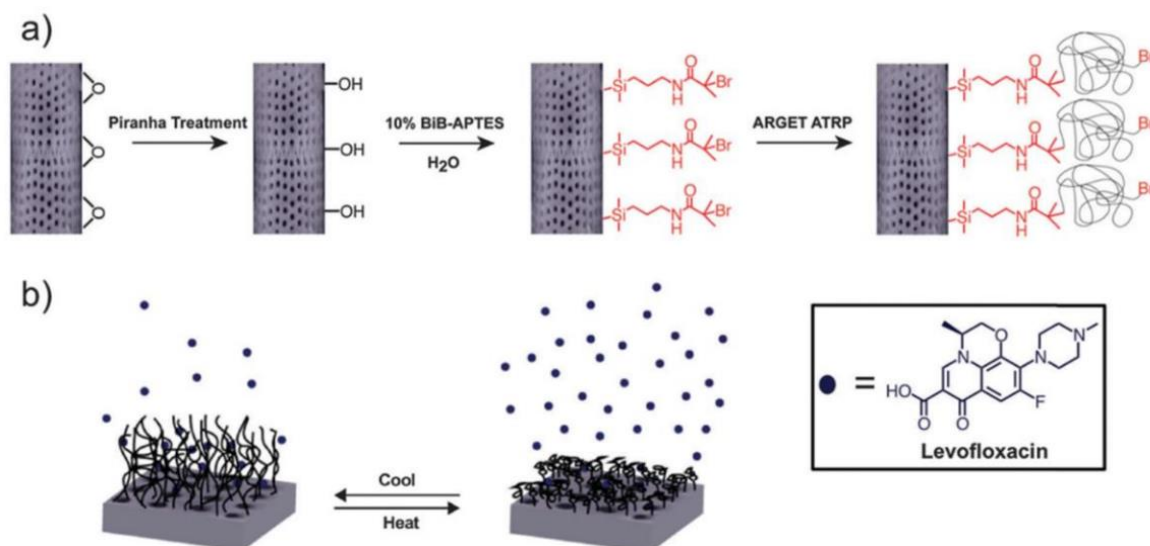
Fig. 19. a) Surface functionalization of diatom biosilica microcapsules.
b) Drug release from thermo-responsive polymer-grafted onto
bio-silica frustules [73].

In addition to chemically modifying diatoms' silica surface for stable and high drug loading, studies accentuate the advantages of incorporating polymers. Terracciano et al. [74]; employ a coating of polyethylene glycol (PEG) and cell-penetrating peptide (CPP) on diatom nanoparticles (DNPs) for delivering the anticancer drug sorafenib, as illustrated in Figure 6.
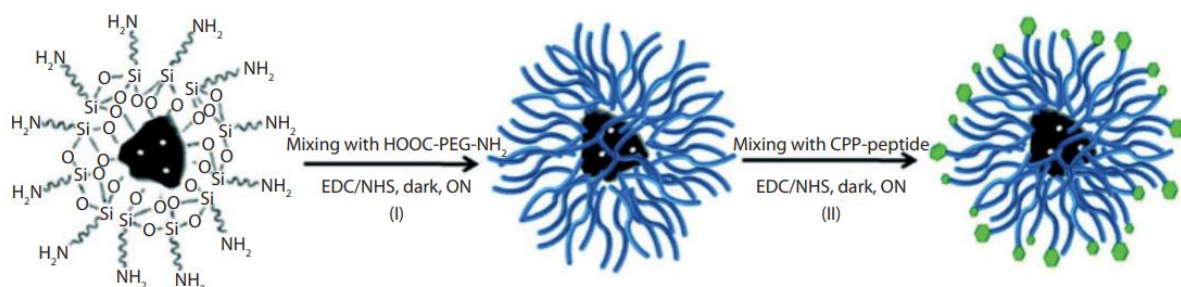
Fig. 20. Schematic illustration of the functionalization of DNPs [74].

Reaction I, PEGylation of DNPs-APT (I) via EDC/NHS, at RT with stirring ON. Reaction II, CPP-peptide bioconjugation of DNPs-APT-PEG via EDC/NHS, at RT with stirring ON. The covalent interaction between the NPs' surface and the biomolecules produced by EDC/NHS chemistry lies at the heart of dual biofunctionalization [74].

References

[1]   M. Elsabahy, K.L. Wooley, Design of polymeric nanoparticles for biomedical delivery applications, Chem. Soc. Rev. 41 (2012) 2545–2561. https://doi.org/10.1039/C2CS15327K.

[2]   M. Karimi, A. Ghasemi, P.S. Zangabad, R. Rahighi, S.M.M. Basri, H. Mirshekari, M. Amiri, Z.S. Pishabad, A. Aslani, M. Bozorgomid, Smart micro/nanoparticles in stimulus-responsive drug/gene delivery systems, Chem. Soc. Rev. 45 (2016) 1457–1501.

[3]   H. Jin, D.A. Heller, M.S. Strano, Single-Particle Tracking of Endocytosis and Exocytosis of Single-Walled Carbon Nanotubes in NIH-3T3 Cells, Nano Lett. 8 (2008) 1577–1585. https://doi.org/10.1021/nl072969s.

[4]   K. Ariga, Q. Ji, W. Nakanishi, J.P. Hill, M. Aono, Nanoarchitectonics: A new materials horizon for nanotechnology, Mater. Horiz. 2 (2015) 406–413.

[5]   T.A. Hilder, J.M. Hill, Modeling the Loading and Unloading of Drugs into Nanotubes, Small 5 (2009) 300–308. https://doi.org/10.1002/smll.200800321.

[6]   R. Yendluri, D.P. Otto, M.M. De Villiers, V. Vinokurov, Y.M. Lvov, Application of halloysite clay nanotubes as a pharmaceutical excipient, Int. J. Pharm. 521 (2017) 267–273.

[7]   V. Bertolino, G. Cavallaro, G. Lazzara, S. Milioto, F. Parisi, Biopolymer-Targeted Adsorption onto Halloysite Nanotubes in Aqueous Media, Langmuir 33 (2017) 3317–3323. https://doi.org/10.1021/acs.langmuir.7b00600.

[8]   P.E. Askenasy, J.B. Dixon, T.R. McKee, Spheroidal Halloysite in a Guatemalan Soil, Soil Sci. Soc. Am. J. 37 (1973) 799–803. https://doi.org/10.2136/sssaj1973.03615995003700050045x.

[9]   Z.X. Teo, W.S. Chow, Impact, Thermal, and Morphological Properties of Poly(Lactic Acid)/Poly(Methyl Methacrylate)/Halloysite Nanotube Nanocomposites, Polym.-Plast. Technol. Eng. 55 (2016) 1474–1480. https://doi.org/10.1080/03602559.2015.1132464.

[10] N.G. Veerabadran, R.R. Price, Y.M. Lvov, Clay nanotubes for encapsulation and sustained release of drugs, Nano 2 (2007) 115–120.

[11] E. Joussein, S. Petit, J. Churchman, B. Theng, D. Righi, B. Delvaux, Halloysite clay minerals—a review, Clay Miner. 40 (2005) 383–426.

[12] G. Cavallaro, G. Lazzara, S. Milioto, F. Parisi, V. Sanzillo, Modified Halloysite Nanotubes: Nanoarchitectures for Enhancing the Capture of Oils from Vapor and Liquid Phases, ACS Appl. Mater. Interfaces 6 (2014) 606–612. https://doi.org/10.1021/am404693r.

[13] V. Bugatti, A. Sorrentino, G. Gorrasi, Encapsulation of Lysozyme into halloysite nanotubes and dispersion in PLA: Structural and physical properties and controlled release analysis, Eur. Polym. J. 93 (2017) 495–506.

[14] M.T. Albdiry, B.F. Yousif, Role of silanized halloysite nanotubes on structural, mechanical properties and fracture toughness of thermoset nanocomposites, Mater. Des. 57 (2014) 279–288.

[15] I. Pereira, M. Saleh, C. Nunes, S. Reis, F. Veiga, A.C. Paiva-Santos, Preclinical developments of natural-occurring halloysite clay nanotubes in cancer therapeutics, Adv. Colloid Interface Sci. 291 (2021) 102406.

[16] E. Abdullayev, Y. Lvov, Halloysite clay nanotubes as a ceramic "skeleton" for functional biopolymer composites with sustained drug release, J. Mater. Chem. B 1 (2013) 2894–2903.

[17] M. Massaro, G. Lazzara, R. Noto, S. Riela, Halloysite nanotubes: a green resource for materials and life sciences, Rendiconti Lincei Sci. Fis. E Nat. 31 (2020) 213–221. https://doi.org/10.1007/s12210-020-00886-x.

[18] W. Chow, W. Tham, P. Seow, Effects of maleated-PLA compatibilizer on the properties of poly(lactic acid)/halloysite clay composites, J. Thermoplast. Compos. Mater. 26 (2013) 1349–1363. https://doi.org/10.1177/0892705712439569.

[19] G.B. Fisher, P.C. Ryan, The smectite-to-disordered kaolinite transition in a tropical soil chronosequence, Pacific Coast, Costa Rica, Clays Clay Miner. 54 (2006) 571–586.

[20] P. Yuan, P.D. Southon, Z. Liu, M.E.R. Green, J.M. Hook, S.J. Antill, C.J. Kepert, Functionalization of Halloysite Clay Nanotubes by Grafting with γ-Aminopropyltriethoxysilane, J. Phys. Chem. C 112 (2008) 15742–15751. https://doi.org/10.1021/jp805657t.

[21] D. Tan, P. Yuan, D. Liu, P. Du, Surface modifications of halloysite, in: Dev. Clay Sci., Elsevier, 2016: pp. 167–201.

[22] F. Bergaya, G. Lagaly, Purification of natural clays, in: Dev. Clay Sci., Elsevier, 2013: pp. 213–221.

[23] S. Jia, M. Fan, Silanization of heat-treated halloysite nanotubes using γ-aminopropyltriethoxysilane, Appl. Clay Sci. 180 (2019) 105204.

[24] Y. Song, P. Yuan, P. Du, L. Deng, Y. Wei, D. Liu, X. Zhong, J. Zhou, A novel halloysite–CeOx nanohybrid for efficient arsenic removal, Appl. Clay Sci. 186 (2020) 105450.

[25] K. Ramadass, G. Singh, K.S. Lakhi, M.R. Benzigar, J.-H. Yang, S. Kim, A.M. Almajid, T. Belperio, A. Vinu, Halloysite nanotubes: Novel and eco-friendly adsorbents for high-pressure CO2 capture, Microporous Mesoporous Mater. 277 (2019) 229–236.

[26] R.D. White, D.V. Bavykin, F.C. Walsh, The stability of halloysite nanotubes in acidic and alkaline aqueous suspensions, Nanotechnology 23 (2012) 065705.

[27] A.-B. Zhang, L. Pan, H.-Y. Zhang, S.-T. Liu, Y. Ye, M.-S. Xia, X.-G. Chen, Effects of acid treatment on the physico-chemical and pore characteristics of halloysite, Colloids Surf. Physicochem. Eng. Asp. 396 (2012) 182–188.

[28] E. Abdullayev, A. Joshi, W. Wei, Y. Zhao, Y. Lvov, Enlargement of Halloysite Clay Nanotube Lumen by Selective Etching of Aluminum Oxide, ACS Nano 6 (2012) 7216–7226. https://doi.org/10.1021/nn302328x.

[29] Q. Wang, J. Zhang, Y. Zheng, A. Wang, Adsorption and release of ofloxacin from acid- and heat-treated halloysite, Colloids Surf. B Biointerfaces 113 (2014) 51–58. https://doi.org/10.1016/j.colsurfb.2013.08.036.

[30] P. Sun, G. Liu, D. Lv, X. Dong, J. Wu, D. Wang, Effective activation of halloysite nanotubes by piranha solution for amine modification via silane coupling chemistry, RSC Adv. 5 (2015) 52916–52925. https://doi.org/10.1039/C5RA04444H.

[31] D. Garcia-Garcia, J.M. Ferri, L. Ripoll, M. Hidalgo, J. López-Martínez, R. Balart, Characterization of selectively etched halloysite nanotubes by acid treatment, in: Appl. Surf. Sci., Elsevier, 2017: pp. 616–625. https://doi.org/10.1016/j.apsusc.2017.06.104.

[32] P. Yuan, D. Tan, F. Annabi-Bergaya, W. Yan, M. Fan, D. Liu, H. He, Changes in Structure, Morphology, Porosity, and Surface Activity of Mesoporous Halloysite Nanotubes Under Heating, Clays Clay Miner. 60 (2012) 561–573. https://doi.org/10.1346/CCMN.2012.0600602.

[33] F. Bergaya, P. Dion, J.-F. Alcover, C. Clinard, D. Tchoubar, TEM study of kaolinite thermal decomposition by controlled-rate thermal analysis, J. Mater. Sci. 31 (1996) 5069–5075. https://doi.org/10.1007/BF00355907.

[34] M. Mousa, N.D. Evans, R.O.C. Oreffo, J.I. Dawson, Clay nanoparticles for regenerative medicine and biomaterial design: A review of clay bioactivity, Biomaterials 159 (2018) 204–214. https://doi.org/10.1016/j.biomaterials.2017.12.024.

[35] V. Vergaro, Y.M. Lvov, S. Leporatti, Halloysite clay nanotubes for resveratrol delivery to cancer cells, Macromol. Biosci. 12 (2012) 1265–1271. https://doi.org/10.1002/mabi.201200121.

[36] M. Massaro, G. Cavallaro, C.G. Colletti, G. Lazzara, S. Milioto, R. Noto, S. Riela, Chemical modification of halloysite nanotubes for controlled loading and release., J. Mater. Chem. B 6 (2018) 3415–3433. https://doi.org/10.1039/c8tb00543e.

[37] G. Cavallaro, S. Milioto, G. Lazzara, Halloysite Nanotubes: Interfacial Properties and Applications in Cultural Heritage, Langmuir 36 (2020) 3677–3689. https://doi.org/10.1021/acs.langmuir.0c00573.

[38] B. Rath, F.A. Qais, R. Patro, S. Mohapatra, T. Sharma, Design, synthesis and molecular modeling studies of novel mesalamine linked coumarin for treatment of inflammatory bowel disease, Bioorg. Med. Chem. Lett. 41 (2021) 128029.

[39] G. Yurtdaş Kırımlıoğlu, Y. Yazan, K. Erol, C. Cengelli Unel, Gamma-Aminobutyric Acid Loaded Halloysite Nanotubes and In Vitro-In Vivo Evaluation for Brain Delivery, Int. J. Pharm. 495 (2015). https://doi.org/10.1016/j.ijpharm.2015.08.087.

[40] Y. Toledano-Magaña, L. Flores-Santos, G. Montes de Oca, A. González-Montiel, J.-C. García-Ramos, C. Mora, N.-A. Saavedra-Ávila, M. Gudiño-Zayas, L.-C. González-Ramírez, J.P. Laclette, J.C. Carrero, Toxicological Evaluations in Macrophages and Mice Acutely and Chronically Exposed to Halloysite Clay Nanotubes Functionalized with Polystyrene, ACS Omega 6 (2021) 29882–29892. https://doi.org/10.1021/acsomega.1c04367.

[41] C. Aguzzi, C. Viseras, P. Cerezo, I. Salcedo, R. Sánchez-Espejo, C. Valenzuela, Release kinetics of 5-aminosalicylic acid from halloysite, Colloids Surf. B Biointerfaces 105 (2013) 75–80. https://doi.org/10.1016/j.colsurfb.2012.12.041.

[42] S.Y. Lee, S.J. Kim, Adsorption of naphthalene by HDTMA modified kaolinite and halloysite, Appl. Clay Sci. 22 (2002) 55–63. https://doi.org/10.1016/S0169-1317(02)00113-8.

[43] K. Krejčová, P.B. Deasy, M. Rabišková, Diclofenac sodium entrapment and release from halloysite nanotubules, Ceska Slov. Farm. Cas. Ceske Farm. Spolecnosti Slov. Farm. Spolecnosti 62 (2013) 28–34.

[44] Z.-L. Cheng, B.-C. Cao, Z. Liu, Study on intercalation in layered structure of halloysite nanotubes (HNTs), Micro Nano Lett. 14 (2019) 585–589. https://doi.org/10.1049/mnl.2018.5625.

[45] Y. Lvov, E. Abdullayev, Functional polymer–clay nanotube composites with sustained release of chemical agents, Prog. Polym. Sci. 38 (2013) 1690–1719. https://doi.org/10.1016/j.progpolymsci.2013.05.009.

[46] K. Fakhruddin, R. Hassan, M.U.A. Khan, S.N. Allisha, S.I.A. Razak, M.H. Zreaqat, H.F.M. Latip, M.N. Jamaludin, A. Hassan, Halloysite nanotubes and halloysite-based composites for biomedical applications, Arab. J. Chem. 14 (2021) 103294. https://doi.org/10.1016/j.arabjc.2021.103294.

[47] H. Hemmatpour, Functionalization of Halloysite Nanotubes for Environmental and Drug Delivery Applications, University of Groningen, [Groningen], 2022. https://doi.org/10.33612/diss.204280083.

[48] E. Abdullayev, Y. Lvov, Halloysite for Controllable Loading and Release, in: Dev. Clay Sci., 2016: pp. 554–605. https://doi.org/10.1016/B978-0-08-100293-3.00022-4.

[49] R.R. Price, B.P. Gaber, Y. Lvov, In-vitro release characteristics of tetracycline HCl, khellin and nicotinamide adenine dineculeotide from halloysite; a cylindrical mineral, J. Microencapsul. 18 (2001) 713–722. https://doi.org/10.1080/02652040010019532.

[50] A. Joshi, E. Abdullayev, A. Vasiliev, O. Volkova, Y. Lvov, Interfacial Modification of Clay Nanotubes for the Sustained Release of Corrosion Inhibitors, Langmuir 29 (2013) 7439–7448. https://doi.org/10.1021/la3044973.

[51] E. Abdullayev, Y. Lvov, Clay nanotubes for corrosion inhibitor encapsulation: Release control with end stoppers, J Mater Chem 20 (2010) 6681–6687. https://doi.org/10.1039/C0JM00810A.

[52] Y.M. Lvov, M.M. DeVilliers, R.F. Fakhrullin, The application of halloysite tubule nanoclay in drug delivery, Expert Opin. Drug Deliv. 13 (2016) 977–986. https://doi.org/10.1517/17425247.2016.1169271.

[53] Y. Lee, G.-E. Jung, S.-J. Cho, K. Geckeler, F. Harald, Cellular interactions of doxorubicin-loaded DNA-modified halloysite nanotubes, Nanoscale 5 (2013). https://doi.org/10.1039/c3nr02665e.

[54] R.F. Fakhrullin, A. Tursunbayeva, V.S. Portnov, Yu.M. L'vov, Ceramic nanotubes for polymer composites with stable anticorrosion properties, Crystallogr. Rep. 59 (2014) 1107–1113. https://doi.org/10.1134/S1063774514070104.

[55] M. Massaro, S. Riela, S. Guernelli, F. Parisi, G. Lazzara, A. Baschieri, L. Valgimigli, R. Amorati, A synergic nanoantioxidant based on covalently modified halloysite–trolox nanotubes with intra-lumen loaded quercetin, J Mater Chem B 4 (2016). https://doi.org/10.1039/C6TB00126B.

[56] M. Massaro, S. Riela, C. Baiamonte, J.L.J. Blanco, C. Giordano, P.L. Meo, S. Milioto, R. Noto, F. Parisi, G. Pizzolanti, G. Lazzara, Dual drug-loaded halloysite hybrid-based glycocluster for sustained release of hydrophobic molecules, RSC Adv. 6 (2016) 87935–87944. https://doi.org/10.1039/C6RA14657K.

[57] H.-Y. Liu, L. Du, Y.-T. Zhao, W.-Q. Tian, In Vitro Hemocompatibility and Cytotoxicity Evaluation of Halloysite Nanotubes for Biomedical Application, J. Nanomater. 2015 (2015) e685323. https://doi.org/10.1155/2015/685323.

[58] M. Liu, Y. Shen, P. Ao, L. Dai, Z. Liu, C. Zhou, The improvement of hemostatic and wound healing property of chitosan by halloysite nanotubes, RSC Adv. 4 (2014) 23540–23553. https://doi.org/10.1039/C4RA02189D.

[59] Y.J. Suh, D.S. Kil, K.S. Chung, E. Abdullayev, Y.M. Lvov, D. Mongayt, Natural nanocontainer for the controlled delivery of glycerol as a moisturizing agent, J. Nanosci. Nanotechnol. 11 (2011) 661–665. https://doi.org/10.1166/jnn.2011.3194.

[60] O. Şan, R. Gören, C. Özgür, Purification of diatomite powder by acid leaching for use in fabrication of porous ceramics, Int. J. Miner. Process. 93 (2009) 6–10. https://doi.org/10.1016/j.minpro.2009.04.007.

[61] Y. Wang, J. Cai, Y. Jiang, X. Jiang, D. Zhang, Preparation of biosilica structures from frustules of diatoms and their applications: current state and perspectives, Appl. Microbiol. Biotechnol. 97 (2013) 453–460. https://doi.org/10.1007/s00253-012-4568-0.

[62] D. Losic, Y. Yu, M.S. Aw, S. Simovic, B. Thierry, J. Addai-Mensah, Surface functionalisation of diatoms with dopamine modified iron-oxide nanoparticles: toward magnetically guided drug microcarriers with biologically derived morphologies, Chem. Commun. 46 (2010) 6323–6325. https://doi.org/10.1039/C0CC01305F.

[63] T. Fuhrmann, S. Landwehr, M. El Rharbi-Kucki, M. Sumper, Diatoms as living photonic crystals, Appl. Phys. B 78 (2004) 257–260. https://doi.org/10.1007/s00340-004-1419-4.

[64] M. De Stefano, L. De Stefano, Nanostructures in Diatom Frustules: Functional Morphology of Valvocopulae in Cocconeidacean Monoraphid Taxa, J. Nanosci. Nanotechnol. 5 (2005) 15–24. https://doi.org/10.1166/jnn.2005.001.

[65] B. Delalat, V.C. Sheppard, S. Rasi Ghaemi, S. Rao, C.A. Prestidge, G. McPhee, M.-L. Rogers, J.F. Donoghue, V. Pillay, T.G. Johns, N. Kröger, N.H. Voelcker, Targeted drug delivery using genetically engineered diatom biosilica, Nat. Commun. 6 (2015) 8791. https://doi.org/10.1038/ncomms9791.

[66] K.M. Wee, T.N. Rogers, B.S. Altan, S.A. Hackney, C. Hamm, Engineering and medical applications of diatoms, J. Nanosci. Nanotechnol. 5 (2005) 88–91. https://doi.org/10.1166/jnn.2005.020.

[67] J.A. Howarter, J.P. Youngblood, Optimization of Silica Silanization by 3-Aminopropyltriethoxysilane, Langmuir 22 (2006) 11142–11147. https://doi.org/10.1021/la061240g.

[68] L. De Stefano, G. Oliviero, J. Amato, N. Borbone, G. Piccialli, L. Mayol, I. Rendina, M. Terracciano, I. Rea, Aminosilane functionalizations of mesoporous oxidized silicon for oligonucleotide synthesis and detection, J. R. Soc. Interface 10 (2013) 20130160. https://doi.org/10.1098/rsif.2013.0160.

[69] I. Rea, M. Terracciano, S. Chandrasekaran, N.H. Voelcker, P. Dardano, N.M. Martucci, A. Lamberti, L. De Stefano, Bioengineered Silicon Diatoms: Adding Photonic Features to a Nanostructured Semiconductive Material for Biomolecular Sensing, Nanoscale Res. Lett. 11 (2016) 405. https://doi.org/10.1186/s11671-016-1624-1.

[70] M. Aw, S. Simovic, J. Addai-Mensah, D. Losic, Porous silica microshells from diatoms as biocarrier for drug delivery applications, Powder Technol. - POWDER TECHNOL 223 (2012). https://doi.org/10.1016/j.powtec.2011.04.023.

[71] M. Bariana, M.S. Aw, M. Kurkuri, D. Losic, Tuning drug loading and release properties of diatom silica microparticles by surface modifications, Int. J. Pharm. 443 (2013) 230–241. https://doi.org/10.1016/j.ijpharm.2012.12.012.

[72] H. Zhang, M.-A. Shahbazi, E.M. Mäkilä, T.H. da Silva, R.L. Reis, J.J. Salonen, J.T. Hirvonen, H.A. Santos, Diatom silica microparticles for sustained release and

permeation enhancement following oral delivery of prednisone and mesalamine, Biomaterials 34 (2013) 9210–9219. https://doi.org/10.1016/j.biomaterials.2013.08.035.

[73] R.B. Vasani, D. Losic, A. Cavallaro, N.H. Voelcker, Fabrication of stimulus-responsive diatom biosilica microcapsules for antibiotic drug delivery, J. Mater. Chem. B 3 (2015) 4325–4329. https://doi.org/10.1039/C5TB00648A.

[74] M. Terracciano, M.-A. Shahbazi, A. Correia, I. Rea, A. Lamberti, L.D. Stefano, H.A. Santos, Surface bioengineering of diatomite based nanovectors for efficient intracellular uptake and drug delivery, Nanoscale 7 (2015) 20063–20074. https://doi.org/10.1039/C5NR05173H.

Chapter IV

Conception of Cellulose/Alginate /Mesalazine microspheres by solvent evaporation technique for drug release: Experimental and theoretical investigations.

Chapter IV

Conception of Cellulose/Alginate /Mesalazine microspheres by solvent evaporation technique for drug release: Experimental and theoretical investigations.

I. Introduction:

Oral drug administration is the widespread way and the most convenient for patients, especially for long term treatment. However, for certain drugs the therapeutic efficacy of this way of treatment can be hindered due to the low bioavailability of the drug, its poor water solubility and its molecule instability in the acidic gastrointestinal (GI) medium[1]. In the case of certain intestine diseases special drugs are needed with the desirable purpose is to target their release in the place where they are wanted to act and this is the case for gastro-resistant formulations.

By protecting drug molecules from GI acidic environment and increasing its passage through the intestinal membrane, encapsulated orally delivered nano/micro drug systems (NDDs) remain promising vehicles by improving drugs bioavailability[2]. The therapeutic efficacy of such drugs is very important in the treatment of colon-related ailments, with particular emphasis on inflammatory bowel disease (IBD)[3].

We should recall that (5-ASA) is a typical anti-inflammatory prescription drug, which has been used for the treatment of IBD such as CD and which is often administered orally (2-4 g/ day) with repeat dosing[4]. This drug molecule inhibits the formation of prostaglandin E2 in inflamed intestinal tissues by blocking the cyclo-oxygenase pathway[5][6]. Over the last few years, it has been reported that 5-ASA can be used as antitumor agent for treatment of colon cancer[7].

It is well established that 5-ASA is swiftly absorbed from the small intestine and mostly from the upper intestine. So, it is necessary as an objective of the present investigation to develop a colon-specific delivery system with a prolonged release and low dosage forms. The 5-ASA molecule has an amphoteric character which affects its intrinsic dissolution rate. So, its release formulation in the colon is problematic and requires a special coating to prevent a gastric release since it is soluble in acidic medium[8][9].

Chapter IV   *Conception of Cellulose/Alginate /Mesalazine*
microspheres by solvent evaporation technique for drug
release: Experimental and theoretical investigations.

Several methods and techniques of microencapsulation are useful to prepare polymeric microparticles for this purpose. Among these ways, the emulsion/evaporation technique is known as very suitable for water insoluble drugs.

EC and SA have been   used as matrices for microencapsulation. EC, is a drug carrier and a biocompatible polymer. It is an extensively studied encapsulating material for the controlled release in microencapsulation and especially when used in the solvent evaporation process since it is insoluble in water but soluble in many polar organic solvents[10][11][12]. SA is a natural unbranched polysaccharide, non-toxic, biocompatible biopolymer slightly soluble in cold water, forming viscous and colloidal solution, insoluble in acidic medium but rapidly breaks down in basic medium, consequently, SA is considered a pH-dependent swelling material[13][14].

In the present study, EC/SA microspheres loaded with 5-ASA are prepared based on the solvent evaporation technique. Different batches were obtained when changing the preparation parameters. The microspheres were characterized using different analytical techniques. The drug entrapment and the drug release were studied and have undergone treatment using data analysis according to Higuchi and Korsmeyer–Peppas modeling. In order to investigate the drug dissolution process, the results have been validated through building the design of experiments (DOE) and modeling using JMP software. To investigate the interaction mechanism involved in binding the 5-ASA and EC/SA system, analysis using the density functional theory (DFT) was performed.

II. Material and methods
II.1. Materials:

Mesalazine (5-ASA) was supplied by SALEM pharmaceutical Laboratories, El-Eulma, Algeria. Ethyl cellulose (EC) (48% of ethoxyl content), Sodium alginate (SA) (medium

Chapter IV   *Conception of Cellulose/Alginate /Mesalazine*
microspheres by solvent evaporation technique for drug
release: Experimental and theoretical investigations.

viscosity) and Polyvinyl alcohol (PVA) 87-90% hydrolyzed with molecular weight (13,000-23,000) g/mol were supplied by Sigma-Aldrich. Dichloromethane (DCM, 99.9%) and ethanol (99.9%) were from Merck. All other used chemicals are of analytical grades and all reagents are used as received.

II.2. Preparation of microspheres:

The microspheres were prepared by an oil/water emulsion solvent evaporation technique. Accurately weighed amounts of 5-ASA, EC and SA (see Table1) were mixed in 20 mL of dichloromethane (DCM). This organic phase was kept under gentle heating and continuous stirring for 2 hours making sure that solvent evaporation was accomplished.

The aqueous phase was prepared by dissolving 2.5g of the emulsifier PVA in 500mL of distilled water under vigorous stirring for 24hoursuntil complete PVA dissolution. Then, the drug/polymers mixture was added in droplets into the aqueous solution using a syringe. The drops were emulsified under continuous mechanical stirring using a paddle stirrer. Different stirring speeds (300 and 800 rpm) were used. This operation lasted for 8 hours ensuring complete evaporation of solvent. The compositions of the prepared formulations are given in Table 1. The resulting wet microspheres floating in the liquid medium were filtered on Whatman paper, and washed several times with distilled water. The collected microspheres were dried in pen air and stored.

Chapter IV

Conception of Cellulose/Alginate /Mesalazine microspheres by solvent evaporation technique for drug release: Experimental and theoretical investigations.

Table1: Composition and process variables for 5-ASA microspheres preparation

Batch	Stirring speed rpm	SA/EC %	SA/EC (m/m) g	Drug% 5-ASA/Pol.	5-ASA weight (g)
1	300	5%	(0.1/1.9)	10%	0.2g
2	800	5%	(0.1/1.9)	10%	0.2g
3	300	30%	(0.6/1.4)	10%	0.2g
4	800	30%	(0.6/1.4)	10%	0.2g
5	300	5%	(0.1/1.9)	50%	1g
6	800	5%	(0.1/1,9)	50%	1g
7	300	30%	(0.6/1.4)	50%	1g
8	800	30%	(0.6/1.4)	50%	1g

II.3. Characterization of 5-ASA microspheres

II.3.1. Determination of drug content

Drug content was determined in duplicate as it follows. 10 mg of microspheres were submerged in 30 ml of distilled water andstirredfor24 hours at room temperature. The resulting mixture was filtered, and the filtrate was analyzed using UV-Vis spectroscopy at 302 nm. Equation 1 is used to determine the active ingredient content.

$$Drug content\% = \frac{mass of active agent extracted * 100}{mass of microspheres} \qquad \text{(IV.1)}$$

II.3.2.Fourier-Transform Infrared Spectroscopy analysis (FT-IR):

The microspheres batches as well pristine 5-ASAand the encapsulating agents (EC and SA) have been analyzed using a Fourier transform infrared (FT–IR) spectrophotometer Shimadzu-8400Japan considering the KBr disc method. For this, microspheres were grounded and all FTIR spectra were recorded from 4000 to 400 cm^{-1}. The obtained spectra were compared to assess whether any alterations had taken place in the chemical structures of the compounds following the micro-encapsulation process.

Chapter IV

Conception of Cellulose/Alginate /Mesalazine
microspheres by solvent evaporation technique for drug
release: Experimental and theoretical investigations.

II.3.3. Optical and Scanning Electronic Microscopies analyzes:

Particle shape and size measurements were evaluated through micrographs obtained using optical microscope (MOTIC, Germany) coupled with a camera and Image J software. The microspheres were placed on a glass slide and viewed at varying magnifications. The mean diameters (d) in micrometers and size distributions (δ) of microparticles were estimated using equations (2, 3, 4 and 5) where (*n*) is the number of 300 microparticles. The surface morphology of microspheres was observed with a scanning electron microscope (SEM) type GEMINI (FESEM) CARL ZEISS equipped with an electron source by Schottky field emission (hot cathode).

$$d_{10} = \sum n_i d_i / \sum n_i \qquad \text{(IV.2)}$$

$$d_{32} = \sum n_i d_i^3 / \sum n_i d_i^2 \qquad \text{(IV.3)}$$

$$d_{43} = \sum n_i d_i^4 / \sum n_i d_i^3 \qquad \text{(IV.4)}$$

$$\delta = \frac{d_{43}}{d_{10}} \qquad \text{(IV.5)}$$

II.3.4. Thermogravimetric Analysis (TGA/DTG):

The thermogravimetric analysis (TGA, DTG) was performed using (TA Instruments SDT Q600). Samples of approximately 5 mg of microspheres (in powder) and those of 5-ASA, EC, and SA were sealed in aluminum pans and heated from ambient temperature to 750°C at a rate of 20°C/min^{-1}, under nitrogen atmosphere.

II.3.5. In vitro drug release studies:

The release of 5-ASA from microspheres was studied *in vitro* in a simulated gastric fluid (SGF, pH 1.2) and in a simulated intestinal fluid (SIF, pH 7.4, *distal ileum and colon*).The tests

were realized in a thermostatic bath containing900 mL of the fluid at 37°C±1°C, stirred with a controlled rate (100 rpm) using a paddle stirrer. A weighed amount of microspheresinclosing100 mg of 5-ASAwas placed in a Soilon bag type (2 x 2 cm) then this later is plunged in the bath containing either SGF or SIF dissolution medium ensuring sink conditions. At appropriate time intervals, 2 mL of liquid were withdrawn, passed through a 0.45 µm membrane filter (Millipore). The concentration of drug in samples was analyzed by UV-vis spectroscopy (Shimadzu Pharmspec UV-1700) at λ_{max}=303 nm. The initial volume of dissolution medium was maintained by adding 2 mL of fresh dissolution medium after each withdrawal. The duration of dissolution test was 120 and 700 min for SGF and SIF respectively. All experiments were performed twice and average values are taken.

II.3.6. Kinetic modeling on drug release

A kinetic modeling analysis was carried out on microspheres in an attempt to determine the phenomena governing the release pattern of 5-ASA. The mechanism and kinetics of drug release were deduced by fitting dissolution curves to Higuchi (equ.6) and Korsmeyer-Peppas (equ.7) models. And for describing the drug release behavior, a better fit was established by using a correlation coefficient the closest to 1,

Higuchi's model $\qquad\qquad M_t/M\infty = K_H t^{1/2}$ $\qquad\qquad\qquad$ (IV.6)

Korsmeyer-Peppas model $\qquad M_t /M\infty = K_P t^n$ $\qquad\qquad\qquad$ (IV.7)

where $M_t/M\infty$ is the fraction of drug released at time t, k_H the Higuchi rate constant, Kp is a kinetic constant including geometric characteristics of microspheres and n is the diffusional exponent indicative of the release mechanism. The value of n depends on the microsphere shape; in the case of n less than 0.45 it is a Fickian release, n between 0.45 and 0.89 described

Chapter IV

Conception of Cellulose/Alginate /Mesalazine microspheres by solvent evaporation technique for drug release: Experimental and theoretical investigations.

a non-Fickian release, while for n greater than 0.89 the mechanism of drug release is considered (case II) as a type in which the erosion of polymers takes place[15].

III. Theoretical study of the microencapsulation
III.1. Computational details

The geometry optimization and theoretical calculations of the electronic state of 5-ASA, EC, and SA molecules were performed using Gaussian 9.0 software, based on the density functional theory (DFT) [16]and which Beck's three parameters hybrid exchange functional[17], 6-31G (d, p) basis set, and Lee-Yang-Parr correlation functional (B3LYP) were selected as calculations parameters[18][19]. To obtain trustworthy results, the influence of the water solvent was considered. These theoretical parameters are adequate for small molecular structure [20] .

The frontier molecular orbitals (FMOs) theory is widely recognized as a valuable approach for gaining insight into the chemical stability and reactivity of molecular materials[21]. it predicts the electronic transfer that may occur within the highest occupied molecular orbital (HOMO) and lowest unoccupied molecular orbital (LUMO) frontier molecular orbitals[22]. The ELUMO, EHOMO were computed and some other related global quantum chemical descriptors (GQCDs) were deduced, including: gap energy (ΔEgap), global hardness (η), chemical potential (μ), global softness (σ), absolute electronegativity (χ) and electrophilicity index (ω) using the following formulas (8 to 13)[23].

$$\Delta E_{Gap} = E_{LUMO} - E_{HOMO} \tag{IV.8}$$

$$\eta = \frac{(E_{LUMO} - E_{HOMO})}{2} \tag{IV.9}$$

Chapter IV

*Conception of Cellulose/Alginate /Mesalazine
microspheres by solvent evaporation technique for drug
release: Experimental and theoretical investigations.*

$$\mu = \frac{(E_{LUMO} + E_{HOMO})}{2} \tag{IV.10}$$

$$\sigma = \frac{1}{\eta} \tag{IV.11}$$

$$\chi = \frac{-(E_{HOMO} + E_{LUMO})}{2} \tag{IV.12}$$

$$\omega = \frac{\chi^2}{2\eta} \tag{IV.13}$$

The adsorption of 5-ASA and water molecules on EC-SA copolymer substrate was modeled by one molecule of 5-ASA and five water molecules on one formal co-monomer unit EC-SA. The adsorption was performed using adsorption locator modulus based on Monte Carlo (MC) theory, in which the DFT-optimized geometries were used as initial configurations. The equilibrium configurations were calculated using the neutral charge of both adsorbent and adsorbate. The time step was 0.1fs and the simulation time was 1ns. Additionally, the equilibrium configurations were considered after 10 cycles and 10^5 steps by cycle, at $2*10^5$Kcal.mol^{-1}.Å^{-1} as cut off energy, 10^{-3} Kcal.mol^{-1}.Å^{-1} as maximum force, and 10^{-6}nm as maximum displacement[24]. We add that a normal thermodynamic ensemble NVT was fixed for all calculations. For the adsorption of small molecules, these theoretical parameters are appropriate[25].

IV. Results and discussion

In the present work 5-ASA/EC/SA microspheres were successfully prepared. Some parameters such as emulsion stirring speed and components ratios were varied and the results were analyzed to determine the best microencapsulation process conditions. The findings are discussed in this section.

Chapter IV

Conception of Cellulose/Alginate /Mesalazine microspheres by solvent evaporation technique for drug release: Experimental and theoretical investigations.

IV.1. Chemical identification

Infrared spectroscopy is a useful tool to confirm the effective presence of 5-ASA in microspheres and to investigate drug/polymers interactions as well as stability of formulations. 5-ASA spectrum (Fig. 1) showed absorption bands between 3200-2500 cm^{-1} which correspond to intramolecular hydrogen bonds. Two bands attributed to the asymmetric and symmetric stretching modes of COOH groups are seen approximately at1651 and 1353 cm^{-1}. Other peaks appeared at 1257 cm^{-1} for C-N stretching vibration and at 1640 cm^{-1} corresponding to the bending vibration of N-H. There were also strong intensity bands corresponding to C-H stretching in aromatic compound at 878 cm^{-1} and peaks at 767 cm^{-1} and 689 cm^{-1} of C-H out of plane bending vibration. Observed peaks are similar to those reported in literature[26][27][28].

The pure SA spectrum exhibited characteristic absorption bands around 1617 cm^{-1}, 1415 cm^{-1} and 1300 cm^{-1}which were attributed to stretching vibrations of asymmetric and symmetric bands of carboxylate anions respectively[27]. The band at 3438 $cm^{-1}$is related to the stretching vibration of the hydroxyl groups(-OH) bonded via hydrogen bonds[29][30].The peak appearing around 2930 cm^{-1} corresponds to aliphatic C-H stretching vibration[31]. At 1030 cm^{-1}a band can be assignable to C-O-C stretching vibration. All of the above characteristics supported the basic properties of natural polysaccharides[29]. On the other hand, the FT-IR spectrum of EC showed a band at 3485 cm^{-1} due to -OH stretching vibration while bands at 2980 and 2876 cm^{-1} correspond to the stretching vibration of aliphatic C-H[30].At 1070 cm^{-1}, the vibrations of glycosidic band C-O-C. The peak at 1370 cm^{-1} corresponds to the C-O ether functions[32].It has been noticed that all the spectra of the microspheres, as seen for batch 8 in (Fig. 1), exhibited the characteristic bands of the drug, the peaks of 5-ASA were maintained. The presence of peaks at the frequencies 1650 cm^{-1} (corresponds to the C = O stretch), 1452 cm^{-1} (C-H bending from the alkane –CH$_2$),770 cm^{-1} (C-H out of plane bending vibrations) and 686 cm^{-1} (Aromatic

C-H out of plane bending vibrations). This indicates that there is no change in the drug structure and the absence of chemical interactions between 5-ASA and EC or SA.

Fig. 1: FT-IR spectra of 5-ASA, SA, EC and batch 8.

IV.2. Optical microscopy and SEM:

Micrographs taken by means of optical microscope showed spherical particles. These were free-flowing and non-aggregated (Fig. 2). In the case of the low agitation speed and the maximum quantity of both active ingredient and polymers during the preparation, larger droplets are formed in the mixing process and consequently larger microspheres are obtained (Fig. 2). The microparticles sizes, as described in the experimental section, were measured using optical microscopy, an example of size frequency classification is displayed on batch 8. In this case,

Chapter IV

Conception of Cellulose/Alginate /Mesalazine microspheres by solvent evaporation technique for drug release: Experimental and theoretical investigations.

300 microparticles were counted and inspected using optical microscopy, and the size distribution is calculated and depicted graphically as shown in fig. 4.
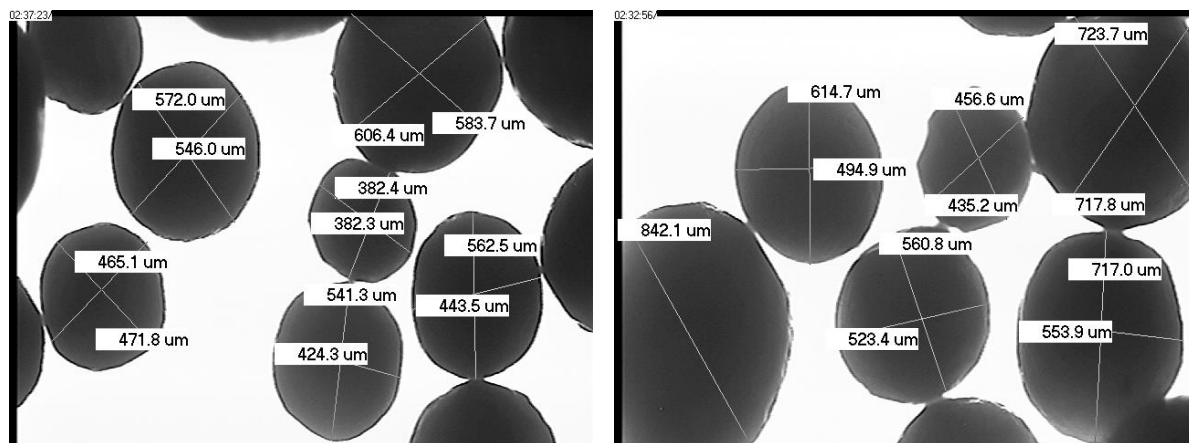
Fig. 2: Optical micrographs of microspheres.

In table 2 are summarized the microparticles size results. The range of mean minimums and maximums diameters (d_{10}) of the produced batches of microparticles varied from 502.3 µm to 748.5 µm and from 555 µm to 813.3 µm, respectively. The stirring speed had a significant influence on the size of the microparticles; when the stirring speed of emulsion was raised, the mean diameter effectively dropped. Furthermore, the results showed that increasing the amount of ethyl cellulose increased the viscosity of the medium, which may reduce emulsion effectiveness, resulting in increased droplet size and hence microsphere size.

Observations made by SEM let think that very small amount of 5-ASA crystals are attached to the surface of the particles from the external medium (Fig. 3). This should be proved by the absence of burst effect in the dissolution test of adsorbed 5-ASA on microspheres. On the other hand, the surface morphology of microparticles (as seen for batch 8) was discovered to be rough, mainly as a result for increased drug concentrations that could be scattered on the surface (Fig. 3 insert).

Chapter IV

Conception of Cellulose/Alginate /Mesalazine microspheres by solvent evaporation technique for drug release: Experimental and theoretical investigations.

Table 2: Microspheres dimensional characteristics (Formulations B1–B8)

Batch	Drug content	d min (µm)				d max (µm)			
	(%)	d_{10}	d_{32}	d_{43}	δ	d_{10}	d_{32}	d_{43}	δ
1	98,3±0.39	752.1	813.0	835.5	1.11	790.6	748.5	869.7	1.10
2	98,5±0.50	727.1	795.1	821.6	1.13	810.0	851.4	867.5	1.07
3	98,4±0.53	682.5	744.5	770.0	1.13	761.8	828.5	852.0	1.12
4	98,5±0.50	774.5	840.9	861.3	1.11	765.0	839.3	862.8	1.13
5	91,5±2.84	714.0	788.2	814.5	1.14	743.5	809.3	834.1	1.12
6	93,3±2.25	684.3	749.5	775.9	1.13	771.5	828.6	849.8	1.10
7	92,4±2.55	673.9	741.1	764.5	1.13	700.0	776.0	811.1	1.16
8	92,8±2.42	502.0	553.2	583.5	1.16	555.0	608.4	639.0	1.15

Fig. 3: Size distribution of (dmax) for batch 8

Chapter IV

Conception of Cellulose/Alginate /Mesalazine microspheres by solvent evaporation technique for drug release: Experimental and theoretical investigations.
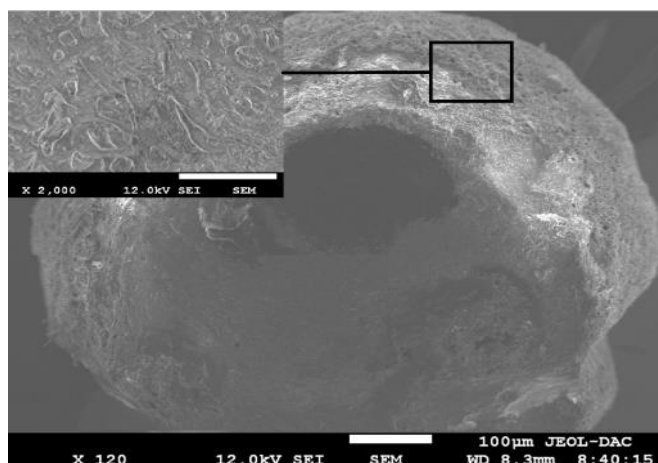
Fig. 4: SEM of 5-ASA loaded EC/SA microspheres (batch 8).

IV.3. Thermogravimetric Analysis

Thermogravimetric analysis (TGA) and derivative (DTG)were carried out to investigate the thermal stability, the oxidation, and the vaporization of the polymers and active ingredient. TGA/DTG thermograms are illustrated in Fig. 5.

For pure 5-ASAa total mass loss is observed in one step at 288°C which corresponds to decomposition of the drug[33]. The thermogram of pure SA showed two events of a mass loss. The first one is observed in the temperature range from36°C to 102°C of about 10% weight loss was attributed to dehydration and volatile products elimination[34][35].The second one may be ascribed to the decomposition of SAin two stages. The first stage starting at approximately 205°C until 350°C is due to decarboxylation (40%). The second one which occurred in the range of350°C -750°C was assigned to the rupture of glycosidic bonds probably leading to volatile fragments and complete degradation of SA backbone corresponding to a mass loss of (7.5%)[36].The TGA/DTG thermogram of pristine EC presented only one step of degradation so it decomposed directly and the maximum decomposition takes place at 365°C[37][38].

Chapter IV   *Conception of Cellulose/Alginate /Mesalazine*
                                 microspheres by solvent evaporation technique for drug
                                 release: Experimental and theoretical investigations.

In the thermogravimetric analysis of microspheres, batch 8 thermogram showed weight loss

and the corresponding DTG indicated the presence of the three ingredients making

microspheres. Through the TGA/DTG thermogram of batch 8 three stages were observed. The

first step in the range between 216 and 279°C corresponds to SA degradation peak. It was

followed by a second step from 279 to 296°C which can be attributed to the decomposition of

5-ASA. It can be noticed that the decomposition of 5-ASA and SA occurred at very similar

temperature ranges so it might not be possible to clearly identify the decomposition events

individually. Finally, the third stage was attributed to the weight loss of EC which occurred

between 305 and 410°C showing a similar decreasing tendency with pristine EC.
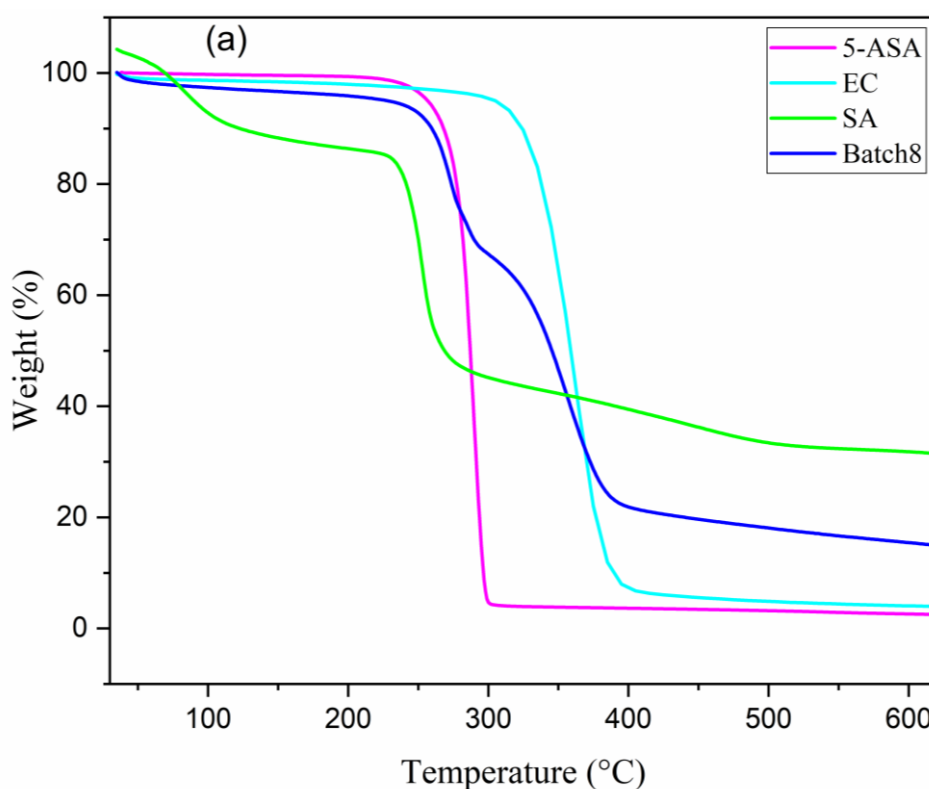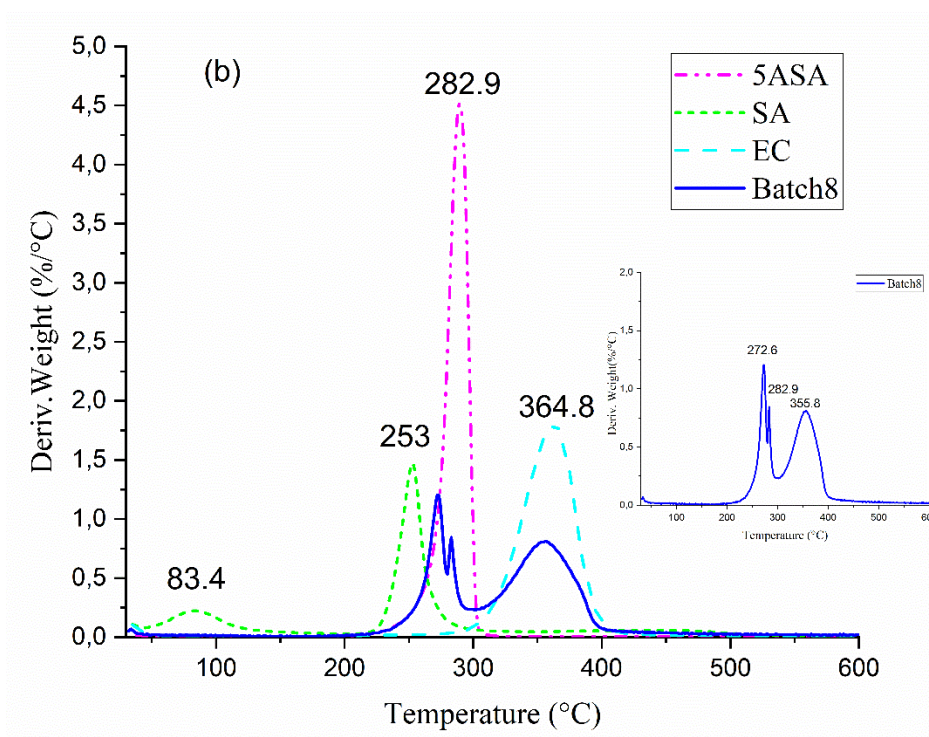
Fig. 5:TGA (a)/DTG (b) patterns of 5-ASA, EC, SA and batch 8

IV.4. Powder X-Ray diffraction pattern (PXRD)

In order to investigate the crystallinity of 5-ASA structure in EC/SA microspheres, the PXRD technique was used. X-ray diffractograms of pure compounds and batch 8 are shown in fig. 6. The PXRD pattern of pristine 5-ASA showed characteristic intense peaks between 2θ(5 and ~16°) indicating its crystalline structure. However, the PXRD analysis of batch 8 microspheres showed also a number of characteristic peaks of 5-ASA but with a low intensity, which suggested the amorphous structure of 5-ASAin the formulations.

Chapter IV   *Conception of Cellulose/Alginate /Mesalazine*
                                          microspheres by solvent evaporation technique for drug
                                          release: Experimental and theoretical investigations.
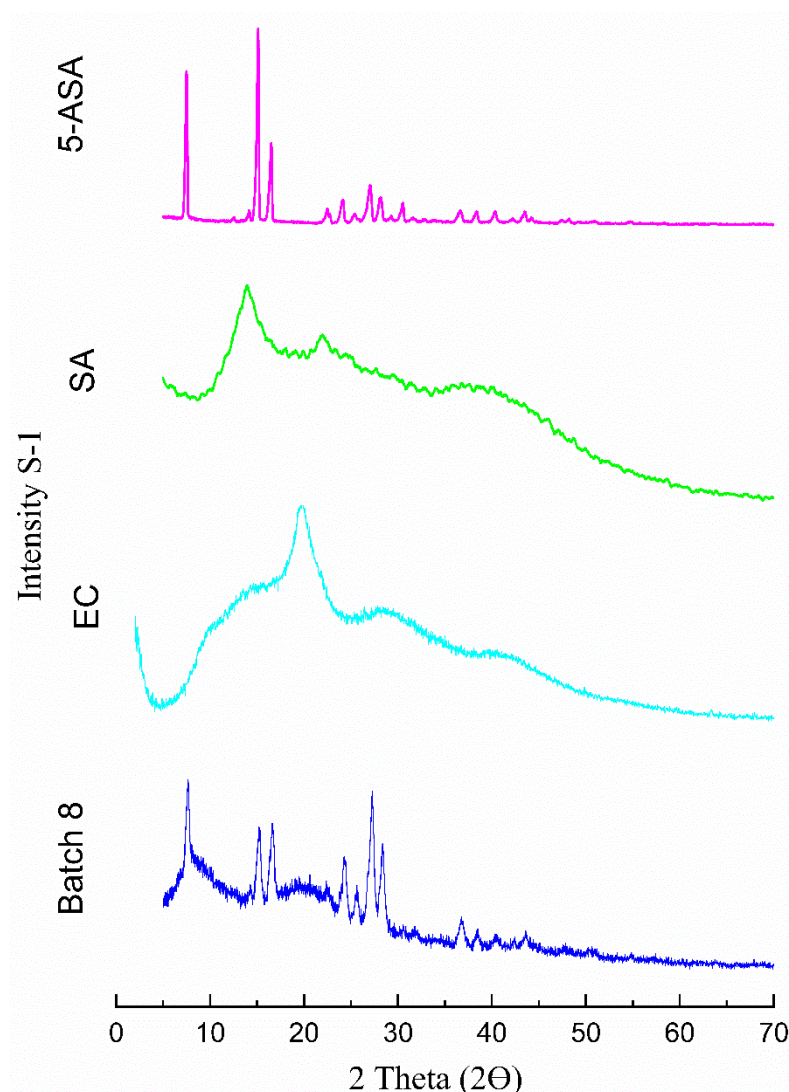
Fig. 6: PXRD pattern of pristine 5-ASA, SA, EC and batch8.

IV.5. *In vitro* drug release studies:

In this study, a delayed delivery drug formulation is desirable because 5-ASA exerts therapeutic effect through local topical activity at the inflamed intestine mucosa. It is also rapidly absorbed by the upper small intestine, hence the drug release must be prolonged until the substance reaches the terminal ileum or the colon[39].

In the *in-vitro* release studies, a successful colon targeted drug delivery with minimum drug release during its transit in the stomach was obtained for all the batches (Fig. 7).

Chapter IV

Conception of Cellulose/Alginate /Mesalazine microspheres by solvent evaporation technique for drug release: Experimental and theoretical investigations.
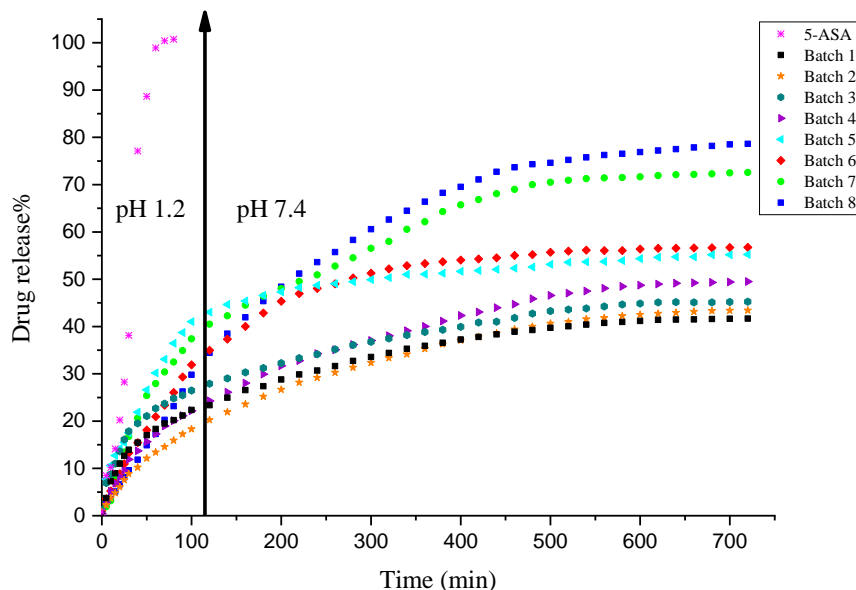
Fig. 7: Percentage release of drug from EC/SA microspheres in (pH 1.2) and (pH 7.4)

As expected, 5-ASA presents a high solubility at acidic pH and this was observed in drug release profile of the pure drug (Fig. 7). Practically, the entire drug is dissolved after 70min of its passage through the first step in the gastrointestinal tract. Contrarily, microspheres containing pure 5-ASA showed a significant stability in these conditions that simulate the stomach medium. From the simulated gastric medium in pH 1.2, the results showed that the drug released after 120min varied from 17.5 %(batch4) to 44.4 %(batch 6) as given in fig. 7. The5-ASA release profiles were compared to determine the effect of agitation speed of emulsion and polymers/drug proportions on drug dissolution.

In the gastric medium, by comparing the percentage of the drug released for the batches having undergone the same stirring speed during the microencapsulation process (batch 1 and 2) and also (3 and 4) it was shown that a faster stirring and higher concentration ratio of SA led to a slightly higher 5-ASA release. In this case since the polymer concentrations are high, they form a barrier which prevents the exit of the drug towards the external environment. Moreover, by

Chapter IV

Conception of Cellulose/Alginate /Mesalazine microspheres by solvent evaporation technique for drug release: Experimental and theoretical investigations.

comparing batches 5 and 6 to 7 and 8, it was observed that the drug release content was increased whatever the stirring speed of emulsion, knowing that in these formulations the rate of the active agent is high, so it is normal for its released fraction to be high.

In the intestinal medium, higher5-ASA release efficiency is noticed; it varied from 41.3% to 77.9%. The batches1and2containing lower drug content exhibited a similar 5-ASA release profile. The effect of each parameter is discussed in the DOE section.

This method allowed a prolonged release of the drug in acidic medium. As it was reported in previous work[40]; when SA is used in solvent evaporation method, it can play a role of coating material for drugs and in this situation electrostatic forces between SA, EC, and 5-ASA produce stable 3D porous network which will be confirmed by DFT studies. This network is easily broken in basic medium due to the solubility of SA in this condition.

IV.6. Drug release kinetics results treatment

The dissolution data were analyzed according to: Higuchi and Korsmeyer-Peppas kinetic model-dependent approaches in order to investigate the drug escape mechanism. The corresponding results are displayed in table 3. The best-fitted release kinetic model is based on the selection in the regression analysis. The kinetic model with the highest value of coefficient (R^2) was considered to be a more suitable model for all dissolutions. By applying the Higuchi model, the value of R^2 was found to be between 0.940-0.994. Moreover, the Drug release mechanism was also investigated from these microspheres using the Korsmeyer-Peppas equation and R^2 values varied from 0.956 to 0.997. The value of "n" was superior to 0.89 for batches (1, 3, 4 and, 5) and closed to this value for the others (2, 6, 7 and, 8). This is associated to an erosion of polymers matrix that takes place during the dissolution test and hence the escape of the drug content. Whereas, ananomalous mode drug release mechanism exhibits both diffusion and erosion of polymers.

Chapter IV

Conception of Cellulose/Alginate /Mesalazine microspheres by solvent evaporation technique for drug release: Experimental and theoretical investigations.

With the increase in EC polymer concentration, the pores surface of the drug was found to decrease preventing its escape which may contribute to prolonging drug release profiles. It is known that the initial drug release from EC usually follows anomalous mode(Korsmeyer-Peppas result)[41]. During dissolution test, microspheres begin to swell by increasing the uptake of water leading to the formation of a barrier. This fact induced erosion decreasing which may prolong the release rate of 5-ASA. Herein, our present study described how the mixture of EC and SA was used to control the balance between erosion and swelling of microspheres. On the other hand, SA polymer is less susceptible to disintegration in the gastric medium then a delayed delivery of 5-ASA in the more distal parts of the small intestine can be achieved. The use of SA/EC mixture helped to maintain extension of drug release and can be a promising matrix for 5-ASAto achieve the desired therapy with minimum side effects.

Table 3: Drug release results and data analysis according to Higuchi and Korsmeyer–Peppas modeling.

Batch	Higuchi's equation			Korsmeyer–Peppas' equation			% 5-ASA released after 120 min
	$K_H(min^{-1/2})$	A	R^2	K_{KP} (min^{-n})	N	R^2	
1	0.06	-0.171	0.988	0.01	0.913	0.997	20
2	0.053	-0.146	0.994	0.01	0.859	0.993	17.5
3	0.061	-0.179	0.988	0.01	0.914	0.991	19.3
4	0.058	-0.164	0.990	0.01	0.885	0.992	18
5	0.134	-0.328	0.940	0.012	0.965	0.984	45.7
6	0.126	-2.264	0.950	0.019	0.867	0.987	44.4
7	0.123	- 0.275	0.943	0.021	0.835	0.956	39.8
8	0.113	-0.227	0.974	0.023	0.805	0.970	37.7

IV.7. Investigation results using design of experiments

Simple 2^3 factorial designs were developed for the microparticles in order to quantify the variables impacts on the microsphere's properties (Table 4).The number of trials necessary for this study is dependent on the number of unrelated variables used such as drug concentration (%Drug), polymer mixtures noted % EC/SA (w/w) and stirring speed (rpm). The responses (Yi) studied were the drug loading(%T), the effect of stirring speed on the d_{10}(dmax) and Higuchi's release constant (K_H), in order to explain the effect of one factor on the other, to know whether this effect is significant or not and how it influences the response. The data obtained for the replies in each run were analyzed with the JMP.13 Software.

The response Yi of the polynomial (Equation 14) was measured for each trial and then interactive statistical first order complete model (Equation 14) was generated to identify statistically significant terms.

$$Y_i = a_0 + a_1 X_1 + a_2 X_2 + a_3 X_3 + a_{12} X_1 X_2 + a_{13} X_1 X_3 + a_{123} X_1 X_2 X_3. \tag{IV.14}$$

Where:

a_0: is the arithmetic mean response of four runs.

a_i: is the estimated coefficient for the factor **X_i**.

Chapter IV

Conception of Cellulose/Alginate /Mesalazine microspheres by solvent evaporation technique for drug release: Experimental and theoretical investigations.

Table 4: Experimental factorial design and results of mesalazine microparticles characteristics

Experiment	X_1	X_2	X_3	Y_1: %T	Y_4: K_H (min$^{-1/2}$)	Y_2:d$_{10}$dmax
(B-1)	-1	-1	-1	98.3	0.06	790.6
(B-6)	+1	-1	+1	93.3	0.126	771.5
(B-7)	+1	+1	-1	92.4	0.123	700.0
(B-5)	+1	-1	-1	91.5	0.134	743.5
(B-3)	-1	+1	-1	98.4	0.061	761.8
(B-2)	-1	-1	+1	98.5	0.053	810.0
(B-4)	-1	+1	+1	98.5	0.068	765.0
(B-8)	+1	+1	+1	92.8	0.113	555.0
Coded values/actual values			−1	+1		
X_1: %Drug			10%	50%		
X_2: % (EC/SA)			5%	30%		
X_3: Stirring speed (rpm)			300	800		

The primary impacts (X_1, X_2 and. X_3) show the average result of changing one element at a time from a lowest (-1) to the highest (+1) values. However, when two factors are altered at the same time the interaction (X_1X_2 and. X_3) illustrates how the response (Y_i) value changes. The primary influence of components X_1, X_2 and X_3 as well as the interacting effect of the two factors on the response Y_i may then be evaluated using these equations.

$$\text{T\%}=95.46-2.96X1 + 0.06X2 + 0.31X_3 +0.03\ X_1X_2+0.24\ X_1X_3-0.19\ X_2X_3-0.17\ X_1X_2X_3 \tag{IV.15}$$

$$\text{K}_H\ (\text{min}^{-1/2}) = 0.09+0.03X1-0.003X2-0.004X_3+0.004\ X_1X_2 -0.001\ X_1X_3+0.0003\ X_2X_3- 0.0007\ X_1X_2X_3 \tag{IV.16}$$

$$\text{d}_{10}\ \text{max (μm)}=733.4 - 40.9X_1 - 37.9X_2 - 8.05X_3 -27.03X_1X_2 -21.2X_1X_3 -27.4\ X_2X_3 -15.85\ X_1X_2X_3 \tag{IV.17}$$

These equations depict the main quantitative effect of factors X_1, X_2 and X_3 as well as the interactive effect of the factors upon the response Y (Drug content %T), the mean diameter (d_{10}), and drug release constant (K_H).The coefficient sign in a regression model indicates how a factor affects the response variable. A positive coefficient means the factor has a synergistic effect, increasing the response variable as it increases from low -1 to a high level +1. A negative

Chapter IV

Conception of Cellulose/Alginate /Mesalazine microspheres by solvent evaporation technique for drug release: Experimental and theoretical investigations.

coefficient means the factor has an inverse or antagonist effect, decreasing the response variable as it increases[11].

The effects of the independent variables and their interactions on the drug loading (%T), the drug release constant (K_H) and the d_{10} microspheres diameter (dmax)can be visualized on the three-dimensional (3D) plots and the Prediction Profiler. This plotting mode is beneficial for evaluating the connection between the independent and dependent variables.

The results obtained for the microspheres as depicted by the estimated coefficient value **(a_i)** in equations(15),(16) and (17) and the main effects representation in fig. 8 showed that; the drug concentration displayed a synergistic effect on drug release constant (K_H), while it exhibited a high but adversary effect on both drug content (%T) and the mean diameter (d_{10}).

The effects of variables on the microspheres size revealed that the stirring speed has a slight but adversary effect on d_{10}; in fact, the mean diameter (d_{10}) decreased when the stirring speed increased. This result approves the initial break-up theory: increasing the stirring speed of emulsification induces small droplets and on the contrary viscous organic phase leads to big droplets[42]. However, the results showed that polymer concentration (% EC/SA) negatively and notably affected the microspheres size. Also, the increase in polymer concentration led to a decrease in drug dissolution.

Finally, the effects of these variables on the responses are significant. Indeed, we highlighted that when the drug concentration increased, the drug release constant (K_H) increased. While drug content (%T) significantly decreases with increasing shaking speed. It is also noticed that an increase in the stirring speed of the emulsion leads to a decrease in the number mean diameter (d10), and on the contrary, the drug dissolution decreased and the size of microspheres (d10) increased with an increase in polymer concentration.
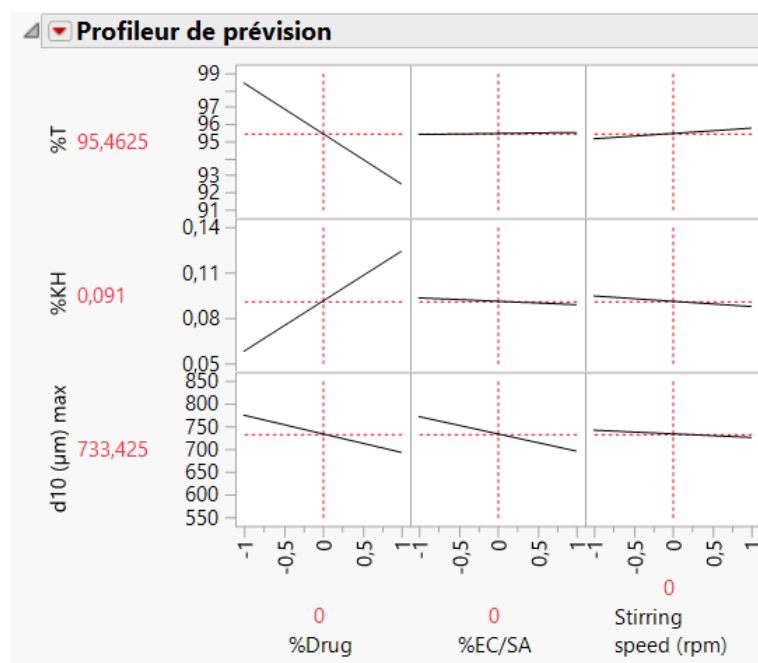
Fig. 8: Optimal conditions obtained by the full factorial model on the 5-ASA microspheres

Building three-dimensional response surfaces allowed us to assess how and which of the variables affected each other and identify the combination that yielded the best results. In fact, the interaction between the variables exhibits no significant interactions separately. But the combination of the variables X_1X_2, X_1X_3, and X_2X_3 can have effect. A strong and notable interaction between drug constant (X_1) and both of EC/SA concentration (X_2) and stirring speed (X_3) is confirmed by a distorted surface plot. Also, a remarkable, soft and control effects interaction between EC/SA concentration (X_2) and stirring speed (X_3) is detected as shown in (Fig. 9).

Evidently; the adequacy and significance of the model were justified by an analysis of variance (ANOVA). This test gives knowledge about the importance and the significance of the effects of the variables and their interactions. In this case, the p values for the effects of drug concentration (%Drug), polymer concentration (%EC/SA), and stirring speed (rpm) from the analysis of variance are 0.011, 0.205, and 0.134, respectively. Nonetheless, because these

Chapter IV   *Conception of Cellulose/Alginate /Mesalazine*
microspheres by solvent evaporation technique for drug
release: Experimental and theoretical investigations.

values are greater than the 0.05 threshold, they imply that the impacts of these factors are not statistically significant except the drug concentration (%Drug) value.

Table 5 presents the comparison between the theoretical equations obtained from the JMP analysis of the factorial design for bathes 6and8, which were created by using drug concentration (X1= +1) and EC/SA concentration (X2= -1) at a stirring speed (X3 = +1). The table includes the theoretical and mean experimental results for the responses %T, K_H, and d_{10} (dmax). We observed that the theoretical values were very similar to the experimental ones. This indicates that the JMP methodology can effectively optimize the appropriate experimental conditions to achieve the desired microsphere characteristics.

Table 5: Theoretical and experimental values of the responses %T, K_H and d_{10} (d max) for the batches 6 and 8

Batch	Responses	Theoretical value	Experimental value
	%T	93.26	93.3
6	K_H	0.11	0.13
	d_{10} (d max)	771.4	771.5
	%T	92.96	92.8
8	K_H	0.12	0.11
	d_{10} (d max)	555.01	555

Chapter IV   *Conception of Cellulose/Alginate /Mesalazine*
                                 microspheres by solvent evaporation technique for drug
                                 release: Experimental and theoretical investigations.

(a) surface plot of %T, %K$_H$ and d$_{10}$ Vs %Drug

(b) surface plot of %T, %K$_H$ and d$_{10}$ Vs%

(EC/SA): Stirring speed (rpm)

Chapter IV

Conception of Cellulose/Alginate /Mesalazine microspheres by solvent evaporation technique for drug release: Experimental and theoretical investigations.

Fig. 9: Surface plots of responses as a function of the selected variables for microspheres,

    (a) surface plot of %T, %K_H and d_{10} Vs %Drug

    (b) surface plot of %T, %K_H and d_{10} Vs % (EC/SA): Stirring speed (rpm)

IV.8. Density Functional Theory (DFT)

The optimized molecular structures, the frontier molecular orbitals FMOs and the mapping electrostatic potential MEP of 5-ASA, EC, and SA were calculated using DFT calculations and the output results are illustrated in (Fig. 10).

The optimized molecular structures of 5-ASA and SA illustrate almost planar geometries due to sp^2 hybridization of the carbon atom of aromatic cycle while the EC molecule occupies a 3D space.

IV.8.1. Frontier molecular Orbitals (FMOs)

The FMOs of 5-ASA are mainly distributed on aromatic cycle and the hydroxyl groups. Moreover, a weak occupancy of the HOMO around the amino group is seen. For EC the FMOs are localized on one part of the molecule. The LUMO can be seen on the organic cycle and some oxygen atoms of its vicinity while the HOMO is localized around the aliphatic chain and

Chapter IV   *Conception of Cellulose/Alginate /Mesalazine*
microspheres by solvent evaporation technique for drug
release: Experimental and theoretical investigations.

a weak part around the organic cycle. Finally, the HOMO of SA is distributed on the whole molecule and its LUMO is localized mainly around on COOH group. Thus, the carboxylate groups may form an active site for the interaction with EC in copolymer building.

Table 6 provides a record of the HOMO and LUMO energies and some related global quantum chemical descriptors (GQCDs) characterized by the used molecules.

The charge transfer between 5-ASA, EC and SA molecules and their external media occurs within the LUMO that accepts electrons and the HOMO that donates electrons. The low values of E_{LUMO} reflect their accepting character (Table 6). In addition, the chemical potential is negative for all molecules which indicates their stabilities[43]. Moreover, the gap energy ΔE_{GAP} is described as the absolute value of the difference between E_{LUMO} and E_{HOMO} and it reflect whether the molecule is hard or soft, i.e., a large gap implies weak chemical reactivity as well as high kinetic stability and vice versa[44][45]. The gap of the EC and SA was found to be 6.958 and 8.052eV respectively indicating the hard character of the used substrate; in return 5-ASA is softer than the others and also its lower η and high σ and |μ| values indicate that its electron transfer may be more effective in chemical interaction[46][47].

Table 6: Values of the FMOs energies (eV) and some related
global quantum chemical descriptors (GQCDs).

Molecule	LUMO	HOMO	ΔE_{GAP}	Global hardness (η)	chemical potential (μ)	Global softness (σ)	Absolute electronegativity (χ)	Electrophilicity index (ω)
5-ASA	-1.067	-5.319	4.252	-2.126	-3.193	-0.470	3.193	-2.398
EC	1.686	-6.366	8.052	-4.026	-2.340	-0.248	2.340	-0.680
SA	-0.282	-7.234	6.958	-3.479	-3.760	-0.287	3.760	-2.032

Chapter IV

Conception of Cellulose/Alginate /Mesalazine microspheres by solvent evaporation technique for drug release: Experimental and theoretical investigations.

Molecular electrostatic potential (MEP)

The calculation of the MEP is routinely used for understanding the relative polarity and to predict electrophilic and nucleophilic regions of the studied molecules[48]. For all studied molecules the negative potential (electron-rich region) is indicated by a red color and positive one (electron-poor region) is indicated by a blue color. The green color indicates the neutral regions and serves as a potential midway between the two extremes of negative and positive regions (Fig. 10).

For 5-ASA molecule, the negative potential is located around the hydroxyl and carboxyl group and is about $-7.33*10^{-2}$V.A weak negative potential can be seen around the organic cycle and the amine group relative to the conjugated π-electrons and electronic doublet of the nitrogen atom respectively. In contrast, the positive potential exists at external surface mainly related to the hydrogen atoms. Its max value is $7.33*10^{-2}$V. Besides, for EC molecule and SA, the most negative potential is centered on OH groups. The C−O−C linkages or COOH group of SA have the highest values $-5.36 10^{-2}$V and $6.69 10^{-2}$V respectively. Elsewhere the potential is positive. The non-homogeneity of the potential is due to the non-equi-distribution of the electronic partial charge on the molecular structure which generates high dipolar moments 3.796, 1.912 and 3.629 Debye for 5-ASA, EC and SA respectively. This may involves these molecules to be in high dipolar interactions.

Chapter IV   *Conception of Cellulose/Alginate /Mesalazine*
microspheres by solvent evaporation technique for drug
release: Experimental and theoretical investigations.

Fig. 10: Optimized molecular structure, frontier molecular orbitals and mapping electrostatic potential of 5-ASA, EC and SA molecules.

Chapter IV

Conception of Cellulose/Alginate /Mesalazine microspheres by solvent evaporation technique for drug release: Experimental and theoretical investigations.

Molecular Dynamic Simulation (MDS)

The most stable equilibrium configurations for the adsorption of 5-ASA and water molecules on SA-EC co-monomer surface model are established through molecular dynamic simulations. The results are shown in (Fig. 11) and the corresponding energies are gathered in table7.

SA is a polysaccharide made up of repeating units of L-guluronic and D-mannuronic acids. The natural polymerization process involves forming 1,4-glycosidic bonds between the monomers, which results in a linear polymer chain. Electrostatic interactions between negatively charged carboxylate groups (-COO⁻) of the monomers and positively charged sodium ions (Na+) stabilize the polymer structure and give sodium alginate its unique properties, such as its ability to form gels in the presence of calcium ions. Additionally, there can be hydrogen bonding interactions between the hydroxyl groups (-OH) of the monomers, which will further stabilize the polymer structure and contribute to the physical properties of sodium alginate.

In order to build the SA/EC complex, L-guluronic acid and EC can interact through hydrogen bonding. L-guluronic acid contains multiple hydroxyl groups (-OH), which can form hydrogen bonds with the ether and hydroxyl groups of EC. Similar to L-guluronic acid, D-mannuronic acid can also interact with EC through hydrogen bonding. These hydrogen bonding interactions can enhance the compatibility and adhesion between L-guluronic or D-mannuronic acids and EC.

The most equilibrium configurations illustrate that 5-ASA is skewed after adsorption. Comparatively to the initial optimized configuration (Fig. 11a) giving a considerable output deformation energy of -20.574 kJ.mol⁻¹(Table 7.b).The negative output values of adsorption energies indicate the spontaneity of the adsorption process. In addition, it is observed that the

Chapter IV

Conception of Cellulose/Alginate /Mesalazine microspheres by solvent evaporation technique for drug release: Experimental and theoretical investigations.

aromatic ring is arranged planar to the adsorbent surface, indicating that π-electrons are strongly involved in the adsorption mechanism. The distance between the aromatic ring and CH_3 of the substrate at the interface is comprised between 3.148 and 3.482Å.This considerable width confirms the absence of covalent bonds. It is worth noting that aromatic compounds have a similar adsorption configurations on polymer complexes[49][50]. On top of that, the interactions π-CH with polymers surfaces and small adsorbed molecules have been extensively remarked and investigated[51][52].

Since5-ASA molecule contains a carbon ring linked to a carboxyl and an amine group, MEP and FMOs proved that these functional groups may form active adsorption sites and enhance the adsorption on copolymer system. The minimum distances between oxygen atoms of the adsorbent and NH_2 and OH groups of 5-ASA are 3.055 and 3.141Å respectively. These distances and the negative partial charges character of these sites may involve them as donor and acceptor in the formation of hydrogen bonds system. Thus, various hydrogen bonds of the type N-H···O. O-H···N and O-H···O were predicted under 3.3Å donor acceptor distance (Fig. 10b).

Furthermore, the water molecule is linked to the adsorbate molecule and the adsorbent via hydrogen bonding mainly of the type O-H···O. Comparatively to adsorption configuration without water molecules, it is seen that these later do not affect strongly the adsorption configuration of 5-ASA molecule. At the same time the adsorption energies are -37.188 (Table 7.a) and -34.449 (Table 7.b). Above this, some water molecules occupy interfacial area and may link indirectly the 5-ASA molecule to the adsorbent surface via a water bridge.

As a summary, it can be concluded that the adsorption of drug molecules is more physical and spontaneous where Van der-Waals-type dipolar interaction, π-electron interactions and hydrogen bonds are predominated.

Chapter IV   *Conception of Cellulose/Alginate /Mesalazine*
                                microspheres by solvent evaporation technique for drug
                                release: Experimental and theoretical investigations.

Table 7: Adsorption energies (kJ.mol^{-1}) of 5-ASA and water molecules
on co-monomer surface model

a.   Complex of L-guluronic acid and ethyl cellulose

Molecules	Total energy	Adsorption energy	Rigid adsorption energy	Deformation energy	5-ASA : dE_{ad}/dN_i	H$_2$O : dE_{ad}/dN_i
5-ASA	2.355	-37.188	-16.791	-20.397	-37.188	/
Water	-3.352	-4.062	-3.352	-0.709	/	-4.062
5-ASA/10H$_2$O	-24.673	-71.317	-43.701	-27.609	-35.678	-3.521

b.   Complex of D-mannuronic acid and ethyl cellulose

Molecules	Total energy	Adsorption energy	Rigid adsorption energy	Deformation energy	5-ASA : dE_{ad}/dN_i	H$_2$O : dE_{ad}/dN_i
5-ASA	5.094	-34.449	-13.875	-20.574	-34.449	/
Water	-3.352	-4.061	-3.352	-0.709	/	-4.061
5-ASA/10H$_2$O	-19.469	-66.106	-38.370	-27.360	-34.265	-2.862

Fig. 11: Magnification at the interface of the most stable adsorption
configuration of one molecule of 5-ASA and five water
molecules adsorbed on EC-SA co-monomer model.

Chapter IV

*Conception of Cellulose/Alginate /Mesalazine
microspheres by solvent evaporation technique for drug
release: Experimental and theoretical investigations.*

Conclusion

The aim of this work is a challenge to produce effective and successfully controlled delivery microspheres systems, through the optimizations of the biopharmaceuticals, pharmacokinetics, and pharmacodynamics of 5-ASA, using the emulsion solvent evaporation technique. These microspheres were formulated by utilizing polymeric mixtures (EC and SA) charged by 5-ASA as active ingredient with different ratios drug: polymer. This approach ensures brightening results concerning the therapeutic efficacy using biodegradable polymers and at the same time produces less side effects of unintended consequences.

As observed through optical microscopy, the particles are spherical, have a rough surface, and fall within the size range of several hundred micrometers. From the FT-IR spectral analysis it can be observed that the selected drug and polymers are compatible without any interactions. Also, from the ATG/DTG it was revealed that the drug was stable inside the microspheres.

From the drug release studies it was found that the mixture of EC and SA encapsulated microspheres provides controlled and targeted drug release, as a result of the hydrophobic interaction between the 5-ASA microspheres and the gastric fluid provided an extra layer of protection against the acidic environment of the stomach. This protection allowed for better control over the release of the drug in the intestine and facilitated more targeted drug delivery. This is a promising *in vitro* dissolution profile for the therapy of the inflammatory bowel disease compared to pure drug.

We also describe the interaction of the 5-ASA- polymer complex at the molecular level by periodic density functional theory (DFT) calculations.

Our research on 5-ASA-polymer complexes has the potential to advance the current understanding of their interactions. Furthermore, in both experimental and theoretical studies, the adsorption of NSAIDs on polymer surfaces is a critical factor in drug delivery, as it affects drug release and efficacy. By using 5-ASA as a model, researchers can gain insights into the

Chapter IV

Conception of Cellulose/Alginate /Mesalazine microspheres by solvent evaporation technique for drug release: Experimental and theoretical investigations.

behavior of NSAIDs on polymer surfaces, which can inform the design and development of more effective drug delivery systems.

Chapter IV

Conception of Cellulose/Alginate /Mesalazine microspheres by solvent evaporation technique for drug release: Experimental and theoretical investigations.

References

[1]   L. M. Ensign, R. Cone, et J. Hanes, « Oral drug delivery with polymeric nanoparticles: the gastrointestinal mucus barriers », Adv. Drug Deliv. Rev., vol. 64, nᵒ 6, p. 557-570, 2012.

[2]   J. Reinholz, K. Landfester, et V. Mailänder, « The challenges of oral drug delivery via nanocarriers », Drug Deliv., vol. 25, nᵒ 1, p. 1694-1705, 2018.

[3]   T. Zhang, G. Zhu, B. Lu, et Q. Peng, « Oral nano-delivery systems for colon targeting therapy », Pharm. Nanotechnol., vol. 5, nᵒ 2, p. 83-94, 2017.

[4]   C. Von Ritter, « Chronisch-entzündliche Darmerkrankungen: Pathophysiologie und medikamentöse Therapie », Radiol. Berl. Print, vol. 38, nᵒ 1, p. 3-7, 1998.

[5]   Y. R. Mahida, C. E. Lamming, A. Gallagher, A. B. Hawthorne, et C. J. Hawkey, « 5-Aminosalicylic acid is a potent inhibitor of interleukin 1 beta production in organ culture of colonic biopsy specimens from patients with inflammatory bowel disease. », Gut, vol. 32, nᵒ 1, p. 50-54, 1991.

[6]   F. Cominelli, C. C. Nast, A. Duchini, et M. Lee, « Recombinant interleukin-1 receptor antagonist blocks the proinflammatory activity of endogenous interleukin-1 in rabbit immune colitis », Gastroenterology, vol. 103, nᵒ 1, p. 65-71, 1992.

[7]   Y. Cheng, « 5-aminosalicylic acid is an attractive candidate agent for chemoprevention of colon cancer in patients with inflammatory bowel disease », World J. Gastroenterol., vol. 11, nᵒ 3, p. 309, 2005, doi: 10.3748/wjg.v11.i3.309.

[8]   D. L. French et J. W. Mauger, « Evaluation of the physicochemical properties and dissolution characteristics of mesalamine: relevance to controlled intestinal drug delivery », Pharm. Res., vol. 10, nᵒ 9, p. 1285-1290, 1993.

[9]   D. L. French, K. J. Himmelstein, et J. W. Mauger, « Physicochemical aspects of controlled release of substituted benzoic and naphthoic acids from Carbopol® gels », J. Controlled Release, vol. 37, nᵒ 3, p. 281-289, 1995.

[10]   M. E. Palomo, M. P. Ballesteros, et P. Frutos, « Solvent and plasticizer influences on ethylcellulose-microcapsules », J. Microencapsul., vol. 13, nᵒ 3, p. 307-318, janv. 1996, doi: 10.3109/02652049609026018.

[11]   N. Assas, Z. Elbahri, M. Baitiche, et F. Djerboua, « Effects of some process parameters on the niflumic acid controlled release polymeric microspheres: Optimization using designs of experiments », Asia-Pac. J. Chem. Eng., vol. 14, nᵒ 2, p. e2283, 2019, doi: 10.1002/apj.2283.

[12]   O. E. Khoukhi, Z. E. Bahri, K. Diaf, et M. Baitiche, « Piroxicam /β-cyclodextrin complex included in cellulose derivatives-based matrix microspheres as new solid dispersion-controlled release formulations », Chem. Pap., vol. 70, nᵒ 6, p. 828-839, juin 2016, doi: 10.1515/chempap-2016-0014.

[13]   Y. Hu, S. Zhang, D. Han, Z. Ding, S. Zeng, et X. Xiao, « Construction and evaluation of the hydroxypropyl methyl cellulose-sodium alginate composite hydrogel system for sustained drug release », J. Polym. Res., vol. 25, nᵒ 7, p. 1-12, 2018.

[14]   T.-L. WU, « Modification of the initial release of a highly water-soluble drug from ethyl cellulose microspheres », J. Microencapsul., vol. 16, nᵒ 5, p. 639-646, 1999.

Chapter IV

Conception of Cellulose/Alginate /Mesalazine microspheres by solvent evaporation technique for drug release: Experimental and theoretical investigations.

[15]   M. S. H. Akash, K. Rehman, N. Li, J.-Q. Gao, H. Sun, et S. Chen, « Sustained delivery of IL-1Ra from pluronic F127-based thermosensitive gel prolongs its therapeutic potentials », Pharm. Res., vol. 29, nº 12, p. 3475-3485, 2012.

[16]   A. Hlel, A. Mabrouk, M. Chemek, I. B. Khalifa, et K. Alimi, « Computational Condensed Matter », 2015.

[17]   A. D. Becke, « Density-functional thermochemistry. III. The role of exact exchange », J. Chem. Phys., vol. 98, nº 7, p. 5648-5652, avr. 1993, doi: 10.1063/1.464913.

[18]   M. Vujović, V. Ragavendran, B. Arsić, E. Kostić, et M. Mladenović, « DFT calculations as an efficient tool for prediction of Raman and infra-red spectra and activities of newly synthesized cathinones », Open Chem., vol. 18, nº 1, p. 185-195, janv. 2020, doi: 10.1515/chem-2020-0021.

[19]   O. Noureddine, N. Issaoui, M. Medimagh, O. Al-Dossary, et H. Marouani, « Quantum chemical studies on molecular structure, AIM, ELF, RDG and antiviral activities of hybrid hydroxychloroquine in the treatment of COVID-19: Molecular docking and DFT calculations », J. King Saud Univ. - Sci., vol. 33, nº 2, p. 101334, mars 2021, doi: 10.1016/j.jksus.2020.101334.

[20]   M. Kebir et al., « Pharmaceutical pollutants adsorption onto activated carbon: isotherm, kinetic investigations and DFT modeling approaches », Comptes Rendus Chim., vol. 25, nº S2, p. 9-25, sept. 2022, doi: 10.5802/crchim.161.

[21]   O. Noureddine, S. Gatfaoui, S. A. Brandán, H. Marouani, et N. Issaoui, « Structural, docking and spectroscopic studies of a new piperazine derivative, 1-Phenylpiperazine-1, 4-diium bis (hydrogen sulfate) », J. Mol. Struct., vol. 1202, p. 127351, 2020.

[22]   T. B. Issa, A. Sagaama, et N. Issaoui, « Computational study of 3-thiophene acetic acid: Molecular docking, electronic and intermolecular interactions investigations », Comput. Biol. Chem., vol. 86, p. 107268, 2020.

[23]   E. E. Ebenso, T. Arslan, F. Kandemirli, N. Caner, et I. Love, « Quantum chemical studies of some rhodanine azosulpha drugs as corrosion inhibitors for mild steel in acidic medium: Rhodanine Azosulpha Drugs as Corrosion Inhibitors », Int. J. Quantum Chem., vol. 110, nº 5, p. 1003-1018, avr. 2010, doi: 10.1002/qua.22249.

[24]   D. Sid et al., « Experimental and theoretical studies of the interaction of ketoprofen in halloysite nanotubes », Colloids Surf. Physicochem. Eng. Asp., vol. 627, p. 127136, 2021.

[25]   M. Radjai et al., « Adsorptive removal of cationic and anionic dyes on a novel mesoporous adsorbent prepared from diatomite and anionic cellulose nanofibrils: Experimental and theoretical investigations », J. Mol. Liq., vol. 361, p. 119670, sept. 2022, doi: 10.1016/j.molliq.2022.119670.

[26]   J. M. Stein, « The effect of adrenaline and of alpha- and beta-adrenergic blocking agents on ATP concentration and on incorporation of 32Pi into ATP in rat fat cells », Biochem. Pharmacol., vol. 24, nº 18, p. 1659-1662, sept. 1975, doi: 10.1016/0006-2952(75)90002-7.

[27]   H. Daemi et M. Barikani, « Synthesis and characterization of calcium alginate nanoparticles, sodium homopolymannuronate salt and its calcium nanoparticles », Sci. Iran., vol. 19, nº 6, p. 2023-2028, 2012.

Chapter IV

Conception of Cellulose/Alginate /Mesalazine microspheres by solvent evaporation technique for drug release: Experimental and theoretical investigations.

[28]   J. Han, Z. Zhou, R. Yin, D. Yang, et J. Nie, « Alginate–chitosan/hydroxyapatite polyelectrolyte complex porous scaffolds: Preparation and characterization », Int. J. Biol. Macromol., vol. 46, n° 2, p. 199-205, 2010.

[29]   M. Singh, « Preparation and structural characterization of melamine–methylurea–formaldehyde resin and its blends separately with ethyl cellulose, starch, teakwood, and almond shell powders by 13C NMR, IR, TGA, and SEM techniques », J. Appl. Polym. Sci., vol. 92, n° 6, p. 3437-3446, 2004.

[30]   V. Suthar, A. Pratap, et H. Raval, « Studies on poly (hydroxy alkanoates)/(ethylcellulose) blends », Bull. Mater. Sci., vol. 23, n° 3, p. 215-219, 2000.

[31]   S. Banerjee, S. Singh, S. S. Bhattacharya, et P. Chattopadhyay, « Trivalent ion cross-linked pH sensitive alginate-methyl cellulose blend hydrogel beads from aqueous template », Int. J. Biol. Macromol., vol. 57, p. 297-307, 2013.

[32]   A. Pineda et A. Hechenleitner, « Characterization of ethylcellulose films containing natural polysaccharides by thermal analysis and FTIR spectroscopy », Acta Farm Bonaer., vol. 23, n° 1, p. 53-7, 2004.

[33]   M. Y. Nassar, M. F. El-Shahat, S. M. Khalile, M. El-Desawy, et E. A. Mohamed, « Structure investigation of mesalazine drug using thermal analyses, mass spectrometry, DFT calculations, and NBO analysis », J. Therm. Anal. Calorim., vol. 117, n° 1, p. 463-471, juill. 2014, doi: 10.1007/s10973-014-3638-1.

[34]   A. Salisu, M. M. Sanagi, A. Abu Naim, K. J. Abd Karim, W. A. Wan Ibrahim, et U. Abdulganiyu, « Alginate graft polyacrylonitrile beads for the removal of lead from aqueous solutions », Polym. Bull., vol. 73, n° 2, p. 519-537, févr. 2016, doi: 10.1007/s00289-015-1504-3.

[35]   M. Zhang et al., « Edible ginger-derived nano-lipids loaded with doxorubicin as a novel drug-delivery approach for colon cancer therapy », Mol. Ther., vol. 24, n° 10, p. 1783-1796, 2016.

[36]   P. Rani, S. Mishra, et G. Sen, « Microwave based synthesis of polymethyl methacrylate grafted sodium alginate: its application as flocculant », Carbohydr. Polym., vol. 91, n° 2, p. 686-692, 2013.

[37]   S. Ş. Başarır et N. P. Bayramgil, « The uranium recovery from aqueous solutions using amidoxime modified cellulose derivatives. I. Preparation, characterization and amidoxime conversion of radiation grafted ethyl cellulose-acrylonitrile copolymers », Radiochim. Acta, vol. 100, n° 12, p. 893-900, 2012.

[38]   M. K. Trivedi, A. Branton, D. Trivedi, G. Nayak, R. Mishra, et S. Jana, « Characterization of physicochemical and thermal properties of biofield treated ethyl cellulose and methyl cellulose », Int. J. Biomed. Mater. Res., vol. 3, n° 6, p. 83-91, 2015.

[39]   A. G. Press et al., « Gastrointestinal pH profiles in patients with inflammatory bowel disease. », Aliment. Pharmacol. Ther., vol. 12, n° 7, p. 673-678, 1998.

[40]   M. Lopes et al., « Preparation methods and applications behind alginate-based particles », Expert Opin. Drug Deliv., vol. 14, n° 6, p. 769-782, juin 2017, doi: 10.1080/17425247.2016.1214564.

Chapter IV

Conception of Cellulose/Alginate /Mesalazine microspheres by solvent evaporation technique for drug release: Experimental and theoretical investigations.

[41]   V. R. Sinha et R. Kumria, « Polysaccharides in colon-specific drug delivery », Int. J. Pharm., vol. 224, nᵒ 1-2, p. 19-38, 2001.

[42]   N. Vankova, S. Tcholakova, N. D. Denkov, I. B. Ivanov, V. D. Vulchev, et T. Danner, « Emulsification in turbulent flow: 1. Mean and maximum drop diameters in inertial and viscous regimes », J. Colloid Interface Sci., vol. 312, nᵒ 2, p. 363-380, 2007.

[43]   M. Kamel, A. Morsali, H. Raissi, et K. Mohammadifard, « Theoretical insights into the intermolecular and mechanisms of covalent interaction of Flutamide drug with COOH and COCl functionalized carbon nanotubes: a DFT approach », Chem. Rev. Lett., vol. 3, nᵒ 1, p. 23-37, 2020.

[44]   K. Fukrd, T. Yomezawa, et H. Skrlnga, « A molecular orbital theory of reactivity in aromatic hydrocarbons. 1 », Chem Phys, vol. 20, p. 722-725, 1952.

[45]   Y. S. Mary et al., « Molecular structure, FT-IR, vibrational assignments, HOMO–LUMO analysis and molecular docking study of 1-[5-(4-Bromophenyl)-3-(4-fluorophenyl)-4, 5-dihydro-1H-pyrazol-1-yl] ethanone », Spectrochim. Acta. A. Mol. Biomol. Spectrosc., vol. 136, p. 473-482, 2015.

[46]   M. R. Jalali Sarvestani et R. Ahmadi, « Investigating the Complexation of a recently synthesized phenothiazine with Different Metals by Density Functional Theory », Int. J. New Chem., vol. 4, nᵒ 4, p. 101-110, 2017.

[47]   M. R. Jalali Sarvestani et S. Majedi, « A DFT study on the interaction of alprazolam with fullerene (C20) », J. Chem. Lett., vol. 1, nᵒ 1, p. 32-38, 2020.

[48]   L. Sinha, O. Prasad, V. Narayan, et S. R. Shukla, « Raman, FT-IR spectroscopic analysis and first-order hyperpolarisability of 3-benzoyl-5-chlorouracil by first principles », Mol. Simul., vol. 37, nᵒ 2, p. 153-163, 2011.

[49]   A. Rochefort et J. D. Wuest, « Interaction of substituted aromatic compounds with graphene », Langmuir, vol. 25, nᵒ 1, p. 210-215, 2009.

[50]   S. K. Kolev, H. A. Aleksandrov, V. A. Atanasov, V. N. Popov, et T. I. Milenov, « Interaction of graphene with out-of-plane aromatic hydrocarbons », J. Phys. Chem. C, vol. 123, nᵒ 35, p. 21448-21456, 2019.

[51]   D. Umadevi et G. N. Sastry, « Saturated vs. unsaturated hydrocarbon interactions with carbon nanostructures », Front. Chem., vol. 2, p. 75, 2014.

[52]   J.-H. Deng et al., « π-π stacking interactions: Non-negligible forces for stabilizing porous supramolecular frameworks », Sci. Adv., vol. 6, nᵒ 2, p. eaax9976, 2020.

Chapter V

Optimizing Colon-Targeted Therapy through Mesalazine Delivery via pH-Sensitive Halloysite/ Polysaccharide Nanocomposites: In vitro, In silico and Computational study.

I.   Introduction

Drug delivery strategies are critical in improving pharmaceutical effectiveness. To regulate dissolution rates and ensure precise drug release, one potential technique includes entrapping drug molecules within micro- and mesoporous materials such as clays or silica. The potential of halloysite nanotubes (HNT), a peculiar hollow tubular form of kaolinite, as a flexible option for drug encapsulation, is investigated in this research. Additionally, we shed light on the fascinating potential of this novel technique by investigating its developing potential in medication, protein, and genetic material delivery [1].

HNT are a naturally occurring two-layered aluminosilicates clay minerals with an empirical formula $Al_2Si_2O_5(OH)_4$. Crystal structure of HNT is consisting of negatively charged siloxane groups (Si–O–Si) located at the outer surface and positively charged aluminol groups (Al–OH) located at the inner surface [2]. The exterior diameter of the tubes ranges from 50 to 200 nm, whereas the diameter of the interior pores ranges from 10 to 40 nm. The nanotubes range in length from 0.5 to 1.5 m, depending on the deposit [3].

Halloysite nanotubes (HNT) encapsulate molecules by three independent mechanisms: (i) adsorption to the tubes' exterior and internal surfaces, (ii) loading into the lumen, and (iii) substance intercalation between layers. The lumen loading is the most significant since it gives the highest loading capability and regulated release. The release duration from halloysite lumen ranges from a few hours to days, depending on the active agent's molecular mass, structure, and solubility in the release medium [4].

Recently, there has been an increasing interest in research incorporating drug molecule by intercalation into different layered silicate structures. This investigation aims to determine the feasibility of using these intercalated compounds as media for mesalazine storage, transport, and, eventually, controlled drug release [5].

5-ASA a member of the salicylate family serves as the first line of defense in the treatment of ulcerative colitis and Crohn's disease. 5-ASA has an anti-inflammatory impact and is the primary choice for treating inflammatory bowel illnesses since it is typically well-tolerated and safe[6].It belongs to Biopharmaceutics Classification System (BCS) Class IV; it has low water solubility, permeability, and limited bioavailability.

Chapter V:

Optimizing Colon-Targeted Therapy through Mesalazine Delivery via pH-Sensitive Halloysite/ Polysaccharide Nanocomposites: In vitro, In silico and Computational study.

Furthermore, it travels via first-pass metabolism in the liver, where 20-30% of it is metabolized away from the drug-rich colon. As a result, substantial dosages are frequently required to establish a therapeutic impact, which might result in major side effects such as nephrotic syndrome and hepatitis[7, 8].

In parallel, current pharmaceutical science is primarily reliant on polymers, which are becoming essential for improving drug delivery. Polymers have an important role in the regulated release of therapeutic substances, as well as in masking the bitter taste of medications and functioning as carriers in targeted treatments. The physicochemical properties of these polymers vary depending on parameters such as molecular weight and structure and properties. As a result, polymers that have been approved for use in medical applications are gaining traction as critical components in the creation of various medication dosage forms.

Sodium alginate (SA) is an anionic polysaccharide, essentially comprising 1 /4 linked β-(D)-guluronic (G) and -L-mannuronic (M) acid residues arranged as -M-G- sequences randomly [9]. As a material, SA has the advantage of being nontoxic, biocompatible, and biodegradable. Moreover, it dissolves easily in water and forms very thick colloidal solutions but is insoluble inorganic solvents like chloroform, ether, or alcohol. In an acidic environment, SA transforms into a porous alginic acid, whereas in the colon it is well established that it transforms into a soluble layer [10]. Furthermore, the quick breakdown of SA at high pH which leads to burst release is a phenomenon which might be utilized to modify the release profile [11]. Alginate composites with HNT have been already reported in the literature as successful material in cosmetics and drug delivery [12].

The key objective of this research is to find a simple and cost-effective method for converting 5-ASA as a drug into a colon-targeted pharmaceutical using halloysite as a friendly drug nanocontainer in the presence of the pH-dependent SA polymer. After its preparation, the 5-ASAloaded HNT/SA nanocomposite was investigated by various instrumental methods which are: Zeta Potential (ζ), X-ray Fluorescence (XRF) Analysis, Fourier Transform Infrared Spectroscopy (FT-IR), Scanning Electron Microscopy (SEM), Transmission Electron Microscopy (TEM), X-ray Diffraction (XRD), and Thermogravimetric Analysis (TGA).Evaluating the safety, efficacy, and stability of the 5-ASA delivery systems requires conducting in vitro release experiments at 37 °C, employing simulated gastrointestinal

Chapter V: *Optimizing Colon-Targeted Therapy through Mesalazine*
Delivery via pH-Sensitive Halloysite/ Polysaccharide
Nanocomposites: In vitro, In silico and Computational study.

mediums with pH levels of 1.2 for the stomach (SGM), 6.8 for the intestines (SIM), and 7.4 for the simulated Colonic Medium (SCM).

For an in-depth support for the use of HNT as excipient and SA as coating agent for colon-targeted drug delivery systems, the adsorption of 5-ASA molecules on kaolinite aluminol (001) and siloxane (00-1) surfaces is explored using atomistic force fields for molecular modeling and quantum mechanics computations. The findings aim to shed light on the interactions between the drug and kaolinite surfaces, predict the potential loading of phyllosilicate, and validate its role as a carrier in pharmaceutical applications. The *in silico* study investigates the molecular docking of 5-ASA against PPAR-γ, COX-1, and COX-2 receptors in order to predict their absorbability, their inhibitory activities and the possibility of their selectivity.

II. Materials and methods

II.1. Materials

The chemical reagents used in this study are analytical grades and used as received.5-ASA was kindly gifted by SALEM Pharmaceutical Laboratories, El-Eulma, Algeria. SA(medium viscosity)obtained from Sigma-Aldrich, USA. The raw halloysite was collected directly from the mine of Djebbel Debbagh, Guelma (Algeria) was ground using porcelain mortar and pestle, sieved in (250 mesh 0.063mm) and dried in an air flowing oven at 100°C for 24 hours. The resulting powder was labeled HNT_R.

II.2. Halloysite purification

As a first stage to purifying the crude HNT_R by removing the water-soluble fraction, the following procedure was considered **[12].** 20 g of the material were spread in 1 L of distilled water and stirred for 24 hours. The resulting suspension was centrifugated at 5000 rpm for 5 minutes and the wet precipitate was collected. To get rid of carbonates by destruction, the precipitate was kept under vigorous agitation for 4 hours in 2 L,0.1 M HCl solution at room temperature. Then the precipitate was recovered by centrifugation and repeatedly washed with portions of distilled water until the supernatant attained a neutral pH in the final cycle. To eliminate organic matter, the already partially purified precipitate was treated with a 10% v/v solution of hydrogen peroxide and agitated at room temperature overnight. By heating the

mixture at 70 °C for 30 minutes, the residual hydrogen peroxide was decomposed. The resultant precipitate was rinsed with hot water and dried for 24 hours at 60 °C. The purified sample referred to as HNT, was stored for further use.

II.3. Preparation of the mixture HNT/ 5-ASA

The Loading of 5-ASA onto HNT nanotubes was accomplished using the following procedure:100 mg of pristine HNT was stirred in 90 ml of water and at the same time, 100 mg of 5-ASAwasaddedto 10 mL of hot water. Then the two preparations were combined creating a homogeneous mixture through sonication for 30min.The resulting dispersion was continuously stirred at 300 rpm at ambient temperature for 24 hours. This time was judged long enough to ensure equilibrium between the adsorbed drug and that in solution. Then, after filtration, the wet material underwent evacuation in vacuum desiccator for 30 min, followed by a return to atmospheric pressure. This cycle was repeated four times to enhance the loading **[13]**. The resulting material was washed with distilled water where the excess of un-adsorbed 5-ASA was eliminated. The powder was dried overnight in an oven at 40°C. The HNT-drug sample was denoted as HNT/5-ASA.

II.4. Preparation of drug halloysite polymer composite

This preparation consists in the encapsulation of HNT/5-ASA previously obtained in the form of beads using SA as a coating agent. For this an aqueous stock solution of SA was prepared by dissolving 2 g of SA in distilled water (100 mL). Then, 2 g of HNT/5-ASA was added to the solution and the mixture was stirred at room temperature for 12 hours until a homogeneous, smooth, and uniform consistency was achieved. Subsequently, the mixture was charged in a syringe and then gently let to fall in drops through the nozzle when pushing the piston, into an excess 2% (m/v) calcium chloride ($CaCl_2$) solution constantly stirred **[14].** The resulting beads were left in the $CaCl_2$solution for 24 hours, followed by careful washing with distilled water to remove any residual material from the bead surfaces. Finally, the HNT/5-ASA/SA beads were filtered and dried at room temperature for 24 hours until a constant weight was reached. This operation was repeated until a sufficient quantity was collected which will be enough for doing all analyses.

II.5. Characterization techniques

To measure the zeta potential (ζ) of the HNT dispersion at different pH levels, the nanoparticle analyzer (SZ-100 Horiba Scientific, Japan) was employed. Furthermore, the pH drift method was utilized to determine the pH. PZC (point of zero charges) of the HNT **[15].** The FT-IR spectra of the complexes and the pristine HNT, 5-ASA, and SA were analyzed using the Shimadzu-8400 model, Japan, using the KBr disc method. The spectra were recorded within the range of 4000–400 cm^{-1}. The acquired spectra were compared to evaluate potential changes in the chemical structures and eventually the interactions of the compounds following the microencapsulation process.

Thermogravimetric analysis (TGA, DTG) was conducted using the TA Instruments Q5000 IR apparatus under nitrogen flow of 25 and 10 cm^3 min^{-1} for the sample and the balance, respectively **[16]**. 5 mg of samples in powder form in sealed aluminum pans were analyzed at a heating rate of 2°C/min^{-1} from ambient temperature to 750°C.

The morphology and microscopic structures of the samples were examined using a JEOL JEM-1400 Flash electron microscope (TEM with a carbon-coated copper grid). A 5 µL droplet of HNT or HNT/5-ASA nanoparticles in distilled water were analyzed. The surplus solution was carefully removed by wiping it with absorbing paper. Before imaging, the sample was left to air-dry overnight.

To verify any changes in the composition of the HNT, X-ray fluorescence (XRF) analysis was performed before and after the purification procedure utilizing Rigaku primus IV apparatus, Japan. The analysis was performed on discs having 1.5 cm in diameter and 0.5 cm in thickness.

X-ray diffraction was used to determine the crystal structure of raw HNT and chemically etched HNT using Bruker D8 Advance X-ray powder diffractometer at 40 KV and 40 mA. The data were gathered at 2θ from 4 to 40° with a step size of 0.05° and a scanning speed of step. Cu-radiation with a wavelength of 1.54Å was employed for the analysis.

II.6. Swelling Index

The swelling index was determined thrice using the shaking method, which consists in immersing 100 mg of microspheres sample in different pH100 ml phosphate buffer (pH 1.2, pH 6.8 and pH 7.4) at room temperature for 12h under gentle shaking. At specific time intervals (1, 2, 4, 6, 8, 10, and 12 h) samples were removed and weight of swollen microspheres was

taken **[17].** The swelling ratio of the HNT/5-ASA/SA beads in simulated gastrointestinal conditions was calculated using equation1**[18].**

$$S\% = \frac{W_f - W_i}{W_i} * 100\% \qquad \textbf{(V.1)}$$

where S is the swelling ratio, W_i (g) and W_f (g) denote the initial and final weights of the beads sample after 12 hours of immersion.

II.7. *In vitro* drug release studies

The effect of simulated gastric-intestinal conditions on the release of 5-ASA from formulations (Pristine 5-ASA, HNT/5-ASA_Powder, and HNT/5-ASA/SA_Beads) was investigated. Three-stage measurements (pH1.2, 6.8 and 7.4) were performed to simulate the *in vivo* drug release process considering the changes in the gastrointestinal pH using the United States Pharmacopeia Paddle Method (Apparatus II) on Heidolph RZR 2041. For this, the experiment of drug release was carried in a closed glass vial containing 900 mL of simulated gastric medium (SGM) solution having a pH 1.2. The paddle apparatus was used at 50 rpm, and the temperature was maintained at $37 \pm 0.5°C$. Samples of the equivalent weight of 100 mg5-ASA were placed in a Soilon bag type (2 × 2 cm) and then immersed in the bath containing (SGM)dissolution medium assuring sink conditions.

Throughout the releasing period, two milliliters' aliquots were periodically withdrawn at a suitable time interval and analyzed for their 5-ASA released content by UV spectroscopy:(λ_{max} = 300 nm for SGM then 330 nm for SIM and 302 nm for SCM).We note that before the analysis, the samples underwent centrifugation for 5 minutes at 10,000 rpm and passed through a 0.45 μm membrane filter (Millipore)to remove any particles. To keep the release medium volume constant this later was replenished with 2 ml volume from the fresh buffer solution after each withdrawal. After 120 min, the release medium was changed by transferring the sample to the solution having pH 6.8 referred to the SIM, and after 360 min, it was further transferred to the SCM with pH 7.4. The release samples were collected at regular intervals over the next 480 minutes for analysis and were examined with a UV-Vis spectrophotometer set at different wavelengths, with a background adjustment of 800 nm.

II.8. Mathematical modeling of release profiles

Different kinetic models were used to examine the average drug release data collected from *in vitro* testing. Including first-order, as log cumulative percentage of drug remaining vs. time **[19]**, Higuchi as cumulative percentage of drug released vs. square root of time and Korsmeyer-Peppas as log cumulative percentage of drug released vs. log time, and the exponent n was calculated through the slope of the straight line **[20,21].** By employing regression analysis, the drug release patterns from the generated matrices were investigated. The model with the greatest coefficient of determination (R^2) was selected as the most suitable one for describing the drug release kinetics.

$$\textbf{Log C = Log C}_0 \textbf{ - kt/2.303} \qquad \textbf{(V.2)}$$

where, C_0 is the initial concentration of drug, k is the first order constant, and t is the time.

$$\textbf{Q = k t}^{1/2} \qquad \textbf{(V.3)}$$

where, k is the constant reflecting the design variables of the system and t is the time in hours. Hence, drug release rate is proportional to the reciprocal of the square root of time.

$$\textbf{M}_t\textbf{/M}_\infty \textbf{ = k t}^n \qquad \textbf{(V.4)}$$

where, M_t/M_0 is the fractional solute release, t is the release time, k is a kinetic constant characteristic of the drug/polymer system, and n is an exponent that characterizes the mechanism of release of tracers **[22]**. For cylindrical matrix tablets, if the exponent n=0.45, then the drug release mechanism is Fickian diffusion, and if 0.45< n <0.89, then it is non-Fickian or anomalous diffusion. An exponent value of 0.89 is indicative of Case-II Transport or typical zero order release **[23].**

III. In silico studies

Molecular docking technique is an attractive scaffold to understand the ligand–protein interactions which can substantiate our experimental results.

Chapter V: ***Optimizing Colon-Targeted Therapy through Mesalazine***
Delivery via pH-Sensitive Halloysite/ Polysaccharide
Nanocomposites: In vitro, In silico and Computational study.

III.1. Data Collection

The receptors/enzymes for molecular docking were selected from a literature review of anti-inflammatories. The crystal structures of the anti-inflammatory proteins were imported from the Protein Data Bank (PDB), an online database (https://www.rcsb.org/). Besides, the ligand structure of mesalazine (CID 4075) was extracted from PubChem.

The crystal structures of Peroxisome Proliferator-Activated Receptor-gamma (PPAR-γ) (PDB ID 4EMA). PPAR-γ is highly expressed in the colon and is known to regulate cellular proliferation, differentiation, and apoptosis **[24].**Activation of PPAR-γ inhibits the formation of aberrant crypt foci and the development of CRC in rodents**[25].** Cyclooxygenase is an enzyme involved in the metabolism of arachidonic acid (AA). It consists of two isoenzymes (COX-1 and COX-2. The Cyclooxygenase-1 (COX-1) enzyme is an intrinsic enzyme and is mostly found in the stomach, kidney, and platelets, which can maintain gastric and renal homeostasis. Cyclooxygenase-2 (COX-2) is an inducible enzyme, and its expression is enhanced in the case of tissue damage and inflammation **[26].**

III.2. Preparation of proteins and ligand

Docking files were created using the BIOVIA Discovery Studio (DS) visualizer and Autodock Tools v.1.5.6 software. Before adding polar hydrogen atoms to proteins, water molecules, additional hetero atoms (HETATM), and the attached ligand(s) were removed. Default assignments were utilized for Kollman charges and salvation parameters. The ligands were given Gasteiger charges and hydrogen atoms, and the compounds were maintained apart. Following that, ligands and receptor coordinate files for PPAR-γ, COX-1, and COX-2 were converted to the PDBQT format using MGL Tools-1.5.6 software, which served as the foundation for future docking activities **[27].**

III.3. Grid box preparation

The Grid box dimensions size at grid points in x*y*z directions were prepared individually for all of PPAR-γ, COX-1, COX-2, and 5-LOX to cover the pocket with the main residues of the enzyme binding site. Table 1 provides specific information on the size and center of the grid for each receptor molecule.

Table 1: Details of the protein grids used for molecular docking in this study.

Protein Number	Protein Name	PDB ID	Size of grid			Center of grid		
			X	Y	Z	X	Y	Z
1	Peroxisome Proliferator-Activated Receptors (PPAR-γ)	4EMA	20	35	40	9.9585	-10.044	32.5655
2	Cyclooxygenase-1 (COX-1)	3N8Y	45	40	40	41.324558	-61.091581	-7.193791
3	Cyclooxygenase-2 (COX-2)	1PXX	40	40	40	30.431	28.4695	21.786

III.4. Molecular docking study

The AutodockVina 1.1.2 software from http://vina.scripps.edu/download.html for protein-ligand interactions was employed for the molecular docking simulations. Vina score, also known as docking energies (kcal/mol), is commonly used to measure the binding affinity of a docked ligand with a protein. Typically, the best-docked conformation has a low final score or docking energies based on a complete docking search (ten runs). The 3D and 2D visualization of PPAR-γ, COX-1, and COX- 2 interaction with the ligand showed by BIOVIA Discovery Studio (DS) Visualizer (BIOVIA, Dassault Systems **[28].**

IV. Theoretical investigation

The Frontier Molecular Orbitals (FMO) hypothesis is a useful approach for studying the chemical stability and reactivity of molecular materials. It predicts electronic transfer possibilities in the Highest Occupied Molecular Orbital (HOMO) and Lowest Unoccupied Molecular Orbital (LUMO) phases**[29]**.Additionally, key global quantum chemical descriptors (GQCDs) like the energy gap (Egap) as well as the MEP (Molecular Electrostatic Potential), give information on nucleophilic and electrophilic reaction sites. The ESP (Electrostatic Potential) is concerned with a molecule charges and electronegativity, which contributes to the understanding of its biological activity and reactivity**[30,31].**

All calculations were methodically carried out using the Gaussian09 program, applying the Becke-3-Parameter-Lee-Yang-Parr (B3LYP) method**,** which was supplemented by the 6-311++G(d,p). Importantly, no limits on molecule geometry were applied throughout these

simulations. Following that, the output check files were carefully inspected and evaluated with Gauss View version 5**[32-34].**

IV.1. Models and computational methodology

The Halloysite Nanotubes (HNT) shares the same crystalline structure as kaolinite and exhibits a similar planar morphology. Kaolinite has two distinct surfaces of interest: the first is the (001) surface, characterized by hydrophilic aluminol groups attached to hydroxyl groups, while the second is the (00-1) surface, featuring hydrophobic siloxane endings (Figure1).

To model kaolinite surfaces for adsorption tests vacuum areas were created along the c-axis, precisely positioned at a distance of c = 30Åabove and below the (001) plane of the kaolinite crystal lattice. This deliberate arrangement effectively created exterior surfaces, isolating them from inter-sheet interactions **[35]**.

IV.2. Optimization of Kaolinite Crystal Structure:

The optimization of the kaolinite crystal structure with the following parameters:
a = 5.18 Å, b = 8.98 Å, c = 7.29 Å, α = 87.2º, β = 105.3º, γ = 90.0º, and d(001) = 7.03 Å, revealed crucial details. Notably, the hydroxyl (OH) groups were predominantly oriented perpendicularly to the (001) plane, except for one OH group oriented towards the vicinal octahedral oxygen (O) atoms **[35,36].**

IV.3. Supercells for Adsorption Studies:

Supercells with dimensions of 2x2x2 unit cells were generated to replicate the conditions for adsorption studies. These specific dimensions were carefully chosen to maintain a ratio of one molecule of 5-ASA to kaolinite surface unit cells, as depicted in figure1.These dimensions were found to be sufficient for both drug and water molecules (insertion). The geometric optimization of the supercells was painstakingly carried out using the Forcite module, with classical theory, Universal Forcefield type, and ultrafine convergence criteria based on basis set requirements being used.

IV.4. Density Functional Theory (DFT)

Density Functional Theory (DFT), a well-known and efficient quantum chemistry technique, was used to get complete insights into the compound's molecular characteristics. This included geometry optimization, Frontier Molecular Orbitals (FMO) analysis, evaluation of global and local reactivity descriptors, and Molecular Electrostatic Potential (MEP) evaluation. The simulation parameters included a 0.1 fs time step and a total simulation period of 1ns. After 10 cycles, with each cycle consisting of 10^5 steps, equilibrium configurations were determined. The maximum force was set at 10^{-3} Kcal.mol^{-1}.Å^{-1}, and the maximum displacement was set at 10^{-6} nm, besides $2*10^5$Kcal.mol^{-1}.Å^{-1} as cut-off energy. Notably, all calculations were carried out within the context of a standard thermodynamic ensemble NVT, which is an appropriate option for small molecule adsorption research **[37].**
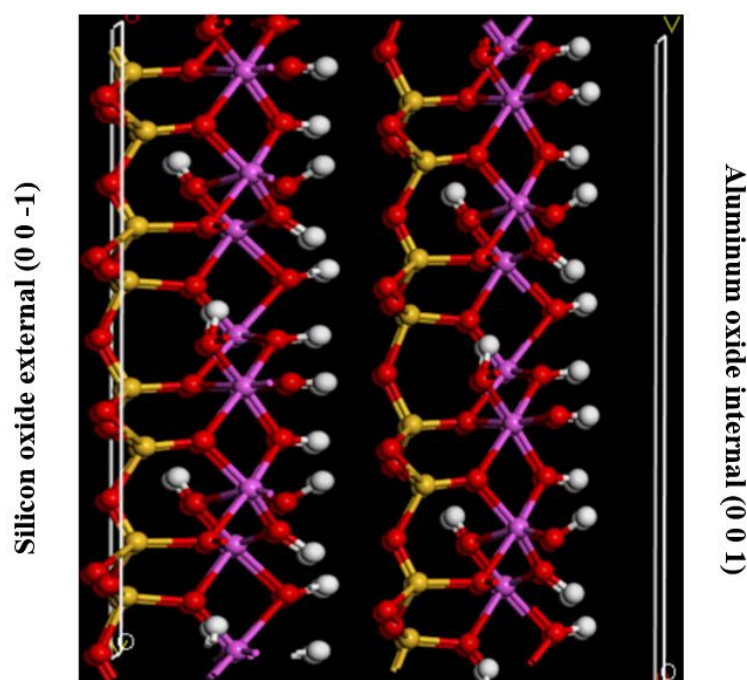
Fig. 1: Supercell of kaolinite structure in the direction (001) (2×2×2)

3. Results and discussion

3.1. Experimental investigation

3.1.1. Characterization of HNT

Chapter V: *Optimizing Colon-Targeted Therapy through Mesalazine*
Delivery via pH-Sensitive Halloysite/ Polysaccharide
Nanocomposites: In vitro, In silico and Computational study.

The atomic percentages of the chemical elements detected by XRF in HNT are shown in table 2. Both silica (SiO_2) and alumina (Al_2O_3) were found, consistent with the chemical structure of aluminosilicates, accounting for more than 90% of the overall composition. The purifying method increased the SiO_2 concentration while decreasing the Al_2O_3 content. Notably, theSiO_2/Al_2O_3 ratio increased slightly from 1.20 to 1.29. According to Panda et al. acid treatment reduced the alumina concentration; this decrease might be attributable to the acid hydrolysis leaching of Al^{3+} cations from the octahedral layer [38].Furthermore, contaminants such as CaO, Fe_2O_3, K_2O, and MnO_2 were decreased during the dealumination process.

Table 2: XRF analysis of untreated and Sulfuric acid etched HNT

	SiO_2	Al_2O_3	CaO	Fe_2O_3	K_2O	MgO	MnO	Na_2O	SiO_2/Al_2O_3	Others
HNT raw	49.8	41.4	0.713	0.593	0.586	0.0995	2.35	0.21	1.20	Traces
HNT Treated	52.4	40.7	0.174	0.521	0.482	0.105	2.09	0.27	1.29	Traces

Zeta potential measurements (ζ) were performed on HNT aqueous dispersions at pH ranging from 2 to 12. The zeta potential of HNT evolves classically, with a positive value at low pH and a progressively negative value as pH increases [39]. The negative surface charge becomes more noticeable when the pH rises, which can be attributed to silica peculiar structure. The outer surfaces of the tubes are rich in silica, whereas the interior surface and margins are fully occupied by alumina. When the material comes into contact with water, surface hydroxyl groups (sur-OH) are formed. The presence of silica on the surface causes the total charge to become more negative throughout a large pH range, as demonstrated in the zeta potential plot. As illustrated in figure 2, HNT has an isoelectric point of approximately 3.6, showing the pH value at which, the surface charge becomes neutral.

Chapter V:

Optimizing Colon-Targeted Therapy through Mesalazine Delivery via pH-Sensitive Halloysite/ Polysaccharide Nanocomposites: In vitro, In silico and Computational study.
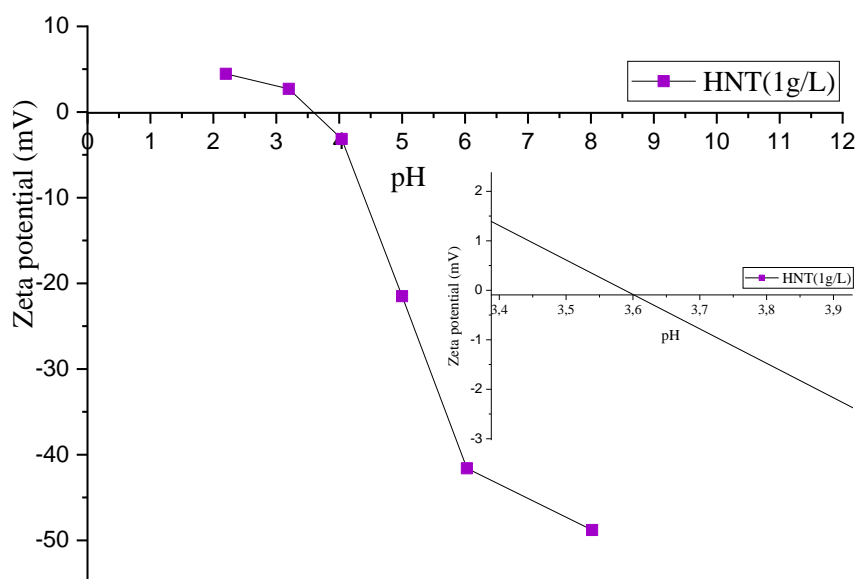
Fig. 2: Zeta potential versus pH for HNT in aqueous dispersion.

3.1.3. Characterization of the HNT based composites

FTIR investigations were carried out to study the interaction of the formulation components. As a result, examinations for raw materials and microparticles were performed. The spectra of the HNT, 5-ASA, and SA (Figure 3) were, as predicted, identical to those discovered in a previous work in our laboratory **[40]**. However, the spectra of raw HNT maintained typical absorption peaks when compared to that of kaolinite. Two bands were present in the hydroxyl region (3000–4000 cm^{-1}) which was centered at $3697 cm^{-1}$ for the stretching vibrations of inner-surface of Al_2-OH groups and at 3624 cm^{-1} assigned to the deformation vibration of interlayer water. While a broad band at 3453 cm^{-1} and a weak one at 1642 cm^{-1} were assigned to the O-H stretching and O-H deformation of physically adsorbed water, respectively. The bands at 1118 and $1031 cm^{-1}$ are related to the in-plane Si-O vibration and the characteristic peaks of Si–O–Si vibration, respectively. The band at 909 cm^{-1} was ascribed to the O-H deformation vibration of inner Al-O-H groups. Also, that at $792 cm^{-1}$ was caused by a symmetrical stretching vibration of Si-O **[41]**. The appearance bands at 753and 687 cm^{-1} were attributed to

perpendicular Si-O stretching. The three remaining bands at 537, 469, and 427 cm^{-1} are related to the deformation of Al-O-Si, Si-O-Si, and Si-O, respectively **[42]**.

Concerning the 5-ASA, the presence of bands that identify its functional groups were observed: The peak at 3458 cm^{-1} owing to the N-H stretching, while, the bands at 3096cm^{-1} and 2977 cm^{-1} are due to the aromatic Ar-CH stretching **[43].** The peak observed at 2784 cm^{-1} corresponds to O-H stretching**[44].**On the other hand; the absorption bands at 2553 cm^{-1} was associated to the vibrations of –NH$_2$ and bending vibration of –C=O which was confirmed by the presence of absorption band at 1651 cm^{-1}. In addition, the peak at 1616 cm^{-1} corresponds to C=C Stretch of aromatic group and N-H primary deformation. Further, the absorption band appeared at 1587cm^{-1} was attributed to the C-N stretch, and he two bands around 1493, 1453 cm^{-1} are due to –C=C stretching **[45].** The peaks at 1352, 1255 cm^{-1} corresponds respectively to the O-H and the C-O bending of primary or secondary alcohol. The C-O stretch of phenol is at 1192 cm^{-1}. The three out-of-plane deformations of C-H in aromatic ring gave absorption bands around 817, 773 and 686 cm^{-1} **[46].** These FTIR spectra confirm the authenticity of the drug sample by identifying peaks as similar to those of pure drug as reference.

From the FTIR spectrum of the sodium alginate, the broad peak around 3445 cm^{-1} ischaracteristic of the stretching vibrations of the hydroxyl groups linked via hydrogen bonds. Also, the absorption band at 2928 cm^{-1} is attributed to the C–H stretching vibration. Moreover, an asymmetric and symmetric COO stretching vibration of the carboxylate salt group of the polymeric backbone gives rise to absorption bands at 1618 cm^{-1} and 1420 cm^{-1}, respectively **[47].** The shoulder at 1029 cm^{-1} is related to the C–O–C (cyclic ether) stretching vibration. Furthermore, the stretching vibration bands observed at approximately 948 cm^{-1}, 887 cm^{-1} and 816 cm^{-1} are specific to the guluronic and mannuronic acids. These data corroborate very well with the literature **[47,48].**
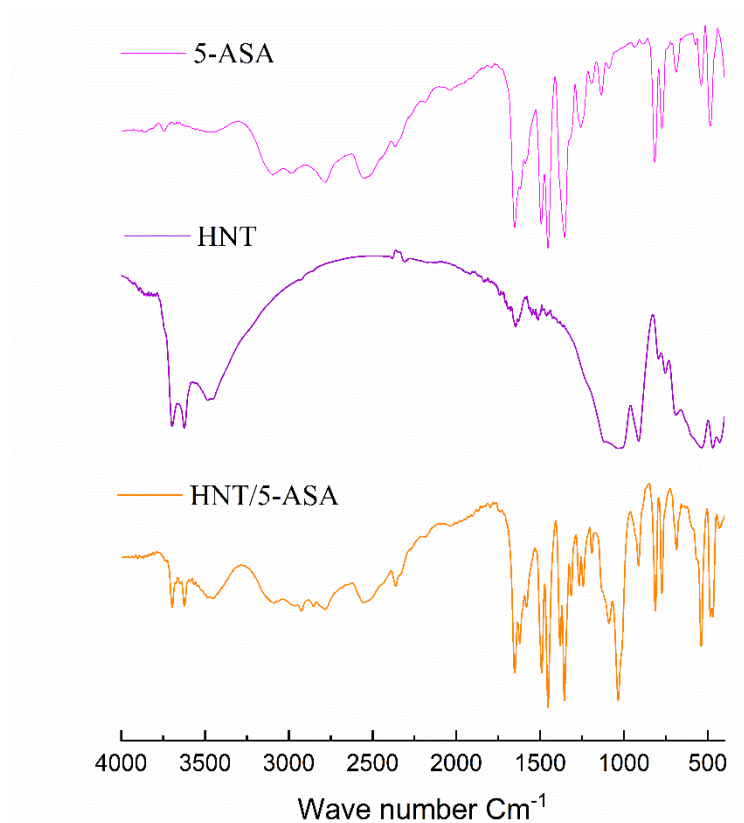
Fig. 3: FTIR spectra of HNT, 5-ASA and HNT/5-ASA samples

The spectra of all samples, as shown in figure4 displayed the unique bands associated with the drug and the mesoporous silica nanoparticles. Specific peaks were consistently detected at frequencies of 2553 cm^{-1} (-NH$_2$ deformation), 1650 cm^{-1} (C=O stretch of carboxylic acid), 1453 cm^{-1} (C=C stretching), and 1350 cm^{-1} (O-H bending). Furthermore, the peaks at 819 and 682 cm^{-1} were recognized as Aromatic C-H out-of-plane bending vibrations. Importantly, the peaks corresponding to 5-ASA are present throughout the spectra. Moreover, the presence of two fine absorption bands at 3628 and 3702 cm^{-1} were attributed to stretching vibrations of inner OH groups located on shared interfaces between the clay layers and external OH groups located on non-shared surfaces, respectively. While the vibrations at 3452 and 916 cm^{-1}are due to the OH bending. Consequently, these bands are the main characteristic peaks of HNT.

Chapter V: *Optimizing Colon-Targeted Therapy through Mesalazine*
                                                Delivery via pH-Sensitive Halloysite/ Polysaccharide
                                                Nanocomposites: In vitro, In silico and Computational study.
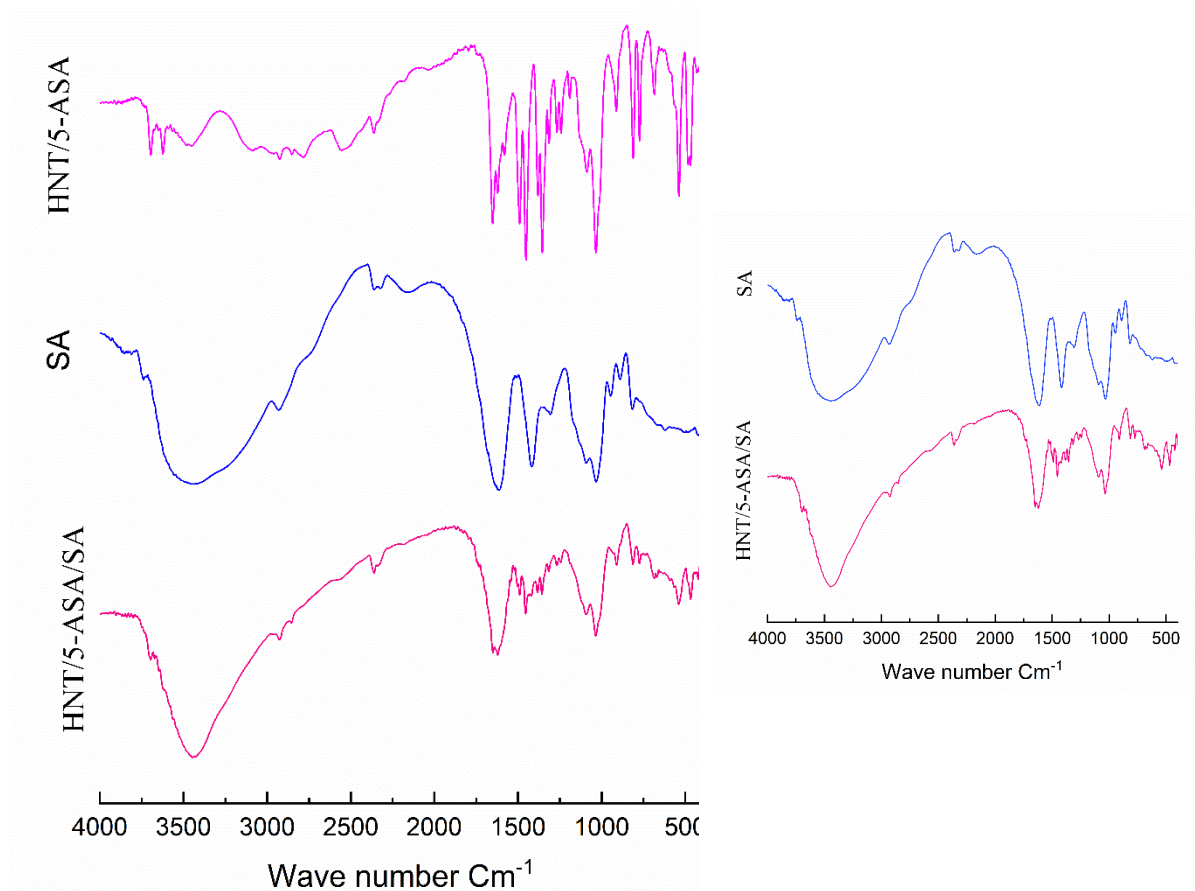
Fig. 4:   FTIR spectra of HNT/5-ASA, SA and, HNT/5-ASA/SA samples.

The thermal stability of microparticles generated is crucial for human beings in drug delivery applications. This analysis can also serve for detecting chemical changes in drug ingredients induced by the preparation process. So, information from its results is critical for determining the success of microparticle production or active component encapsulation **[49]**.

The thermal gravimetric analysis curves (TGA) obtained under nitrogen atmosphere for the HNT/5-ASA and HNT/5-ASA/SA in comparison with the HNT; 5-ASA and, SA samples are shown in figure 5. It is clear that the TGA curve of pristine HNT reveals a first loss (5%)in the temperature range 25-120°C which is ascribed to the dehydration of the material, including removal of the physically adsorbed and the interlayer water. Further, a significant loss (13.3%) in the range 150-550°C has been attributed to the dihydroxylation of the structural aluminol (Al-OH) and silanol (Si-OH) groups of HNT (figure 5.A).

Chapter V: *Optimizing Colon-Targeted Therapy through Mesalazine*
Delivery via pH-Sensitive Halloysite/ Polysaccharide
Nanocomposites: In vitro, In silico and Computational study.

The TG analysis of 5-ASA exhibits a complete mass loss occurring in one step within the temperature range of 225-367°C with a maximum at approximately 290°C reflecting the progressive decarboxylation leading to the breakdown of the molecular structure of mesalazine(See figure 5B)**[45-50].**

While the TGA/DTG curve of sodium alginate (figure 5. C) revealed a two-steps weight loss. The initial of about 11.9% and which takes place at 45-120°C was attributed to moisture evaporation, in the second stage, a considerable weight loss of around 36.55% was detected at temperatures ranging from 200 to 310°C. The existence of numerous functional groups and molecular interactions inside the sodium alginate molecule contributes to the complicated character of the degradation process **[51]**. The breakdown of the polymer structure results in the creation of water, methane, and (carbon dioxide).
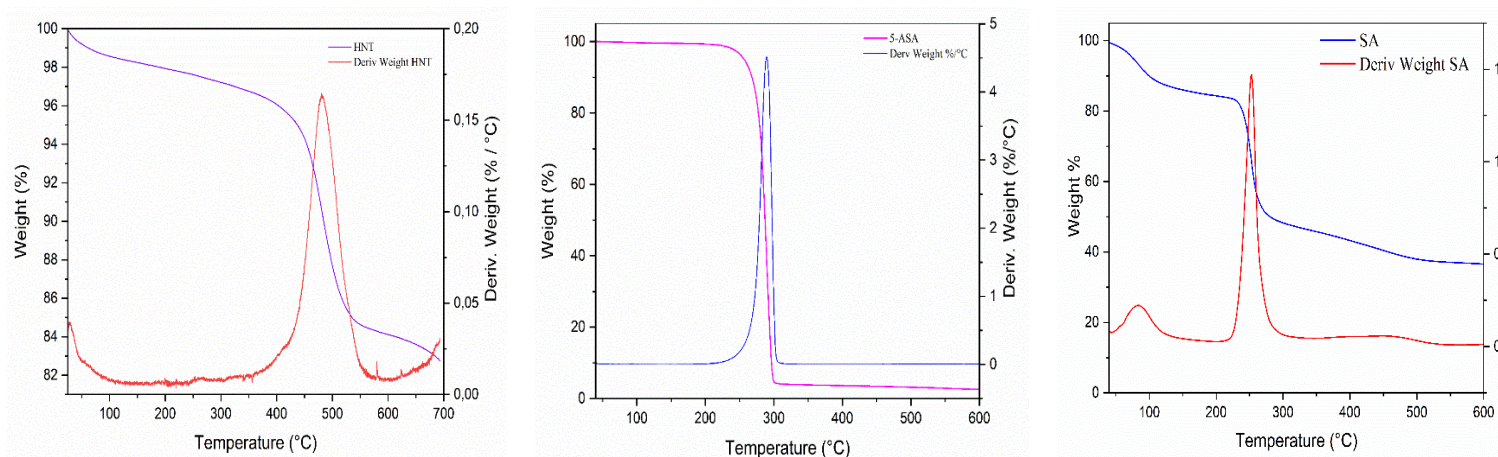
Fig. 5: TGA /DTG patterns of (A) HNT,(B) 5-ASA, (C) SA.

For the evaluation of the amount of drug loading in the inorganic carriers, the TGA method was performed. As depicted in figure6, the thermal stability and degradation behavior of HNT/5-ASA system exhibited two-weight losses in the intervals 220–300°C and 320–550°C. Upon the incorporation of sodium alginate to form HNT/5-ASA/SA biocomposite, the initial weight loss step before reaching 100°C is attributed to the evaporation of water content present in the material. The thermal behavior shows several levels of weight loss. The initial weight loss step before reaching 100°C is related to the evaporation of the alginate water content. Following that, a second stage of weight loss which happens between 200°C and 280°C is a

Chapter V: *Optimizing Colon-Targeted Therapy through Mesalazine*
Delivery via pH-Sensitive Halloysite/ Polysaccharide
Nanocomposites: In vitro, In silico and Computational study.

result of the thermal and mechanical disintegration of the alginate networks and mesalazine molecules. Furthermore, the mass loss ranging from 350°C to 600°C is related to alumina group degradation and dihydroxylation in HNT, as well as thermal disintegration of the alginate network [52,53].
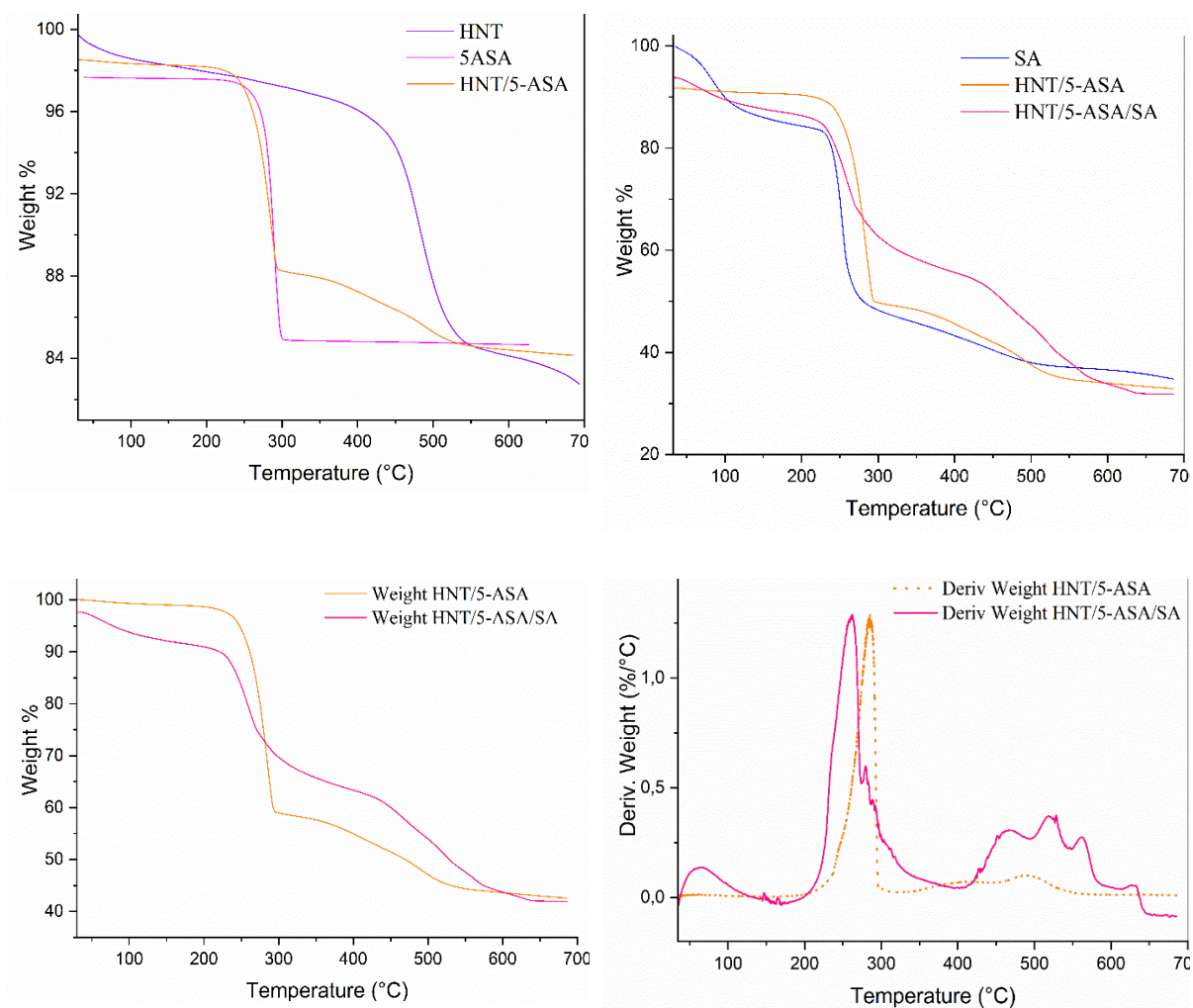
Fig. 6: TGA /DTG of the samples (HNT/5-ASA and HNT/5-ASA/SA).

Transmission electron microscopy (TEM) and scanning electron microscopy (SEM) were used to examine the structure of the HNT nanotubes. Foremost, the HNT transmission electron microscopy (TEM) images exhibit consistent elongated shapes. Besides, figure7(a)confirms that the inner region of the HNT is hollow and possesses open ends with smooth and crisp

Chapter V: *Optimizing Colon-Targeted Therapy through Mesalazine*
Delivery via pH-Sensitive Halloysite/ Polysaccharide
Nanocomposites: In vitro, In silico and Computational study.

surfaces. Figure7(a) displays a variety of nanotubular in shapes with varying sizes, ranging from 40 to 1300 nm in length. This observation aligns with the typical dimensions of clay minerals, which generally range from 20 to 2000 nm. The TEM images after the addition of 5-ASA show that the drug successfully enters the interior of HNT. The darkening of the tube cavity shown in figure 7(b) indicates that the 5-ASA molecules are adsorbed on both the interior and exterior surfaces of the tubes **[54]**.

The dispersion of exterior diameters for HNT and HNT/5-ASA is shown in figure8(a, b). The findings show relatively uniform deposition, with average exterior diameters of 37±8 nm for HNT and 42±4 nm for HNT/5-ASA, respectively. Both samples have a width at mid-height distribution curve of around 30 nm. Based on these data, the thickness of the 5-ASA deposition on the outer surface is expected to be 2.5 nm, computed as (42 - 37) / 2. Similarly, the average internal diameter of the empty nanotube volume in HNT/5-ASA and HNT is expected to be 11±3 nm and 16±3 nm, respectively, assuming uniform deposition as illustrated in figure9(a, b). As a consequence, the average uniform thickness of the deposited material is projected to be about 2.5 nm, which is calculated as (16-11) / 2.

The dried HNT/5-ASA/SA hybrid beads were characterized by SEM, and the surface morphology can be observed in figure10 as somewhat rough, and shriveled.
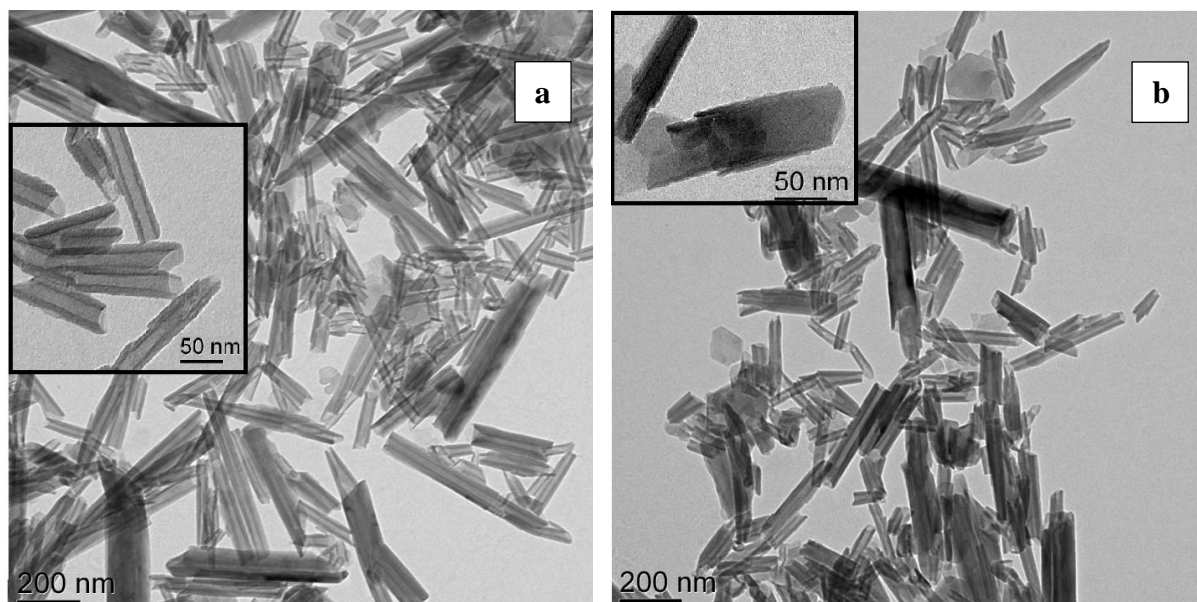
Fig. 7: TEM images of (a) HNT and (b) HNT/5-ASA.
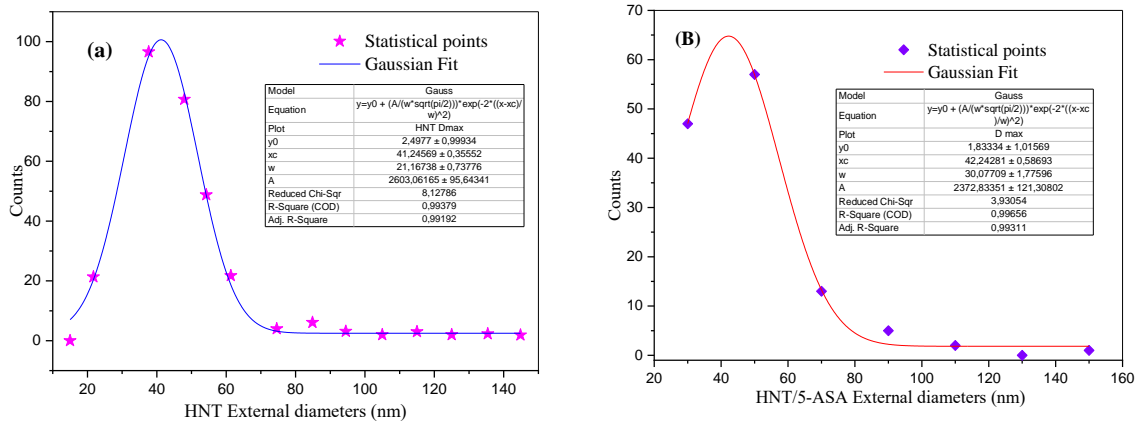
Fig. 8: Distribution of the external diameters of (A) HNT and (B) HNT/5-ASA.
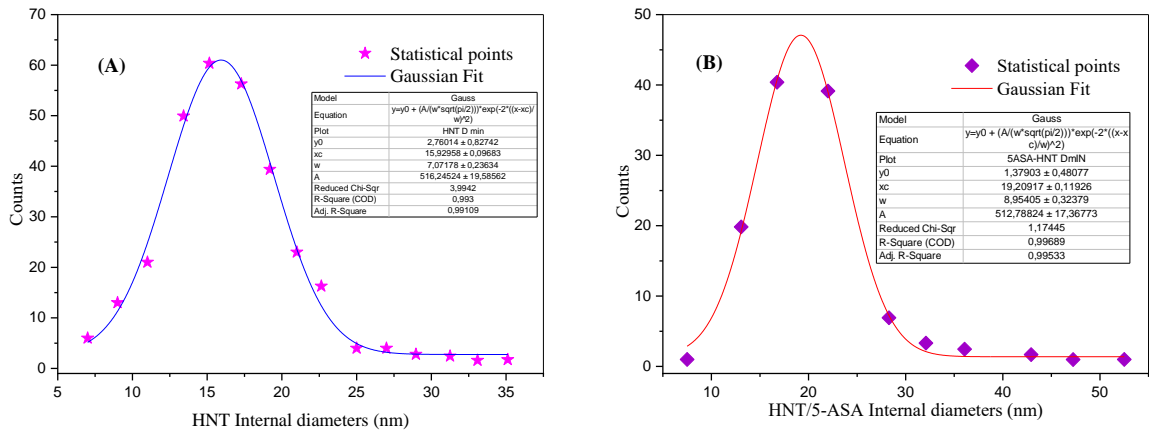
Fig. 9: Distribution of the internal diameters of (A) HNT and (B) HNT/5-ASA.
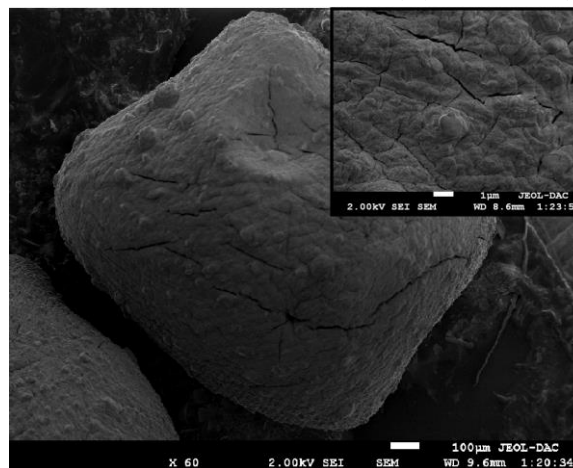
Fig. 10: SEM images of HNT/5-ASA/SA bead.

126

Chapter V: *Optimizing Colon-Targeted Therapy through Mesalazine*
Delivery via pH-Sensitive Halloysite/ Polysaccharide
Nanocomposites: In vitro, In silico and Computational study.

3.1.6. The X-ray diffraction (XRD)

The state of the molecules in the powder samples was determined using X-ray diffraction (XRD). Figure 11 depicts the XRD patterns of HNT_R, HNT, 5-ASA, and HNT/5-ASAas well as HNT/5-ASA/SA. Figure 11 displays as well the halloysite layouts. The basal spacing reflections reveal a high peak at 12.27°2θ, which equates to a 001 the basal spacing of 7.12 Å using Bragg's Law. There is also no peak around 8°2θ, indicating the absence of the 10Å form, which is typical of hydrated halloysite. The XRD investigation shows the presence of particular Miller indices corresponding to lattice planes at (020), (002), (003), (200), (211), and (3 to 31), corresponding respectively to the basal reflection at 20.3°, 24.86°, 35.34°, 36.02°, 54.96°, and 62.48°**[55].**

The HNT_R and HNT samples unquestionably contain traces of crystalline phases such as quartz, carbonate, alumina, and cristobalite. Furthermore, their interarticular distances, specifically $d_{(001)} = 0.712$ nm and $d_{(020)} = 0.436$ nm are suggestive of the dehydrated phase of HNT ($Al_2Si_2O_5$), which unequivocally exhibits a tubular morphology**[54].**

On the other hand, the crystalline character of 5-ASA was validated through the presence of distinct crystalline peaks at varying angles: 7.54°, 15.14°, 16.57°, 24.2°, 27.04°, and 28.31°. These typical peaks, however, disappear in the case of 5-ASA/loaded HNT (HNT/5-ASA), indicating a change of 5-ASA structure from crystalline to amorphous.

 Furthermore, sodium alginate XRD patterns show frequently crystalline structure as a result of the tight contact between the alginate chains via intermolecular hydrogen bonding. The reflection of their (110) plane of poly-guluronate unit, (200) plane from poly-mannuronate, and others from amorphous halo resulted in three diffraction peaks for sodium alginate at 2θvalues 13.9°,21.9° and 39.4° **[56]**. These findings also indicate the dispersion of 5-ASA molecules within the HNT structure. This observation aligns with the conclusions drawn in other prior studies involving drug-loaded HNT **[57]**.
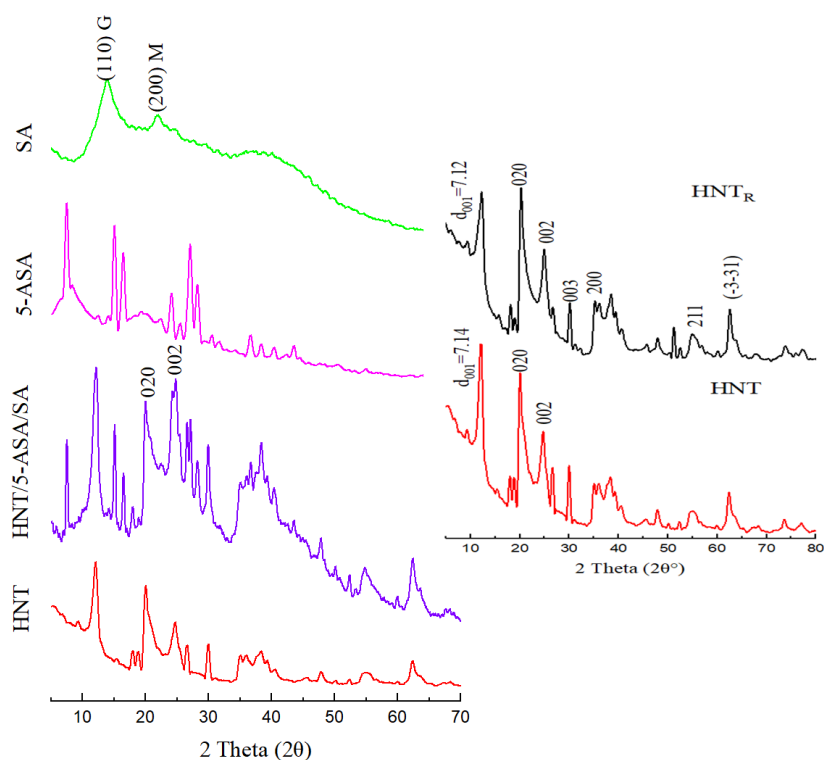
Fig. 11: XRD patterns of HNT_R, HNT, 5-ASA and HNT/5-ASA provided by

the main characteristic plane Miller indices.

3.1.7. Swelling Index

Swelling test for HNT/5-ASA/SA formulation was carried out at three distinct pH levels (1.2, 6.8 and 7.4) as shown in figure 12(a), to simulate the transition of beads in GIT. During 12 hours, the swelling index at pH 1.2 remains quite modest, ranging from 10% to 25% depending on the immersion time. This result indicates little swelling in an acidic environment. This phenomenon might be explained by the fact that sodium alginate is less sensitive to acidic environments, resulting in just a little increase in size of the beads. Extended swelling time (24 hours) seems to have negligible effect on the modest fluctuations in the swelling index. Contrarily and for the beads swelled moderately (15% to 30%) at pH 6.8 which reflects a slightly acidic to a neutral environment effect. This shows that the beads absorbed more water and expanded in size. However, the relatively substantial standard deviations show that the swelling behavior of the beads in this pH range is variable. The observed disintegration over time (increasing swelling followed by disappearance, after 24 hours) might be attributed

128

to sodium alginate sensitivity to pH and the probable destruction of the polymer structure. In the alkaline environment, pH 7.4, the swelling index reveals considerable swelling ranging from 20% to 45% throughout the 6 first hours. The beads absorbed water and enlarged as a result of this action. The quick rise in size followed by the beginning of bead disappearance implies that the beads are extremely sensitive to alkaline environments. At this pH, this behavior might be attributed to a combination of water absorption and probable breakdown or deterioration of the beads as depicted infigure12(b).
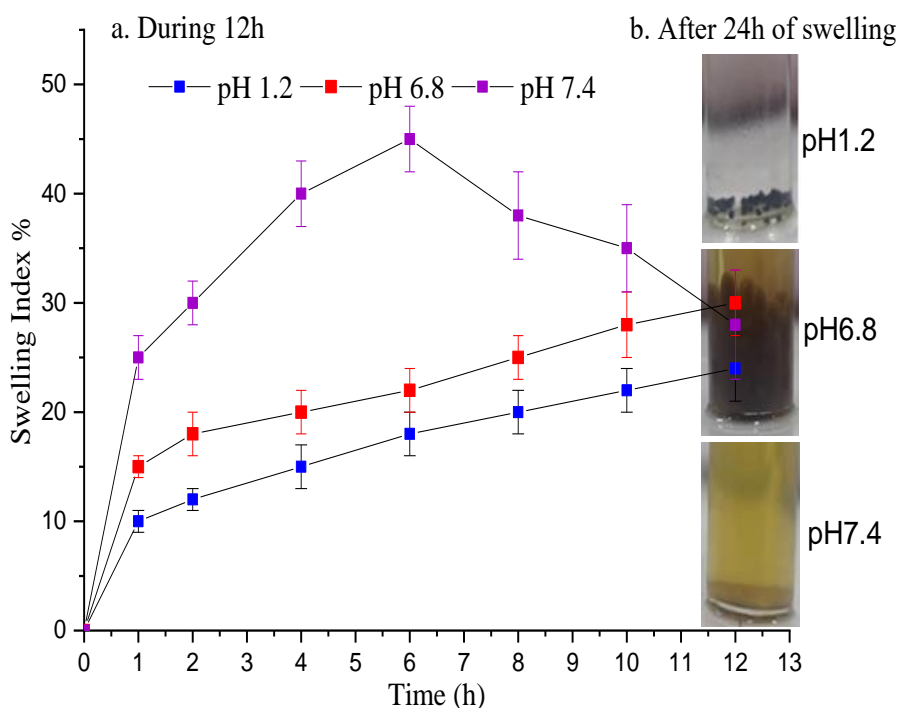
Fig.12: a) Swelling index of 5-ASA loaded halloysite bead during first12h.
b) Result of swelling after 24h.

3.1.8. *In vitro* **Drug Release Study**

Halloysite nanotubes have been extensively researched for medication delivery purposes. One interesting outcome is the possibility of targeting drug localization within the nanomaterial, which might lead to adjustable release rates using various preparation processes. This breakthrough holds the promise of expanding the scope of these systems applications. Based

on these possibilities, *in vitro*, experiments were carried out with 5-ASA incorporated into both powdered Halloysite and beads (Figure 13). For this purpose, the drug release profiles of HNT/5-ASA$_{powder}$, HNT/5-ASA/SA $_{Beads}$, and 5-ASApure, were tested individually in simulated gastro-intestinal fluids. The results showed a certain sustained release effects associated to 5-ASA entrapment into the HNT beads system.

As illustrated in Figure 13 at pH 1.2, the release profile of pure 5-ASA revealed a fast and total drug release during the first 45 min. In the case of the HNT/5-ASA powder formulation, the drug release occurs in two distinct phases: during the first two hours: an immediate burst release from the outer surface of about 60% of the drug. This swift release is likely attributed to the weak binding of surface-loaded 5-ASA through hydrogen interactions. The subsequent sustained release is linked to the liberation of lumen-loaded 5-ASA, which is delayed by the pseudo-one-dimensional nanotube structure of Halloysite **[58]**.Interestingly, the slow-release behavior of HNT/5-ASA/SA$_{Beads}$ in an acidic environment, with approximately 18% has been assigned to the presence of sodium alginate, which forms a protective gel layer around the drug-loaded halloysite particles. This gel layer acts as a barrier, hindering the diffusion of mesalazine from the halloysite reservoir to the surrounding acidic medium. The percentage of 5-ASA release from HNT/5-ASA$_{Powder}$ at simulated intestinal pH shows a quick and complete liberation profile (480 min) compared to the HNT beads. In contrast, the release from HNT/5-ASA/SA formulation was quite insignificant for period of 45 min, and then presented a remarkable controlled release, reaching 80% at 500 min caused by the presence of the polymer barrier which slows down the drug release process. In pH 7.4 case, the *in vitro* release profile from HNT/5-ASA/SA$_{Beads}$ demonstrates an exceptional 5-ASA controlled release achieving 100% in 750 min. The incorporation of SA enhanced further the precision of drug release, leading to a more regulated and controlled liberation of 5-ASA which may be due to mucoadhesive property of the sodium alginate.

Chapter V: *Optimizing Colon-Targeted Therapy through Mesalazine*
Delivery via pH-Sensitive Halloysite/ Polysaccharide
Nanocomposites: In vitro, In silico and Computational study.
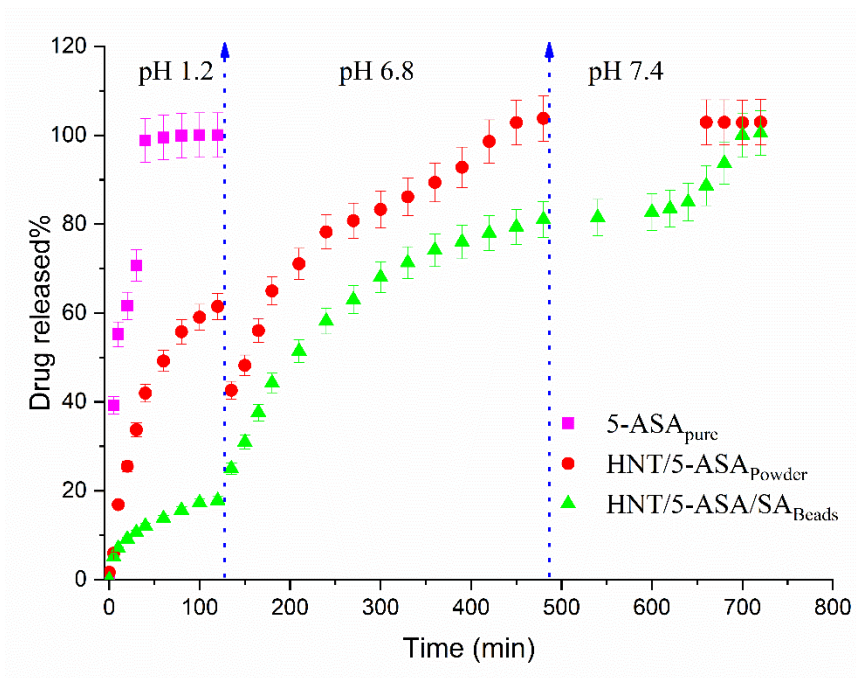
Fig. 13: Drug release of 5-ASA from hybrid materials at different pH values.

3.1.8. Drug Release Kinetics treatment

The investigation of drug release kinetics is crucial for understanding the behavior of drug delivery systems and optimizing their therapeutic efficacy. Subsequently, various kinetic models were utilized to analyze the mesalazine release from different matrices, and the results are summarized intable3.

Table 3: Kinetic treatment release results of prepared 5-ASA formulations.

Formulations	First order		Higuchi square root		Korsmeyer-Peppas model		
	K	R^2	K_H	R^2	K_P	N	R^2
HNT/5-ASA	0.024	0.981	6.115	0.991	4.936	0.536	0.969
HNT/5-ASA/SA	0.037	0.946	1.591	0.983	2.877	0.385	0.999

As a result, the release kinetic results of 5-ASA of the formulations showed that data were well-fitted for each case investigated (Table 3). It was found that the *in vitro* drug release of HNT/5-ASA powder was accurately described by the Higuchi model provided a superior linearity of the plots (R^2 = 0.991) closer to 1, indicating that the release kinetics are described

by a Higuchi square root equation. This observation implies that the release of 5-ASA from the nanotube carrier is primarily governed by diffusion, as further supported by a zero-order model (R^2 = 0.981). However, to confirm the release mechanism, the *in vitro* release results of HNT/5-ASA/SA beads were fitted to the Korsmeyer-Peppas model indicating the highest value of n= 0.385 with R^2 = 0.999. This indicates that the drug release is primarily controlled by Fickian diffusion, and the release mechanism is consistent with the Higuchi model**.**

3. Docking study

Molecular docking of test compounds into the active sites of PPAR-γ, COX-1, and COX-2 was done separately and was shown to be effective based on the formation of complexes of PPAR-γ, COX-1, and COX-2 with the ligand, as depicted in figure14. Table 4 displays the binding energy and interacting amino acids from the docking data.

Table 4: Binding affinity and types of binding energy of 5-ASA with each receptor.

Receptors	Score	Total. Energy (Kcal/mol)	Internal. Energy (Kcal/mol)	VDW's Energy	Electrostatic Energy
PPAR-γ	-6.846	-13.077	-28.895	-7.283	-21.612
COX-1	-6.989	-27.866	-46.407	-3.663	-42.744
COX-2	-7.083	-17.328	-38.213	-13.025	-25.188

PPAR-γ plays a pivotal role in regulating inflammation and metabolism. After conducting the docking study, the results of the interaction between ligand(5-ASA) and PPAR- γ revealed a favorable docking score of -6.848 kcal/mol indicating a high binding affinity, with conventional hydrogen bonds in Arginine (ARG: B173) and Glutamic acid (GLU: B100) at a distance of 1.66 Å, and 2 Å respectively. However, ligand and Tyrosine (TYR: B96) formed π –Alkyl and π – π T-shaped interactions, respectively. The Total Energy -13.077 kcal/mol implies a stable complex, while the Internal Energy -28.895 kcal/mol suggests a favorable binding conformation. The presence of favorable interactions is shown by Van Der Waal's Energy of -7.283 kcal/mol and Electrostatic Energy of -21.612 kcal/mol. These findings contribute to our understanding of 5-ASA pharmacological properties and highlight PPAR- γ as a promising target for therapeutic interventions.

A. Molecular docked complex   B. 3D   C. 2D
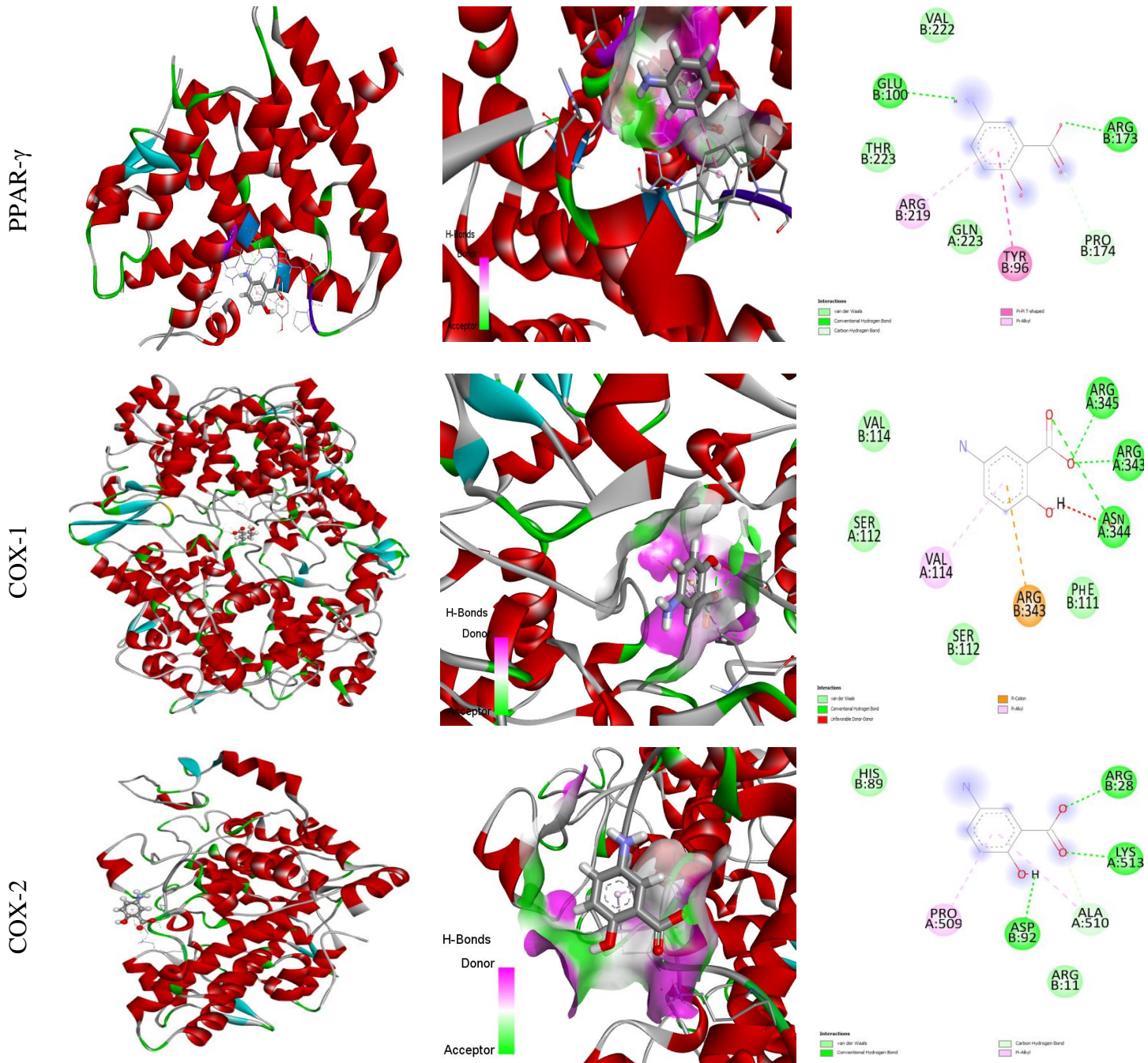
Fig. 14: A (3D) Molecular docked complexes of PPAR-γ, COX-1, and COX-2 with 5-ASA.

B(3D) image of H-binding of the 5-ASA with PPAR-γ, COX-1, and COX-2.

C(2D) diagram involving various amino acid residues after docking

of the 5-ASA with PPAR-γ, COX-1, and COX-2.

133

Unlike traditional nonsteroidal anti-inflammatory drugs (NSAIDs), 5-ASA does not directly inhibit COX-1 and COX-2 enzymes. As a result, the docking research revealed the kind of interaction between Ligand and COX-1, with a significant score of -6.989 Kcal/mol.The binding interactions were characterized by hydrogen bonding between 5-ASA and key amino acids such as Arginine (ARG: A343), Asparagine (ASN: A344), and Arginine(ARG:A345)at defined distances of 1.66 Å, 2.6 Å and 1.63 Å, respectively. The total Energy -27.866 Kcal/mol suggests a stable complex formation, with lower values indicating a higher likelihood of successful binding. The internal energy, determined to be -46.407 Kcal/mol, signifies that 5-ASA is adopting a conformation conducive to binding within the COX-1 receptor. The van der Waals (VDW) energy of -3.663suggests that adjacent atoms have advantageous non-covalent interactions. Furthermore, the Coulomb energy of -42.744 emphasizes the strong electrostatic connection between charged groups in the ligand and receptor. Collectively, these energy components provide a comprehensive view of the binding interactions.

Moreover, COX-2 is a crucial enzyme in the prostanoid biosynthesis pathway. Leveraging advanced molecular docking techniques. A key docking score of -7.083 Kcal/mol with a total Energy value of -17.328 shows that mesalamine and COX-2 complex have a strong binding affinity and stability. The engagement of typical hydrogen bonds Lysine (LYS: A513), Arginine (ARG: B28), and Aspartic (ASP: B92) and ligand with distances of 1.71 Å, 1.93 Å, and 2 Å demonstrates the complicated nature of the interaction. These connections represent particular and directed interactions, emphasizing the binding process accuracy. Additionally, the participation of carbon-hydrogen bonds and hydrophobic interactions as in Alanine (ALA: A510) greatly adds to the binding energy. Furthermore, the presence of π-alkyl interactions highlights the contribution of π-cloud interactions between aromatic systems to the binding mechanism.

In summary, these findings shed light on the molecular interactions of 5-ASA with important enzymes involved in inflammation and metabolism regulation. The reported binding affinities and stability of 5-ASA point to its potential as a therapeutic intervention, specifically targeting the PPAR- γ and COX-2 pathways.

4. Density Functional Theory (DFT)

DFT calculations were used to construct the optimal molecular structures, frontier molecular orbitals FMOs, and mapping electrostatic potential MEP of 5-ASA and SA. The results are shown in figure15.Based on the aromatic cycle carbon atom sp^2hybridization; the optimal molecular structures of 5-ASA and SA have almost planar geometries (Figure15(A)).

4.1. Frontier Molecular Orbitals (FMOs)

The charge transfer between 5-ASA and SA molecules and their external environment relies on the Lowest Unoccupied Molecular Orbital (LUMO) considering the electron acceptor and the Highest Occupied Molecular Orbital (HOMO) as the electron donor. This electron transfer process is evident from the low values of E_{LUMO}, which signifies their electron-accepting tendencies, as depicted in figure15(B). Furthermore, all molecules exhibit a negative chemical potential, a key indicator of their stability[31]. We add that the gap energy (E_{GAP}), defined as the absolute difference between E_{LUMO} and E_{HOMO}, plays a vital role in characterizing molecular reactivity. A larger gap implies reduced chemical reactivity coupled with increased kinetic stability, whereas a smaller gap suggests the opposite [37-45]. The calculated gap for SA is 6,958 eV, indicating its hardness and a decreased chemical reactivity. In contrast, 5-ASA exhibits a softer nature $\Delta E_{GAP} = 4,252$ eV compared to SA, as evidenced by its smaller gap, signifying heightened chemical reactivity [45].

4.2. Molecular Electrostatic Potential (MEP)

The MEP (Molecular Electrostatic Potential) provides crucial insights into the locations where nucleophilic and electrophilic reactions are likely to occur. ESP (Electro-Static Potential) is closely related to the molecule partial charges and electronegativity characteristics. It serves as a fundamental tool for understanding how a molecule is recognized as biologically active and how it responds to electrophilic and nucleophilic attacks. By examining the surfaces and contours, one can gain an understanding of how various molecular geometries interact [59]. As shown in figure15(C), a uniform distribution of electron density across the molecules, while the ESP bar data reveals localized negative ESP regions within specific areas of the molecules

under investigation. Various colors on the ESP bar correspond to distinct electrostatic potential values. The red color highlights highly negative electrostatic potential, notably concentrated around the hydroxyl and carboxyl groups in the case of the 5-ASA molecule, measuring approximately $-7.33*10^{-2}$V. Additionally, a weaker negative potential is observed surrounding the organic cycle and the amine group, relative to the conjugated π-electrons and electronic doublet of the nitrogen atom, respectively. Conversely, the blue color signifies a highly positive potential mainly associated with hydrogen atoms, reaching a maximum value of $7.33*10^{-2}$V on the external surface.

In the SA molecule, the most negative potential is prominently centered on the COOH group, represented by red or orange color, extending across multiple regions of the alginate molecule. Particularly active sites, such as certain oxygen atoms, besides the highest values of SA reach approximately $6.69*10^{-2}$V.

A. Optimized molecular structures

5-ASA	SA

B. Frontier molecular orbitals (FMO)

LUMO PLOT

$E_{LUMO} = -1.067$

LUMO PLOT

$E_{LUMO} = -0.282$

$\Delta E_{GAP} = 4,252$ eV

$\Delta E_{GAP} = 6,958$ eV

HOMO PLOT

HOMO PLOT

$E_{HOMO} = -5.319$

$E_{HOMO} = -7.234$

C. Mapping electrostatic potential (MEP)

$-7.33 10^{-2}$ $7.33 10^{-2}$ V

$-6.69 10^{-2}$ $6.69 10^{-2}$ V
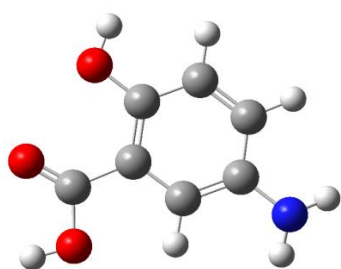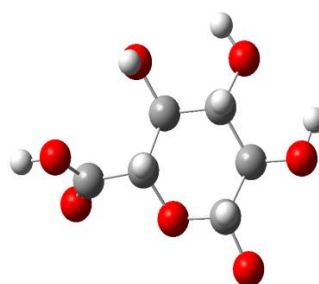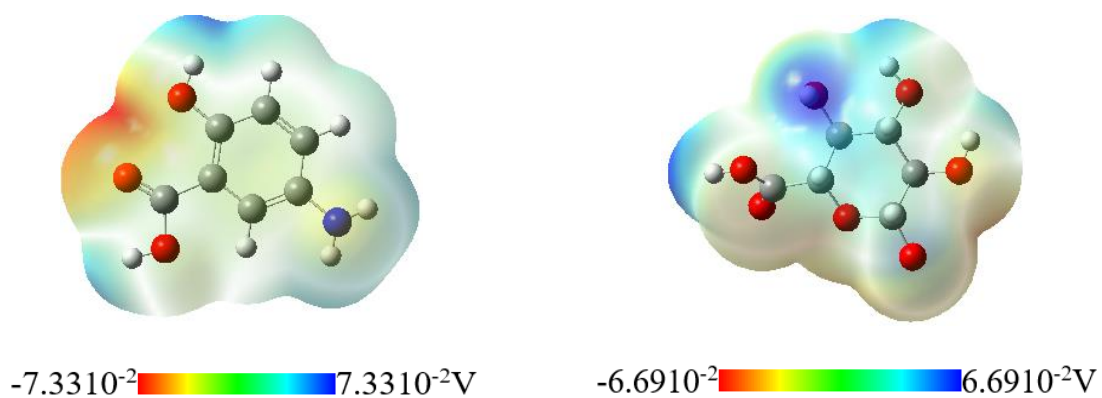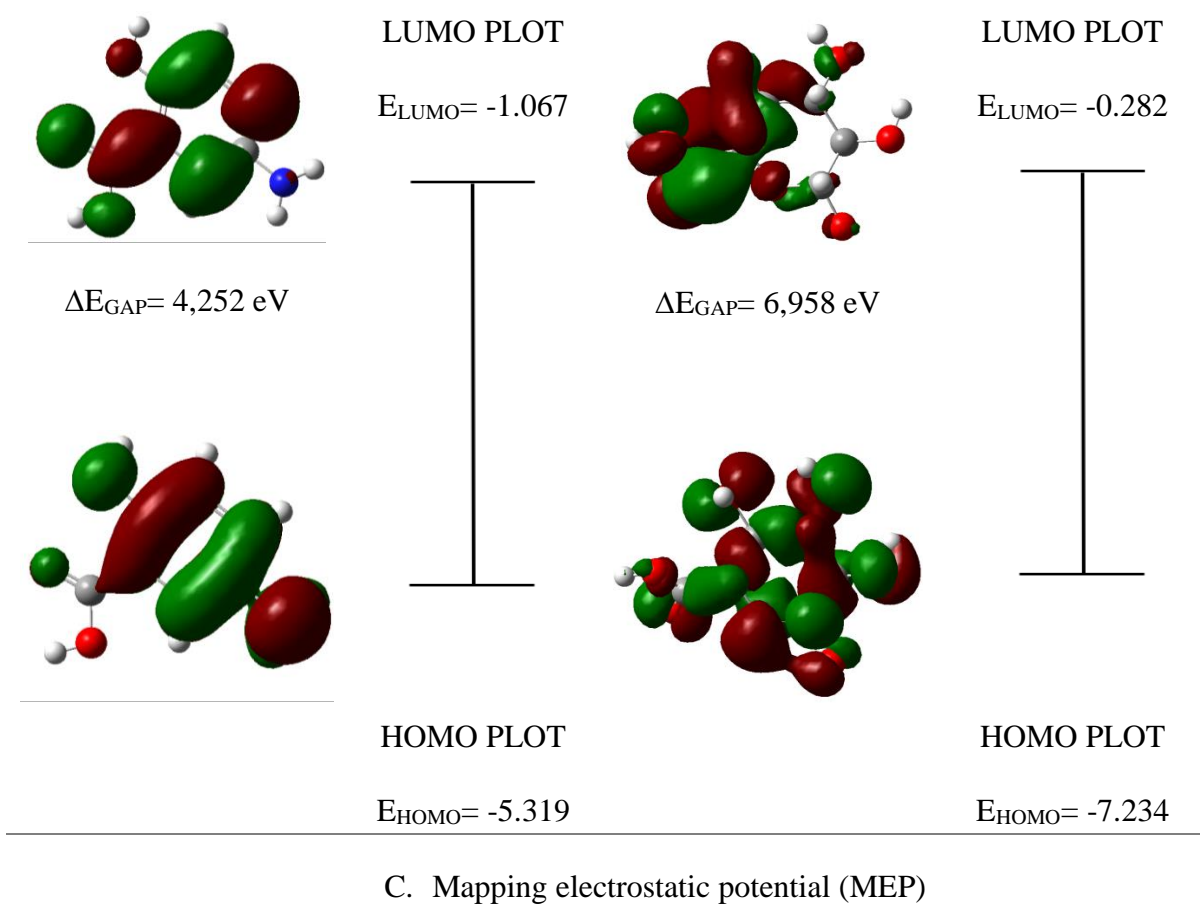
Fig.15: 5-ASA and SA optimized molecular structure, frontier molecular orbitals, and electrostatic potential mapping.

4.3. Molecular Dynamic Simulation (MDS)

In the arrangement of the halloysite structure, various OH groups are discernible: ones positioned vertically to the surface, others lying parallel to it, and those within the inner region oriented towards the siloxane surface (Figure 1). Because of their varied electrostatic interactions, the H and O atoms within these groups have different atomic charges.

Molecular Modeling of the Adsorption of 5-ASA in the HNT was then investigated to identify the most essential interaction sites with the mineral as depicted in figure 16(A,B).

The outcomes of the adsorption demonstrate that the adsorbate and the surface have significant interactions. These interactions are primarily hydrogen bonds and electrostatic forces and involve specific atomic groups. In the case of the negatively charged O atoms within the carbonyl and hydroxyl groups of 5-ASA interact with the positively charged H atoms of the surface aluminol groups. These interactions occur at distances of approximately 1.80 Å between the carbon-oxygen bond (C=O) and the hydrogen-oxygen bond (HOAl), and 1.92 Å for the carbon-carbon (C-C) bond adjacent to the hydrogen-oxygen bond (HOAl), indicating a stronger hydrogen bond interaction. Moreover, the interactions extend to the 5-ASA amino group, where the hydrogen atoms interact with the oxygen atoms of the surface aluminol groups. These interactions are detected at distances of 2.29, 2.34 and, 2.48 Å, corresponding to different amino group orientations and locations relative to the aluminol groups. Finally, there are interactions between the amino nitrogen atoms of 5-ASA and the surface oxygen atoms. These interactions occur at a distance of around 2.013Å showing that the interacting atoms are separated by a large distance. The adsorption energy of the complex was −40.348 kcal/mol (Table5), indicating that this phenomenon is spontaneous and energetically a favorable process.

In contrast to the strong hydrogen bonding interactions with Al-OH groups, the interaction between 5-ASA and the hydrophobic siloxane (-Si-O-) regions is weaker. This is primarily because the siloxane regions are non-polar and do not readily form hydrogen bonds with 5-ASA. Instead, this later interacts with the siloxane groups primarily through Van der Waals forces, which are relatively weaker forces of attraction between molecules. Since 5-ASA is

Chapter V: *Optimizing Colon-Targeted Therapy through Mesalazine*
Delivery via pH-Sensitive Halloysite/ Polysaccharide
Nanocomposites: In vitro, In silico and Computational study.

hydrophobic and lacks strong polar functional groups, its interaction with the hydrophobic siloxane regions is less significant compared to its interaction with the Al-OH groups.

Table 5: Adsorption energies (kJ.mol^{-1}) of 5-ASA and water molecules
on halloysite surface model.

001 Surface	Total energy	Adsorption energy	Rigid adsorption energy	Deformation energy	5-ASA : dE_{ad}/dN_i	H_2O : dE_{ad}/dN_i
5-ASA	-0,931	-40,474	-19,927	-20,547	-40,474	/
Water	-3,637	-4,347	-3,638	-0,709	/	-4,347
5-ASA/50H_2O	-114,063	-189,077	-133,099	-55,978	-2,029	-41,327

00-1 Surface	Total energy	Adsorption energy	Rigid adsorption energy	Deformation energy	5-ASA : dE_{ad}/dN_i	H_2O : dE_{ad}/dN_i
5-ASA	-0,805	-40,348	-19,709	-20,638	-40,348	/
Water	-3,591	-4,300	-3,591	-0,709	/	-4,300
5-ASA/50H_2O	-93,976	-168,991	-112,933	-56,0578	-1,724	-39,616

a)Silicon oxide external(00-1)   b)Aluminum oxide internal (00 1)
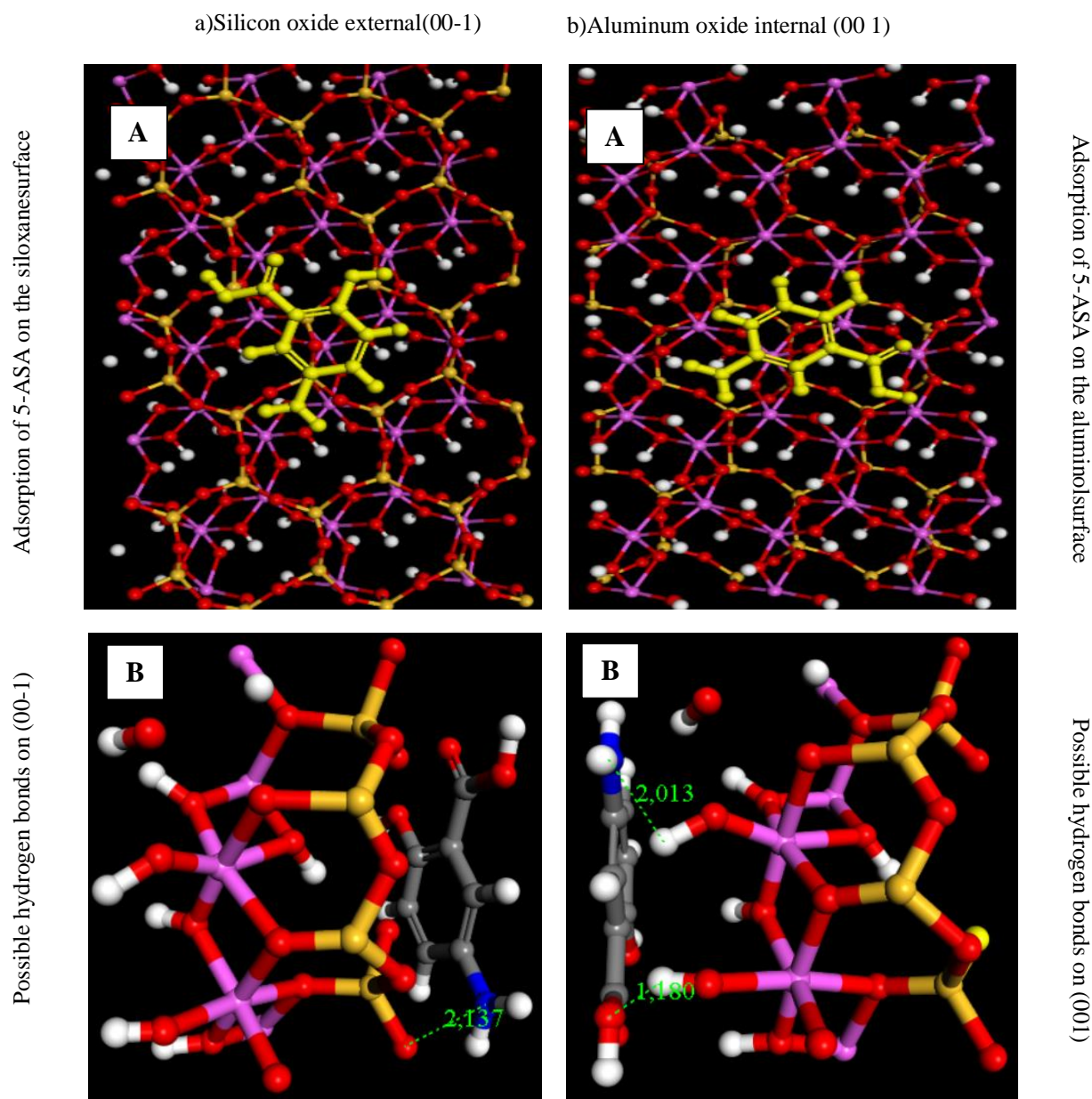
Fig. 16: A: Adsorption complexes of the 5-ASA on the kaolinite. (a)siloxane surface (00-1) and (b) aluminol surface (001) optimized with DFT.

B: The possible hydrogen bonding adsorption arrangement (00-1) and (001) surfaces.

As shown in figure. 17(1), one alternate configuration for 5-ASA entails putting it perpendicular to the mineral surface, allowing for simultaneous interactions with both the aluminol and siloxane surfaces. This structure has been confirmed and agrees with the observed interaction patterns inside kaolinite exterior and interior monolayers. With a distance of d(COH…O(H)Al) = 1.527Å, a strong hydrogen connection arises between the carboxylic hydrogen atom and the oxygen atoms inside the aluminol groups of the mineral surface.

Chapter V:

Optimizing Colon-Targeted Therapy through Mesalazine Delivery via pH-Sensitive Halloysite/ Polysaccharide Nanocomposites: In vitro, In silico and Computational study.

Notably, the orientation of the OH bond is parallel to the mineral surface (001) plane. Furthermore, the amino hydrogen atoms form weaker hydrogen bonds with the siloxane oxygen atoms of the mineral surface, at a distance of $d(NH…OSi) = 2.041$ Å.
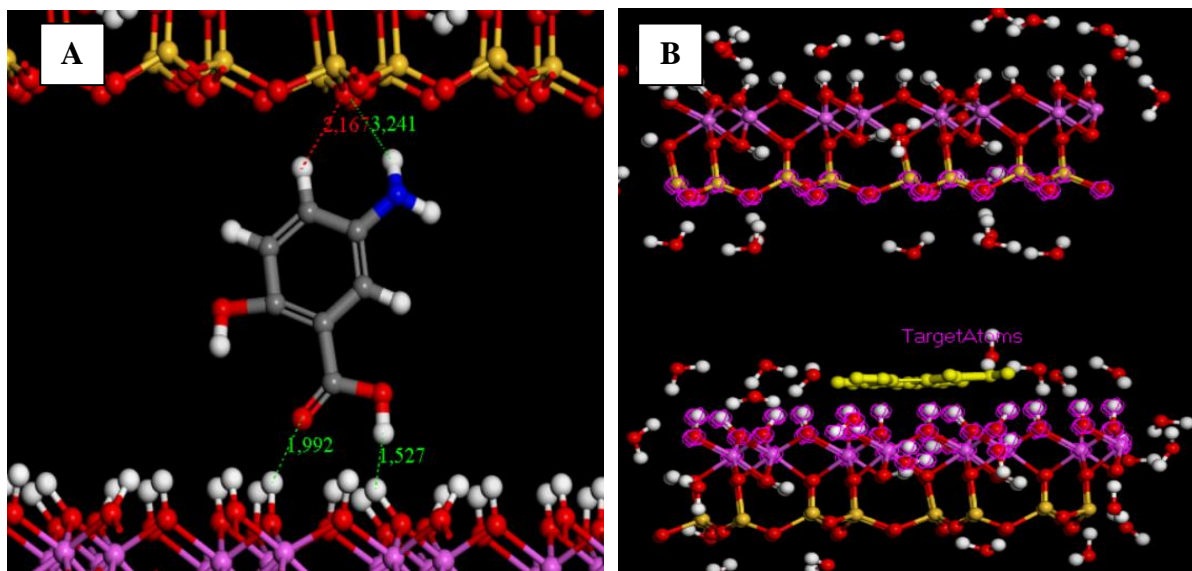
Fig. 17. A. Intercalation of a 5-ASA molecule between the aluminol and siloxane surfaces of kaolinite. **B.** The adsorption of 5-ASA on water-filled Optimized Halloysite model.

When the same experiment was carried out in the presence of water molecules, following halloysite optimization, the interior and exterior zones were filled with water, and it was observed that: water molecules located outside the halloysite nanotube maintained an approximate distance of 2.268-3.093 Å from the basal tetrahedral O atoms. On the other hand, internal water molecules confined within the nanotube were positioned in closer proximity to the aluminol surface, exhibiting an average distance of 1.504-1.833 Å. These measurements, indicating shorter distances between water molecules and the aluminol surface as compared to the outer siloxane surface, strongly imply that the aluminol surface demonstrates greater hydrophilicity.

Parallel to the mineral surface near the aluminol surface of the halloysite, the adsorption of 5-ASA was observed. Notably, the intramolecular hydrogen bond of the 5-ASA molecule remained stable, with distances around approximately 1.753 Å between hydroxyl group (C-COH) and the carbonyl group (O(H)-CO) with an adsorption energies -184,405 kcal/mol.

141

Furthermore, it is worth noting that no water molecule entered the space between 5-ASA and the mineral surface, as illustrated in figure17(2).

Table 6: Adsorption energies ($kJ.mol^{-1}$) of mesalazine and water molecules on halloysite/ sodium alginate model.

00-1 Surface	Total energy	Adsorption energy	Rigid adsorption energy	Deformation energy	5-ASA : dE_{ad}/dN_i	H_2O : dE_{ad}/dN_i
SA	8,765	-30,777	-10,108	-20,670	-30,777	/
Water	-2,6844	-3,3931	-2,684	-0,709	/	-3,394
SA/50H_2O	-87,970	-123,442	-87,978	-35,465	/	-2,195
SA/5-ASA/50H_2O	-58,404	-173,318	-98,285	-75,033	-39,887	-33,856

The components in the complex HNT/5-ASA/SA can interact in a variety of ways. Primarily due to the chemical nature of the compounds involved. These interactions can include:

In the case of the direct interaction between HNT surface and SA: Sodium alginate contains negatively charged carboxylate (-COO$^-$) groups, while the halloysite surface has negatively charged siloxane groups (Si-O-Si). This charge complementarity leads to electrostatic attraction, promoting the adsorption of sodium alginate onto the halloysite surface. Additionally, As depicted in figure. 17(3.A). the external surface of HNT is rich in siloxane groups while the SA features oxygen-rich units, acting as hydrogen bond acceptors. On the other hand, the hydrogen atoms in halloysite siloxane groups serve as hydrogen bond donors. These hydrogen bonds are weaker than covalent bonds but can play a significant role in the adsorption process. Besides, this interaction plays a crucial role in controlled drug delivery, where it facilitates stable encapsulation and controlled release due to strong hydrogen bonding which reveals the precision of substance release. Van der Waals forces, like hydrogen bonds, are relatively weak non-covalent interactions caused by oscillations in electron distribution around atoms and molecules. These forces may help to attach SA molecules to the HNT surface. Additionally, as depicted in table 6. Water molecules present in the solution can mediate the interaction between SA and the HNT surface by forming a hydration layer around the particles, affecting SA adsorption behavior.

According to Lisuzzo et al. **[60]**, capillarity causes nanotubes to fill quickly impacted by the Gibbs-Thomson effect, reducing the requirement for vacuum removal of air from the interior. However, the filling process generated by water confinement shows that vacuum operation and lower pressure boost halloysite nanotube loading even more due to the loading is not restricted to the lumen of the HNT, it might occur at the surface. And, considering that 5-ASA possesses both donor and acceptor hydrogen bonding sites (NH_2 and $-COO^-$), it can interact with SA and the HNT surface through hydrogen bonding (Figure 18(B)), potentially involving electrostatic attraction or repulsion. Additionally, hydrogen bonding may develop as a result of the oxygen-rich units in the SA and the functional groups in 5-ASA, which increases the complex stability. When the components are close together, Van der Waals forces may contribute to binding. These interactions, together with the possibility of covalent bonding, impact the complex behavior and stability. Furthermore, the particular structure of 5-ASA may comprise aromatic rings, that can engage in π-π interactions with other aromatic components present in SA or on the HNT surface.
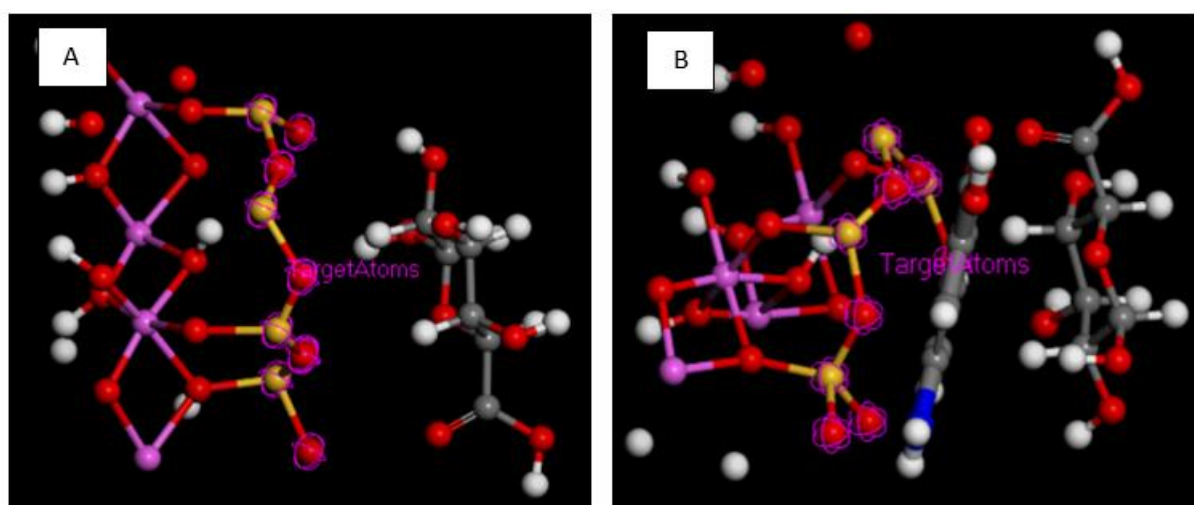
Fig. 18: Adsorption complexes of: (A) HNT/SA system,(B) HNT/5-ASA/SA system.

Conclusion

In the treatment of Crohn's disease, 5-ASA plays a crucial role as a specialized, colon-targeted medication. Achieving controlled release of mesalazine is essential to reduce unintended dispersion within the gastrointestinal tract, thereby enhancing the absorption of the medication. The current investigation effectively supported the creation and assessment of a new formulation that provides both an improvement in 5-ASA therapeutic efficacy and a decrease in its principal adverse effects. The challenge is to produce an effective pH-sensitive complex HNT/5-ASA/SA beads. The findings demonstrated the pH sensitivity of the HNT/5-ASA/SA complex, as 5-ASA release was significantly increased at pH values of 6.8 and 7.4, in contrast to its restricted release at pH 1.2. The interactions of 5-ASA with key enzymes involved in the control of inflammation and metabolism. The favorable docking results and strong binding affinity observed between 5-ASA and PPAR-γ underscore the potential of PPAR-γ as a therapeutic target. The formation of stable complexes and precise interactions between 5-ASA and essential amino acids in COX-1 highlight the potential of 5-ASA as an alternative to conventional NSAIDs for inflammation management. Additionally, the significant binding affinity and stability of the 5-ASA-COX-2 complex demonstrated through various types of interactions, suggest its effectiveness in targeting the prostaglandin biosynthesis pathway. Besides our findings shed light on the interaction of HNT, 5-ASA, and SA within the lumen region and on the outer surfaces was confirmed through physicochemical characterization. The Monte Carlo theory-based study demonstrates a strong affinity for 5-ASA adsorption on both internal and external surfaces, and these adsorption affinities are not significantly affected by the presence of water molecules. The interaction mechanism between 5-ASA and HNT is physical, with multiple hydrogen bonds and electrostatic interactions playing a predominant role. Additionally, Interactions in the HNT/5-ASA/SA complex include electrostatic attraction between the carboxylate groups of sodium alginate and the siloxane groups of halloysite, as well as hydrogen bonding with oxygen-rich units. Because of its aromatic composition, 5-ASA also helps through hydrogen bonding and potential - interactions.

References

[1] N.G. Veerabadran, R.R. Price, Y.M. Lvov, Clay nanotubes for encapsulation and sustained release of drugs, Nano. 2 (2007) 115–120.https://www.worldscientific.com/doi/abs/10.1142/S1793292007000441

[2] M. Massaro, G. Cavallaro, C.G. Colletti, G. Lazzara, S. Milioto, R. Noto, S. Riela, Chemical modification of halloysite nanotubes for controlled loading and release, J. Mater. Chem. B. 6 (2018) 3415–3433.https://doi.org/10.1039/C8TB00543E

[3] G. Cavallaro, L. Chiappisi, P. Pasbakhsh, M. Gradzielski, G. Lazzara, A structural comparison of halloysite nanotubes of different origin by Small-Angle Neutron Scattering (SANS) and Electric Birefringence, Appl. Clay Sci. 160 (2018) 71–80. https://doi.org/10.1016/j.clay.2017.12.044

[4] G. Cavallaro, G. Lazzara, S. Milioto, Nanocomposites based on halloysite nanotubes and sulphated galactan from red seaweed Gloiopeltis: Properties and delivery capacity of sodium diclofenac, Int. J. Biol. Macromol. 234 (2023) 123645. https://doi.org/10.1016/j.ijbiomac.2023.123645

[5] P. Tang, Q. Sun, L. Zhao, H. Pu, H. Yang, S. Zhang, R. Gan, N. Gan, H. Li, Mesalazine/hydroxypropyl-β-cyclodextrin/chitosan nanoparticles with sustained release and enhanced anti-inflammation activity, Carbohydr. Polym. 198 (2018) 418–425. https://doi.org/10.1016/j.carbpol.2018.06.106

[6] H.-J. Hong, J. Kim, Y.J. Suh, D. Kim, K.-M. Roh, I. Kang, pH-sensitive mesalazine carrier for colon-targeted drug delivery: A two-fold composition of mesalazine with a clay and alginate, Macromol. Res. 25 (2017) 1145–1152. https://doi.org/10.1007/s13233-017-5150-5

[7] R. Deshmukh, R.K. Harwansh, Preformulation considerations development and evaluation of mesalamine loaded polysaccharide-based complex mucoadhesive beads for colon targeting, Indian J Pharm Educ Res. 55 (2021) 95–106. http://dx.doi.org/10.5530/ijper.55.1.13

[8]M. Sharma, B. Joshi, M. Bansal, M. Goswami, Formulation and evaluation of colon

targeted tablets of mesalazine, J. Drug Deliv. Ther. 2 (2012).

https://doi.org/10.22270/jddt.v2i5.290

[9] K. Mallikarjuna Reddy, V. Ramesh Babu, K.S.V. Krishna Rao, M.C.S. Subha, K. Chowdoji Rao, M. Sairam, T.M. Aminabhavi, Temperature sensitive semi-IPN microspheres from sodium alginate and N-isopropylacrylamide for controlled release of 5-fluorouracil, J. Appl. Polym. Sci. 107 (2008) 2820–2829.https://doi.org/10.1002/app.27305

[10]M. George, T.E. Abraham, Polyionic hydrocolloids for the intestinal delivery of protein drugs: alginate and chitosan—a review, J. Controlled Release. 114 (2006) 1–14.https://doi.org/10.1016/j.jconrel.2006.04.017

[11] S. Takka, A. Gürel, Evaluation of chitosan/alginate beads using experimental design: formulation and in vitro characterization, AapsPharmscitech. 11 (2010) 460–466.https://doi.org/10.1208/s12249-010-9406-z

[12] F. Bergaya, G. Lagaly, Introduction to clay science: techniques and applications, in: Dev. Clay Sci., Elsevier, 2013: pp. 1–7.https://doi.org/10.1016/B978-0-08-098259-5.00001-9

[13] L. Lisuzzo, G. Cavallaro, S. Milioto, G. Lazzara, Halloysite nanotubes filled with salicylic acid and sodium diclofenac: effects of vacuum pumping on loading and release properties, J. Nanostructure Chem. 11 (2021) 663–673. https://doi.org/10.1007/s40097-021-00391-z.

[14] L. Liu, Y. Wan, Y. Xie, R. Zhai, B. Zhang, J. Liu, The removal of dye from aqueous solution using alginate-halloysite nanotube beads, Chem. Eng. J. 187 (2012) 210–216.https://doi.org/10.1016/j.cej.2012.01.136

[15] S. Sahnoun, M. Boutahala, H. Zaghouane-Boudiaf, L. Zerroual, Trichlorophenol removal from aqueous solutions by modified halloysite: kinetic and equilibrium studies, Desalination Water Treat. 57 (2016) 15941–15951.https://www.tandfonline.com/doi/abs/10.1080/19443994.2015.1075159

[16] I. Blanco, L. Abate, F.A. Bottino, P. Bottino, Thermal behaviour of a series of novel aliphatic bridged polyhedral oligomeric silsesquioxanes (POSSs)/polystyrene (PS) nanocomposites: The influence of the bridge length on the resistance to thermal degradation, Polym. Degrad. Stab. 102 (2014) 132–137.https://doi.org/10.1016/j.polymdegradstab.2014.01.029

[17] B. Singh, S. Purohit, G. Saini, A. Bhandari, D. Awasthi, Colon specific chronotherapeutic drug delivery for nocturnal asthma: Eudragit S-100 coated calcium alginate gel beads-entrapped salbutamol sulphate, Int J Pharm Pharm Sci. 5 (2013) 362–7.https://www.researchgate.net/profile/Bhupendra-Singh-5/publication/236949533

[18] C. Gao, M. Liu, J. Chen, X. Zhang, Preparation and controlled degradation of oxidized sodium alginate hydrogel, Polym. Degrad. Stab. 94 (2009) 1405–1410.https://doi.org/10.1016/j.polymdegradstab.2009.05.011

[19] M.L. Vueba, L.B. De Carvalho, F. Veiga, J.J. Sousa, M.E. Pina, Influence of cellulose ether polymers on ketoprofen release from hydrophilic matrix tablets, Eur. J. Pharm. Biopharm. 58 (2004) 51–59.https://doi.org/10.1016/j.ejpb.2004.03.006

[20] T. Higuchi, Mechanism of sustained-action medication. Theoretical analysis of rate of release of solid drugs dispersed in solid matrices, J. Pharm. Sci. 52 (1963) 1145–1149.https://onlinelibrary.wiley.com/doi/abs/10.1002/jps.2600521210

[21] P.L. Ritger, N.A. Peppas, A simple equation for description of solute release II. Fickian and anomalous release from swellable devices, J. Controlled Release. 5 (1987) 37–42.https://onlinelibrary.wiley.com/doi/abs/10.1002/jps.2600521210

Chapter V: *Optimizing Colon-Targeted Therapy through Mesalazine*
Delivery via pH-Sensitive Halloysite/ Polysaccharide
Nanocomposites: In vitro, In silico and Computational study.

[22] R.W. Korsmeyer, R. Gurny, E. Doelker, P. Buri, N.A. Peppas, Mechanisms of solute release from porous hydrophilic polymers, Int. J. Pharm. 15 (1983) 25–35.https://doi.org/10.1016/0378-5173(83)90064-9

[23] J. Siepmann, N.A. Peppas, Modeling of drug release from delivery systems based on hydroxypropyl methylcellulose (HPMC), Adv. Drug Deliv. Rev. 64 (2012) 163–174.https://doi.org/10.1016/j.addr.2012.09.028

[24] M.W. Matthiessen, G. Pedersen, T. Albrektsen, S. Adamsen, J. Fleckner, J. Brynskov, Peroxisome proliferator-activated receptor expression and activation in normal human colonic epithelial cells and tubular adenomas, Scand. J. Gastroenterol. 40 (2005) 198–205.https://doi.org/10.1080/00365520410009573

[25] T. Shimada, K. Kojima, K. Yoshiura, H. Hiraishi, A. Terano, Characteristics of the peroxisome proliferator activated receptor γ (PPARγ) ligand induced apoptosis in colon cancer cells, Gut. 50 (2002) 658–664.https://doi.org/10.1136%2Fgut.50.5.658

[26] G. de Gaetano, M.B. Donati, C. Cerletti, Prevention of thrombosis and vascular inflammation: benefits and limitations of selective or combined COX-1, COX-2 and 5-LOX inhibitors, Trends Pharmacol. Sci. 24 (2003) 245–252.https://doi.org/10.1016/S0165-6147(03)00077-4

[27] B. Rath, F.A. Qais, R. Patro, S. Mohapatra, T. Sharma, Design, synthesis and molecular modeling studies of novel mesalamine linked coumarin for treatment of inflammatory bowel disease, Bioorg. Med. Chem. Lett. 41 (2021) 128029.https://doi.org/10.1016/j.bmcl.2021.128029

[28] N.A. Alsaif, M.A. Bhat, M.A. Al-Omar, H.M. Al-Tuwajiri, A.M. Naglah, A. Al-Dhfyan, Synthesis of novel diclofenac hydrazones: molecular docking, anti-inflammatory, analgesic, and ulcerogenic activity, J. Chem. 2020 (2020) 1–12.https://doi.org/10.1155/2020/4916726

[29] T.B. Issa, A. Sagaama, N. Issaoui, Computational study of 3-thiophene acetic acid: Molecular docking, electronic and intermolecular interactions investigations, Comput. Biol. Chem. 86 (2020) 107268.https://doi.org/10.1016/j.compbiolchem.2020.107268

[30] E.E. Ebenso, T. Arslan, F. Kandemirli, N. Caner, I. Love, Quantum chemical studies of some rhodanineazosulpha drugs as corrosion inhibitors for mild steel in acidic medium, Int. J. Quantum Chem. 110 (2010) 1003–1018.https://doi.org/10.1002/qua.22249

[31] M. Kamel, A. Morsali, H. Raissi, K. Mohammadifard, Theoretical insights into the intermolecular and mechanisms of covalent interaction of Flutamide drug with COOH and COCl functionalized carbon nanotubes: a DFT approach, Chem. Rev. Lett. 3 (2020) 23–37. https://doi.org/10.22034/crl.2020.221149.1039

[32] R. Dennington, T.A. Keith, J.M. Millam, GaussView, version 6.0. 16, Semichem Inc Shawnee Mission KS. (2016).https://scholar.google.com/scholar?cluster=9146009410332145197&hl=fr&as_sdt=2005&sciodt=0,5

Chapter V: *Optimizing Colon-Targeted Therapy through Mesalazine*
                                                    Delivery via pH-Sensitive Halloysite/ Polysaccharide
                                                    Nanocomposites: In vitro, In silico and Computational study.

[33] D. Villemin, T. Abbaz, A. Bendjeddou, Molecular structure, HOMO, LUMO, MEP, natural bond orbital analysis of benzo and anthraquinodimethane derivatives, Pharm. Biol. Eval. 5 (2018).https://dx.doi.org/10.26510/2394-0859.pbe.2018.04

[34] M.E. Awad, E. Escamilla-Roa, A. Borrego-Sánchez, C. Viseras, A. Hernández-Laguna, C.I. Sainz-Díaz, Adsorption of 5-aminosalicylic acid on kaolinite surfaces at a molecular level, Clay Miner. 54 (2019) 49–56.https://doi.org/10.1180/clm.2019.13

[35] M.E. Awad, A. López-Galindo, M. Setti, M.M. El-Rahmany, C.V. Iborra, Kaolinite in pharmaceutics and biomedicine, Int. J. Pharm. 533 (2017) 34–48.https://doi.org/10.1016/j.ijpharm.2017.09.056

[36] Y.S. Mary, C.Y. Panicker, M. Sapnakumari, B. Narayana, B.K. Sarojini, A.A. Al-Saadi, C. Van Alsenoy, J.A. War, H.K. Fun, Molecular structure, FT-IR, vibrational assignments, HOMO–LUMO analysis and molecular docking study of 1-[5-(4-Bromophenyl)-3-(4-fluorophenyl)-4, 5-dihydro-1H-pyrazol-1-yl] ethanone, Spectrochim. Acta. A. Mol. Biomol. Spectrosc. 136 (2015) 473–482. https://doi.org/10.1016/j.saa.2014.09.060

[37] W.O. Yah, A. Takahara, Y.M. Lvov, Selective modification of halloysite lumen with octadecylphosphonic acid: new inorganic tubular micelle, J. Am. Chem. Soc. 134 (2012) 1853–1859.https://doi.org/10.1021/ja210258y

[38] A.K. Panda, B.G. Mishra, D.K. Mishra, R.K. Singh, Effect of sulphuric acid treatment on the physico-chemical characteristics of kaolin clay, Colloids Surf. Physicochem. Eng. Asp. 363 (2010) 98–104. https://doi.org/10.1016/j.colsurfa.2010.04.022

[39] Brett, C.; Cataldo, S.; Gianguzza, A.; Lando, G.; Lazzara, G.; Pettignano, A.; Sammartano, S. Thermodynamics of Proton Binding of Halloysite Nanotubes - Recherche Google, (n.d.).https://doi.org/10.1021/acs.jpcc.6b01127

[40] D. Sid, M. Baitiche, R. Bourzami, R. Merir, F. Djerboua, A. Gil, M. Boutahala, Experimental and theoretical studies of the interaction of ketoprofen in halloysite nanotubes, Colloids Surf. Physicochem. Eng. Asp. 627 (2021) 127136. https://doi.org/10.1016/j.colsurfa.2021.127136

[41] M.M. Yallapu, M. Jaggi, S.C. Chauhan, Poly (β-cyclodextrin)/curcumin self-assembly: a novel approach to improve curcumin delivery and its therapeutic efficacy in prostate cancer cells, Macromol. Biosci. 10 (2010) 1141–1151.https://doi.org/10.1002/mabi.201000084

[42] H. Sabahi, M. Khorami, A.H. Rezayan, Y. Jafari, M.H. Karami, Surface functionalization of halloysite nanotubes via curcumin inclusion, Colloids Surf. Physicochem. Eng. Asp. 538 (2018) 834–840.https://doi.org/10.1016/j.colsurfa.2017.11.038

[43] A.R. Pawar, P.V. Mundhe, V.K. Deshmukh, R.B. Pandhare, T.D. Nandgude, Enrichment of aqueous solubility and dissolution profile of mesalamine: In vitro evaluation of solid dispersion, J. Pharm. Biol. Sci. 9 (2021) 127.https://doi.org/10.18231/j.jpbs.2021.018

Chapter V: *Optimizing Colon-Targeted Therapy through Mesalazine*
Delivery via pH-Sensitive Halloysite/ Polysaccharide
Nanocomposites: In vitro, In silico and Computational study.

[44] A.M.J. Newton, P. Lakshmanan, Effect of HPMC-E15 LV premium polymer on release profile and compression characteristics of chitosan/pectin colon targeted mesalamine matrix tablets and in vitro study on effect of pH impact on the drug release profile, Recent Pat. Drug Deliv. Formul. 8 (2014) 46–62.https://www.ingentaconnect.com/content/ben/ddf/2014/00000008/00000001/art00006

[45] R. Merir, M. Baitiche, Z. Elbahri, R. Bourzami, F. Djerboua, M. Boutahala, Conception of Cellulose/Alginate/Mesalazine microspheres by solvent evaporation technique for drug release: Experimental and theoretical investigations, Int. J. Biol. Macromol. 243 (2023) 124894. https://doi.org/10.1016/j.ijbiomac.2023.124894

[46] M.M. Alam, F. Tasneem, A.L. Kabir, A.S.S. Rouf, Study of Drug-Drug and Drug-Food Interactions of Mesalazine Through FTIR and DSC, Dhaka Univ. J. Pharm. Sci. 18 (2019) 257–269. https://doi.org/10.3329/dujps.v18i2.44466

[47] L. Nie, C. Liu, J. Wang, Y. Shuai, X. Cui, L. Liu, Effects of surface functionalized graphene oxide on the behavior of sodium alginate, Carbohydr. Polym. 117 (2015) 616–623. https://doi.org/10.1016/j.carbpol.2014.08.104

[48] B. Huang, M. Liu, Z. Long, Y. Shen, C. Zhou, Effects of halloysite nanotubes on physical properties and cytocompatibility of alginate composite hydrogels, Mater. Sci. Eng. C. 70 (2017) 303–310. https://doi.org/10.1016/j.msec.2016.09.001

[49] S.R. Schaffazick, S.S. Guterres, L. de L. Freitas, A.R. Pohlmann, Caracterização e estabilidadefísico-química de sistemaspoliméricosnanoparticulados para administração de fármacos, Quím. Nova. 26 (2003) 726–737. https://doi.org/10.1590/S0100-40422003000500017

[50] M.Y. Nassar, M.F. El-Shahat, S.M. Khalile, M. El-Desawy, E.A. Mohamed, Structure investigation of mesalazine drug using thermal analyses, mass spectrometry, DFT calculations, and NBO analysis, J. Therm. Anal. Calorim. 117 (2014) 463–471. https://doi.org/10.1007/s10973-014-3638-1

[51] A. Salisu, M.M. Sanagi, A. Abu Naim, K.J. Abd Karim, W.A. Wan Ibrahim, U. Abdulganiyu, Alginate graft polyacrylonitrile beads for the removal of lead from aqueous solutions, Polym. Bull. 73 (2016) 519–537. https://doi.org/10.1007/s00289-015-1504-3

[52] Q. Zhao, T. Wang, J. Wang, L. Zheng, T. Jiang, G. Cheng, S. Wang, Template-directed hydrothermal synthesis of hydroxyapatite as a drug delivery system for the poorly water-soluble drug carvedilol, Appl. Surf. Sci. 257 (2011) 10126–10133. https://doi.org/10.1016/j.apsusc.2011.06.161

[53] M.K.L. Coelho, J. de F. Giarola, A.T.M. Da Silva, C.R.T. Tarley, K.B. Borges, A.C. Pereira, Development and application of electrochemical sensor based on molecularly imprinted polymer and carbon nanotubes for the determination of carvedilol, Chemosensors. 4 (2016) 22. https://doi.org/10.3390/chemosensors4040022

[54] E. Joussein, S. Petit, J. Churchman, B. Theng, D. Righi, B. Delvaux, Halloysite clay minerals—a review, Clay Miner. 40 (2005) 383–426. https://doi.org/10.1180/0009855054040180

[55] G. Brown, Crystal structures of clay minerals and their X-ray identification, The mineralogical society of Great Britain and Ireland, 1982. https://books.google.com/books

[56] One Pot Synthesis and Characterization of Alginate StabilizedSemiconductor Nanoparticles, (n.d.).https://www.researchgate.net/publication/233424649

[57] O.S. Reddy, M.C.S. Subha, T. Jithendra, C. Madhavi, K.C. Rao, Curcumin encapsulated dual cross linked sodium alginate/montmorillonite polymeric composite beads for controlled drug delivery, J. Pharm. Anal. 11 (2021) 191–199. https://doi.org/10.1016/j.jpha.2020.07.002

[58] Y. Lvov, W. Wang, L. Zhang, R. Fakhrullin, Halloysite Clay Nanotubes for Loading and Sustained Release of Functional Compounds, Adv. Mater. 28 (2016) 1227–1250. https://doi.org/10.1002/adma.201502341

[59] A. Saeed, S.A. Ejaz, M. Sarfraz, N. Tamam, F. Siddique, N. Riaz, F.A. Qais, S. Chtita, J. Iqbal, Discovery of phenylcarbamoylazinane-1, 2, 4-triazole amides derivatives as the potential inhibitors of aldo-keto reductases (AKR1B1 & AKRB10): Potential lead molecules for treatment of colon cancer, Molecules. 27 (2022) 3981. https://doi.org/10.3390/molecules27133981

[60] L. Lisuzzo, G. Cavallaro, P. Pasbakhsh, S. Milioto, G. Lazzara, Why does vacuum drive to the loading of halloysite nanotubes? The key role of water confinement, J. Colloid Interface Sci. 547 (2019) 361–369. https://doi.org/10.1016/j.jcis.2019.04.012

Chapter VI

Computational Insights and Nanocarrier Technologies with pH-Responsive Polymers for Improving Drug Delivery in Inflammatory Bowel Disease.

I.   Introduction

In the realm of drug delivery systems, various structural frameworks have been devised for nanocarrier-based methodologies, aiming to proficiently hinder Inflammatory bowel disease (IBD) progression and amplify the therapeutic index. Notwithstanding the effectiveness of these systems, a primary constraint endures in the simplicity of their design, resulting in compromised stability and a proclivity for sudden drug release. To overcome these obstacles, continuing research takes an innovative method that focuses on combining polymers with pH-sensitive properties into nanostructures.

As Ulcerative colitis poses a substantial global hazard to human health, numerous studies have been undertaken to search for efficient anti-inflammatory therapeutic agents. Traditional treatment options induce various side effects, and regimens appear to have high toxicity while their response is relatively low. Therefore, effective and more secure treatments are needed to manage and hopefully resolve these problems **[1,2]**.

Nowadays, natural compounds have been preferred as alternative drug delivery agents due to their fewer side effects, combined mild mechanisms, and lower cost **[3]**.

Diatomite, often known as diatomaceous earth, is a naturally occurring sedimentary rock formed by biogenic processes. It is easily available and affordable. Diatomite is mostly composed of amorphous silica and well-preserved diatom frustules **[4]**. Numerous studies have looked at both unmodified and modified versions of diatomite as possible carriers of tiny drugs and macromolecules. Various studies emphasize the advantages of diatomite as a drug carrier, including its high porosity, low density, non-toxicity, high drug loading capacity, thermal stability, mechanical durability, and chemical resistance **[5]**. To improve diatomite's overall performance in pharmaceutical applications while also ensuring safety, biodegradability, and biocompatibility, it was functionalized or modified by incorporating various chemical groups, common biopolymers, and non-toxic inorganic compounds **[6]**.

Microencapsulated pharmaceutical forms have found widespread use in pharmaceutical technology due to their established safety and effectiveness in drug release systems. The development of new biomaterials, particularly those that are more reliable, biocompatible, biodegradable, and non-toxic, is better suited for advancing pharmaceutical systems compared to traditional pharmaceuticals. The selection of microencapsulation excipients

Chapter V: *Computational Insights and Nanocarrier Technologies with*
pH Responsive Polymers for Improving Drug Delivery in
Inflammatory Bowel Disease.

can influence chemical cross-linking and annealing during the immobilization of active ingredients. Anionic natural polymers like sodium alginate, recognized as advantageous microencapsulation materials, contribute to drug release kinetics by degrading in the body, as supported by studies [7,8].

Sodium alginate is a biodegradable, biocompatible, and non-toxic natural polysaccharide with a linear structure. It has gelling, viscous, and stabilizing characteristics. Its capacity to hold water enhances tissue strength and flexibility, making it useful in a variety of industrial contexts. High-purity alginate is required in biomedical and pharmaceutical applications to assure safety and biocompatibility. When crude alginate is exposed to a multistage extraction procedure that successfully removes or minimizes the presence of contaminants, it may be ingested orally without eliciting an immunological response [9].

Chitosan is widely utilized as an adjuvant for alginate microcapsules, reinforcing the structure of the alginate gel by coating it. In the absence of chitosan covering, stomach acid was shown to enter the alginate structure's interfacial pores, reaching the core and reducing drug viability within the microcapsules destined for intestinal diseases [10]. Chitosan, a well-known biopolymer, is used extensively in a variety of sectors, including pharmaceuticals and medicine research, principally as a drug carrier [11,12]. This polyamino-saccharide polymer has significant technical benefits and is easily made from the chitin component found in many biogenic resources [13]. Chitosan chains provide significant advantages in terms of safety, hemostatic efficiency, biological activity, compatibility, and biodegradability, as well as outstanding mechanical and adsorption properties [14].

Molecular docking is the most extensively used computational tool, and its primary application is in structure-based drug discovery to identify novel active molecules for a certain target protein. Molecular docking involves two fundamental steps: first, sampling ligand conformations in the protein's active site, and second, rating these conformations using a scoring system [15]. Scoring functions aid in distinguishing between proper and wrong postures, or binders and inactive substances, in a fair amount of calculation time. Molecular docking is accomplished using a variety of techniques, including rigid ligand and rigid receptor docking, flexible ligand and stiff receptor docking, flexible ligand and flexible receptor docking, and others [16,17].

Chapter V: *Computational Insights and Nanocarrier Technologies with*
pH Responsive Polymers for Improving Drug Delivery in
Inflammatory Bowel Disease.

The objective of this study is to design a drug delivery system that can overcome these limitations and provide sustained and targeted release of 5-ASA. The proposed system involves loading 5-ASA onto diatomite particles encapsulated in sodium alginate, followed by applying a chitosan coating for enteric protection and improved stability. Various analytical techniques, such as dynamic light scattering, X-ray fluorescence, X-ray diffraction, Fourier transform-infrared spectroscopy, and thermogravimetric analysis, besides Scanning Electron Microscope are employed to characterize the physical, chemical, and morphological properties of the developed drug delivery system. On the other side, the *in-silico* study examines the molecular docking of 5-ASA against TNF-α and 5-LOX receptors to predict its absorbability, inhibitory activity, and potential selectivity.

II.   Materials and methods

II.1. Materials

The raw diatomite (DTM) used in this study was collected from the Sig deposit in West Algeria. 5-ASA was generously given by SALEM Pharmaceutical Laboratories, El-Eulma, Algeria. The principal materials applied were medical-grade. chitosan obtained from Biotech Surindo (Cirebon, Indonesia) and applied directly without treatment. Chitosan has an 80% deacetylation rate (DD) and a viscosity-average molecular weight (Mv) of 3783 kDa. Sodium alginate (SA) with medium viscosity was obtained from Sigma-Aldrich, USA. Anhydrous glacial acetic acid was acquired from Merck KGaA, Darmstadt, Germany. All compounds were used without further purification.

II.1.1. Purification of diatomite powder

The diatomite nanopowder was prepared through the following process: 10 g of crushed diatomite rocks were added to 500 ml of absolute ethanol and sonicated in 5 cycles for 30 min to disrupt large aggregates. The resulting dispersion was initially filtered through a nylon net with a pore size of 41 μm, followed by a subsequent filtration step with a 0.45 μm pore size filter (Millipore, Billerica, MA, USA) [9,10].

The material was centrifuged for purification before being treated with Piranha solution (2 M H_2SO_4, 10% H_2O_2) for 30 min at 80°C. The nanoparticle dispersion was centrifuged at $21,500 \times g$ for 30 min, rinsed twice with distilled water, and then resuspended in 5 M HCl. The suspension was incubated at 80°C overnight. The diatomite nanoparticles were

Chapter V: *Computational Insights and Nanocarrier Technologies with*
pH Responsive Polymers for Improving Drug Delivery in
Inflammatory Bowel Disease.

centrifuged again at $21,500 \times g$ for 30 min, then washed twice with distilled water to eliminate any remaining HCl.

II.2. Diatomite preparation

The diatomite was dried overnight in an oven set to 105°C. Then, it was placed in a laboratory-type ash furnace at 500°C for 240 minutes to eliminate organic compounds. Because, according to the literature [18], temperatures between 500 and 600 °C are commonly utilized for removing organic contaminants. While it may not be completely effective at lower temperatures, structural breakdown may develop in the inorganic material as temperatures rise [19].

II.3. Drug loading DTM

Ultrasounds were used to decrease the average size of diatomite powder to a nanometric scale, and a uniform distribution was achieved by repeated cycles of settling and recovery [20], before collecting. The 5-ASA was then dissolved in 1 M hydrochloric acid at a concentration of 100 mg/mL by immersion [21]. Ethanol-wetted DTM (100 mg) was added to the 5-ASA solution at a 1:5 (w/w) ratio and swirled for 12 hours. The particles were then centrifuged at 1000Xg, collected, and dried at room temperature to form a stable drug delivery system (5-ASA/DTM powder).

II.4. Preparation of 5-ASA/DTM/SA$_{Beads}$

The extrusion process was used to create 5-ASA/DTM beads with sodium alginate as a pH-sensitive polymeric coating agent.

The procedure consisted of the following stages. An aqueous stock solution of SA was made by dissolving 2 g in 100 mL of distilled water. The solution was then mixed with 2 g of 5-ASA/DTM and agitated overnight at room temperature until it reached a homogenous, smooth, and uniform consistency. The mixture was then put in a syringe and gently allowed to drip in drops via the nozzle while pressing the piston into an excess 2% (m/v) cross-linking calcium chloride ($CaCl_2$) bath, which was continually agitated [22]. After an incubation period of 24 h in the agitated cross-linking $CaCl_2$ solution. the resulting product was taken out and washed several times with distilled water to remove unbound $CaCl_2$ from the surface of the beads. to obtain the 5-ASA/DTM/SA Beads. A part of the obtained

samples was dried for 72 h at ambient temperature till constant weight then stocked. the other part was used in the next stage.

II.5. Preparation of chitosan-coated 5-ASA/DTM/SA_{Beads}

 In the final step, the 5-ASA/DTM sodium alginate beads undergo coating with chitosan. The beads were transformed and submerged in a chitosan solution for enteric coating.

The chitosan solution was prepared by dissolving 2 g of chitosan in 400 mL of 0.1 M acetic acid and adjusting the pH to 6.0 with 1 M NaOH. The resultant mixture was filtered using Whatman #4 filter paper. The suspension was then heated on a hot plate for 30 seconds at 72 °C before being rapidly cooled in an ice bath **[23]**. This solution was then used for coating applications. After 60 min, the enteric-coated beads were removed, rinsed with distilled water, and allowed to dry for 72 hours at room temperature before being stored and labeled 5-ASA/DTM/SA/Cts.

II.6. Characterization Methods

Dynamic Light Sattering Analysis (DLS)

Dynamic light scattering analysis was used to investigate the size and surface charge Zeta potential (ζ) of the pure diatomite. Using Malvern Zetasizer Nano-ZS ZEN 3600. The auto correlation functions of the samples were analyzed using the Contin algorithm through the Zetasizer 7.12 software. Samples were run in triplicates **[24]**. To examine diatomite's surface charge properties, measurements were conducted in water with pH= 7.12 with a solid (DTM) ratio of 0.01%.

X-ray Fluorescence (XRF)

The key elements of the DTM sample were identified using X-ray fluorescence (XRF) spectroscopy. The analysis was carried out on discs measuring 1.5 cm in diameter and 0.5 cm in thickness. Using the Rigaku Primus IV equipment from Japan.

X-ray Diffraction (XRD)

To investigate the structural arrangement and properties of impurities found in diatomite and all samples, X-ray diffraction data were collected using a Bruker D8 Advance X-ray powder

Chapter V: *Computational Insights and Nanocarrier Technologies with*
pH Responsive Polymers for Improving Drug Delivery in
Inflammatory Bowel Disease.

diffractometer. The instruments used a Cu Kα anode ($\lambda = 0.1542$ nm) and operated at 40 kV/40 mA. The data collection ranged from 4 to 40°, with a 0.05° step size and commensurate scanning speed.

Fourier Transform-Infrared Spectroscopy (FTIR)

To assess possible alterations in the chemical structures, aiming to discern the interactions among the compounds resulting from the microencapsulation process. A comparative analysis of the obtained spectra was performed. The FT-IR spectra of both the complexes and the pristine compounds were examined using the Shimadzu-8400 model from Japan, employing the KBr disc method. The spectra were recorded in the expansive range of 4000-400 cm^{-1}.

Thermogravimetric Analysis Examination (TGA)

Thermogravimetric analysis (TA Instruments Q5000 IR apparatus) was performed to assess the thermal stability of the samples. The analysis was carried out under a nitrogen flow, with rates set at 25 cm^3 min^{-1} for the sample and 10 cm^3 min^{-1} for the balance system. with a microprocessor-driven temperature control unit **[25]**. The sample masses varied from 2-3 mg in dried and powdered form and were placed in an alumina pan. The sample pan was placed in the balancing system equipment, and the temperature was gradually increased from room temperature to 800 °C at a rate of 10 °C/min.

Scanning Electron Microscope (SEM)

The morphology of the unloaded and loaded Diatomite besides the coating formulation surface was investigated by using a scanning electron microscope (SEM, AIS2100, Seron Technology, South Korea) at an operating voltage of 25 kV.

III.   *In silico* studies

The *in-silico* method is widely used to anticipate and validate drug design. This approach is cost-effective, time-saving, and less likely to isolate inactive molecules **[26]**.

III. 1. Data Collection

The receptors and enzymes utilized for molecular docking were chosen based on a comprehensive review of the literature on anti-inflammatory agents. The crystal structures of

Chapter V: *Computational Insights and Nanocarrier Technologies with*
pH Responsive Polymers for Improving Drug Delivery in
Inflammatory Bowel Disease.

these anti-inflammatory proteins were obtained from the Protein Data Bank (PDB), an online repository available at https://www.rcsb.org.

Additionally, the ligand SDF data of mesalazine (CID 4075) was extracted from PubChem. Since the SDF files cannot be utilized directly in docking studies. the SDF files were converted into PDB files using the Discovery Visualizer.

Since the Tumor necrosis factor alpha (TNF-α) plays a crucial role in several immunological phenomena, encompassing inflammation, infection, and antitumor responses. Its indispensability extends to acute and chronic neuroinflammation, as well as diverse neurodegenerative disorders **[27]**. The crystal structure of TNF-α (PDB ID 2AZ5) with X-ray diffraction 2.1 Å On the other hand, Lipoxygenase (LOX) is well-known for its function in the production of pro-inflammatory mediators, particularly in the human body. 5-lipoxygenase (5-LOX) with PDB ID 3O8Y and X-ray resolution 2.39 A is a lipoxygenase family member that has garnered interest due to its possible medicinal use **[28]**.

III.2. Target protein retrieval and preparation

The BIOVIA Discovery Studio Visualizer (DS) was used to eliminate all chains from the protein except chain A. All heteroatoms, including water molecules, were then removed, along with their associated ligands. Afterward, default assignments were used for Kollman charges and salvation parameters. Following that, ligand and receptor coordinate data for TNF-α and 5-LOX were converted to PDBQT format with MGL Tools-1.5.6 software, which served as the foundation for subsequent docking efforts **[1,29]**. Before performing docking.

IV. Results and discussion

IV.1. Experimental investigation

The ζ (zeta) values of diatomite particles are illustrated in Fig. 1(A), depicting the size and zeta-potential distributions with average values of 504 ± 60 nm and -21.6 ± 4.7 mV Fig. 1(C), respectively. The negative surface charge is attributed to the deprotonation of surface Si–OH groups. Additionally, Fig. 1(B) reveals a bimodal distribution in intensity-average hydrodynamic sizes over 100 repeated measurements.

The submicron size contributes to the colloidal stability of diatomite particles in a non-aqueous suspension, and the bimodal size distribution is expected to provide high packing efficiency.

Chapter V: *Computational Insights and Nanocarrier Technologies with*
pH Responsive Polymers for Improving Drug Delivery in
Inflammatory Bowel Disease.

Consequently, the colloidal stability of diatomite particles is anticipated to be elevated, facilitated by the strong electrostatic repulsive forces between their surfaces **[30,31]**.
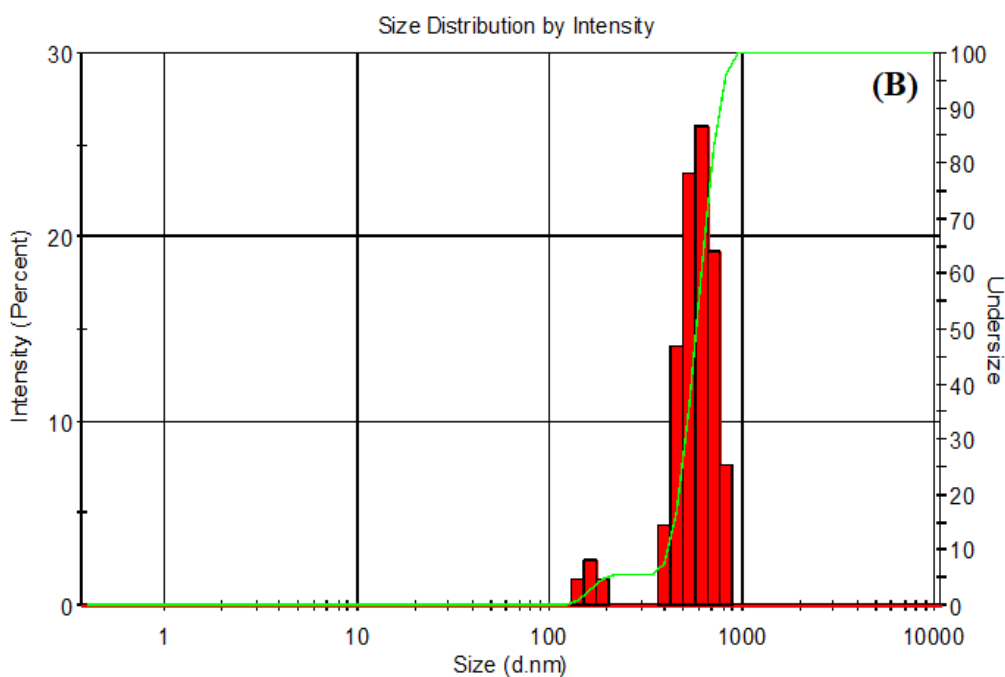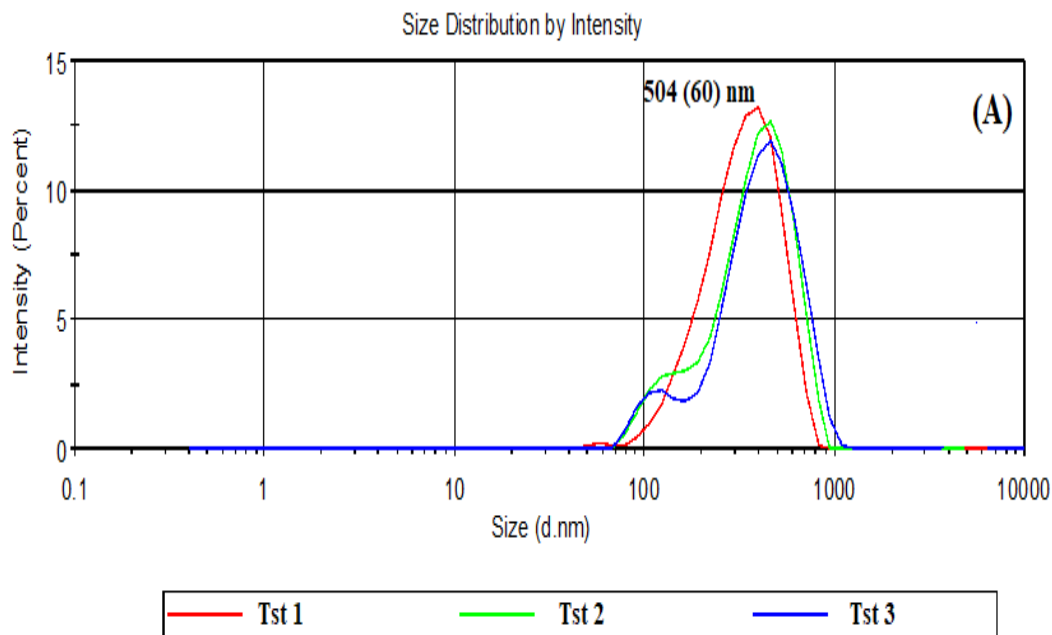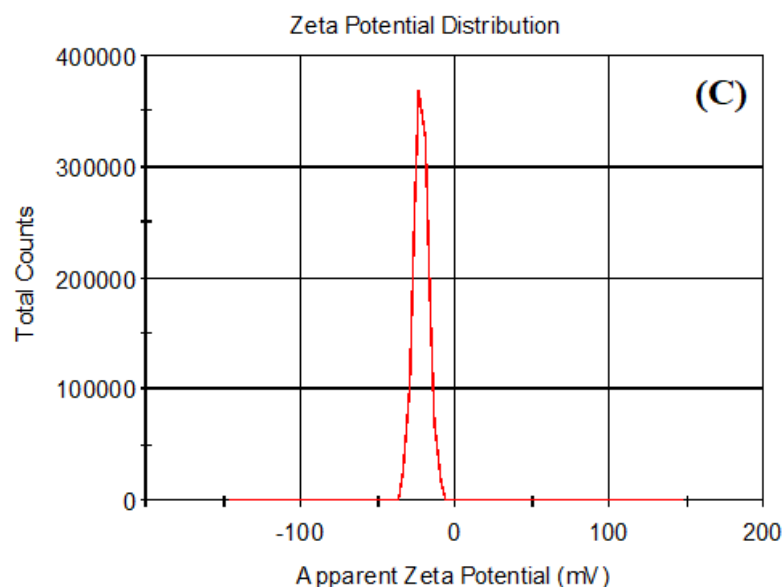
Fig. 1. Size (A), Hydrodynamic size distribution graph (B) and, zeta-potential (C) of diatomite nanoparticles in pH 7 at 25 °C.

The intrinsic chemical composition and intricate crystal structure of DTM wield profound influence over the intricate dynamics of medication release. In the X-ray fluorescence (XRF) analysis of diatomite, as detailed in Table 2, Silicon Dioxide (SiO_2) emerged as the predominant component, constituting 73.85% of the composition. These findings underscore the importance of knowing diatomite chemical constitution in the context of medication delivery systems. The observed 2.3% increase in glow loss is likely attributed to the presence of organic impurities that have precipitated within the pores of the diatomite.

Table 1: The natural diatomite bulk chemical composition using the XRF analysis.

	SiO_2	Al_2O_3	CaO	Fe_2O_3	K_2O	MgO	MnO	Others
DTM	73.85	3.14	3.21	1.19	0.63	2.15	0.01	2.33

Connecting this chemical composition study to Fig. 2(A) X-ray diffraction (XRD) spectrum reveals that amorphous opal-A is the prevailing mineral component in the raw DTM sample. The wide band at $2\theta = 22°(2\Theta)$ indicates the presence of amorphous silica, a distinctive feature of diatomite. Despite the dominance of SiO_2, there are trace impurities such as quartz (Q) and mica (M) [5]. Additionally, the XRD analysis of 5-ASA, as shown in Fig. 2(B), reveals specific 2θ values at 15.1°, 16.5°, and 26.9°, indicating the crystalline nature of the drug.

Chapter V: *Computational Insights and Nanocarrier Technologies with*
pH Responsive Polymers for Improving Drug Delivery in
Inflammatory Bowel Disease.

In the context of sodium alginate, the X-ray diffraction (XRD) patterns illustrate a crystalline arrangement resulting from robust intermolecular hydrogen bonding interactions among alginate chains. Fig. 2(B) shows peaks at 2θ values of 13.8º, 21.9º, and 37.5º. These correspond to the reflection of the (110) plane from the polyguluronate unit, the (200) plane from polymannuronate, and an extra peak attributable to the amorphous halo [32]. The signals observed at 12.1° and 20° are attributed to crystal-I and crystal-II within the chitosan framework. These particular peaks signify a notable level of crystallinity of the chitosan used [33].

The typical peaks of pure DTM emerged in the final product's XRD patterns (5-ASA/DTM/SA/Cts), demonstrating that the crystal phase structure of DTM was created, retained in the drug formulation, and effectively assembled. Moreover, the presence of distinct 5-ASA peaks, albeit with a diminished intensity, pointing conclusively to an amorphous structure of 5-ASA within the formulations. Interestingly, the disappearance of the chitosan crystalline peak at $2\Theta = 12°$ (110) is persuasive evidence of structural changes caused by complexation due to the disrupting of hydrogen bonding between amino and hydroxyl groups in chitosan [34].

163
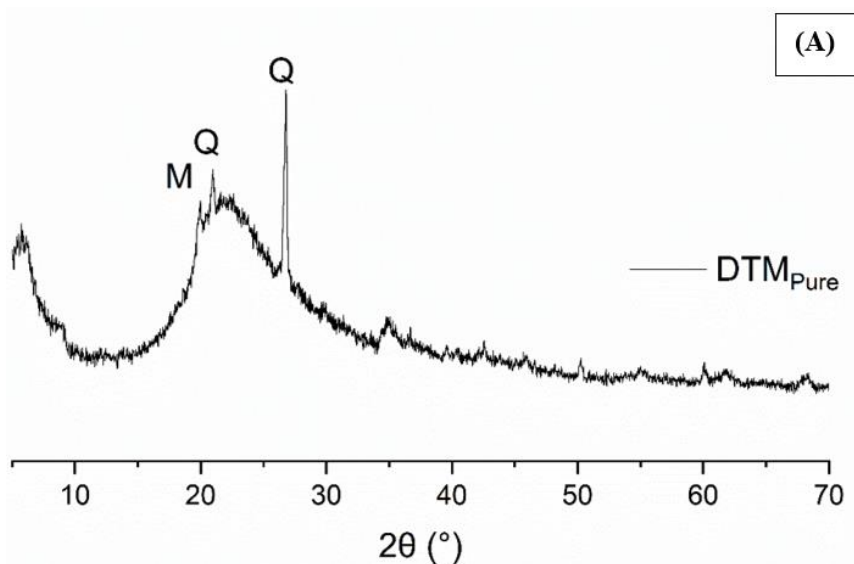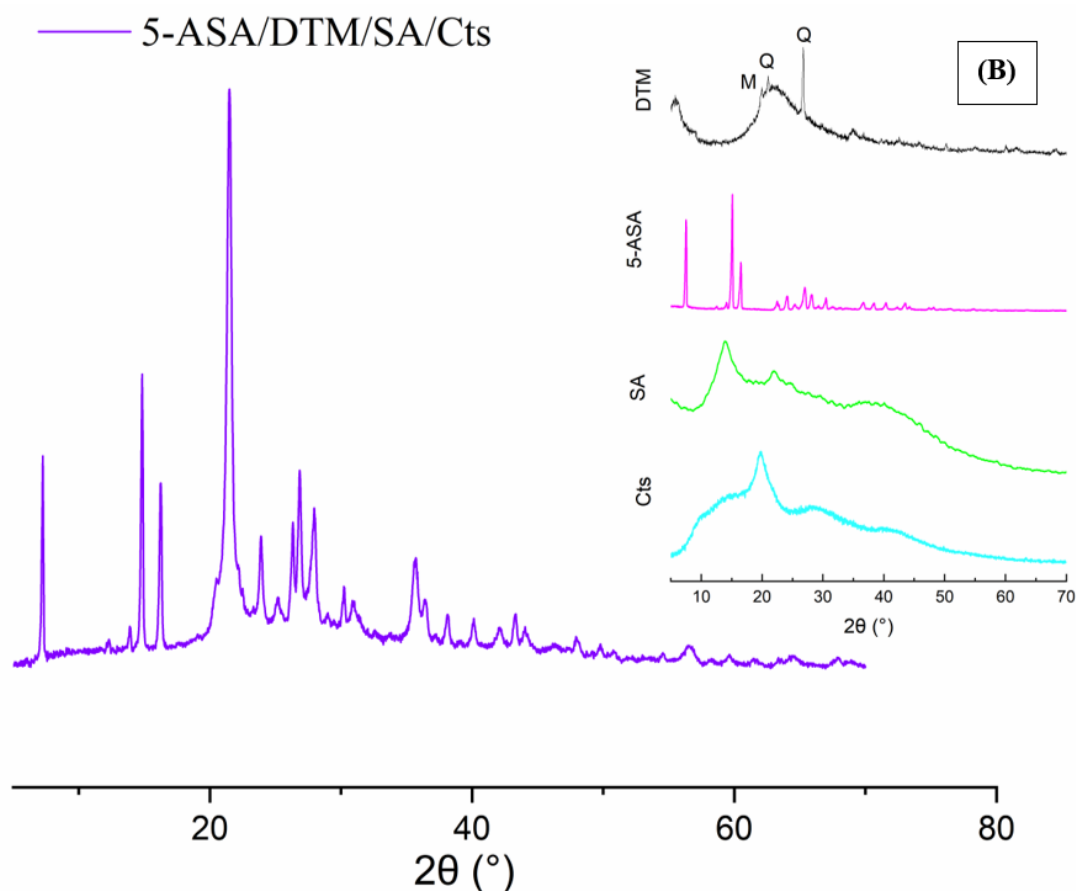
Fig. 2. Powder XRD patterns of DTM$_{Pure}$ (A) and the samples: 5-ASA/DTM/SA/Cts formulation, DTM, 5-ASA, SA and, Cts (B).

Embarking on the analysis of the Fourier Transform Infrared (FTIR) spectra for DTM, 5-ASA, SA, Cts, and the drug formulations reveals distinctive features that offer insights into their molecular structures and the interactions within these pharmaceutical components (Fig. 3). It is seen that Diatomite's absorption spectra show a significant peak at 3622.3 cm⁻¹ due to the stretching vibration of -OH. The stretching vibrations of physically adsorbed and zeolitic water are indicated by peaks at 3448 and 1634 cm⁻¹. The Si−O−Si bonds exhibit both symmetrical and asymmetrical vibrations at 788 and 1090 cm⁻¹, respectively. A prominent signal at 477 cm⁻¹ is related to the stretching mode of siloxane (Si-O–Si) **[35,36]**.

In the pristine 5-ASA spectrum displays distinctive absorption bands suggesting functional groups. The peak at 3458 cm⁻¹ indicates N-H stretching, supported by vibrations of –NH2 at 2553 cm⁻¹. Peaks at 3096 cm⁻¹ and 2977 cm⁻¹ correspond to aromatic Ar-CH stretching, consistent with the identification of the C=C stretch at 1616 cm⁻¹. The peak at 2784 cm⁻¹ corresponds to O-H stretching, while peaks at 1352 cm⁻¹ and 1255 cm⁻¹ indicate O-H bending

Chapter V: *Computational Insights and Nanocarrier Technologies with*
pH Responsive Polymers for Improving Drug Delivery in
Inflammatory Bowel Disease.

and C-O bending, suggesting the presence of alcohol groups. The absorption band at 1651 cm^{-1} confirms –C=O bending, and bands at 1587 cm^{-1}, 1493 cm^{-1}, and 1453 cm^{-1} signify C-N, –C=C stretching, providing evidence of the compound's structure. The C-O stretch of phenol appears at 1192 cm^{-1}, and three bands at 817 cm^{-1}, 773 cm^{-1}, and 686 cm^{-1} confirm the out-of-plane deformation of C-H in aromatic rings [37,38].

The success of mesalamine loadings was emphasized by the presence of peaks from 1095 to 1654 cm^{-1}. These bands suggest the presence of main and secondary alcohol groups. Furthermore, it supports the existence of carbonyl groups in mesalazine. matched with the medicines' C=O stretching. As depicted in Fig. 3(A).

within the framework of sodium alginate Fig. 3(B), the FTIR spectrum displays important molecular characteristics. The large peak at 3445 cm^{-1} indicates hydroxyl groups' (O-H) stretching vibrations, highlighting their presence in the structure. The absorption band at 2931 cm^{-1} indicates C-H stretching vibrations, adding to the aliphatic component (C-H). The polymeric backbone may be identified by distinct asymmetric and symmetric COO stretching vibrations of carboxylate salt groups at 1622 cm^{-1} and 1417 cm^{-1}, respectively. The 1093 cm^{-1} band was related to the C-O stretching vibration of the pyranosyl ring. Besides, the shoulder at 1039 cm^{-1} indicates C-O-C (cyclic ether) stretching vibrations. The stretching vibration bands at 944 cm^{-1}, 891 cm^{-1}, and 815 cm^{-1} are exclusive to guluronic and mannuronic acids, providing insights into alginate's composition [39,40].

Regarding chitosan, its spectrum shows a band between 3600-3000 cm^{-1}, which represents the stretching of hydroxyl (OH) groups, indicating hydrogen bonding. This broad peak, which indicates significant hydrogen bonding [41]. Complemented by absorption bands at 2920 cm^{-1} and 2860 cm^{-1}, illustrating symmetric and asymmetric stretching of C-H bonds, respectively. Notably, the band at 1655 cm^{-1} corresponds to C=O stretching, specifically Amine I. The band at 1318 cm^{-1} reveals the C-N stretching, also known as Amine III. Also, certain additional significant bands reveal more details regarding the molecular structure of chitosan on the spectrum. The bands at 1590 cm^{-1} and 1383 cm^{-1} demonstrate NH and CH bending, respectively. The band at 1034 cm^{-1} indicates C-O stretching [42]. Moreover, the peak at 890 cm^{-1} supports the existence of saccharide groups in chitosan [11].

The disappearing bands as shown in Fig. 3(C) belong to the chitosan formulation. This suggests that the dominating peaks of diatomite absorb the peaks of chitosan's weaker amide and amine groups which was confirmed in a study by **[43]**.
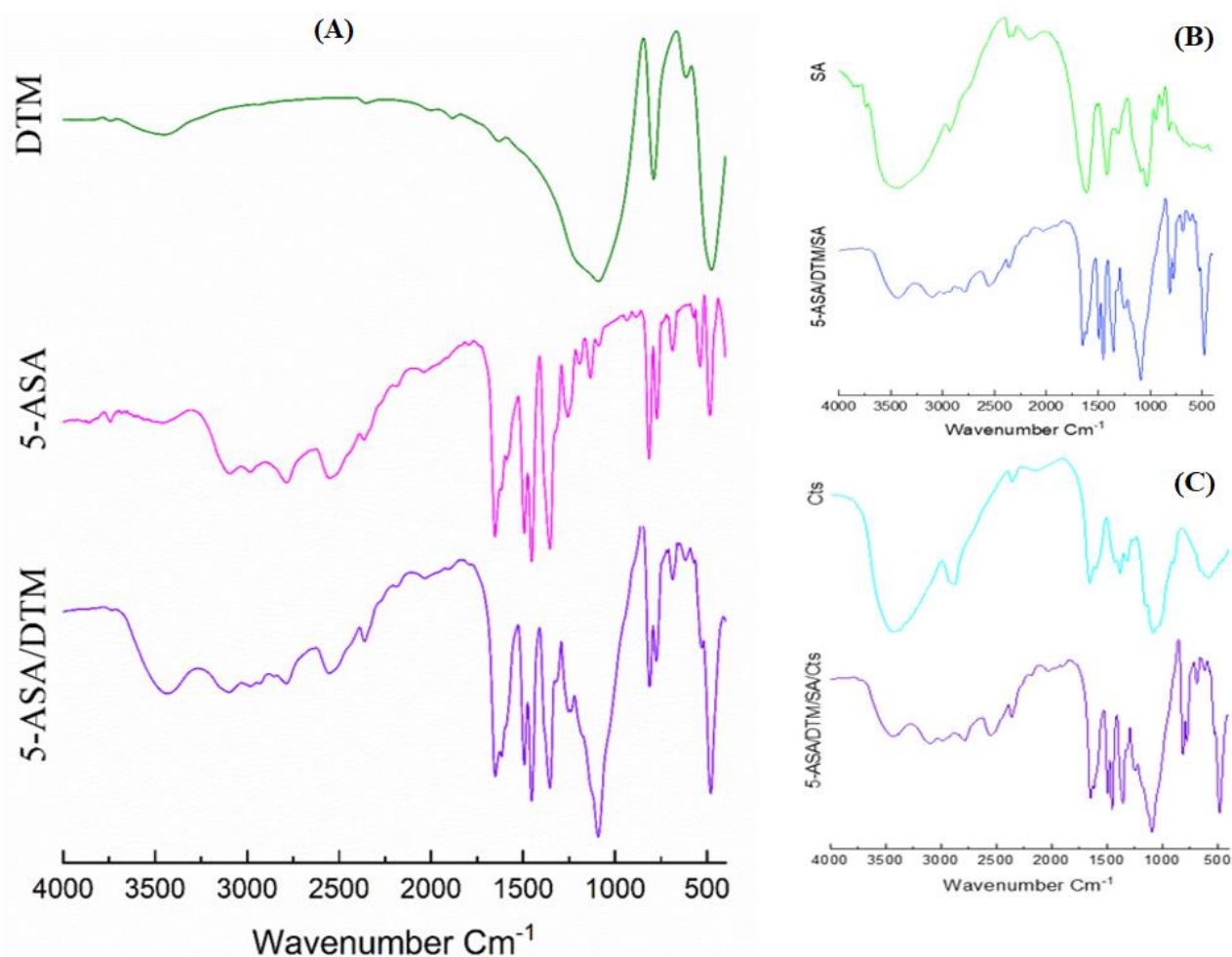
Fig. 3. FTIR spectra of DTM, 5-ASA, SA, Cts and all drug formulations samples.

Thermogravimetric analysis (TGA) has been widely used for exploring thermal stability and discerning the attributes of thermal decomposition in the pristine compounds DTM, 5-ASA, and polymers as depicted in Fig. 4(A) and Drug formulations Fig. 4(B).

The TG analysis of DTM reveals distinct phases. Initially, between ambient temperature and 265°C, a 3.3% weight loss occurs, owing to the release of water vapors, suggesting humidity. Subsequently, between 295 and 630°C, a 2.13% weight loss occurs, caused by the dehydration of chemically connected water in the opal structure and the burning of organic components inside the diatomite **[44,45]**. In addition, the 5-ASA TG analysis reveals a single-step mass loss

Chapter V: *Computational Insights and Nanocarrier Technologies with*
pH Responsive Polymers for Improving Drug Delivery in
Inflammatory Bowel Disease.

between 225 and 367°C. indicating a gradual decarboxylation process that contributes to the breakdown of the molecular structure of mesalazine. This information is visually represented in Figure 5B **[37,46]**.

Furthermore, the TG study of sodium alginate shows a two-stage weight decrease pattern. The first weight loss, occurring between 25 and 127°C, is around 13.3%, showing moisture evaporation-induced weight loss **[25]**. The following weight loss of roughly 32.36% occurs in the temperature range of 200 to 250 degrees Celsius. This second step is caused by a complicated degradation mechanism that breaks down the sodium alginate sample and produces water, methane, and CO2 **[47]**.

For the TGA curve of pure chitosan unequivocally demonstrates distinct phases of weight loss. The initial stage, spanning from 45 to 106 °C, is attributed to the evaporation of water molecules, resulting in a precisely measured weight loss of approximately 4%. The subsequent stage involves deacetylation, where acetyl groups are removed, followed by vaporization and the elimination of volatile products. This step is crucial in the breakdown of chitosan. The process is initiated by amino groups, leading to the creation of unsaturated structures. During the subsequent pyrolysis of polysaccharides, glycosidic linkages within the chitosan molecule break randomly. This results in the degradation of the polysaccharide structure, and as a consequence, acetic and butyric acids are formed. Additionally, a series of lower fatty acids, with a prevalence of C2, C3, and C6, is generated. This Non-oxidative thermal degradation of chitosan happens between 264°C to 376°C under nitrogen flow with about a weight loss of 51% **[48,49]**.

Chapter V: *Computational Insights and Nanocarrier Technologies with*
pH Responsive Polymers for Improving Drug Delivery in
Inflammatory Bowel Disease.
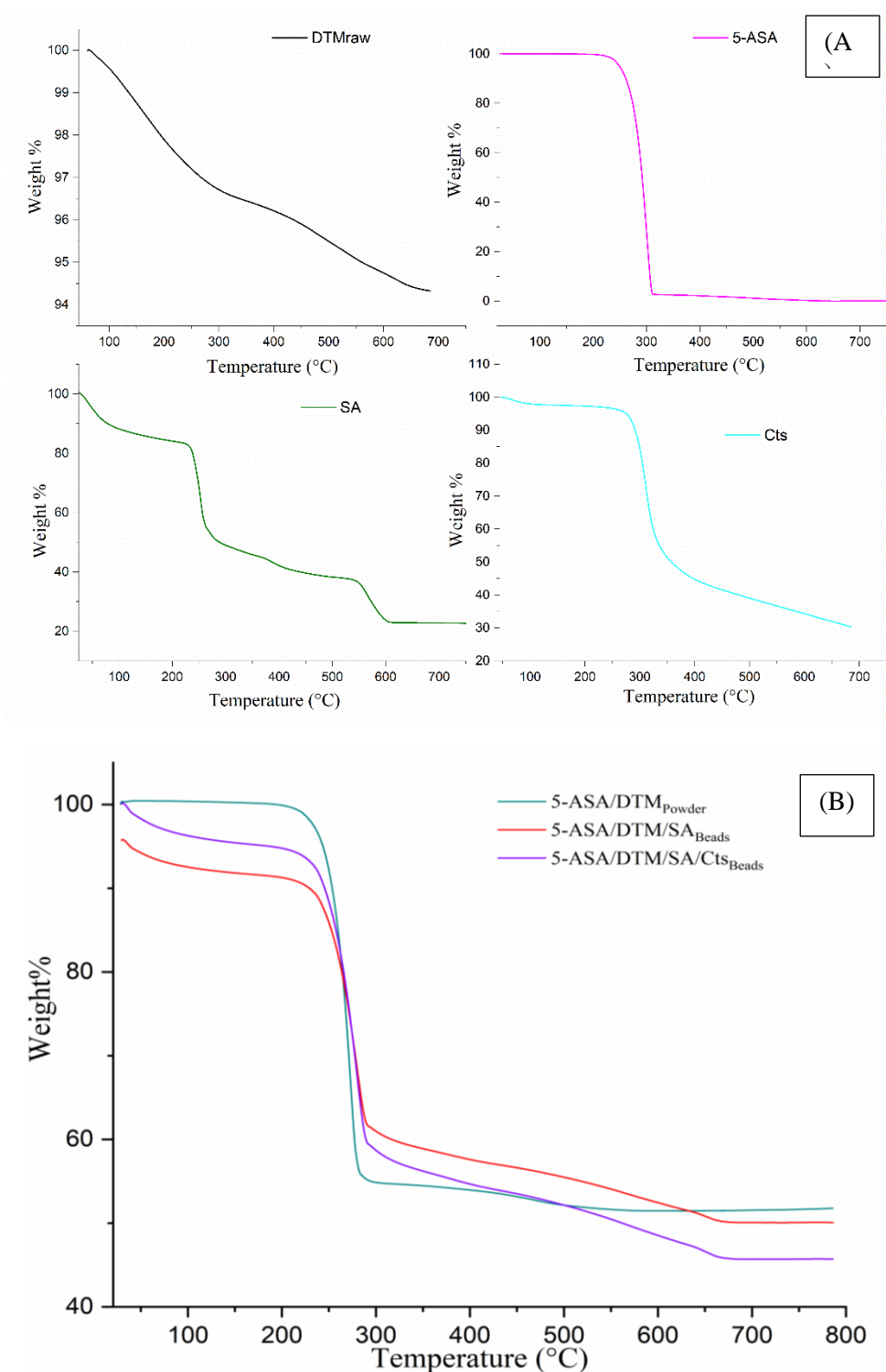
Fig. 4. The thermogravimetric TGA curves of: (A) DTM, 5-ASA, SA, Cts and,
(B) the drug formulation samples.

The morphological characteristics of diatomite powder were examined before and after mesalazine loading using SEM micrographs. The initial diatomite exhibited disc-shaped central frustules with pore rows extending from circular valves, suggesting a honeycomb-like porosity

Chapter V: *Computational Insights and Nanocarrier Technologies with*
pH Responsive Polymers for Improving Drug Delivery in
Inflammatory Bowel Disease.

with a well-defined macroporous and mesoporous structure. However, the raw diatomite surface displayed numerous inclusions, likely attributed to the presence of clayey minerals [30], this is depicted in Figure 5. The cylindrical-shaped central frustules with straight pore rows are also noticeable on the mantle, albeit to a lesser degree (Fig. 6(A)). After drug loading through an immersion approach, the pores became saturated with pharmaceuticals, as depicted in Fig. 6(B).
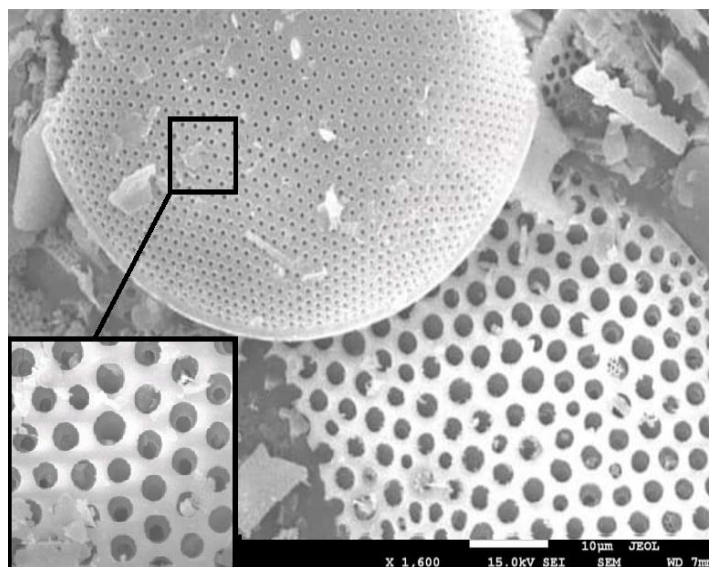
Fig. 5. SEM micrography of the diatomite powder.
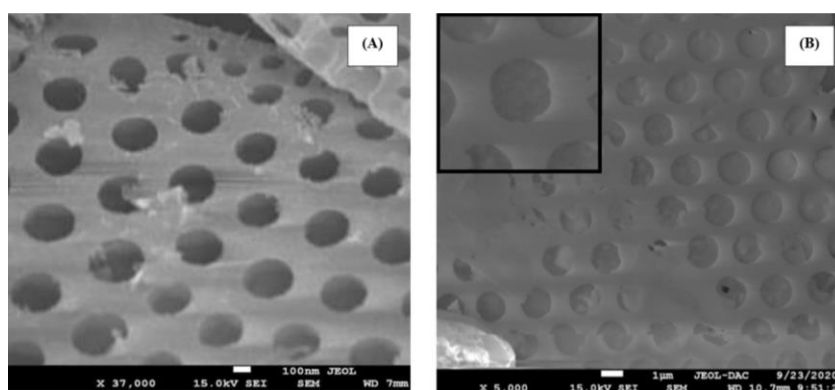
Fig. 6. Comparison of Pore Structure in Diatom (A) Before and (B) After Drug Loading.

Chapter V: *Computational Insights and Nanocarrier Technologies with*
pH Responsive Polymers for Improving Drug Delivery in
Inflammatory Bowel Disease.
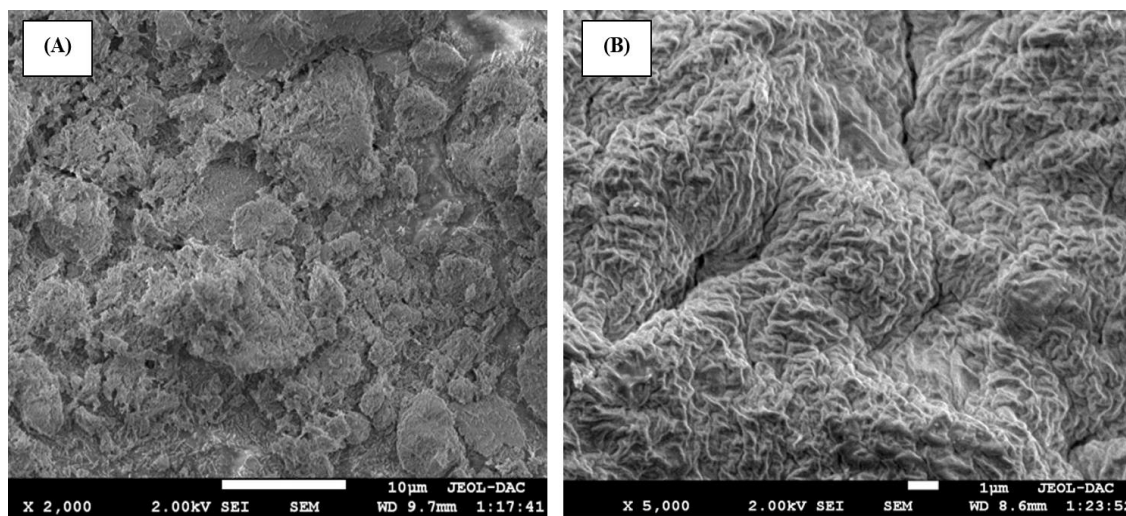
Fig. 7. SEM images of the surface morphology examination of Uncoated 5-ASA/DTM/SA Bead (A) and Coated 5-ASA/DTM/SA/Cts Bead (B).

Based on the SEM images of 5-ASA/DTM/SA$_{Beads}$ in Fig. 7. Powder was trapped in the matrix of the beads, as shown by their rough texture (Fig. 7(A)). However, after coating the 5-ASA/DTM/SA$_{Beads}$ with Cts, the surface beads became shrunken but smoother, with fewer snaps and nanoparticles visible on the surface (Fig. 7(B)). This alteration might be attributed to ionotropic/external gelation interactions that occur during the creation of the beads, causing chitosan molecules to diffuse into the alginate gel core **[50]**.

IV.2. Virtual screening through molecular docking

The present study found that the two proteins TNF-α and 5-LOX were effectively docked with binding affinities -5.5 and -6.3 kcal/mol, respectively.

The detailed insights from the docking study, combined with specific interactions identified, suggest a nuanced and intricate binding mode between 5-ASA and proteins (TNF-α, 5-LOX). These diverse interactions collectively enhance the overall binding affinity.

Understanding TNF-α broader role as a proinflammatory cytokine, and its impact on immune regulation, induction of apoptosis, fever induction, and tissue remodeling, emphasizes the significance of targeting TNF-α for therapeutic purposes **[1]**. 5-ASA potential to modulate these interactions provides valuable insights into its mechanism of action in treating inflammatory and autoimmune conditions. The observed hydrogen bonds, notably those between N1 and GLY121 (O) and TYR151 (OH) as depicted in figure. 8(B), are critical for molecular recognition and binding with a distance of 2.83 A in both interactions. These interactions greatly

help to stabilize the overall interaction between mesalamine and TNF-α. In addition, to improve our understanding of the polar contacts in the 5-ASA-TNF-α interaction. Polar interactions, such as H1 with TYR151 (OH) and H2 with TYR151 (OH), provide additional specificity and stability to the binding.

The previously reported hydrophobic interaction between C7 and TYR119 demonstrates the role of hydrophobic forces in maintaining the binding contact. These interactions help to maintain the overall stability of the 5-ASA/TNF-α complex. Besides, Pi-pi Interactions are critical in molecular recognition and affect total binding affinity. Such as those between C5 and TYR59, C4 and TYR119, C6 and TYR119, C1 and TYR119, and C3 and TYR119, help us understand the aromatic interactions at play.

The 5-LOX is a pivotal enzyme involved in the biosynthesis of leukotrienes, lipid mediators that play a crucial role in inflammation and immune responses **[51]**. The interplay between 5-ASA and 5-LOX involves potential interactions such as Hydrogen bonds that could form between specific atoms in mesalamine and amino acid residues on 5-LOX. For example, interactions like those between O2 and ARG347 or N1 and LEU409 suggest the potential for hydrogen bonding which stabilizes molecular interactions (Fig. 8(B)). On the other side, Polar interactions may occur between 5-ASA polar functional groups and 5-LOX polar residues playing a role in the binding process, as evidenced by O3 and H6 interacting with ARG347 while O1, O2, and H6 with GLN510. Moreover, the observed interactions between nonpolar 5-ASA regions and hydrophobic amino acid residues in the 5-LOX binding site, such as C7 with ARG347 and C2 with LEU409, emphasize the importance of hydrophobic forces in preserving the binding interface.

TNF-α   **5-LOX**

(A) 3D

Chapter V: *Computational Insights and Nanocarrier Technologies with*
pH Responsive Polymers for Improving Drug Delivery in
Inflammatory Bowel Disease.

(B) 2D

(C) H-Bonds
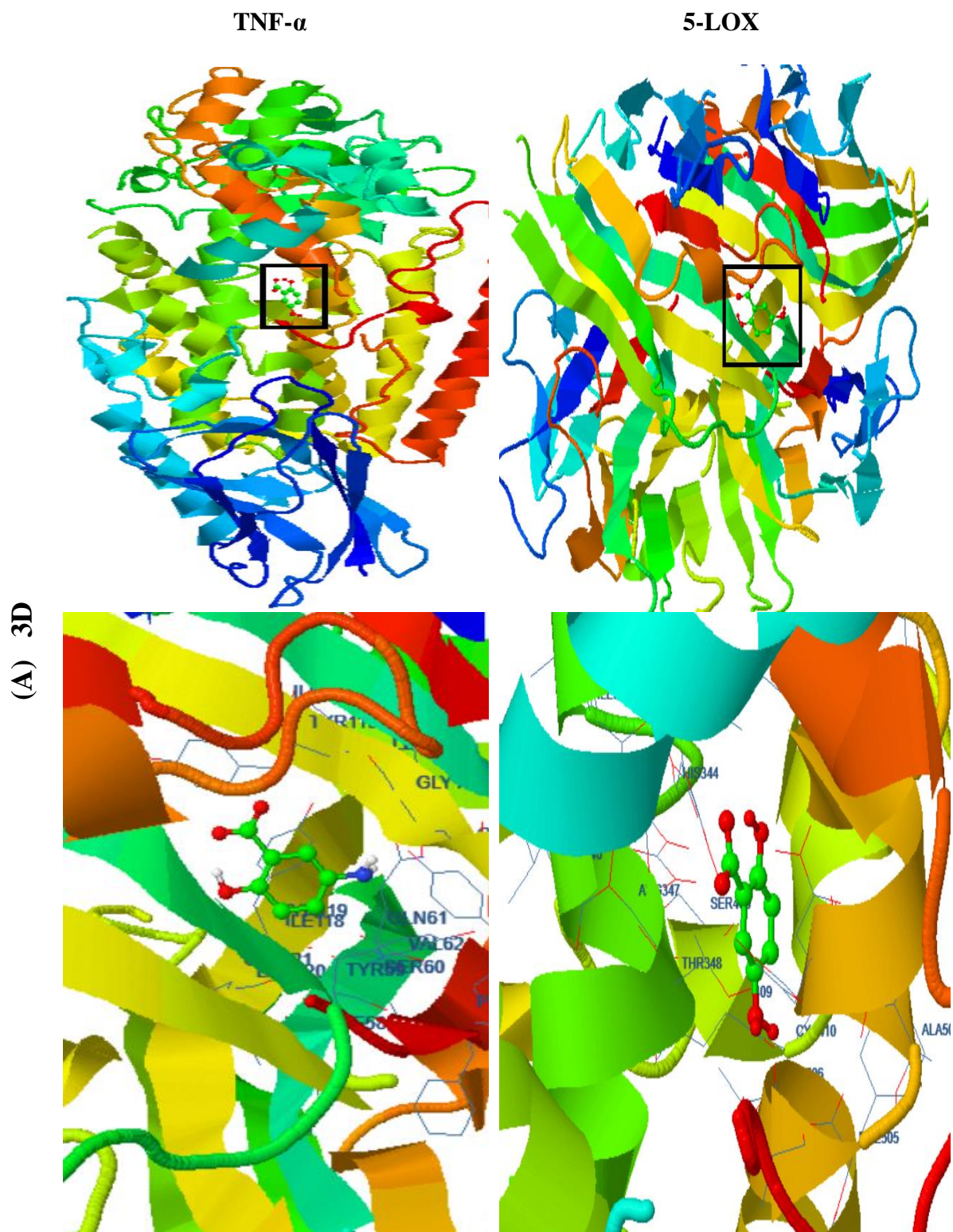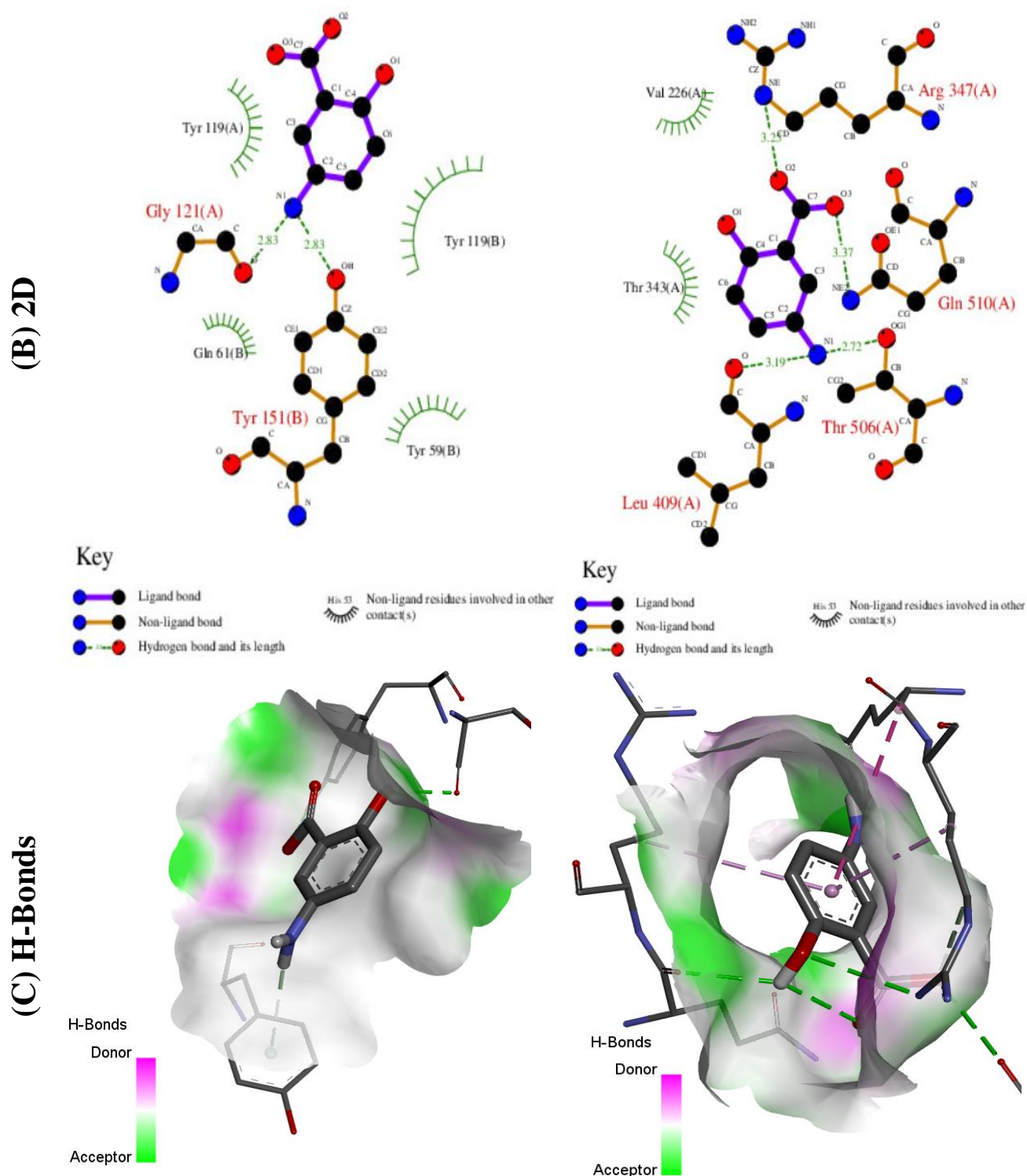
Fig.8. A(3D) Molecular docked complexes of TNF-α and, 5-LOX with 5-ASA.
B(2D) diagram involving various amino acid residues after docking.
C(2D) image of H-binding of the 5-ASA with TNF-α and, 5-LOX.

173

Conclusion

Overall, in this research paper, we highlight the modification of diatomite-loaded mesalazine to improve its performance, safety, and biocompatibility by incorporating biopolymers. Microencapsulation techniques utilizing sodium alginate enable controlled drug release, while chitosan serves as an adjuvant to enhance the structural integrity of the drug-loaded capsules. on the other hand, Targeting the expression levels of TNF-α and 5-LOX receptors in colon tissues could provide a means for early detection and assessment of therapeutic effectiveness, in Ulcerative colitis. Using molecular docking, we can virtually screen and assess the binding affinity of potential drug candidates to these target proteins, providing valuable insights for the design and development of new therapeutics.

References

[1] B. Rath, F.A. Qais, R. Patro, S. Mohapatra, T. Sharma, Design, synthesis and molecular modeling studies of novel mesalamine linked coumarin for treatment of inflammatory bowel disease, Bioorg. Med. Chem. Lett. 41 (2021) 128029. https://www.sciencedirect.com/science/article/pii/S0960894X21002559

[2] M.H. Sanad, S.F.A. Rizvi, F.A. Marzook, A.B. Farag, In-Silico Study, Preparation and Biological Evaluation of 99MTC-Mesalamine Complex as Radiotracer for Diagnostics and Monitoring of Ulcerative Colitis in Mice, Pharm. Chem. J. 56 (2022) 754–761. https://doi.org/10.1007/s11094-022-02706-y

[3] P. Silva, B. Bonifácio, M. Ramos, K. Negri, T. Maria Bauab, M. Chorilli, Nanotechnology-based drug delivery systems and herbal medicines: a review, Int. J. Nanomedicine (2013) 1. https://doi.org/10.2147/IJN.S52634

[4] T.A. Saleh, M. Tuzen, A. Sarı, Evaluation of poly(ethylene diamine-trimesoyl chloride)-modified diatomite as efficient adsorbent for removal of rhodamine B from wastewater samples, Environ. Sci. Pollut. Res. 28 (2021) 55655–55666. https://doi.org/10.1007/s11356-021-14832-3

[5] G. Liu, M.R. Abukhadra, A.M. El-Sherbeeny, A.M. Mostafa, M.A. Elmeligy, Insight into the photocatalytic properties of diatomite@ Ni/NiO composite for effective photo-degradation of malachite green dye and photo-reduction of Cr (VI) under visible light, J. Environ. Manage. 254 (2020) 109799. https://www.sciencedirect.com/science/article/pii/S0301479719315178

[6] Y. Zhao, G. Tian, X. Duan, X. Liang, J. Meng, J. Liang, Environmental Applications of Diatomite Minerals in Removing Heavy Metals from Water, Ind. Eng. Chem. Res. 58 (2019) 11638–11652. https://doi.org/10.1021/acs.iecr.9b01941

[7] H. Jiang, Y. Sheng, T. Ngai, Pickering emulsions: Versatility of colloidal particles and recent applications, Curr. Opin. Colloid Interface Sci. 49 (2020) 1–15. https://www.sciencedirect.com/science/article/pii/S135902942030039X

[8] Polymers | Free Full-Text | Preparation and Characterization of Chitosan-Alginate Microspheres Loaded with Quercetin, (n.d.). https://www.mdpi.com/2073-4360/14/3/490

[9] L. Agüero, D. Zaldivar-Silva, L. Peña, M.L. Dias, Alginate microparticles as oral colon drug delivery device: A review, Carbohydr. Polym. 168 (2017) 32–43. https://www.sciencedirect.com/science/article/pii/S0144861717302898

[10] F.-L. Mi, H.-W. Sung, S.-S. Shyu, Drug release from chitosan–alginate complex beads reinforced by a naturally occurring cross-linking agent, Carbohydr. Polym. 48 (2002) 61–72. https://www.sciencedirect.com/science/article/pii/S0144861701002120

[11] S.M. Ibrahim, M.N. Bin Jumah, S.I. Othman, R.S. Alruhaimi, N. Al-Khalawi, Y.F. Salama, A.A. Allam, M.R. Abukhadra, Synthesis of Chitosan/Diatomite Composite as an Advanced Delivery System for Ibuprofen Drug; Equilibrium Studies and the Release Profile, ACS Omega 6 (2021) 13406–13416. https://doi.org/10.1021/acsomega.1c01514

[12] Y. Jiang, M.R. Abukhadra, N.M. Refay, M.F. Sharaf, M.A. El-Meligy, E.M. Awwad, Synthesis of chitosan/MCM-48 and β-cyclodextrin/MCM-48 composites as bio-adsorbents for environmental removal of Cd2+ ions; kinetic and equilibrium studies, React. Funct. Polym. 154 (2020) 104675. https://www.sciencedirect.com/science/article/pii/S138151482030376X

[13] A.M. Saad, M.R. Abukhadra, S.A.-K. Ahmed, A.M. Elzanaty, A.H. Mady, M.A. Betiha, J.-J. Shim, A.M. Rabie, Photocatalytic degradation of malachite green dye using chitosan supported ZnO and Ce–ZnO nano-flowers under visible light, J. Environ. Manage. 258 (2020) 110043. https://www.sciencedirect.com/science/article/pii/S030147971931761X

[14] D. Zhao, S. Yu, B. Sun, S. Gao, S. Guo, K. Zhao, Biomedical Applications of Chitosan and Its Derivative Nanoparticles, Polymers 10 (2018) 462. https://doi.org/10.3390/polym10040462

[15] J. De Ruyck, G. Brysbaert, R. Blossey, M. Lensink, Molecular docking as a popular tool in drug design, an in silico travel, Adv. Appl. Bioinforma. Chem. Volume 9 (2016) 1–11. https://doi.org/10.2147/AABC.S105289

[16] N.S. Pagadala, K. Syed, J. Tuszynski, Software for molecular docking: a review, Biophys. Rev. 9 (2017) 91–102. https://doi.org/10.1007/s12551-016-0247-1

[17] G. Bottegoni, I. Kufareva, M. Totrov, R. Abagyan, Four-Dimensional Docking: A Fast and Accurate Account of Discrete Receptor Flexibility in Ligand Docking, J. Med. Chem. 52 (2009) 397–406. https://doi.org/10.1021/jm8009958

[18] P. Yuan, D. Liu, D.-Y. Tan, K.-K. Liu, H.-G. Yu, Y.-H. Zhong, A.-H. Yuan, W.-B. Yu, H.-P. He, Surface silylation of mesoporous/macroporous diatomite (diatomaceous earth) and its function in Cu(II) adsorption: The effects of heating pretreatment, Microporous Mesoporous Mater. 170 (2013) 9–19. https://doi.org/10.1016/j.micromeso.2012.11.030

[19] M.R. Abukhadra, S.M. Ibrahim, J.S. Khim, A.A. Allam, J.S. Ajarem, S.N. Maodaa, Enhanced decontamination of pefloxacin and chlorpyrifos as organic pollutants using chitosan/diatomite composite as a multifunctional adsorbent; equilibrium studies, J. Sol-Gel Sci. Technol. 99 (2021) 650–662. https://doi.org/10.1007/s10971-021-05613-y

[20] G. Zhang, D. Cai, M. Wang, C. Zhang, J. Zhang, Z. Wu, Microstructural modification of diatomite by acid treatment, high-speed shear, and ultrasound, Microporous Mesoporous Mater. 165 (2013) 106–112. https://www.sciencedirect.com/science/article/pii/S1387181112005033

[21] S. Nalinbenjapun, C. Ovatlarnporn, Chitosan-5-aminosalicylic acid conjugates for colon-specific drug delivery: Methods of preparation and in vitro evaluations, J. Drug Deliv. Sci. Technol. 57 (2020) 101397. https://www.sciencedirect.com/science/article/pii/S1773224719309475

[22] L. Liu, Y. Wan, Y. Xie, R. Zhai, B. Zhang, J. Liu, The removal of dye from aqueous solution using alginate-halloysite nanotube beads, Chem. Eng. J. 187 (2012) 210–216. https://www.sciencedirect.com/science/article/pii/S1385894712001787

[23] S. Nualkaekul, M.T. Cook, V.V. Khutoryanskiy, D. Charalampopoulos, Influence of encapsulation and coating materials on the survival of Lactobacillus plantarum and Bifidobacterium longum in fruit juices, Food Res. Int. 53 (2013) 304–311. https://www.sciencedirect.com/science/article/pii/S0963996913002470

[24] Frontiers | Strong Antimicrobial Activity of Silver Nanoparticles Obtained by the Green Synthesis in Viridibacillus sp. Extracts, (n.d.). https://www.frontiersin.org/articles/10.3389/fmicb.2022.820048/full

[25] I. Blanco, L. Abate, F.A. Bottino, P. Bottino, Thermal behaviour of a series of novel aliphatic bridged polyhedral oligomeric silsesquioxanes (POSSs)/polystyrene (PS) nanocomposites: The influence of the bridge length on the resistance to thermal degradation, Polym. Degrad. Stab. 102 (2014) 132–137. https://www.sciencedirect.com/science/article/pii/S0141391014000408

[26] S. Yatam, S.S. Jadav, K.P. Gundla, K. Paidikondala, A.R. Ankireddy, B.N. Babu, M.J. Ahsan, R. Gundla, 2-Mercapto Benzthiazole Coupled Benzyl Triazoles as New COX-2 Inhibitors: Design, Synthesis, Biological Testing and Molecular Modeling Studies, ChemistrySelect 4 (2019) 11081–11092. https://doi.org/10.1002/slct.201902972

[27] S.E. Abechi, S. Ejeh, A. Abduljelil, In silico screening of potential Tumor necrosis factor alpha (TNF-α) inhibitors through molecular modeling, molecular docking, and pharmacokinetics evaluations, Sci. Afr. 21 (2023) e01830. https://doi.org/10.1016/j.sciaf.2023.e01830

[28] S. Singh, V. Nair, S. Jain, Y.K. Gupta, Evaluation of anti-inflammatory activity of plant lipids containingα–linolenic acid, (2008). https://nopr.niscpr.res.in/handle/123456789/4500

[29] G.M. Morris, R. Huey, A.J. Olson, Using AutoDock for Ligand-Receptor Docking, Curr. Protoc. Bioinforma. 24 (2008). https://doi.org/10.1002/0471250953.bi0814s24

[30] M. Terracciano, L. De Stefano, H.A. Santos, N.M. Martucci, A. Tino, I. Ruggiero, I. Rendina, N. Migliaccio, C. Tortiglione, A. Lamberti, I. Rea, Silica-Based Nanovectors: From Mother Nature to Biomedical Applications, in: N. Thajuddin, D. Dhanasekaran (Eds.), Algae - Org. Imminent Biotechnol., InTech, 2016. https://doi.org/10.5772/63191

[31] U.T. Uthappa, V. Brahmkhatri, G. Sriram, H.-Y. Jung, J. Yu, N. Kurkuri, T.M. Aminabhavi, T. Altalhi, G.M. Neelgund, M.D. Kurkuri, Nature engineered diatom biosilica as drug delivery systems, J. Controlled Release 281 (2018) 70–83. https://doi.org/10.1016/j.jconrel.2018.05.013

[32] P. Sundarrajan, P. Eswaran, A. Marimuthu, L.B. Subhadra, P. Kannaiyan, One pot synthesis and characterization of alginate stabilized semiconductor nanoparticles, Bull. Korean Chem. Soc. 33 (2012) 3218–3224.

[33] E. Günister, D. Pestreli, C.H. Ünlü, O. Atıcı, N. Güngör, Synthesis and characterization of chitosan-MMT biocomposite systems, Carbohydr. Polym. 67 (2007) 358–365.

[34] J.H. Kim, Y.M. Lee, Synthesis and properties of diethylaminoethyl chitosan, Polymer 34 (1993) 1952–1957.

[35] E. Gültürk, M. Güden, Thermal and acid treatment of diatom frustules, J. Achiev. Mater. Manuf. Eng. (2011).

[36] K. Khezri, Y. Fazli, Characterization of Diatomite Platelets and Its Application for In Situ Atom Transfer Radical Random Copolymerization of Styrene and Butyl Acrylate: Normal Approach, J. Inorg. Organomet. Polym. Mater. 27 (2017) 266–274. https://doi.org/10.1007/s10904-016-0469-5

[37] R. Merir, M. Baitiche, Z. Elbahri, R. Bourzami, F. Djerboua, M. Boutahala, Conception of Cellulose/Alginate/Mesalazine microspheres by solvent evaporation technique for drug release: Experimental and theoretical investigations, Int. J. Biol. Macromol. 243 (2023) 124894. https://doi.org/10.1016/j.ijbiomac.2023.124894

[38] A.R. Pawar, P.V. Mundhe, V.K. Deshmukh, R.B. Pandhare, T.D. Nandgude, Enrichment of aqueous solubility and dissolution profile of mesalamine: In vitro evaluation of solid dispersion, J. Pharm. Biol. Sci. 9 (2021) 127–135. https://doi.org/10.18231/j.jpbs.2021.018

[39] L. Nie, C. Liu, J. Wang, Y. Shuai, X. Cui, L. Liu, Effects of surface functionalized graphene oxide on the behavior of sodium alginate, Carbohydr. Polym. 117 (2015) 616–623. https://www.sciencedirect.com/science/article/pii/

[40] C. Jiang, Z. Wang, X. Zhang, X. Zhu, J. Nie, G. Ma, Crosslinked polyelectrolyte complex fiber membrane based on chitosan–sodium alginate by freeze-drying, RSC Adv. 4 (2014) 41551–41560. https://pubs.rsc.org/en/content/articlehtml/2014/ra/c4ra04208e

[41] Y. Zheng, A. Wang, Enhanced Adsorption of Ammonium Using Hydrogel Composites Based on Chitosan and Halloysite, J. Macromol. Sci. Part A 47 (2009) 33–38. https://doi.org/10.1080/10601320903394421

[42] G. Thakur, A. Singh, I. Singh, Formulation and evaluation of transdermal composite films of chitosan-montmorillonite for the delivery of curcumin, Int. J. Pharm. Investig. 6 (2016) 23.

[43] X.-J. Wu, J.-D. Wang, L.-Q. Cao, Characterization and adsorption performance of chitosan/diatomite membranes for Orange G removal, E-Polym. 16 (2016) 99–109

[44] S. Nasir, T. Theye, H.-J. Massonne, Elaboration and characterization of natural diatomite in Aktyubinsk/Kazakhstan, Open Mineral. J. 3 (2009). https://benthamopen.com/ABSTRACT/TOMJ-3-17

[45] J.B. Holt, I.B. Cutler, M.E. Wadsworth, Rate of Thermal Dehydration of Muscovite, J. Am. Ceram. Soc. 41 (1958) 242–246. https://doi.org/10.1111/j.1151-2916.1958.tb13548.x

[46] M.M. Alam, F. Tasneem, A.L. Kabir, A.S.S. Rouf, Study of Drug-Drug and Drug-Food Interactions of Mesalazine Through FTIR and DSC, Dhaka Univ. J. Pharm. Sci. 18 (2019) 257–269.

[47] A. Salisu, M.M. Sanagi, A. Abu Naim, K.J. Abd Karim, W.A. Wan Ibrahim, U. Abdulganiyu, Alginate graft polyacrylonitrile beads for the removal of lead from aqueous solutions, Polym. Bull. 73 (2016) 519–537. https://doi.org/10.1007/s00289-015-1504-3

[48] S.F. Wang, L. Shen, Y.J. Tong, L. Chen, I.Y. Phang, P.Q. Lim, T.X. Liu, Biopolymer chitosan/montmorillonite nanocomposites: preparation and characterization, Polym. Degrad. Stab. 90 (2005) 123–131. https://www.sciencedirect.com/science/article/pii/S0141391005001321

[49] S. Kumar, P.K. Dutta, J. Koh, A physico-chemical and biological study of novel chitosan–chloroquinoline derivative for biomedical applications, Int. J. Biol. Macromol. 49 (2011) 356–361. https://www.sciencedirect.com/science/article/pii/S0141813011002005

[50] V. Mokale, N. Jitendra, S. Yogesh, K. Gokul, Chitosan reinforced alginate controlled release beads of losartan potassium: design, formulation and in vitro evaluation, J. Pharm. Investig. 44 (2014) 243–252. https://doi.org/10.1007/s40005-014-0122-7

[51] D. Swami, S. Siddiqui, U. Kumar, S. Devarajan, J. Aich, One of the 5-aminosalicylates drug, mesalamine as a drug repurposing lead against breast cancer, Bull. Natl. Res. Cent. 46 (2022) 1–13.

Conclusion

This research aimed to develop effective and controlled delivery microspheres systems for 5-ASA, optimizing its biopharmaceutical, pharmacokinetic, and pharmacodynamic properties through the emulsion solvent evaporation technique. We achieved promising results regarding therapeutic efficacy and reduced side effects by using polymeric mixtures of ethyl cellulose (EC) and sodium alginate (SA) in various drug-to-polymer ratios. The spherical microspheres, observed through optical microscopy, exhibited a rough surface with a size range of several hundred micrometers. FT-IR spectral analysis confirmed compatibility between the drug and polymers, while ATG/DTG analysis revealed the drug's stability within the microspheres.

Drug release studies demonstrated that the EC and SA encapsulated microspheres provided controlled and targeted drug release, offering protection against the stomach's acidic environment and ensuring better drug delivery to the intestine. This in vitro dissolution profile is promising for treating inflammatory bowel disease compared to the pure drug. Additionally, periodic density functional theory (DFT) calculations described the molecular interactions of the 5-ASA-polymer complex, enhancing our understanding of NSAID adsorption on polymer surfaces.

In treating Crohn's disease, controlled release of mesalazine is critical to enhancing absorption and reducing adverse effects. The HNT/5-ASA/SA complex exhibited pH sensitivity, with increased drug release at pH 6.8 and 7.4. Docking results and strong binding affinity between 5-ASA and PPAR-γ, as well as stable complexes with COX-1 and COX-2, underscore the therapeutic potential of 5-ASA for inflammation management.

Our research further highlighted the improvement of diatomite-loaded mesalazine's performance, safety, and biocompatibility by incorporating biopolymers. Microencapsulation techniques utilizing sodium alginate and chitosan enhance controlled drug release and structural integrity. Targeting TNF-α and 5-LOX receptors in colon tissues provides a means for early detection and assessment of therapeutic effectiveness in ulcerative colitis. Molecular docking offers insights into the binding affinity of potential drug candidates, aiding the design and development of new therapeutics.

Overall, this research advances the development of more effective drug delivery systems for 5-ASA, providing significant potential for improved treatment of inflammatory bowel diseases.

Abstract

The purpose of this research is to improve and optimize drug delivery systems for 5-aminosalicylic acid (5-ASA) to treat inflammatory bowel diseases such as Crohn's disease and ulcerative colitis. We used the emulsion solvent evaporation technique, which allows for the encapsulation of 5-ASA within a polymer matrix, creating microspheres that can control drug release. Our in vitro release studies in simulated gastric and intestinal fluids demonstrated controlled, pH-dependent drug release, which we successfully modeled using Higuchi's and Korsmeyer–Peppas' models. Additionally, we employed Design of Experiments (DOE) and Density Functional Theory (DFT) analyses to optimize molecular interactions and evaluate their effects on drug entrapment and microparticle sizes.

For prolonged release in acidic medium, sodium alginate (SA) acts as a coating material, forming a stable 3D porous network with ethylcellulose (EC) and 5-ASA. This network is easily broken in basic conditions, leading to drug release. Chitosan (Cts) enhances the structural integrity of the drug-loaded beads, providing additional stability and ensuring that the drug remains effective within the gastrointestinal environment.

In the optimization of colon-targeted therapy via halloysite, the biocompatibility, encapsulation capability, and pH-responsive release properties of halloysite nanotubes make them a promising material for developing targeted and controlled 5-ASA delivery systems.

Diatomite serves as a promising material for drug delivery systems due to its unique properties. When combined with polymers such as sodium alginate and chitosan, diatomite can enhance the stability, biocompatibility, and controlled release of therapeutic agents.

Docking experiments showed strong binding of 5-ASA to PPAR-γ and stable interactions with COX-2 enzymes, suggesting 5-ASA's potential to effectively reduce inflammation.

Keywords: *5-aminosalicylic acid, Inflammatory bowel disease, Microencapsulation, Molecular docking, Density functional theory, Design of experiments, Therapeutic efficacy.*

Résumé

Le but de cette recherche est d'améliorer et d'optimiser les systèmes d'administration de médicaments pour l'acide 5-aminosalicylique (5-ASA) afin de traiter les maladies inflammatoires de l'intestin telles que la maladie de Crohn et la colite ulcéreuse. Nous avons utilisé la technique d'évaporation de solvant en émulsion, qui permet l'encapsulation du 5-ASA dans une matrice polymère, créant des microsphères capables de contrôler la libération du médicament. Nos études de libération in vitro dans des fluides gastriques et intestinaux simulés ont démontré une libération contrôlée et dépendante du pH, que nous avons modélisée avec succès en utilisant les modèles de Higuchi et de Korsmeyer–Peppas. De plus, nous avons employé des analyses de plan d'expériences (DOE) et de théorie de la fonctionnelle de la densité (DFT) pour optimiser les interactions moléculaires et évaluer leurs effets sur l'entrapment du médicament et la taille des microparticules.

Pour la libération prolongée en milieu acide, l'alginate de sodium (SA) agit comme un matériau de revêtement, formant un réseau poreux 3D stable avec l'éthylcellulose (EC) et le 5-ASA. Ce réseau est facilement dégradé en conditions basiques, ce qui conduit à la libération du médicament. Le chitosane (Cts) renforce l'intégrité structurelle des billes chargées de médicament, fournissant une stabilité supplémentaire et garantissant que le médicament reste efficace dans l'environnement gastro-intestinal.

Dans l'optimisation de la thérapie ciblée sur le côlon via l'halloysite, la biocompatibilité, la capacité d'encapsulation et les propriétés de libération dépendantes du pH des nanotubes d'halloysite en font un matériau prometteur pour développer des systèmes de délivrance contrôlée et ciblée du 5-ASA.

La diatomite est un matériau prometteur pour les systèmes d'administration de médicaments en raison de ses propriétés uniques. Lorsqu'elle est combinée avec des polymères tels que l'alginate de sodium et le chitosane, la diatomite peut améliorer la stabilité, la biocompatibilité et la libération contrôlée des agents thérapeutiques.

Les expériences de docking ont montré une forte liaison du 5-ASA avec PPAR-γ et des interactions stables avec les enzymes COX-2, suggérant le potentiel du 5-ASA à réduire efficacement l'inflammation.

Mots-clés : *Acide 5-aminosalicylique, Maladie inflammatoire de l'intestin, Microencapsulation, Docking moléculaire, Théorie de la fonctionnelle de la densité, Plan d'expériences, Efficacité thérapeutique.*

ملخص

الغرض من هذا البحث هو تحسين وتحسين أنظمة توصيل الدواء لحمض الخماسي الأميني (5-ASA) لعلاج الأمراض الالتهابية في الأمعاء مثل مرض كرون والتهاب القولون التقرحي. لقد استخدمنا تقنية تبخير المذيبات بالتشتت الإمولسيوني، التي تسمح بتغليف 5-ASA داخل مصفوفة بوليمرية، مما ينتج عنه ميكروسفيرات يمكن أن تسيطر على إطلاق الدواء ؛أظهرت دراساتنا لإطلاق الدواء في الأنابيب الهضمية والأمعاء المحاكية إطلاق دواء متحكم به يعتمد على درجة الحموضة، وقد نمذجنا بنجاح ذلك باستخدام نماذج هيغوتشي وكورسماير–بيباس. بالإضافة إلى ذلك، استخدمنا تصميم التجارب (DOE) ونظرية الدوال الكثافية (DFT) لتحسين التفاعلات الجزيئية وتقييم تأثيراتها على احتجاز الدواء وأحجام الميكروبارتيكل.

بالنسبة للإطلاق المطول في وسط حمضي، يعمل الألجينات الصوديوم (SA) كمادة طلاء، مكونة شبكة مسامية ثلاثية الأبعاد مستقرة مع الإيثيل سيليلوز (EC) و 5-ASA. هذه الشبكة يمكن تفكيكها بسهولة في ظروف قاعدية، مما يؤدي إلى إطلاق الدواء. يعزز الكيتوزان (Cts) تكامل بنية الخرز المحملة بالدواء، مما يوفر استقرارًا إضافيًا ويضمن بقاء الدواء فعالًا داخل البيئة الهضمية.

في تحسين العلاج المستهدف على مستوى القولون عبر الهالويسيت، تجعل قدرة التحميل الحيوي، وقابلية التغليف، وخواص إطلاق الحمض النووي المستجيبة لدرجة الحموضة لأنابيب الهالويسيت نانوتيوبز منهجاً واعداً لتطوير أنظمة توصيل مستهدفة ومتحكمة لـ 5-ASA.

تعتبر الدياتوميت مادة واعدة لأنظمة توصيل الدواء بفضل خصائصها الفريدة. عندما تُدمج مع البوليمرات مثل الألجينات الصوديوم والكيتوزان، يمكن للدياتوميت تعزيز الاستقرار والتوافق مع الأنسجة الحية والإفراج المتحكم عن الوكلاء العلاجيين.

أظهرت التجارب الموضوعية ربط قوي لـ 5-ASA بـ PPAR-γ وتفاعلات مستقرة مع إنزيمات COX-2، مما يشير إلى إمكانية 5-ASA للحد من الالتهاب بفعالية.

الكلمات الرئيسية: *حمض الخماسي الأميني (5-ASA)، مرض الأمعاء التهابية، التغليف المجهري، التحسين المولكي، نظرية الوظيفة الكثافية، تصميم التجارب، الفعالية العلاجية .*

Conception of Cellulose/Alginate/Mesalazine microspheres by solvent evaporation technique for drug release: Experimental and theoretical investigations

Roufaida Merir [a,d], Milad Baitiche [a], Zineb Elbahri [b], Riadh Bourzami [c], Ferhat Djerboua [a], Mokhtar Boutahala [d,*]

[a] Laboratory of Multiphasic Polymeric Materials, Department of Process Engineering, Faculty of Technology, Ferhat Abbas Sétif 1University, 19000 Sétif, Algeria
[b] Laboratory of Materials and Catalysis, Faculty of Exact Sciences, Djillali Liabes University, Sidi Bel Abbes 22000, Algeria
[c] Research Unit on Emergent Materials, Ferhat Abbas Sétif1University, 19000 Sétif, Algeria
[d] Laboratory of Chemical Process Engineering, Department of Process Engineering, Faculty of Technology, Ferhat Abbas Sétif1University, 19000 Sétif, Algeria

A B S T R A C T

Preparation of microspheres containing Mesalazine referred to as 5-aminosalicylic acid (5-ASA) for colon targeting drug was carried out using the emulsion solvent evaporation technique. The formulation was based on 5-ASA as the active agent, sodium Alginate (SA) andEthylcellulose (EC) as encapsulating agents, with polyvinyl alcohol (PVA) as emulsifier. The effects ofthe following processing parameters, 5-ASA %, EC:SA ratio and stirring rate on the properties of the resulting products in the form microspheres were considered. The samples were characterized using Optical microscopy, SEM, PXRD, FTIR, TGA, and DTG.

In vitro release of 5-ASA from the different batches of microspheres was tested in biologically simulated fluids, (gastric; SGF, pH 1.2 for 2 h), then (intestinal fluid SIF, pH 7.4for 12 h) at 37 °C. The release kinetic results have been treated mathematically relaying on Higuchi's and Korsmeyer–Peppas' models for drug liberation. DOE study was performed to evaluate the interactive effects of variables on the drug entrapment and microparticle sizes. Molecular chemical interactions in structures were optimized using DFT analysis.

1. Introduction

Oral drug administration is popular and the most convenient for patients, especially for long term treatment. However, for certain drugs the therapeutic efficacy of this way of treatment can be hindered due to the low bioavailability of the drug, its poor water solubility and its molecule instability in the acidic gastrointestinal (GI) medium [1]. In the case of certain intestine diseases, special drugs are needed with aim of targeting their release at the site of action as is the case for gastro-resistant formulations.

By protecting drug molecules from GI acidic environment and increasing its passage through the intestinal membrane, encapsulated orally-delivered nano/micro drug systems (NDDs) remain promising vehicles by improving drugs bioavailability [2]. The therapeutic efficacy of such drugs is very important in the treatment of colon-related ailments, with particular emphasis on inflammatory bowel disease (IBD) [3].

Mesalazine (5-ASA) is a typical anti-inflammatory prescription drug, which has been used for the treatment of IBD such as Crohn's disease and which is often administered orally (2–4 g/ day) with repeat dosing [4]. This drug molecule inhibits the formation of prostaglandin E2 in inflamed intestinal tissues by blocking the cyclo-oxygenase pathway [5,6]. Over the last few years, it has been reported that 5-ASA can be used as antitumor agent for treatment of colon cancer [7].

It is well established that 5-ASA is swiftly absorbed from the small intestine and mostly from the upper intestine. So, it is necessary as an objective of the present investigation to develop a colon-specific delivery system with a prolonged release and low dosage forms. The 5-ASA molecule has an amphoteric character which affects its intrinsic dissolution rate. So, its release formulation in the colon is problematic and requires a special coating to prevent a gastric release since it is soluble in acidic medium [8,9].

Several methods and techniques of microencapsulation are useful to prepare polymeric microparticles for this purpose. Among these ways,

the emulsion/evaporation technique is known as very suitable for water insoluble drugs.

Ethyl cellulose (EC) and sodium alginate (SA) have been used as matrices for microencapsulation. EC is a drug carrier and a biocompatible polymer. It is an extensively studied encapsulating material for the controlled release in microencapsulation and especially when used in the solvent evaporation process since it is insoluble in water but soluble in many polar organic solvents [10–12]. SA is a natural unbranched polysaccharide, non-toxic, biocompatible biopolymer slightly soluble in cold water, forming viscous and colloidal solution, insoluble in acidic medium but rapidly breaks down in basic medium, consequently, SA is considered a pH-dependent swelling material [13,14].

In the present study, EC/SA microspheres loaded with 5-ASA are prepared based on the solvent evaporation technique. Different batches were obtained by changing the preparation parameters. The microspheres were characterized using different analytical techniques. The drug entrapment and the drug release were studied and subjected to data analysis according to Higuchi and Korsmeyer–Peppas modeling. In order to investigate the drug dissolution process, the results have been validated through building the design of experiments (DOE) and modeling using JMP software. To investigate the interaction mechanism involved in binding the 5-ASA and EC/SA system, analysis using the density functional theory (DFT) was performed.

2. Material and methods

2.1. Materials

Mesalazine (5-ASA) was supplied by SALEM Pharmaceutical Laboratories, El-Eulma, Algeria. Ethyl cellulose (EC) (48 % of ethoxyl content), Sodium alginate (SA) (medium viscosity) and Polyvinyl alcohol (PVA) 87–90 % hydrolyzed with molecular weight $(13,000-23,000)$ g/mol were supplied by Sigma-Aldrich, USA. Dichloromethane (DCM, 99.9 %) and ethanol (99.9 %) were from Merck, Germany. All other used chemicals are of analytical grades and all reagents are used as received.

2.2. Preparation of microspheres

The microspheres were prepared by an oil/water emulsion solvent evaporation technique. Accurately weighed amounts of 5-ASA, EC and SA (see Table 1) were mixed in 20 mL of dichloromethane (DCM). This organic phase was kept under gentle heating and continuous stirring for 2 h making sure that solvent evaporation was accomplished. The aqueous phase was prepared by dissolving 2.5 g of the emulsifier PVA in 500 mL of distilled water under vigorous stirring for 24 h until complete PVA dissolution. Then, the drug/polymers mixture was added in droplets into the aqueous solution using a syringe. The drops were emulsified under continuous mechanical stirring using a paddle stirrer. Different stirring speeds (300 and 800 rpm) were used. This operation lasted for 8 h ensuring complete evaporation of solvent. The compositions of the prepared formulations are given in Table 1. The resulting wet microspheres floating in the liquid medium were filtered on Whatman paper, and washed several times with distilled water. The collected

Table 1
Composition and process variables for 5-ASA microspheres preparation.

Batch	Stirring speed rpm	SA/EC %	SA/EC (m/m) g	Drug% 5-ASA/Pol.	5-ASA weight (g)
1	300	5 %	(0.1/1.9)	10 %	0.2 g
2	800	5 %	(0.1/1.9)	10 %	0.2 g
3	300	30 %	(0.6/1.4)	10 %	0.2 g
4	800	30 %	(0.6/1.4)	10 %	0.2 g
5	300	5 %	(0.1/1.9)	50 %	1 g
6	800	5 %	(0.1/1,9)	50 %	1 g
7	300	30 %	(0.6/1.4)	50 %	1 g
8	800	30 %	(0.6/1.4)	50 %	1 g

microspheres were dried in open air (48 h) until constant weight and stored.

2.3. Characterization of 5-ASA microspheres

2.3.1. Determination of drug content

Drug content was determined in duplicate as it follows. 10 mg of microspheres were submerged in 30 mL of distilled water and stirred for 24 h at room temperature. The resulting mixture was filtered, and the filtrate was analyzed using UV–Vis spectroscopy at 302 nm. Eq. (1) is used to determine the active ingredient content.

$$Drug\ content\% = \frac{mass\ of\ active\ agent\ extracted * 100}{mass\ of\ microspheres} \quad (1)$$

2.3.2. Fourier-Transform Infrared Spectroscopy analysis (FT-IR)

The microspheres batches as well pristine 5-ASA and the encapsulating agents (EC and SA) have been analyzed using a Fourier transform infrared (FT–IR) spectrophotometer Shimadzu-8400 Japan considering the KBr disc method. For this, microspheres were grounded and all FTIR spectra were recorded from 4000 to 400 cm^{-1}. The obtained spectra were compared to assess whether any alterations had taken place in the chemical structures of the compounds following the microencapsulation process.

2.3.3. Optical and scanning electronic microscopies analyzes

Particle shape and size measurements were evaluated through micrographs obtained using optical microscope (MOTIC, Germany) coupled with a camera and Image J software. The microspheres were placed on a glass slide and viewed at varying magnifications. The mean diameters (d) in micrometers and size distributions (δ) of microparticles were estimated using Eqs. (2)-(5) where (n) is the number of 300 microparticles. The surface morphology of microspheres was observed with a scanning electron microscope (SEM) type GEMINI (FESEM) CARL ZEISS equipped with an electron source by Schottky field emission (hot cathode).

$$d_{10} = \sum n_i d_i \Big/ \sum n_i \quad (2)$$

$$d_{32} = \sum n_i d_i^3 \Big/ \sum n_i d_i^2 \quad (3)$$

$$d_{43} = \sum n_i d_i^4 \Big/ \sum n_i d_i^3 \quad (4)$$

$$\delta = \frac{d_{43}}{d_{10}} \quad (5)$$

2.3.4. Thermogravimetric Analysis (TGA/DTG)

The thermogravimetric analysis (TGA, DTG) was performed using (TA Instruments SDTQ600). Samples of approximately 5 mg of microspheres (in powder) and those of 5-ASA, EC, and SA were sealed in aluminum pans and heated from ambient temperature to 750 °C at a rate of 20 °C/min^{-1}, under nitrogen atmosphere.

2.3.5. In vitro drug release studies

The release of 5-ASA from microspheres was studied in vitro in a simulated gastric fluid (SGF, pH 1.2) and in a simulated intestinal fluid (SIF, pH 7.4, distal ileum and colon). The tests were carried out in a thermostatic bath containing 900 mL of the fluid at 37 °C ± 1 °C, stirred with a controlled rate (100 rpm) using a paddle stirrer. A weighed amount of microspheres containing 100 mg of 5-ASA was placed in a Soilon bag type (2 × 2 cm) then this later was plunged in the bath containing either SGF or SIF dissolution medium ensuring sink conditions. At appropriate time intervals, 2 mL of liquid were withdrawn, passed through a 0.45 μm membrane filter (Millipore). The concentration of drug in samples was analyzed by UV–vis spectroscopy (Shimadzu

Pharmspec UV-1700) at λ_{max} = 302 nm for SGF then 330 nm for SIF, respectively. The initial volume of dissolution medium was maintained by adding 2 mL of fresh dissolution medium after each withdrawal. The duration of dissolution test was 120 and 700 min for SGF and SIF respectively. All experiments were performed twice and average values were determined.

2.3.6. Kinetic modeling on drug release

A kinetic modeling analysis was carried out on microspheres in an attempt to determine the phenomena governing the release pattern of 5-ASA. The mechanism and kinetics of drug release were deduced by fitting dissolution curves to Higuchi (Eq. (6)) and Korsmeyer-Peppas (Eq. (7)) models. And for describing the drug release behavior, a better fit was established by using a correlation coefficient the closest to 1,

Higuchi's model

$$M_t/M\infty = K_H t^{1/2} \qquad (6)$$

Korsmeyer-Peppas model

$$M_t/M\infty = K_P t^n \qquad (7)$$

Where $M_t/M\infty$ is the fraction of drug released at time t, k_H the Higuchi rate constant, Kp is a kinetic constant including geometric characteristics of microspheres and n is the diffusion exponent indicative of the release mechanism. The value of n depends on the microsphere shape; in the case of n less than 0.45 it is a Fickian release, n between 0.45 and 0.89 described a non-Fickian release, while for n greater than 0.89 the mechanism of drug release is considered (case II) as a type in which the erosion of polymers takes place [15].

3. Theoretical study of the microencapsulation

3.1. Computational details

The geometry optimization and theoretical calculations of the electronic state of 5-ASA, EC, and SA molecules were performed using Gaussian 09W 9.0, Cincinnati, USA software, based on the density functional theory (DFT) [16] and which Beck's three parameters hybrid exchange functional [17], 6-31G (d, p) basis set, and Lee-Yang-Parr correlation functional (B3LYP) were selected as calculations parameters [18,19]. To obtain trustworthy results, the influence of the water solvent was considered. These theoretical parameters are adequate for small molecular structure [20] .

The frontier molecular orbitals (FMOs) theory is widely recognized as a valuable approach for gaining insight into the chemical stability and reactivity of molecular materials [21]. it predicts the electronic transfer that may occur within the highest occupied molecular orbital (HOMO) and lowest unoccupied molecular orbital (LUMO) frontier molecular orbitals [22]. The ELUMO, EHOMO were computed and some other related global quantum chemical descriptors (GQCDs) were deduced, including: gap energy (ΔEgap), global hardness (η), chemical potential (μ), global softness (σ), absolute electronegativity (χ) and electrophilicity index (ω) using the following Eqs. (8) to (13) [23]:

$$\Delta E_{Gap} = E_{LUMO} - E_{HOMO} \qquad (8)$$

$$\eta = \frac{(E_{LUMO} - E_{HOMO})}{2} \qquad (9)$$

$$\mu = \frac{(E_{LUMO} + E_{HOMO})}{2} \qquad (10)$$

$$\sigma = \frac{1}{\eta} \qquad (11)$$

$$\chi = \frac{-(E_{HOMO} + E_{LUMO})}{2} \qquad (12)$$

$$\omega = \frac{x^2}{2\eta} \qquad (13)$$

The adsorption of 5-ASA and water molecules on EC-SA copolymer substrate was modeled by one molecule of 5-ASA and five water molecules on one formal co-monomer unit EC-SA. The adsorption was performed using adsorption locator modulus based on Monte Carlo (MC) theory, in which the DFT-optimized geometries were used as initial configurations. The equilibrium configurations were calculated using the neutral charge of both adsorbent and adsorbate. The time step was 0.1 fs and the simulation time was 1 ns. Additionally, the equilibrium configurations were considered after 10 cycles and 10^5 steps by cycle, at $2*10^5$ Kcal.mol^{-1}.Å^{-1} as cut off energy, 10^{-3} Kcal.mol^{-1}.Å^{-1} as maximum force, and.

10^{-6} nm as maximum displacement [24]. We add that a normal thermodynamic ensemble NVT was fixed for all calculations. For the adsorption of small molecules, these theoretical parameters are appropriate [25].

4. Results and discussion

In the present work 5-ASA/EC/SA microspheres were successfully prepared. Some parameters such as emulsion stirring speed and components ratios were varied and the results were analyzed to determine the best microencapsulation process conditions. The findings are discussed in this section.

4.1. Chemical identification

Infrared spectroscopy is a useful tool to confirm the effective presence of 5-ASA in microspheres and to investigate drug/polymers interactions as well as stability of formulations. 5-ASA spectrum Fig. 1 showed absorption bands between 3200 and 2500 cm^{-1} which correspond to intermolecular hydrogen bonds. Two bands attributed to the asymmetric and symmetric stretching modes of COOH groups are seen approximately at1651 and 1353 cm^{-1}. Other peaks appeared at 1257 cm^{-1} for C—N stretching vibration and at 1640 cm^{-1} corresponding to the bending vibration of N—H. There were also strong intensity bands corresponding to C—H stretching in aromatic compound at 878 cm^{-1} and peaks at 767 cm^{-1} and 689 cm^{-1} of C—H out of plane bending vibration. Observed peaks are similar to those reported in literature [26–28].

The pure SA spectrum exhibited characteristic absorption bands around 1617 cm^{-1}, 1415 cm^{-1} and 1300 cm^{-1} which were attributed to stretching vibrations of asymmetric and symmetric bands of carboxylate anions respectively [27]. The band at 3438 cm^{-1} is related to the stretching vibration of the hydroxyl groups (-OH) bonded via hydrogen bonds [29,30].The peak appearing around 2930 cm^{-1} corresponds to aliphatic C—H stretching vibration [31]. At 1030 cm^{-1}a band can be assignable to C-O-C stretching vibration. All of the above characteristics supported the basic properties of natural polysaccharides [29]. On the other hand, the FT-IR spectrum of EC showed a band at 3485 cm^{-1} due to -OH stretching vibration while bands at 2980 and 2876 cm^{-1} correspond to the stretching vibration of aliphatic C—H [30]. At 1070 cm^{-1}, the vibrations of glycosidic band C-O-C were observed. The peak at 1370 cm^{-1} corresponds to the C—O ether functions [32]. It has been noticed that all the spectra of the microspheres, as seen for Batch 8 in (Fig. 1), exhibited the characteristic bands of the drug, the peaks of 5-ASA were maintained. The presence of peaks at the frequencies 1650 cm^{-1} (corresponds to the C=O stretch), 1452 cm^{-1} (C—H bending from the alkane –CH$_2$), 770 cm^{-1} (C—H out of plane bending vibrations) and 686 cm^{-1} (Aromatic C—H out of plane bending vibrations). This indicates that there is no change in the drug structure and the absence of chemical interactions between 5-ASA and EC or SA.
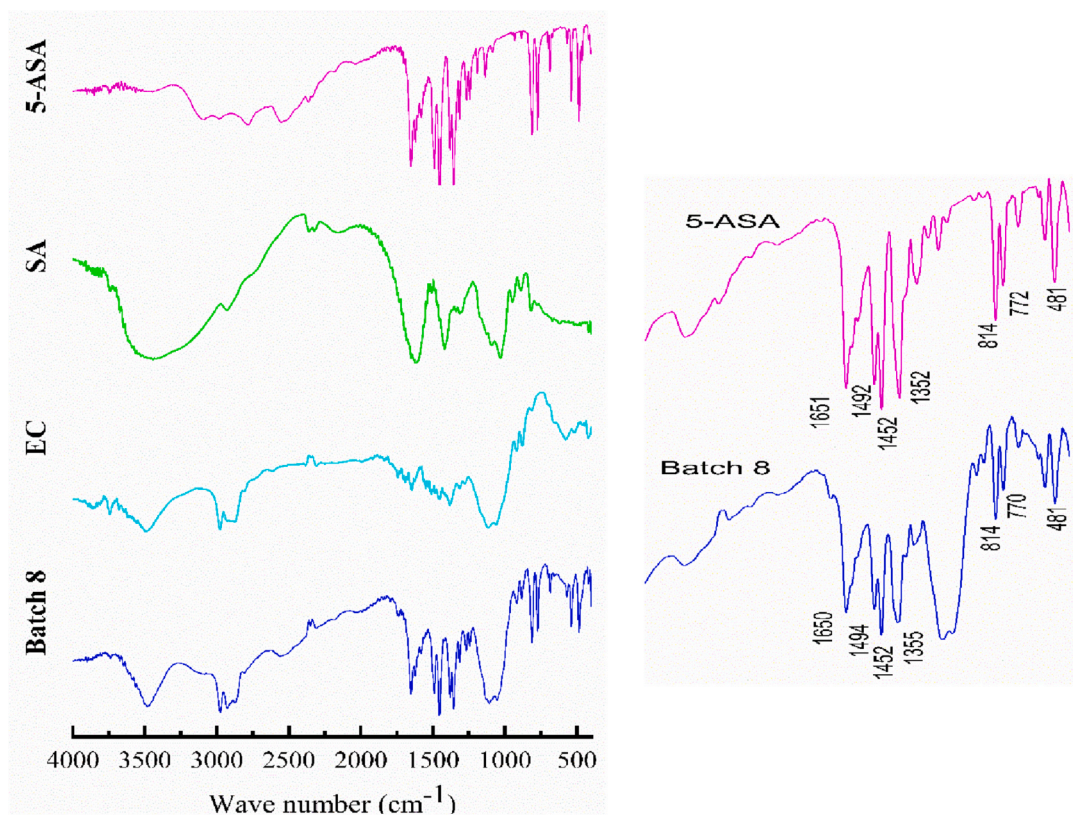
Fig. 1. FT-IR spectra of 5-ASA, SA, EC and batch 8.

4.2. Optical microscopy and SEM

Micrographs taken by means of optical microscope showed spherical particles. These were free-flowing and non-aggregated Fig. 2. In the case of the low agitation speed and the maximum quantity of both active ingredient and polymers during the preparation, larger droplets were formed in the mixing process and consequently larger microspheres were obtained Fig. 2. The microparticles sizes, as described in the experimental section, were measured using optical microscopy, an example of size frequency classification is displayed on Batch 8. In this case, 300 microparticles were counted and inspected using optical microscopy, and the size distribution is calculated and depicted graphically as shown in Fig. 3. In Table 2 are summarized the microparticles size results. The range of mean minimums and maximums diameters (d_{10}) of the microparticles varied from 502.3 μm to 748.5 μm and from 555 μm to 813.3 μm, respectively. The stirring speed had a significant influence on the size of the microparticles; when the stirring speed of emulsion was raised, the mean diameter effectively decreases. Furthermore, the results showed that increasing the amount of ethyl cellulose increased the viscosity of the medium, which may reduce emulsion effectiveness, resulting in increased droplet size and hence microsphere size.

Observations made by SEM suggests that very small amount of 5-ASA crystals are attached to the surface of the particles from the external medium Fig. 4. This is supported by the absence of burst effect in the dissolution test of adsorbed 5-ASA on microspheres. On the other hand, the surface morphology of microparticles (as seen for Batch 8) was observed to be rough, mainly as a result for increased drug concentrations that could be scattered on the surface (insertion in Fig. 4).

4.3. Thermogravimetric analysis

Thermogravimetric analysis (TGA) and derivative (DTG) were carried out to investigate the thermal stability, the oxidation, and the vaporization of the polymers and active ingredient. TGA/DTG thermograms are illustrated in Fig. 5. For pure 5-ASA a total mass loss is observed in one step at 288 °C which corresponds to decomposition of the drug [33]. The thermogram of pure SA showed two events of a mass loss. The first one is observed in the temperature range from 36 °C to 102 °C of about 10 % weight loss was attributed to dehydration and volatile products elimination [34,35]. The second one may be ascribed to the decomposition of SA in two stages. The first stage starting at approximately 205 °C until 350 °C is due to decarboxylation (40 %). The second one which occurred in the range of 350 °C–750 °C was assigned to the rupture of glycosidic bonds probably leading to volatile fragments and complete degradation of SA backbone corresponding to a mass loss of (7.5 %) [36]. The TGA/DTG thermogram of pristine EC presented only one step of degradation so it decomposed directly and the maximum decomposition takes place at 365 °C [37,38].

In the thermogravimetric analysis of microspheres, Batch 8 thermogram showed weight loss and the corresponding DTG indicated the presence of the three ingredients that made the microspheres. Through the TGA/DTG thermogram of Batch 8 three stages were observed. The first step in the range between 216 and 279 °C corresponds to SA degradation peak. It was followed by a second step from 279 to 296 °C which can be attributed to the decomposition of 5-ASA. It can be noticed that the decomposition of 5-ASA and SA occurred at very similar temperature ranges so it might not be possible to clearly identify the decomposition events individually. Finally, the third stage was attributed to the weight loss of EC which occurred between 305 and 410 °C showing a similar decreasing tendency with pristine EC.

4.4. Powder X-ray diffraction pattern (PXRD)

In order to investigate the crystallinity of 5-ASA structure in EC/SA microspheres, the PXRD technique was used. X-ray diffractograms of pure compounds and batch 8 are shown in Fig. 6. The PXRD pattern of
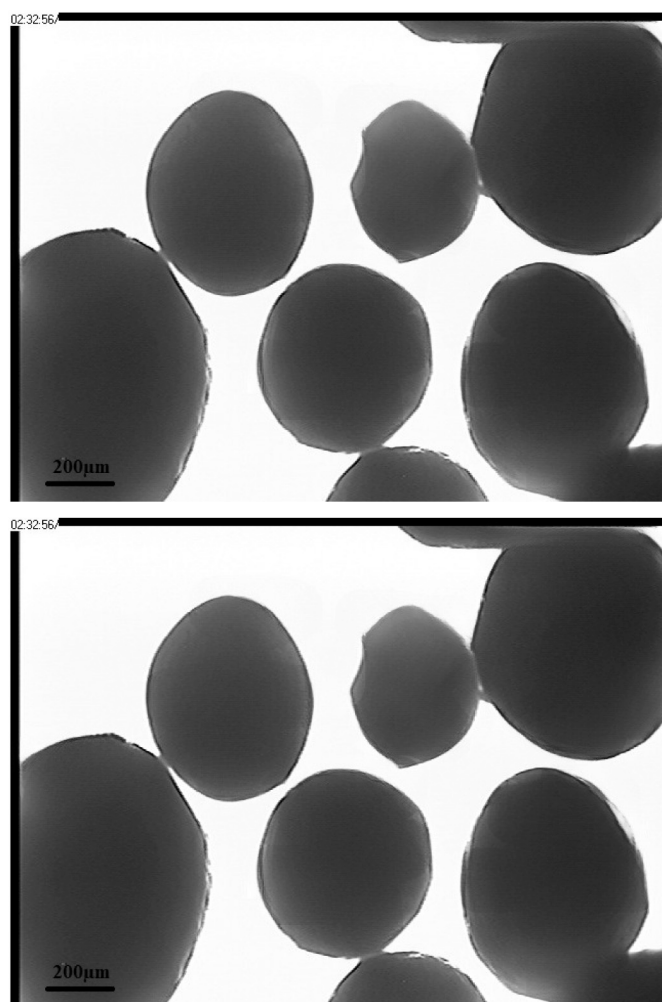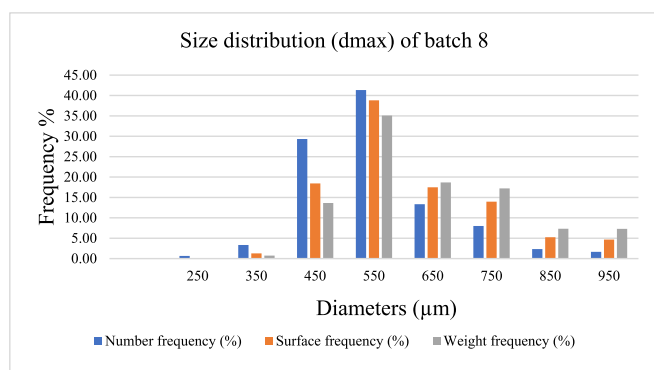
Fig. 2. Optical micrographs of microspheres.

Fig. 3. Size distribution of (dmax) for Batch 8.

pristine 5-ASA showed characteristic intense peaks between 2θ (5 and ~16°) indicating its crystalline structure. However, the PXRD analysis of batch 8 microspheres showed also a number of characteristic peaks of 5-ASA but with a low intensity, which suggested the amorphous structure of 5-ASA in the formulations.

4.5. In vitro drug release studies

In this study, a delayed delivery drug formulation is desirable because 5-ASA exerts therapeutic effect through local topical activity at the inflamed intestine mucosa. It is also rapidly absorbed by the upper small intestine, hence the drug release must be prolonged until the substance reaches the terminal ileum or the colon [39]. In the in-vitro release studies, a successful colon targeted drug delivery with minimum drug release during its transit in the stomach was obtained for all the batches Fig. 7. As expected, 5-ASA presents a high solubility at acidic pH and this was observed in drug release profile of the pure drug (Fig. 7). Practically, the entire drug is dissolved after 70 min of its passage through the first step in the gastrointestinal tract. Contrarily, microspheres containing pure 5-ASA showed a significant stability in these conditions that simulate the stomach medium. From the simulated gastric medium in pH 1.2, the results showed that the drug released after 120 min varied from 17.5 % (Batch4) to 44.4 % (Batch 6) as shown in Fig. 7. The5-ASA release profiles were compared to determine the effect of agitation speed of emulsion and polymers/drug proportions on drug dissolution. In the gastric medium, by comparing the percentage of the drug released for the batches prepared using the same stirring speed during the microencapsulation process (Batch 1 and 2) and also (3 and 4) it was shown that a faster stirring and higher concentration ratio of SA led to a slower 5-ASA release. In this case since the polymer concentrations are high, they form a barrier which prevents the exit of the drug towards the external environment. Moreover, by comparing Batches 5 and 6 to 7 and 8, it was observed that the drug release content was increased whatever the stirring speed of emulsion, knowing that in these formulations the rate of the active agent is high, so it is normal for its released fraction to be high. In the intestinal medium, higher 5-ASA release efficiency is noticed; it varied from 41.3 % to 77.9 %. The Batches 1 and 2 containing lower drug content exhibited a similar 5-ASA release profile. The effect of each parameter is discussed in the DOE section. This method allowed a prolonged release of the drug in acidic medium. As it was reported in previous work [40]; when SA is used in solvent evaporation method, it can play a role of coating material for drugs and in this situation electrostatic forces between SA, EC, and 5-ASA produce stable 3D porous network which will be confirmed by DFT studies. This network is easily broken in basic medium due to the solubility of SA in this condition.

4.6. Drug release kinetics results treatment

The dissolution data were analyzed according to: Higuchi and Korsmeyer-Peppas kinetic model-dependent approaches in order to investigate the drug release mechanism. The corresponding results are displayed in Table 3. The best-fitted release kinetic model is based on the selection in the regression analysis. The kinetic model with the highest value of coefficient (R^2) was considered to be a more suitable model for all dissolutions. By applying the Higuchi model, the value of R^2 was found to be between 0.940 and 0.994. Moreover, the drug release mechanism was also investigated from these microspheres using the Korsmeyer-Peppas equation and R^2 values varied from 0.956 to 0.997. The value of "n" was superior to 0.89 for batches (1, 3, 4 and, 5) and closed to this value for the others (2, 6, 7 and, 8). This is associated to an erosion of polymers matrix that takes place during the dissolution test and hence the escape of the drug content. Whereas, an anomalous mode drug release mechanism exhibits both diffusion and erosion of polymers. With the increase in EC polymer concentration, the pores surface of the drug was found to decrease preventing its escape which may contribute to prolonging drug release profiles. It is known that the initial drug release from EC usually follows anomalous mode (Korsmeyer-Peppas result) [41]. During dissolution test, microspheres begin to swell by increasing the uptake of water leading to the formation of a barrier. This fact induced erosion decreasing which may prolong the release rate of 5-ASA. Herein, our present study described how the mixture of EC and SA was used to control the balance

Table 2
Microspheres dimensional characteristics (Formulations B1–B8).

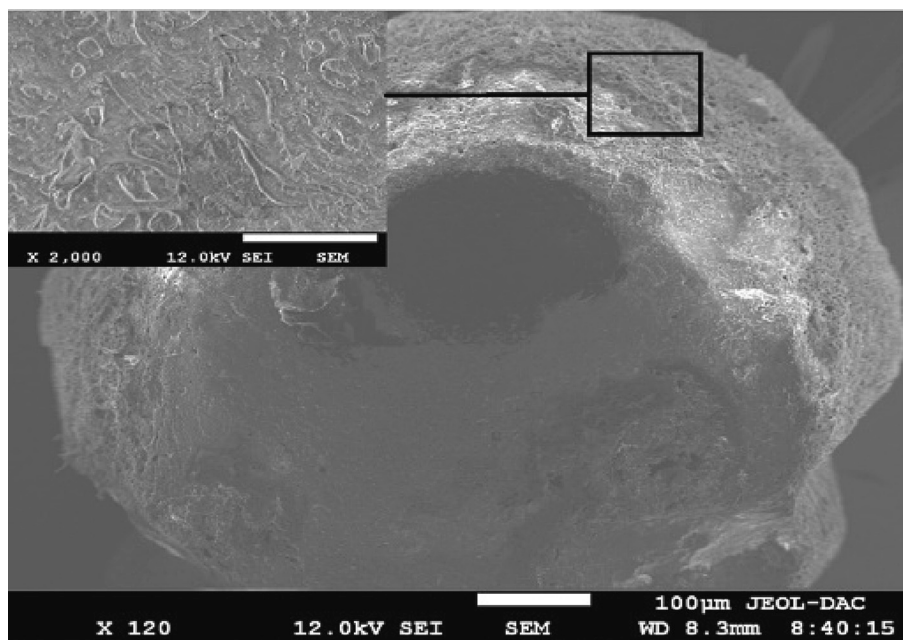| Batch	Drug content	d min (μm)				d max (μm)			
	(%)	d_{10}	d_{32}	d_{43}	δ	d_{10}	d_{32}	d_{43}	δ
1	98,3 ± 0.39	752.1	813.0	835.5	1.11	790.6	748.5	869.7	1.10
2	98,5 ± 0.50	727.1	795.1	821.6	1.13	810.0	851.4	867.5	1.07
3	98,4 ± 0.53	682.5	744.5	770.0	1.13	761.8	828.5	852.0	1.12
4	98,5 ± 0.50	774.5	840.9	861.3	1.11	765.0	839.3	862.8	1.13
5	91,5 ± 2.84	714.0	788.2	814.5	1.14	743.5	809.3	834.1	1.12
6	93,3 ± 2.25	684.3	749.5	775.9	1.13	771.5	828.6	849.8	1.10
7	92,4 ± 2.55	673.9	741.1	764.5	1.13	700.0	776.0	811.1	1.16
8	92,8 ± 2.42	502.0	553.2	583.5	1.16	555.0	608.4	639.0	1.15

Fig. 4. SEM of 5-ASA loaded EC/SA microspheres (Batch 8).

between erosion and swelling of microspheres. On the other hand, SA polymer is less susceptible to disintegration in the gastric medium then a delayed delivery of 5-ASA in the more distal parts of the small intestine can be achieved. The use of SA/EC mixture helped to prolong drug release and can be a promising matrix for 5-ASA to achieve the desired therapy with minimum side effects.

4.7. Investigation results using design of experiments

Simple 2^3 factorial designs were developed for the microparticles in order to quantify the variables impacts on the microsphere's properties (Table 4). The number of trials necessary for this study is dependent on the number of unrelated variables used such as drug concentration (% Drug), polymer mixtures noted % EC/SA (*w/w*) and stirring speed (rpm). The responses (Yi) studied were the drug loading (% T), the effect of stirring speed on the d_{10} (dmax) and Higuchi's release constant (K_H), in order to explain the effect of one factor on the other, to know whether this effect is significant or not and how it influences the response. The data obtained for the replies in each run were analyzed with the JMP.13 Software. The response Yi of the polynomial (Eq. (14)) was measured for each trial and then interactive statistical first order complete model (Eq. (14)) was generated to identify statistically significant terms.

$$Y_i = a_0 + a_1X_1 + a_2X_2 + a_3X_3 + a_{12}X_1X_2 + a_{13}X_1X_3 + a_{123}X_1X_2X_3 \quad (14)$$

where: a_0: is the arithmetic mean response of four runs, a_i: is the estimated coefficient for the factor X_i.

The primary impacts (X_1, X_2 and X_3) show the average result of changing one element at a time from a lowest (−1) to the highest (+1) values. However, when two factors are altered at the same time the interaction (X_1X_2 and X_3) illustrates how the response (Y_i) value changes. The primary influence of components X_1, X_2 and X_3 as well as the interacting effect of the two factors on the response Y_i may then be evaluated using these equations.

$$\begin{aligned} T\% = 95.46 - 2.96X1 + 0.06X2 + 0.31X3 + 0.03\ X_1X_2 + 0.24\ X_1X_3 \\ - 0.19\ X_2X_3 - 0.17\ X_1X_2X_3 \end{aligned} \quad (15)$$

$$\begin{aligned} K_H\left(min^{-1/2}\right) = 0.09 + 0.03X1 - 0.003X2 - 0.004X3 + 0.004\ X_1X_2 \\ - 0.001\ X_1X_3 + 0.0003\ X_2X_3 - 0.0007\ X_1X_2X_3 \end{aligned} \quad (16)$$

$$\begin{aligned} d_{10}max\ (\mathbf{μm}) = 733.4 - 40.9X_1 - 37.9X_2 - 8.05X_3 - 27.03X_1X_2 \\ - 21.2X_1X_3 - 27.4\ X_2X_3 - 15.85\ X_1X_2X_3 \end{aligned} \quad (17)$$

These equations depict the main quantitative effect of factors X_1, X_2 and X_3 as well as the interactive effect of the factors upon the response Y (Drug content % T), the mean diameter (d_{10}), and drug release constant (K_H). The coefficient sign in a regression model indicates how a factor affects the response variable. A positive coefficient means the factor has a synergistic effect, increasing the response variable as it increases from low −1 to a high level + 1. A negative coefficient means the factor has an inverse or antagonist effect, decreasing the response variable as it increases [11]. The effects of the independent variables and their
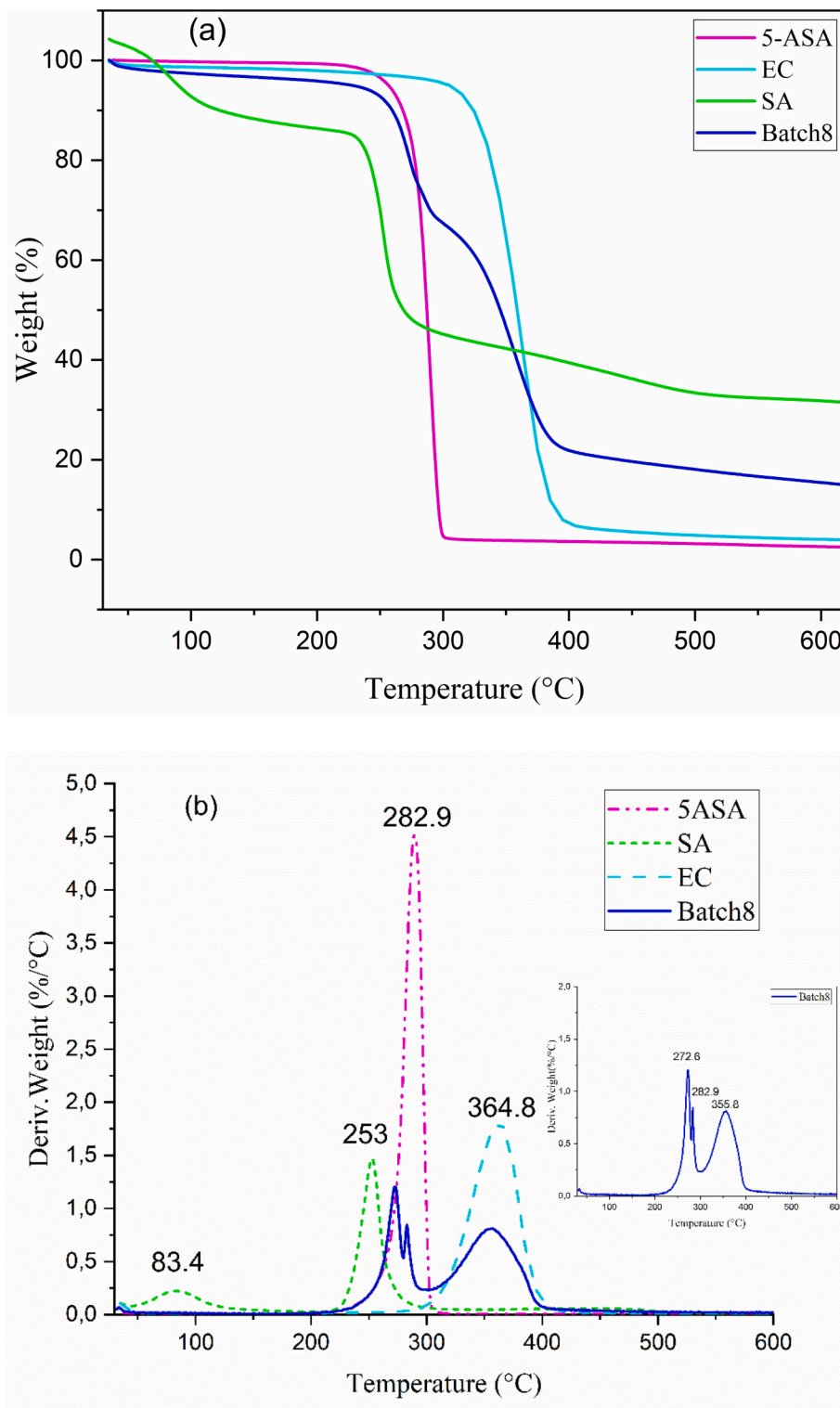
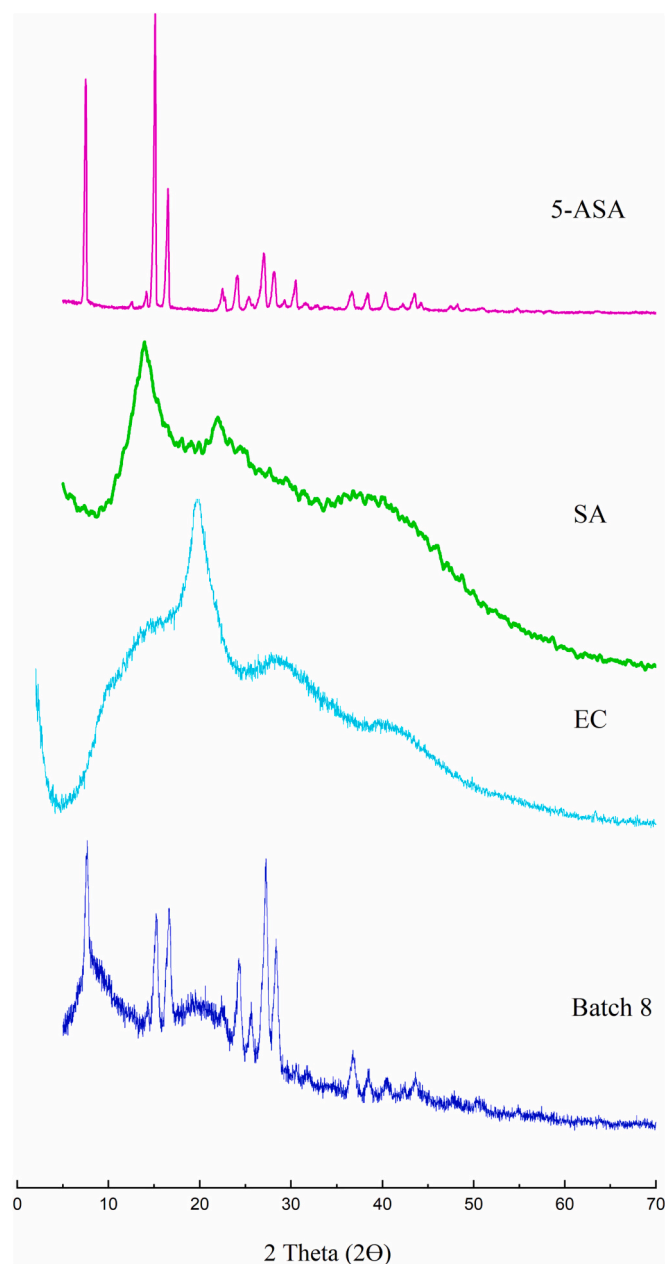**Fig. 5.** TGA (a)/DTG (b) patterns of 5-ASA, EC, SA and Batch 8.

Fig. 6. XRD patterns of 5-ASA, SA, EC and Batch8.

interactions on the drug loading (% T), the drug release constant (K_H) and the d_{10} microspheres diameter (dmax) can be visualized on the three-dimensional (3D) plots and the Prediction Profiler. This plotting mode is beneficial for evaluating the connection between the independent and dependent variables.

The results obtained for the microspheres as depicted by the estimated coefficient value (**a_i**) in Eqs. (15), (16) and (17) and the main effects representation in Fig. 8 showed that; the drug concentration displayed a synergistic effect on drug release constant (K_H), while it exhibited a high but adverse effect on both drug content (% T) and the mean diameter (d_{10}).

The effects of variables on the microspheres size revealed that the stirring speed has a slight but adverse effect on d_{10}; in fact, the mean diameter (d_{10}) decreased when the stirring speed increased. This result approves the initial break-up theory: increasing the stirring speed of emulsification induces small droplets and on the contrary viscous organic phase leads to big droplets [42]. However, the results showed

that polymer concentration (% EC/SA) negatively and notably affected the microspheres size. Also, the increase in polymer concentration led to a decrease in drug dissolution.

Finally, the effects of these variables on the responses are significant. Indeed, it was highlighted that when the drug concentration increased, the drug release constant (K_H) increased. While drug content (% T) significantly decreases with increasing shaking speed. It is also noticed that an increase in the stirring speed of the emulsion leads to a decrease in the value of mean diameter (d10), and on the contrary, the drug dissolution decreased and the size of microspheres (d10) increased with an increase in polymer concentration.

Building three-dimensional response surfaces allowed us to assess how and which of the variables affected each other and identify the combination that yielded the best results. In fact, the interaction between the variables exhibits no significant interactions separately. But the combination of the variables X_1X_2, X_1X_3, and X_2X_3 can have effect. A strong and notable interaction between drug constant (X_1) and both of EC/SA concentration (X_2) and stirring speed (X_3) is confirmed by a distorted surface plot. Also, a remarkable, soft and control effects interaction between EC/SA concentration (X_2) and stirring speed (X_3) is detected as shown in Fig. 9.

Evidently; the adequacy and significance of the model were justified by an analysis of variance (ANOVA). This test gives knowledge about the importance and the significance of the effects of the variables and their interactions. In this case, the *p* values for the effects of drug concentration (% Drug), polymer concentration (% EC/SA), and stirring speed (rpm) from the analysis of variance are 0.011, 0.205, and 0.134, respectively. Nonetheless, because these values are greater than the 0.05 threshold, they imply that the impacts of these factors are not statistically significant except the drug concentration (% Drug) value.

Table 5 shows the comparison between the theoretical equations obtained from the JMP analysis of the factorial design for Bathes 6 and 8, which were created by using drug concentration (X1 = +1) and EC/SA concentration (X2 = −1) at a stirring speed (X3 = +1). The table includes the theoretical and mean experimental results for the responses % T, K_H, and d_{10} (dmax). We observed that the theoretical values were very similar to the experimental ones. This indicates that the JMP methodology can effectively optimize the appropriate experimental conditions to achieve the desired microsphere characteristics.

4.8. Density functional theory (DFT)

The optimized molecular structures, the frontier molecular orbitals FMOs and the mapping electrostatic potential MEP of 5-ASA, EC, and SA were calculated using DFT calculations and the output results are illustrated in Fig. 10. The optimized molecular structures of 5-ASA and SA illustrate almost planar geometries due to sp^2 hybridization of the carbon atom of aromatic cycle while the EC molecule occupies a 3D space.

4.8.1. Frontier molecular orbitals (FMOs)

The FMOs of 5-ASA are mainly distributed on aromatic cycle and the hydroxyl groups. Moreover, a weak occupancy of the HOMO around the amino group is seen. For EC the FMOs are localized on one part of the molecule. The LUMO can be seen on the organic cycle and some oxygen atoms of its vicinity while the HOMO is localized around the aliphatic chain and a weak part around the organic cycle. Finally, the HOMO of SA is distributed on the whole molecule and its LUMO is localized mainly around on COOH group. Thus, the carboxylate groups may form an active site for the interaction with EC in copolymer building.

Table 6 provides a record of the HOMO and LUMO energies and some related global quantum chemical descriptors (GQCDs) characterized by the used molecules.

The charge transfer between 5-ASA, EC and SA molecules and their external media occurs within the LUMO that accepts electrons and the HOMO that donates electrons. The low values of E_{LUMO} reflect their
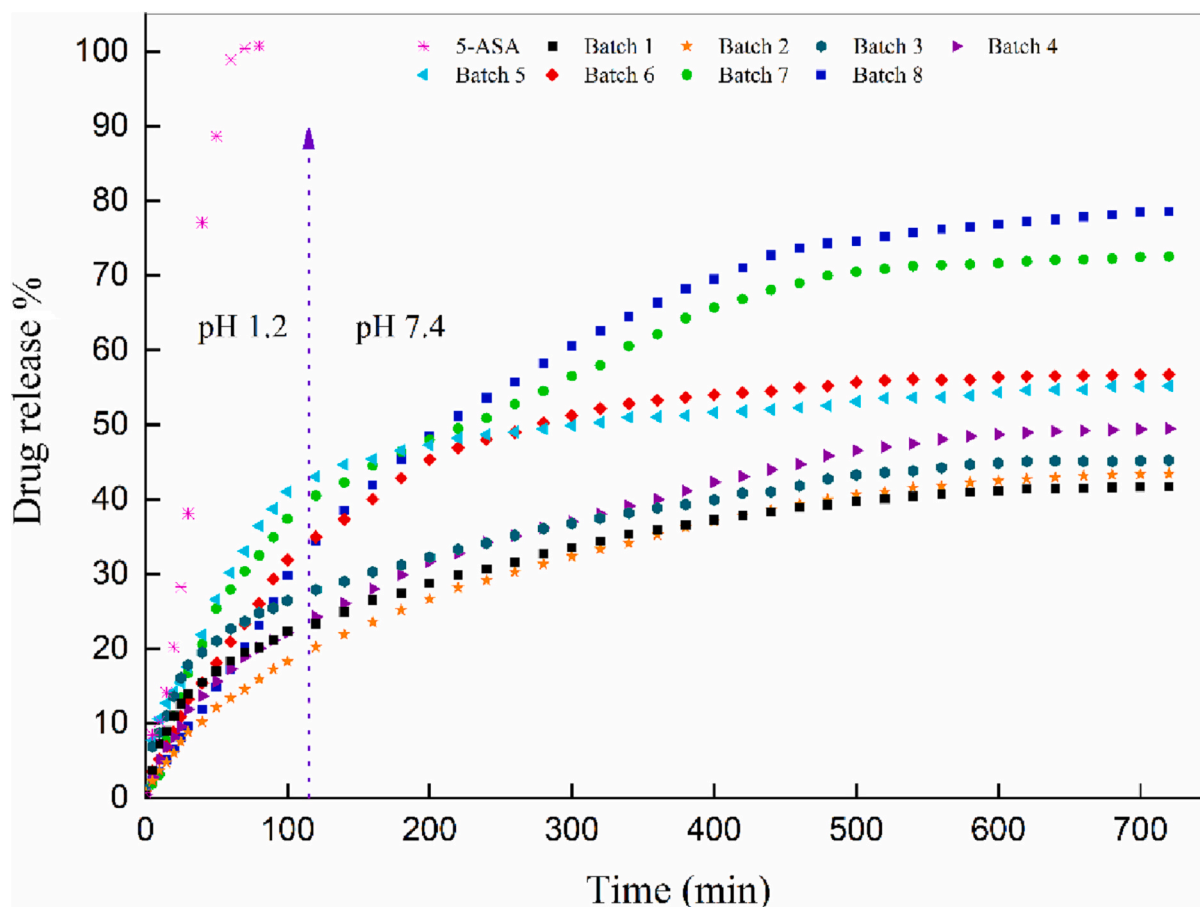
Fig. 7. Percentage release of 5-ASA from EC/SA microspheres in (pH 1.2) and (pH 7.4).

Table 3
Drug release results and data analysis according to Higuchi and Korsmeyer–Peppas modeling.

Batch	Higuchi's equation			Korsmeyer–Peppas' equation			% 5-ASA released after 120 min
	$K_H (min^{-1/2})$	A	R^2	$K_{KP} (min^{-n})$	N	R^2	
1	0.06	−0.171	0.988	0.01	0.913	0.997	20
2	0.053	−0.146	0.994	0.01	0.859	0.993	17.5
3	0.061	−0.179	0.988	0.01	0.914	0.991	19.3
4	0.058	−0.164	0.990	0.01	0.885	0.992	18
5	0.134	−0.328	0.940	0.012	0.965	0.984	45.7
6	0.126	−2.264	0.950	0.019	0.867	0.987	44.4
7	0.123	−0.275	0.943	0.021	0.835	0.956	39.8
8	0.113	−0.227	0.974	0.023	0.805	0.970	37.7

Table 4
Experimental factorial design and results of mesalazine microparticles characteristics.

Experiment	X_1	X_2	X_3	Y_1: %T	Y_4: K_H $(min^{-1/2})$	Y_2:d_{10}dmax
(B − 1)	−1	−1	−1	98.3	0.06	790.6
(B-6)	+1	−1	+1	93.3	0.126	771.5
(B-7)	+1	+1	−1	92.4	0.123	700.0
(B-5)	+1	−1	−1	91.5	0.134	743.5
(B-3)	−1	+1	−1	98.4	0.061	761.8
(B-2)	−1	−1	+1	98.5	0.053	810.0
(B-4)	-1	+1	+1	98.5	0.068	765.0
(B-8)	+1	+1	+1	92.8	0.113	555.0
Coded values/actual values			−1	+1		
X_1: %Drug			10 %	50 %		
X_2: % (EC/SA)			5 %	30 %		
X_3: Stirring speed (rpm)			300	800		

accepting character (Table 6). In addition, the chemical potential is negative for all molecules which indicates their stabilities [43]. Moreover, the gap energy ΔE_{GAP} is described as the absolute value of the difference between E_{LUMO} and E_{HOMO} and it reflect whether the molecule is hard or soft, i.e., a large gap implies weak chemical reactivity as well as high kinetic stability and vice versa [44,45]. The gap of the EC and SA was found to be 6.958 and 8.052 eV respectively indicating the hard character of the used substrate; in return 5-ASA is softer than the others and also its lower η and high σ and |μ| values indicate that its electron transfer may be more effective in chemical interaction [46,47].

4.8.2. Molecular electrostatic potential (MEP)

The calculation of the MEP is routinely used for understanding the relative polarity and to predict electrophilic and nucleophilic regions of the studied molecules [48]. For all studied molecules the negative
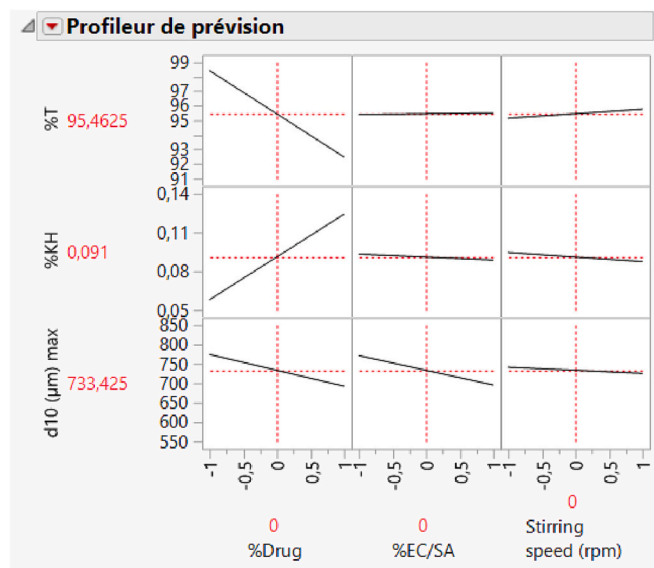
Fig. 8. Optimal conditions obtained by the full factorial model on the 5-ASA microspheres.

potential (electron-rich region) is indicated by a red color and positive one (electron-poor region) is indicated by a blue color. The green color indicates the neutral regions and serves as a potential midway between the two extremes of negative and positive regions Fig. 10. For 5-ASA molecule, the negative potential is located around the hydroxyl and carboxyl group and is about $-7.33*10^{-2}$ V. A weak negative potential can be seen around the organic cycle and the amine group relative to the conjugated π-electrons and electronic doublet of the nitrogen atom respectively. In contrast, the positive potential exists at external surface mainly related to the hydrogen atoms. Its max value is $7.33*10^{-2}$ V. Besides, for EC molecule and SA, the most negative potential is centered on OH groups. The C−O−C linkages or COOH group of SA have the highest values -5.3610^{-2} V and 6.6910^{-2} V respectively. Elsewhere the potential is positive. The non-homogeneity of the potential is due to the non-equi-distribution of the electronic partial charge on the molecular structure which generates high dipolar moments 3.796, 1.912 and 3.629 Debye for 5-ASA, EC and SA respectively. This may involve these molecules to be in high dipolar interactions.

4.8.3. Molecular dynamic simulation (MDS)

The most stable equilibrium configurations for the adsorption of 5-ASA and water molecules on SA-EC co-monomer surface model are established through molecular dynamic simulations. The results are shown in Fig. 11 and the corresponding energies are gathered in Table 7. SA is a polysaccharide made up of repeating units of L-guluronic and D-mannuronic acids. The natural polymerization process involves forming 1,4-glycosidic bonds between the monomers, which results in a linear polymer chain. Electrostatic interactions between negatively charged carboxylate groups (-COO⁻) of the monomers and positively charged sodium ions (Na+) stabilize the polymer structure and give sodium alginate its unique properties, such as its ability to form gels in the presence of calcium ions. Additionally, there can be hydrogen bonding interactions between the hydroxyl groups (-OH) of the monomers, which will further stabilize the polymer structure and contribute to the physical properties of sodium alginate.

In order to build the SA/EC complex, L-guluronic acid and EC can interact through hydrogen bonding. L-guluronic acid contains multiple hydroxyl groups (-OH), which can form hydrogen bonds with the ether and hydroxyl groups of EC. Similar to L-guluronic acid, D-mannuronic acid can also interact with EC through hydrogen bonding. These

hydrogen bonding interactions can enhance the compatibility and adhesion between L-guluronic or D-mannuronic acids and EC. The most equilibrium configurations illustrate that 5-ASA is skewed after adsorption. Comparatively to the initial optimized configuration (Fig. 11a) giving a considerable output deformation energy of -20.574 kJ.mol^{-1} (Table 7.b). The negative output values of adsorption energies indicate the spontaneity of the adsorption process. In addition, it is observed that the aromatic ring is arranged planar to the adsorbent surface, indicating that π-electrons are strongly involved in the adsorption mechanism. The distance between the aromatic ring and CH$_3$ of the substrate at the interface is comprised between 3.148 and 3.482 Å. This considerable width confirms the absence of covalent bonds. It is worth noting that aromatic compounds have a similar adsorption configurations on polymer complexes [49,50]. On top of that, the interactions π-CH with polymers surfaces and small adsorbed molecules have been extensively remarked and investigated [51,52].

Since 5-ASA molecule contains a carbon ring linked to a carboxyl and an amine group, MEP and FMOs proved that these functional groups may form active adsorption sites and enhance the adsorption on copolymer system. The minimum distances between oxygen atoms of the adsorbent and NH$_2$ and OH groups of 5-ASA are 3.055 and 3.141 Å respectively. These distances and the negative partial charges character of these sites may involve them as donor and acceptor in the formation of hydrogen bonds system. Thus, various hydrogen bonds of the type N—H···O. O—H···N and O—H···O were predicted under 3.3 Å donor acceptor distance (Fig. 10b). Furthermore, the water molecule is linked to the adsorbate molecule and the adsorbent via hydrogen bonding mainly of the type O—H···O. Comparatively to adsorption configuration without water molecules, it is seen that these later do not affect strongly the adsorption configuration of 5-ASA molecule. At the same time the adsorption energies are -37.188 (Table 7.a) and -34.449 (Table 7.b). Above this, some water molecules occupy interfacial area and may link indirectly the 5-ASA molecule to the adsorbent surface via a water bridge. As a summary, it can be concluded that the adsorption of drug molecules is more physical and spontaneous where Van der-Waals-type dipolar interaction, π-electron interactions and hydrogen bonds are predominated.

5. Conclusion

The aim of this study is to produce an effective and successful controlled delivery system based on microspheres where Mesalazine (5-ASA) as the active ingredient was encapsulated using a mixture of biopolymers, ethyl cellulose (EC), and sodium alginate (SA), prepared through the emulsion solvent evaporation technique. The process variables including the EC/SA/5-ASA ratio and stirring rate were varied to produce eight batches with distinct characteristics. Microspheres were successfully obtained in all cases with improved drug encapsulation efficiency. The microspheres were characterized using optical microscopy, SEM, FTIR, TGA analysis, XRD, and drug content evaluation, which revealed spherical particles with rough surfaces and sizes range of hundreds of micrometers. Mesalazine was seen to be chemically stable when encapsulated and primarily in an amorphous state. The polymers were compatible without any chemical interactions. The in vitro drug delivery properties of Mesalazine in pH 1.2 and 7.4 aqueous media showed controlled release from microspheres compared to pristine drugs. Delayed and prolonged delivery was observed when the microspheres were exposed to pH 1.2, while higher dissolution efficiency was observed at pH 7.4. The fitting results of the Higuchi's and Korsmeyer-Peppas' models provided insight into the release mechanism. The theoretical DOE and DFT studies impart a deeper analysis of compound interactions, and the approach yielded promising results of therapeutic efficacy using biodegradable polymers while minimizing side effects.
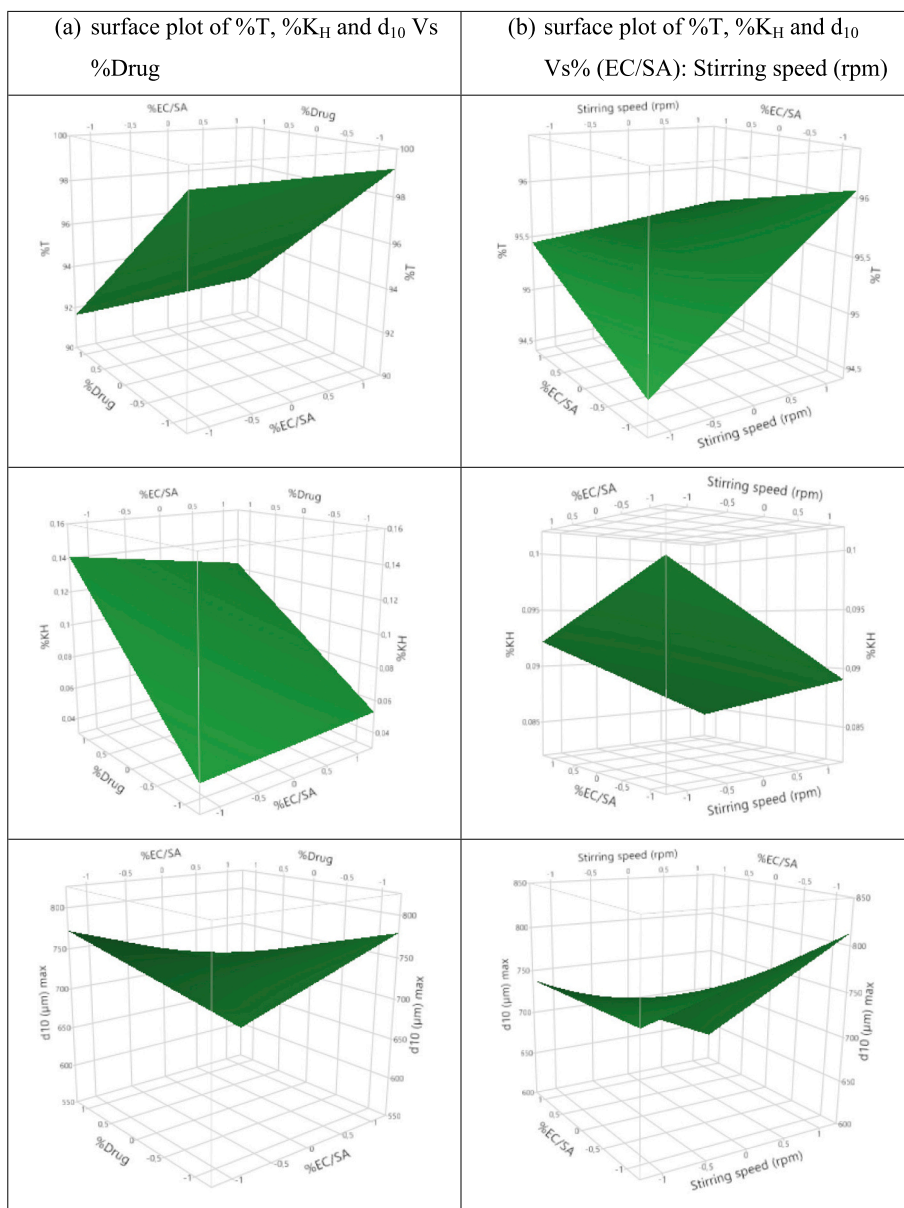
(a) surface plot of %T, %K_H and d_{10} Vs %Drug	(b) surface plot of %T, %K_H and d_{10} Vs% (EC/SA): Stirring speed (rpm)

Fig. 9. Surface plots of responses as a function of the selected variables for microspheres preparation,
(a) surface plot of %T, %K_H and d_{10} Vs %Drug
(b) surface plot of %T, %K_H and d_{10} Vs % (EC/SA): Stirring speed (rpm).

Table 5
Theoretical and experimental values of the responses %T, K_H and d_{10} (d max) for the batches 6 and 8.

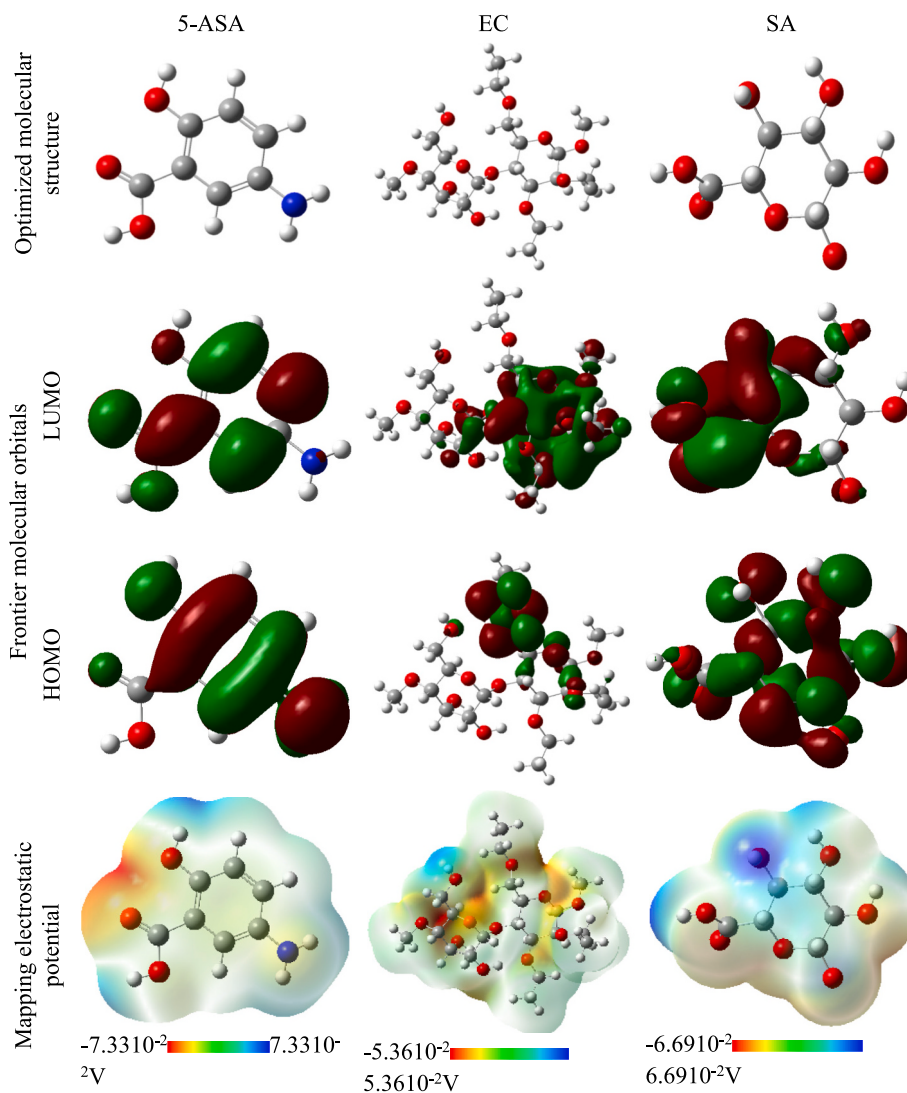| Batch	Responses	Theoretical value	Experimental value
6	%T	93.26	93.3
	K_H	0.11	0.13
	d_{10} (d max)	771.4	771.5
8	%T	92.96	92.8
	K_H	0.12	0.11
	d_{10} (d max)	555.01	555

Fig. 10. Optimized molecular structure, frontier molecular orbitals and mapping electrostatic potential of 5-ASA, EC and SA molecules.

Table 6

Values of the FMOs energies (eV) and some related global quantum chemical descriptors (GQCDs).

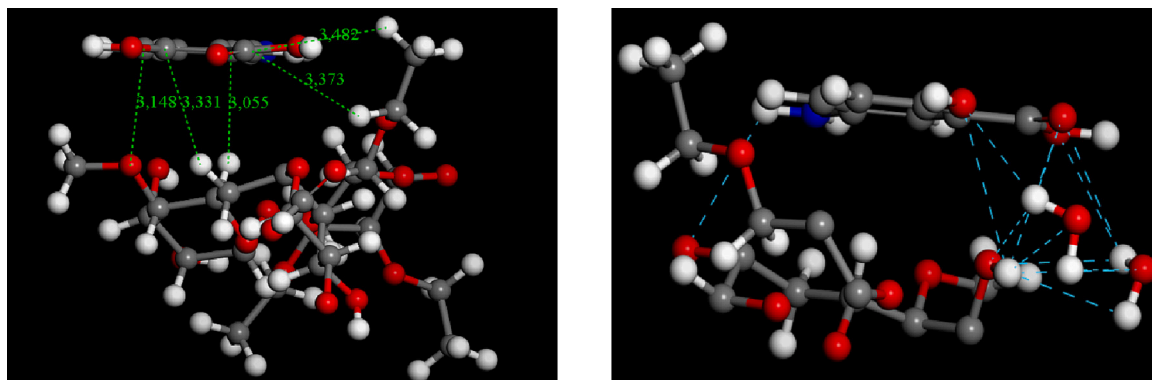| Molecule	LUMO	HOMO	ΔE_{GAP}	Global hardness (η)	chemical potential (μ)	Global softness (σ)	Absolute electronegativity (χ)	Electrophilicity index (ω)
5-ASA	−1.067	−5.319	4.252	−2.126	−3.193	−0.470	3.193	−2.398
EC	1.686	−6.366	8.052	−4.026	−2.340	−0.248	2.340	−0.680
SA	−0.282	−7.234	6.958	−3.479	−3.760	−0.287	3.760	−2.032

Fig. 11. Magnification at the interface of the most stable adsorption configuration of one molecule of 5-ASA and five water molecules adsorbed on EC-SA co-monomer model.

Table 7
Adsorption energies (kJ.mol^{-1}) of 5-ASA and water molecules on co-monomer surface model.

a. Complex of L-guluronic acid and ethyl cellulose

Molecules	Total energy	Adsorption energy	Rigid adsorption energy	Deformationenergy	5-ASA: dE$_{ad}$/dN$_i$	H$_2$O: dE$_{ad}$/dN$_i$
5-ASA	2.355	−37.188	−16.791	−20.397	−37.188	/
Water	−3.352	−4.062	−3.352	−0.709	/	−4.062
5-ASA/10H$_2$O	−24.673	−71.317	−43.701	−27.609	−35.678	−3.521

b. Complex of D-mannuronic acid and ethyl cellulose

Molecules	Total energy	Adsorption energy	Rigid adsorption energy	Deformationenergy	5-ASA: dE$_{ad}$/dN$_i$	H$_2$O: dE$_{ad}$/dN$_i$
5-ASA	5.094	−34.449	−13.875	−20.574	−34.449	/
Water	−3.352	−4.061	−3.352	−0.709	/	−4.061
5-ASA/10H$_2$O	−19.469	−66.106	−38.370	−27.360	−34.265	−2.862

CRediT authorship contribution statement

Roufaida MERIR: Methodology, Conceptualization, Visualization, Formal analysis, writing. **Milad BAITICHE:** Methodology, Conceptualization**,** Data and graphs analyses, Review. **Zineb ELBAHRI:** Methodology, Micrographic Analysis, Simulation analysis. **Riad BOURZAMI:**, Simulation analysis and modeling. **Ferhat DJERBOUA:** Reviewing and English checking. **Mokhtar BOUTAHALA:** Conceptualization, Visualization, Review.

Declaration of competing interest

There are no known competing interests to declare.

Acknowledgements

References

[1] L.M. Ensign, R. Cone, J. Hanes, Oral drug delivery with polymeric nanoparticles: the gastrointestinal mucus barriers, Adv. Drug Deliv. Rev. 64 (2012) 557–570, https://doi.org/10.1016/j.addr.2011.12.009.

[2] J. Reinholz, K. Landfester, V. Mailänder, The challenges of oral drug delivery via nanocarriers, Drug Deliv. 25 (2018) 1694–1705, https://doi.org/10.1080/10717544.2018.1501119.

[3] T. Zhang, G. Zhu, B. Lu, Q. Peng, Oral nano-delivery systems for colon targeting therapy, Pharm. Nanotechnol. 5 (2017) 83–94, https://doi.org/10.2174/2211738505666170424122722.

[4] C. Von Ritter, Chronisch-entzündlicheDarmerkrankungen: Pathophysiologie und medikamentöseTherapie, Radiol. Berl. Print. 38 (1998) 3–7.

[5] Y.R. Mahida, C.E. Lamming, A. Gallagher, A.B. Hawthorne, C.J. Hawkey, 5-Aminosalicylic acid is a potent inhibitor of interleukin 1 beta production in organ culture of colonic biopsy specimens from patients with inflammatory bowel disease, Gut. 32 (1991) 50–54, https://doi.org/10.1136/gut.32.1.50.

[6] F. Cominelli, C.C. Nast, A. Duchini, M. Lee, Recombinant interleukin-1 receptor antagonist blocks the proinflammatory activity of endogenous interleukin-1 in rabbit immune colitis, Gastroenterology. 103 (1992) 65–71, https://doi.org/10.1016/0016-5085(92)91096-M.

[7] Y. Cheng, 5-aminosalicylic acid is an attractive candidate agent for chemoprevention of colon cancer in patients with inflammatory bowel disease, World J. Gastroenterol. 11 (2005) 309, https://doi.org/10.3748/wjg.v11.i3.309.

[8] D.L. French, J.W. Mauger, Evaluation of the physicochemical properties and dissolution characteristics of mesalamine: relevance to controlled intestinal drug delivery, Pharm. Res. 10 (1993) 1285–1290, https://doi.org/10.1023/A:1018909527659.

[9] D.L. French, K.J. Himmelstein, J.W. Mauger, Physicochemical aspects of controlled release of substituted benzoic and naphthoic acids from Carbopol® gels, J. Control. Release 37 (1995) 281–289, https://doi.org/10.1016/0168-3659(95)00086-0.

[10] M.E. Palomo, M.P. Ballesteros, P. Frutos, Solvent and plasticizer influences on ethylcellulose-microcapsules, J. Microencapsul. 13 (1996) 307–318, https://doi.org/10.3109/02652049609026018.

[11] N. Assas, Z. Elbahri, M. Baitiche, F. Djerboua, Effects of some process parameters on the niflumicacid controlled release polymeric microspheres: optimization using designs of experiments, Asia Pac. J. Chem. Eng. 14 (2019), e2283, https://doi.org/10.1002/apj.2283.

[12] O.E. Khoukhi, Z.E. Bahri, K. Diaf, M. Baitiche, Piroxicam /β-cyclodextrin complex included in cellulose derivatives-based matrix microspheres as new solid dispersion-controlled release formulations, Chem. Pap. 70 (2016) 828–839, https://doi.org/10.1515/chempap-2016-0014.

[13] Y. Hu, S. Zhang, D. Han, Z. Ding, S. Zeng, X. Xiao, Construction and evaluation of the hydroxypropyl methyl cellulose-sodium alginate composite hydrogel system for sustained drug release, J. Polym. Res. 25 (2018) 1–12, https://doi.org/10.1007/s10965-018-1546-y.

[14] T.-L. Wu, Modification of the initial release of a highly water-soluble drug from ethyl cellulose microspheres, J. Microencapsul. 16 (1999) 639–646, https://doi.org/10.1080/026520499288825.

[15] M.S.H. Akash, K. Rehman, N. Li, J.-Q. Gao, H. Sun, S. Chen, Sustained delivery of IL-1Ra from pluronic F127-based thermosensitive gel prolongs its therapeutic potentials, Pharm. Res. 29 (2012) 3475–3485, https://doi.org/10.1007/s11095-012-0843-0.

[16] A. Hlel, A. Mabrouk, M. Chemek, I.B. Khalifa, K. Alimi, Computational Condensed Matter, 2015, https://doi.org/10.1016/j.cocom.2015.02.001.

[17] A.D. Becke, Density-functional thermochemistry. III. The role of exact exchange, J. Chem. Phys. 98 (1993) 5648–5652, https://doi.org/10.1063/1.464913.

[18] M. Vujović, V. Ragavendran, B. Arsić, E. Kostić, M. Mladenović, DFT calculations as an efficient tool for prediction of Raman and infra-red spectra and activities of newly synthesized cathinones, Open Chem. 18 (2020) 185–195, https://doi.org/10.1515/chem-2020-0021.

[19] O. Noureddine, N. Issaoui, M. Medimagh, O. Al-Dossary, H. Marouani, Quantum chemical studies on molecular structure, AIM, ELF, RDG and antiviral activities of hybrid hydroxychloroquine in the treatment of COVID-19: molecular docking and DFT calculations, J. King Saud Univ. Sci. 33 (2021) 101334, https://doi.org/10.1016/j.jksus.2020.101334.

[20] M. Kebir, R. Bourzami, N. Nasrallah, S.E.I. Lebouachera, F. Dergal, R. Ladji, M. Trari, H. Ben Harharah, A. elJery, A.A. Azzaz, L. Khezami, Pharmaceutical pollutants adsorption onto activated carbon: isotherm, kinetic investigations and DFT modeling approaches, ComptesRendusChim. 25 (2022) 9–25, https://doi.org/10.5802/crchim.161.

[21] O. Noureddine, S. Gatfaoui, S.A. Brandán, H. Marouani, N. Issaoui, Structural, docking and spectroscopic studies of a new piperazine derivative, 1-Phenylpiperazine-1, 4-diium bis (hydrogen sulfate), J. Mol. Struct. 1202 (2020), 127351, https://doi.org/10.1016/j.molstruc.2019.127351.

[22] T.B. Issa, A. Sagaama, N. Issaoui, Computational study of 3-thiophene acetic acid: molecular docking, electronic and intermolecular interactions investigations, Comput. Biol. Chem. 86 (2020), 107268, https://doi.org/10.1016/j.compbiolchem.2020.107268.

[23] E.E. Ebenso, T. Arslan, F. Kandemirli, N. Caner, I. Love, Quantum chemical studies of some rhodanineazosulpha drugs as corrosion inhibitors for mild steel in acidic medium: RhodanineAzosulpha drugs as corrosion inhibitors, Int. J. Quantum Chem. 110 (2010) 1003–1018, https://doi.org/10.1002/qua.22249.

[24] D. Sid, M. Baitiche, R. Bourzami, R. Merir, F. Djerboua, A. Gil, M. Boutahala, Experimental and theoretical studies of the interaction of ketoprofen in halloysite nanotubes, Colloids Surf. A Physicochem. Eng. Asp. 627 (2021), 127136, https://doi.org/10.1016/j.colsurfa.2021.127136.

[25] M. Radjai, H. Ferkous, Z. Jebali, H. Majdoub, R. Bourzami, G. Raffin, M. Achour, A. Gil, M. Boutahala, Adsorptive removal of cationic and anionic dyes on a novel mesoporous adsorbent prepared from diatomite and anionic cellulose nanofibrils: experimental and theoretical investigations, J. Mol. Liq. 361 (2022), 119670, https://doi.org/10.1016/j.molliq.2022.119670.

[26] J.M. Stein, The effect of adrenaline and of alpha- and beta-adrenergic blocking agents on ATP concentration and on incorporation of 32Pi into ATP in rat fat cells, Biochem. Pharmacol. 24 (1975) 1659–1662, https://doi.org/10.1016/0006-2952(75)90002-7.

[27] H. Daemi, M. Barikani, Synthesis and characterization of calcium alginate nanoparticles, sodium homopolymannuronate salt and its calcium nanoparticles, Sci. Iran. 19 (2012) 2023–2028, https://doi.org/10.1016/j.scient.2012.10.005.

[28] J. Han, Z. Zhou, R. Yin, D. Yang, J. Nie, Alginate–chitosan/hydroxyapatite polyelectrolyte complex porous scaffolds: preparation and characterization, Int. J.

Biol. Macromol. 46 (2010) 199–205, https://doi.org/10.1016/j.ijbiomac.2009.11.004.

[29] M. Singh, Preparation and structural characterization of melamine–methylurea–formaldehyde resin and its blends separately with ethyl cellulose, starch, teakwood, and almond shell powders by 13C NMR, IR, TGA, and SEM techniques, J. Appl. Polym. Sci. 92 (2004) 3437–3446, https://doi.org/10.1002/app.20279.

[30] V. Suthar, A. Pratap, H. Raval, Studies on poly (hydroxy alkanoates)/(ethylcellulose) blends, Bull. Mater. Sci. 23 (2000) 215–219, https://doi.org/10.1007/BF02719913.

[31] S. Banerjee, S. Singh, S.S. Bhattacharya, P. Chattopadhyay, Trivalent ion cross-linked pH sensitive alginate-methyl cellulose blend hydrogel beads from aqueous template, Int. J. Biol. Macromol. 57 (2013) 297–307, https://doi.org/10.1016/j.ijbiomac.2013.03.039.

[32] A. Pineda, A. Hechenleitner, Characterization of ethylcellulose films containing natural polysaccharides by thermal analysis and FTIR spectroscopy, Acta Farm. Bonaer. 23 (2004) 53–57.

[33] M.Y. Nassar, M.F. El-Shahat, S.M. Khalile, M. El-Desawy, E.A. Mohamed, Structure investigation of mesalazine drug using thermal analyses, mass spectrometry, DFT calculations, and NBO analysis, J. Therm. Anal. Calorim. 117 (2014) 463–471, https://doi.org/10.1007/s10973-014-3638-1.

[34] A. Salisu, M.M. Sanagi, A. Abu Naim, K.J. Abd Karim, W.A. Wan Ibrahim, U. Abdulganiyu, Alginate graft polyacrylonitrile beads for the removal of lead from aqueous solutions, Polym. Bull. 73 (2016) 519–537, https://doi.org/10.1007/s00289-015-1504-3.

[35] M. Zhang, B. Xiao, H. Wang, M.K. Han, Z. Zhang, E. Viennois, C. Xu, D. Merlin, Edible ginger-derived nano-lipids loaded with doxorubicin as a novel drug-delivery approach for colon cancer therapy, Mol. Ther. 24 (2016) 1783–1796, https://doi.org/10.1038/mt.2016.159.

[36] P. Rani, S. Mishra, G. Sen, Microwave based synthesis of polymethyl methacrylate grafted sodium alginate: its application as flocculant, Carbohydr. Polym. 91 (2013) 686–692, https://doi.org/10.1016/j.carbpol.2012.08.023.

[37] S.Ş. Başarır, N.P. Bayramgil, The uranium recovery from aqueous solutions using amidoxime modified cellulose derivatives. I. Preparation, characterization and amidoxime conversion of radiation grafted ethyl cellulose-acrylonitrile copolymers, Radiochim. Acta 100 (2012) 893–900, https://doi.org/10.18596/jotcsa.310947.

[38] M.K. Trivedi, A. Branton, D. Trivedi, G. Nayak, R. Mishra, S. Jana, Characterization of physicochemical and thermal properties of biofield treated ethyl cellulose and methyl cellulose, Int. J. Biomed. Mater. Res. 3 (2015) 83–91, https://doi.org/10.18596/jotcsa.310947.

[39] A.G. Press, I.A. Hauptmann, L. Hauptmann, B. Fuchs, M. Fuchs, K. Ewe, G. Ramadori, Gastrointestinal pH profiles in patients with inflammatory bowel disease, Aliment. Pharmacol. Ther. 12 (1998) 673–678, https://doi.org/10.1046/j.1365-2036.1998.00358.x.

[40] M. Lopes, B. Abrahim, F. Veiga, R. Seiça, L.M. Cabral, P. Arnaud, J.C. Andrade, A. J. Ribeiro, Preparation methods and applications behind alginate-based particles, Expert Opin. Drug Deliv. 14 (2017) 769–782, https://doi.org/10.1080/17425247.2016.1214564.

[41] V.R. Sinha, R. Kumria, Polysaccharides in colon-specific drug delivery, Int. J. Pharm. 224 (2001) 19–38, https://doi.org/10.1016/S0378-5173(01)00720-7.

[42] N. Vankova, S. Tcholakova, N.D. Denkov, I.B. Ivanov, V.D. Vulchev, T. Danner, Emulsification in turbulent flow: 1. Mean and maximum drop diameters in inertial and viscous regimes, J. Colloid Interface Sci. 312 (2007) 363–380, https://doi.org/10.1016/j.jcis.2007.03.059.

[43] M. Kamel, A. Morsali, H. Raissi, K. Mohammadifard, Theoretical insights into the intermolecular and mechanisms of covalent interaction of Flutamide drug with COOH and COCl functionalized carbon nanotubes: a DFT approach, Chem. Rev. Lett. 3 (2020) 23–37, https://doi.org/10.22034/crl.2020.221149.1039.

[44] K. Fukrd, T. Yomezawa, H. Skrlnga, A molecular orbital theory of reactivity in aromatic hydrocarbons. 1, Chem. Phys. 20 (1952) 722–725, https://doi.org/10.1063/1.1700523.

[45] Y.S. Mary, C.Y. Panicker, M. Sapnakumari, B. Narayana, B.K. Sarojini, A.A. Al-Saadi, C. Van Alsenoy, J.A. War, H.K. Fun, Molecular structure, FT-IR, vibrational assignments, HOMO–LUMO analysis and molecular docking study of 1-[5-(4-Bromophenyl)-3-(4-fluorophenyl)-4, 5-dihydro-1H-pyrazol-1-yl] ethanone, Spectrochim. Acta A Mol. Biomol. Spectrosc. 136 (2015) 473–482, https://doi.org/10.1016/j.saa.2014.09.060.

[46] M.R. JalaliSarvestani, R. Ahmadi, Investigating the complexation of a recently synthesized phenothiazine with different metals by density functional theory, Int. J. New Chem. 4 (2017) 101–110, https://doi.org/10.22034/ijnc.2017.30984.

[47] M.R. JalaliSarvestani, S. Majedi, A DFT study on the interaction of alprazolam with fullerene (C20), J. Chem. Lett. 1 (2020) 32–38, https://doi.org/10.22034/jchemlett.2020.108111.

[48] L. Sinha, O. Prasad, V. Narayan, S.R. Shukla, Raman, FT-IR spectroscopic analysis and first-order hyperpolarisability of 3-benzoyl-5-chlorouracil by first principles, Mol. Simul. 37 (2011) 153–163, https://doi.org/10.1080/08927022.2010.533273.

[49] A. Rochefort, J.D. Wuest, Interaction of substituted aromatic compounds with graphene, Langmuir. 25 (2009) 210–215, https://doi.org/10.1021/la802284j.

[50] S.K. Kolev, H.A. Aleksandrov, V.A. Atanasov, V.N. Popov, T.I. Milenov, Interaction of graphene with out-of-plane aromatic hydrocarbons, J. Phys. Chem. C 123 (2019) 21448–21456, https://doi.org/10.1021/acs.jpcc.9b03550.

[51] D. Umadevi, G.N. Sastry, Saturated vs. unsaturated hydrocarbon interactions with carbon nanostructures, Front. Chem. 2 (2014) 75, https://doi.org/10.3389/fchem.2014.00075.

[52] J.-H. Deng, J. Luo, Y.-L. Mao, S. Lai, Y.-N. Gong, D.-C. Zhong, T.-B., Lu, π-π stacking interactions: non-negligible forces for stabilizing porous supramolecular frameworks, Sci. Adv. 6 (2020) eaax9976, https://doi.org/10.1126/sciadv.aax9976.

Abstract

The purpose of this research is to improve and optimize drug delivery systems for 5-aminosalicylic acid (5-ASA) to treat inflammatory bowel diseases such as Crohn's disease and ulcerative colitis. We used the emulsion solvent evaporation technique, which allows for the encapsulation of 5-ASA within a polymer matrix, creating microspheres that can control drug release. Our in vitro release studies in simulated gastric and intestinal fluids demonstrated controlled, pH-dependent drug release, which we successfully modeled using Higuchi's and Korsmeyer–Peppas' models. Additionally, we employed Design of Experiments (DOE) and Density Functional Theory (DFT) analyses to optimize molecular interactions and evaluate their effects on drug entrapment and microparticle sizes.

For prolonged release in acidic medium, sodium alginate (SA) acts as a coating material, forming a stable 3D porous network with ethylcellulose (EC) and 5-ASA. This network is easily broken in basic conditions, leading to drug release. Chitosan (Cts) enhances the structural integrity of the drug-loaded beads, providing additional stability and ensuring that the drug remains effective within the gastrointestinal environment.

In the optimization of colon-targeted therapy via halloysite, the biocompatibility, encapsulation capability, and pH-responsive release properties of halloysite nanotubes make them a promising material for developing targeted and controlled 5-ASA delivery systems.

Diatomite serves as a promising material for drug delivery systems due to its unique properties. When combined with polymers such as sodium alginate and chitosan, diatomite can enhance the stability, biocompatibility, and controlled release of therapeutic agents.

Docking experiments showed strong binding of 5-ASA to PPAR-γ and stable interactions with COX-2 enzymes, suggesting 5-ASA's potential to effectively reduce inflammation.

Keywords: 5-aminosalicylic acid, Inflammatory bowel disease, Microencapsulation, Molecular docking, Density functional theory, Design of experiments, Therapeutic efficacy.

Résumé

Le but de cette recherche est d'améliorer et d'optimiser les systèmes d'administration de médicaments pour l'acide 5-aminosalicylique (5-ASA) afin de traiter les maladies inflammatoires de l'intestin telles que la maladie de Crohn et la colite ulcéreuse. Nous avons utilisé la technique d'évaporation de solvant en émulsion, qui permet l'encapsulation du 5-ASA dans une matrice polymère, créant des microsphères capables de contrôler la libération du médicament. Nos études de libération in vitro dans des fluides gastriques et intestinaux simulés ont démontré une libération contrôlée et dépendante du pH, que nous avons modélisée avec succès en utilisant les modèles de Higuchi et de Korsmeyer–Peppas. De plus, nous avons employé des analyses de plan d'expériences (DOE) et de théorie de la fonctionnelle de la densité (DFT) pour optimiser les interactions moléculaires et évaluer leurs effets sur l'entrapment du médicament et la taille des microparticules.

Pour la libération prolongée en milieu acide, l'alginate de sodium (SA) agit comme un matériau de revêtement, formant un réseau poreux 3D stable avec l'éthylcellulose (EC) et le 5-ASA. Ce réseau est facilement dégradé en conditions basiques, ce qui conduit à la libération du médicament. Le chitosane (Cts) renforce l'intégrité structurelle des billes chargées de médicament, fournissant une stabilité supplémentaire et garantissant que le médicament reste efficace dans l'environnement gastro-intestinal.

Dans l'optimisation de la thérapie ciblée sur le côlon via l'halloysite, la biocompatibilité, la capacité d'encapsulation et les propriétés de libération dépendantes du pH des nanotubes d'halloysite en font un matériau prometteur pour développer des systèmes de délivrance contrôlée et ciblée du 5-ASA.

La diatomite est un matériau prometteur pour les systèmes d'administration de médicaments en raison de ses propriétés uniques. Lorsqu'elle est combinée avec des polymères tels que l'alginate de sodium et le chitosane, la diatomite peut améliorer la stabilité, la biocompatibilité et la libération contrôlée des agents thérapeutiques.

Les expériences de docking ont montré une forte liaison du 5-ASA avec PPAR-γ et des interactions stables avec les enzymes COX-2, suggérant le potentiel du 5-ASA à réduire efficacement l'inflammation.

Mots-clés : Acide 5-aminosalicylique, Maladie inflammatoire de l'intestin, Microencapsulation, Docking moléculaire, Théorie de la fonctionnelle de la densité, Plan d'expériences, Efficacité thérapeutique.

ملخص

الغرض من هذا البحث هو تحسين وتحسين أنظمة توصيل الدواء لحمض الخماسي الأميني (5-ASA) لعلاج الأمراض الالتهابية في الأمعاء مثل مرض كرون والتهاب القولون التقرحي. لقد استخدمنا تقنية تبخير المذيبات بالتشتت الإمولسيوني، التي تسمح بتغليف 5-ASA داخل مصفوفة بوليمريّة، مما ينتج عنه ميكروسفيرات يمكن أن تسيطر على إطلاق الدواء؛ أظهرت دراساتنا لإطلاق الدواء في الأنابيب الهضمية والأمعاء المحاكية إطلاق دواء متحكم به يعتمد على درجة الحموضة، وقد نمذجنا بنجاح ذلك باستخدام نماذج هيغوتشي وكورسماير-بيباس. بالإضافة إلى ذلك، استخدمنا تصميم التجارب (DOE) ونظرية الدوال الكثافية (DFT) لتحسين التفاعلات الجزيئية وتقييم تأثيراتها على احتجاز الدواء وأحجام الميكروبارتيكل.

بالنسبة للإطلاق المطول في وسط حمضي، يعمل الألجينات الصوديوم (SA) كمادة طلاء، مكونة شبكة مسامية ثلاثية الأبعاد مستقرة مع الإيثيل سيليلوز (EC) و 5-ASA. هذه الشبكة يمكن تفكيكها بسهولة في ظروف قاعدية، مما يؤدي إلى إطلاق الدواء. يعزز الكيتوزان (Cts) تكامل بنية الخرز المحملة بالدواء، مما يوفر استقرارًا إضافيًا ويضمن بقاء الدواء فعالاً داخل البيئة الهضمية.

في تحسين العلاج المستهدف على مستوى القولون عبر الهالويسيت، تجعل قدرة التحميل الحيوي، وقابلية التغليف، وخواص إطلاق الحمض النووي المستجيبة لدرجة الحموضة لأنابيب الهالويسيت نانوتيوبز منهجاً واعداً لتطوير أنظمة توصيل مستهدفة ومتحكمة لـ 5-ASA.

تعتبر الدياتوميت مادة واعدة لأنظمة توصيل الدواء بفضل خصائصها الفريدة. عندما تُدمج مع البوليمرات مثل الألجينات الصوديوم والكيتوزان، يمكن للدياتوميت تعزيز الاستقرار والتوافق مع الأنسجة الحية والإفراج المتحكم عن الوكلاء العلاجيين.

أظهرت التجارب الموضوعية ربط قوي لـ 5-ASA بـ PPAR-γ وتفاعلات مستقرة مع إنزيمات COX-2، مما يشير إلى إمكانية 5-ASA للحد من الالتهاب بفعالية.

الكلمات الرئيسية: حمض الخماسي الأميني (5-ASA)، مرض الأمعاء التهابية، التغليف المجهري، التحسين المولكي، نظرية الوظيفة الكثافية، تصميم التجارب، الفعالية العلاجية.